Preparation and Characterization of Hydrophilic Polysulfone Ultrafiltration Membranes

Thesis submitted in partial fulfillment of the requirements

for the degree of

DOCTOR OF PHILOSOPHY

by

Nilay Sharma

Department of Chemical Engineering

Indian Institute of Technology Guwahati

Guwahati-781039, India

Preparation and Characterization of Hydrophilic Polysulfone Ultrafiltration Membranes

Nilay Sharma

Preparation and Characterization of Hydrophilic Polysulfone Ultrafiltration Membranes

Thesis submitted in partial fulfillment of the requirements

for the degree of

DOCTOR OF PHILOSOPHY

by

Nilay Sharma

Roll No: 126107020

Department of Chemical Engineering

Indian Institute of Technology Guwahati

Guwahati-781039, India

Dedicated to my Parents and husband for their faith, love, understanding and support

Department of Chemical Engineering

Indian Institute of Technology Guwahati

Guwahati 781039, India

CERTIFICATE

It is certified that the work reported in the thesis entitled "**Preparation and Characterization of Hydrophilic Polysulfone Ultrafiltration Membranes**", by **Nilay Sharma**, has been carried out under my supervision. The work documented in this thesis has not been submitted to any other University or Institute for the award of any degree or diploma.

Dr. Mihir Kumar Purkait

Professor

Department of Chemical Engineering

Indian Institute of Technology Guwahati

Guwahati 781039, India

Date:

Acknowledgements

I owe a debt of gratitude to many people who have helped me in completing this research work directly and indirectly. I would like to acknowledge them all. To begin with, I wish to express my deepest acknowledgement to my supervisor, **Dr. Mihir Kumar Purkait** for providing me inspiring guidance throughout the entire course of this work. I am indebted to him for his useful suggestions and constant encouragement throughout the entire period. I am grateful to him for his great support, encouragement which helped me to finish this work within time. I always admire his advises, energy and hard work for all his students. Besides this, I feel very fortunate that I got a chance to work with such experienced and enthusiastic supervisor, whom I will admire throughout my career.

I would like to thank my doctoral committee members, **Prof. Pallab Ghosh**, **Dr. Chandan Das** (Department of Chemical Engineering), and **Dr. Bhuwneshwar Mondal** (Chemistry Department) for their valuable suggestions and constructive criticism during the project evolutions, which helped me to make necessary improvements in various stages of my research work. I would specially like to thank **Prof. Pallab Ghosh** for the rigorous and remarkable questions that he raised during the seminar presentations which had helped me a lot in understanding many facts related to my work.

I am also thankful to all the faculty members of the Chemical Engineering Department for their encouragement and help at various stages during my stay in this Department. In this regard, I would specially like to mention the name of **Dr. Chandan Das.**

I must thank to all the technical staffs of my Department specially, **Mr. Lukumoni Borah**, **Mr. Dipak Kumar Barman, Mr. Prasun Bhattacharjee**, **Mr. Kaustavmoni Deka**, **Mr. Debajit Borah**, and the Scientific Officers, **Mrs. Ritumoni Kalita** and **Mr. Harsaraj Biswanath.** The experimental works presented in this thesis would never have been possible without the help of these proficient technicians. I am also very thankful to **Mr. Bijoy Kumar**

Choudhury (Senior Technician, Department of Mechanical Engineering), who helped me in installing my experimental setup.

I am thankful to the **Central Instrument Facility** and **Centre of Excellence** for **Sustainable polymers (CoE-SusPol)** of IIT Guwahati for allowing me to utilize their experimental resources. I am also thankful to the **Central Workshop** of IIT Guwahati for helping me in the fabrication part of my experimental setup which was essential in my research work.

I was fortunate enough to get excellent lab-mates like, **Murchana, Piyal**, **Anushree, Shyam** and **Somnath**. Thanks to all of them for their friendly support, timely assistance and co-operation throughout my research work. I am also thankful to **Sayan, Harsha, Rohan, Indra and Madhusmita** for their friendly behavior and assistance.

I have no word to thank **GOD** who is my strength and wisdom.

I also wish to extend my loving thanks to my father **Mr. Akhilesh Kumar Sharma** and my mother **Mrs. Seema Shrama** for their constant moral support. Their love, affection, blessings and sacrifices made me stronger to overcome my huddles and achieve my goal. I express my humble regards to my parents-in-law and acknowledge their love and blessings. Also, I would like to give my love to my sweet niece **Nivedita**. A special thanks to **Rangmala** for her caring efforts to me and my family during these years.

Finally, I express my enormous gratitude and indebtedness to my husband, **Brajesh** for his utmost care, unlimited patience and constant endorsement at all stages of this work during these four years. This work would not have been possible without his support.

Nilay Sharma

Abstract

The main objective of this work is to prepare asymmetric polymeric membranes with increased hydrophilic properties. It is well known that three surface modification techniques are mainly used for increasing the hydrophilicity of membrane. First by plasma treatment, second by coating and third by blending. Among these three methods, blending is a simple technique and it does not require complicated steps. So, in the present work polymeric membranes were modified by blending different additives. All the additives used in this thesis, increased the hydrophilicity of modified membranes compared to plain membranes. Apart from this, Tartaric acid (both enantiomeric and racemic) provides the electrostatic repulsive property to the modified membranes.

First of all, flat sheet asymmetric polymeric membranes were prepared by phase inversion process using polysulfone (PSF) as base polymer in N-methyl-2-pyrrolidone (NMP) as a solvent. Consequences of the addition of polyvinyl pyrrolidone (PVP) of different molecular weights with constant molecular weight of polyacrylic acid (PAA) on the morphology and permeation properties of PSF membranes were studied. The surface structure and morphology of the prepared membranes were analyzed by field emission scanning electron microscope (FESEM) and atomic force microscopy (AFM). The pore number, average pore size and area of pores for all the membranes were determined by liquid displacement porosimetry (LLDP) method. These ultrafiltration membranes were subjected to characterizations such as measurement of pure water flux (PWF) and compaction factor (CF). Bovine serum albumin (BSA) of molecular weight 68,000 Da was used to study the permeation performance of prepared membranes using a batch cell of 400 mL capacity. Whereas equilibrium water content (EWC), porosity and ion exchange capacity (IEC) are measured for evaluating the hydrophilicity. Results demonstrate that the flux performance of the membranes and morphological parameters own a crucial inter-relationship with the

molecular weight of PVP. The membrane pore area and pore number were found to be increased by increasing molecular weight of PVP with constant molecular weight of PAA. A detailed comparative study was done with Chakrabarty et al. [15] and found better in almost all the aspects. All the resulting parameters were compared and concluded with the fact that addition of small amount of PAA in PSF/PVP/NMP casting solution can be better than addition of PVP alone.

Keeping hydrophilicity as key factor for anti-fouling property for polymeric membrane, PSF ultrafiltration membranes with pH sensitivity were prepared using the copolymer poly(N vinyl pyrrolidone-co-isatoic anhydride) poly(VP-co-IAH) as an additive. Radical initiated copolymerization was used for the preparation of copolymer poly(VP-co-IAH) from N-vinyl pyrrolidone and isatoic anhydride. Azobisisobutyronitrile (AIBN) was taken as initiator. Asymmetric membranes were prepared by blending of copolymer poly(VP-co-IAH) directly in the membrane casting solution. FTIR and ^{1}HNMR spectra proved the formation of copolymer poly(VP-co-IAH). Whereas, presence of copolymer in blended membranes was confirmed by comparing FTIR spectra of plain and polymer containing membranes. Field emission scanning electron microscope (FESEM) and atomic force microscopy (AFM) were used for morphological study. Characterization of membrane was done in terms of PWF, hydrophilicity and hydraulic permeability. PWF increased from 44.4 L/m^{2}h to 76.6 L/m^{2}h for plain and 4 wt % copolymer containing PSF membrane, respectively. Likewise, water contact angle was also found to be reduced from 76.25^0 to 61.65^0. BSA solution was used for studying the permeation and rejection behaviour of the membranes. A substantial rise in BSA flux (which is from 6.6 L/m^{2}h for unmodified membrane to 18.1 L/m^{2}h for copolymer containing membrane) and maximum BSA rejection was increased by 47.9 % for the modified membrane. FESEM images affirm that the pore size of the membranes decreases. The membrane permeability was also increased from 0.16 to 0.28 by the addition of poly(VP-

co-IAH) in the membrane. 4 wt % of copolymer in PSF membrane gave best performance among all the membranes for each parameter.

Further, enantiomeric and racemic effect of tartaric acid (TA) was studied on the properties of PSF ultrafiltration membranes. Asymmetric membranes were prepared by direct blending of PVP with D-TA and DL-TA in membrane casting solution. FTIR spectra of plain and TA containing PSF membranes was taken to confirm the presence of PVP and TA in blended membranes. Morphological study of the prepared membranes was done by FESEM, scanning electron microscope (SEM) and AFM. The membranes were characterized in terms of PWF, hydraulic permeability and hydrophilicity. PWF increased from 52 L/m^2h to 79.9 L/m^2h for plain and D-TA containing PSF membrane, respectively. The measurements of water contact angle provide evidence that the hydrophilicity of PSF membrane increases by addition of the D-TA in the casting solution. Additionally, permeation and rejection behaviour of prepared membranes was studied by BSA solution. A considerable increase in BSA flux (from 19.1 L/m^2h for plain membrane to 32.1 L/m^2h for D-TA containing membrane) was observed. FESEM images affirm that the pore size of the membranes decreases by the addition of D-TA in the membrane. D-TA increases the hydrophilicity whereas; DL-TA decreases the hydrophilicity of PSF membrane. PVP (average molecular weight of 40000 Da) with D-TA (1 wt %) gave best performance among all the membranes for each parameter.

Investigation was also done in terms of permeation and rejection behaviour of fabricated membranes for crystal violet dye (CVD). Anionic surfactant sodium dodecyl sulphate was used for micellar enhanced ultrafiltration of CVD from aqueous media.

Finally, PSF ultrafiltration membranes with increased hydrophilicity were prepared using the amino alcohol plasticizers (AAPs). The AAPs were synthesized by the reaction between polyethylene glycol (PEG) and isatoic anhydride (IAH). Different molecular weight of PEG and IAH (molecular weight 163 Da) were used for preparing the AAP. Asymmetric

membranes were fabricated by blending these plasticizers in membrane casting solution. Formation of AAP was confirmed by FTIR and ^{1}HNMR spectra of AAP. Characterization of membranes was done in terms of hydraulic permeability, PWF and hydrophilicity. PWF was found to be increased from 29.3 L/m^{2}h to 110.1 L/m^{2}h and water contact angle also reduced from 72^0 to 62^0 for plain and AAP containing PSF membrane, respectively. The morphological and structural analysis of the membranes was done by SEM and FESEM. Permeation and rejection behaviour of fabricated membranes was studied by BSA solution. Maximum BSA rejection was increased by 21.75 % for the modified membrane. FESEM images affirm that the pore size of the membranes decreased by the addition of AAP. PEG with molecular weight of 400 Da based AAP gave best performance among all the membranes for each parameter.

Research Publications

Published

1. **N Sharma,** M K Purkait, Impact of synthesized amino alcohol plasticizer on the morphology and hydrophilicity of polysulfone ultrafiltration membrane, J. Membr. Sci. 522 (2017) 202–215.
2. **N Sharma**, M K Purkait, Enantiomeric and racemic effect of tartaric acid on polysulfone membrane during crystal violet dye removal by MEUF process, J. Water Proc. Eng. 10 (2016) 104–112.
3. **Nilay Sharma**, M K Purkait, Racemic and enantiomeric effect of tartaric acid on the hydrophilicity of polysulfone membrane, Membr. Water Treat. 7 (3) (2016) 257-275.
4. **Nilay Sharma**, M K Purkait, Preparation of hydrophilic polysulfone membrane using polyacrylic acid with polyvinyl pyrrolidone, J. Appl. Poly. Sci. 132 (2015), 41964 DOI: 10.1002/app.41964.

Submitted

5. **N Sharma**, M K Purkait, Effect of synthesized copolymer poly(vinyl pyrrolidone-co-isatoic anhydride) on the pH responsive and hydrophilic behavior of polysulfone ultrafiltration membrane, J. Membr. Sci. (Submitted on 17/10/2016).
6. **N Sharma**, M K Purkait, Fabrication and characterization of polysulfone ultrafiltration membrane using polyethylene glycol and tartaric acid: morphology and performance in protein separation, Chem. Eng. Comm. (Submitted on 15/10/2016).

Conference Publications

1. **Nilay Sharma**, Mihir Kumar Purkait, "Enantiomeric and Racemic effect of Tartaric acid on Brilliant Green dye Removal on Polysulfone based Membrane by MEUF process", 5th International Science Congress (ISC-2015), Tribhuvan University Kirtipur, Kathmandu, NEPAL, 8th & 9th December, 2015. pp 27-32 (2016), Research Journal of Recent Sciences.
2. **Nilay Sharma**, M K Purkait, "Improving the hydrophilicity of polysulfone membrane by the addition of imidazol with polyvinyl pyrrolidone for crystal violet dye removal" International Conference on Waste Management (Recycle 2016), IIT Guwahati, Assam, India, 1st -2nd April, 2016, To be published.

Conference/Presentations

1. Presented paper in DAE-BRNS Symposium on "Emerging Trends in Separation Science and Technology (SESTEC-2016)" held at IIT Guwahati on 17th-20th May 2016.
2. Presented poster in Annual Session of Indian Institute of Chemical Engineers "CHEMCON 2015" on 27th December 2015 at IIT Guwahati.
3. Presented paper in National conference on "Challenges in Environmental Research" June 4th-6th, 2015 at IIT Guwahati.
4. Presented poster in Annual Symposium "Reflux 2015" of Department of Chemical Engineering, March 27th – 29th, 2015 at IIT Guwahati.
5. Presented a poster in International Symposium on "Advances in Sustainable Polymers (ASP-15)" January 21st-22nd, 2015 organized at IIT Guwahati.
6. Given oral presentation on "Commercial use of waste polythene" in annual Symposium "Recycle 2014", on solid waste management organized by Department of Civil Engineering at IIT Guwahati on 6th April 2014.

CONTENTS

LIST OF FIGURES

LIST OF TABLES

Nomenclature

Notations

A	effective membrane area (m^2)
A_t	total area (m^2)
C_f	concentration in the feed (mg/L)
C_p	concentration in permeate (mg/L)
F_{ir}	irreversible fouling
F_r	reversible fouling
F_t	total fouling
h	hour
J_p	BSA solution flux (L/m^2h)
J_w	pure water flux (L/m^2h)
J_{w1}	initial water flux (L/m^2h)
J_{w2}	water flux in second run (L/m^2h)
L	length of pore in equations (m)
P	pressure (kPa)
P_m	hydraulic permeability (L/m^2hkPa)
ΔP	transmembrane pressure in equations (kPa)
Q	volume of water permeated (L)
r	radius of pores (nm)
r_m	mean pore radius (nm)
V	volume of membrane in wet state (m^3)
W_d	weight of dry membrane
W_w	weight of wet membrane
η	viscosity (Pa s)

ε	porosity
σ	interfacial surface tension

Abbreviations

AAP	amino alcohol plasticizer
AFM	atomic force microscopy
AIBN	Azobisisobutyronitrile
ATR	attenuated total reflectance
BSA	bovine serum albumin
CA	cellulose acetate
CF	compaction factor
CVD	crystal violet dye
Da	Dalton
DMAc	dimethylacetamide
D-TA	dextro-tartaric acid
DL-TA	racemic-tartaric acid
EWC	equilibrium water content
FESEM	field emission scanning electron microscope
FTIR	Fourier transform infrared
IAH	isatoic anhydride
IEP	isoelectric point
IEC	ion exchange capacity
LLDP	liquid-liquid displacement porosimetry
MA	malic acid
MU	microfiltration

NF	nanofiltration
NMP	N-methyl-2-pyrrolidone
NMR	nuclear magnetic resonance
PAA	poly-acrylic acid
PBI	poly[2,2′-(m-phenylene)-5,5′-dibenzimidazole]
PDMAEMA	poly(N,N–dimethylamino-2-ethyl methacrylate)
PEG	polyethylene glycol
PEGMA	polyethylene glycol methyl ether methacrylate
PEGME	polyethylene glycol methyl ether
PES	polyethersulfone
(P(MMA -co-DMA))	poly (methyl methacrylate-co-dimethylaminoethyl methacrylate)
Poly(VP-S)	poly(1-vinylpyrrolidone-co-styrene)
PVC	polyvinyl chloride
PVCL	poly-vinylcaprolactam
PVDF	polyvinylidene fluoride
PVP	polyvinylpyrrolidone
P(VP–AN)	poly(1-vinylpyrrolidone-co-acrylonitrile)
PWF	pure water flux
PU	polyurethane
RO	reverse osmosis
SDS	sodium dodecyl sulphate
SEM	scanning electron microscope
TA	tartaric acid
THF	tetrahydrofuran

TMP	transmembrane pressure
UF	ultrafiltration
WCA	water contact angle

Chapter 1
Introduction

This chapter discusses a brief summary of the fundamentals involved in membrane technology. It summarizes the state-of-the art in polymeric membranes, their applications and the background of the problem undertaken in this work i.e. the problem associated with the hydrophobicity fouling of the polymeric membrane. It discusses the features of different techniques of membrane preparation. The chapter subsequently presents detailed literature review that includes the basis of major problem of polymeric membranes in applications, i.e. membrane hydrophobicity. Finally, the hydrophilic modification methods are comprehensively reviewed as well as the objectives of the present work are highlighted.

1.1. Background

Membranes are defined as semi-permeable barriers that prevent intimate contact between two homogeneous phases, but allow preferential passage of certain species across their structures. In recent years, membranes and membrane separation processes have grown from a simple laboratory tool to an industrial process with considerable technical and commercial impact. The roles of membranes are to change the composition of a solution on the basis of relative permeation rates (membrane separation processes), physically or chemically modify the permeating species (ion-exchange membranes and bio-functional membranes), conduct electric current and prevent permeation (packaging or coating) or regulate the rate of permeation (controlled release). Membrane processes are currently gaining a lot of interest in separation technology. Separation operation in fact occupies a key position in process industries that include foods, pharmaceuticals and other industries. The rapid growth in membrane technology has made it a serious competitor for other conventional separation technologies like crystallization, distillation, etc. particularly for small scale operations.

Nowadays, membrane technology is seen to be applied in various industrial areas such as food and beverages, metallurgy, pulp and paper, textile, pharmaceutical, automotive, dairy, biotechnology and chemical industries etc. [1]. The membrane separation processes offer following advantages over other means of separation:

- ✓ Separation can be carried out continuously;
- ✓ Hybrid process development, i.e. membrane unit operations are used as part of a process design with other unit operations;
- ✓ Low energy utilization as no phase change or temperature change is involved;
- ✓ Low maintenance as the systems are easy to operate and maintain;
- ✓ Constituents in the concentrated stream remain chemically unaltered due to non-requirement of any chemical addition which facilitated their subsequent utilization;
- ✓ Capability of generating permeates of acceptable quality which can be reused as make-up water for emulsification and discharged directly into a receiving water body.

However, membrane separation processes suffer from the following drawbacks due to membrane fouling and concentration polarization:

- Low membrane life time
- Low selectivity or flux.

Measures are explored to reduce membrane fouling and concentration polarization so as to overcome these limitations.

1.1.1. Classification of membrane

In the most general sense, a synthetic membrane is a barrier which separates two phases and restricts the transport of various chemical species in a rather specific manner. Membranes can be solid or liquid. They may be either neutral or may carry negative or positive charges or

both. They can be homogeneous (i.e. completely uniform in composition and structure) or heterogeneous (i.e. containing pores of finite dimensions or consisting of some form of layered structure). Membranes can be further classified depending on (i) nature, (ii) structure and (iii) mechanism of action [1 - 3]. On the basis of nature, membranes can be classified as biological and synthetic membranes. These two types of membranes are entirely different in structure and functionality. Biological membranes can be subdivided into living and non-living membranes. Synthetic membranes can be subdivided into organic (polymeric, liquid) and inorganic (ceramic, metal) membranes. This study emphasizes only on the polymeric membranes.

According to morphology or structure, solid membranes can be divided into two main classes: symmetric (or isotropic) and asymmetric (or anisotropic). The symmetric membranes can be subdivided further into porous, nonporous or dense and electrically charged membranes. Symmetric porous membranes have a rigid, highly voided structure with randomly distributed, interconnected pores. In general, only molecules that differ considerably in size can be separated effectively by such membranes, e.g. ultrafiltration and micro filtration. On the other hand, nonporous, dense membranes consist of a dense film through which permeates are transported by diffusion under the driving force of a pressure, concentration, or electrical potential gradient. The separation of various components of a mixture is related directly to their relative transport rate within the membrane, which is determined by their diffusivity and solubility in the membrane material e.g. pervaporation and reverse osmosis. Electrically charged membranes (or ion-exchanged membranes) can be dense or porous, but are most commonly very finely microporous, with the pore walls carrying fixed positively or negatively charged ions. The separation is affected by the charge and concentration of the ions in solution e.g. electro dialysis.

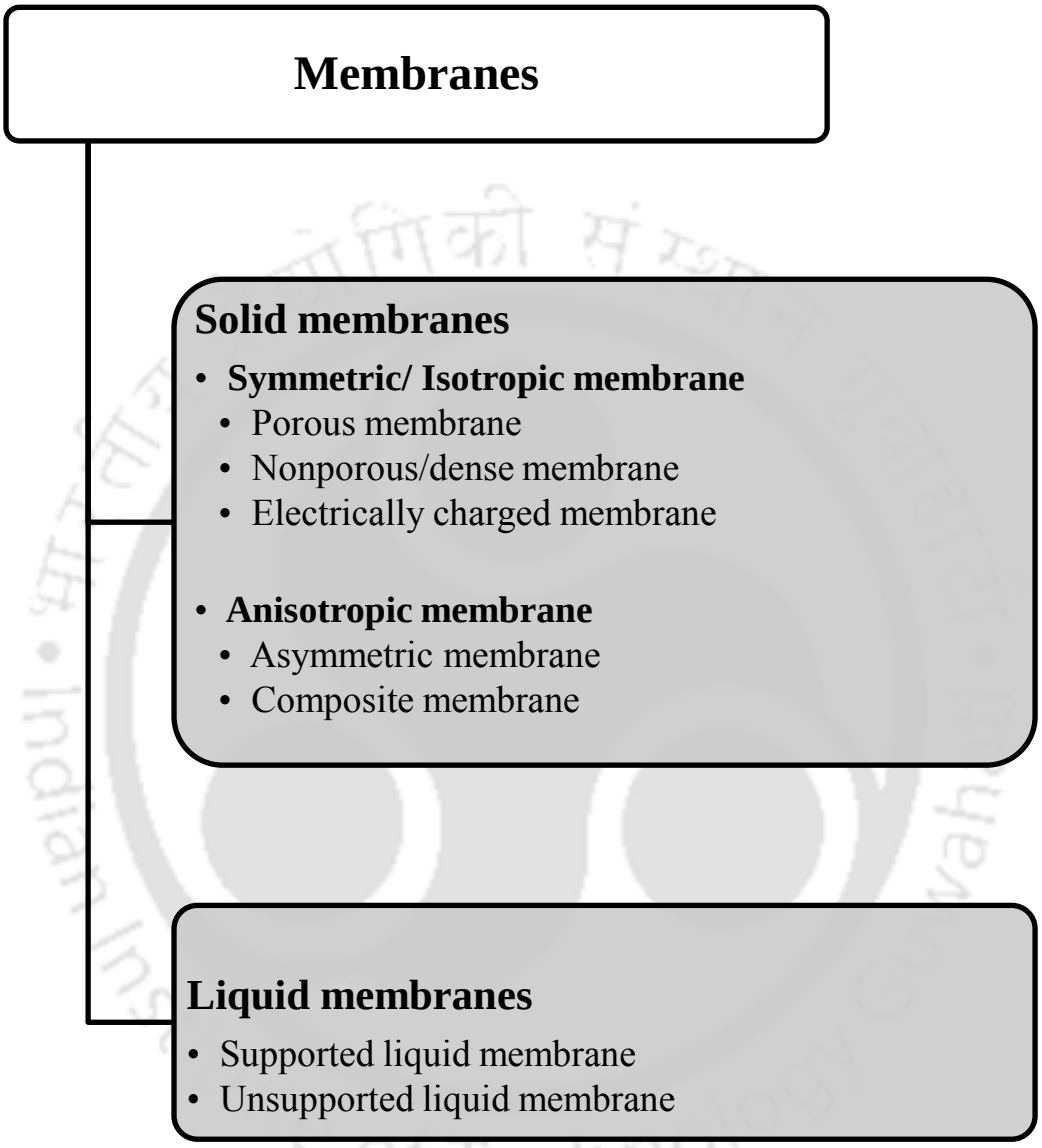

Figure 1.1: Membrane classifications according to the morphology.

Asymmetric membranes consist of a very dense top layer or skin of thickness 0.1 – 0.5 μm supported by a porous sub-layer with a thickness of about 50 -150 μm. The top layer and its

substructure may be formed in a single operation or separately. In composite membranes, the layers are usually made from different polymers; each layer of which can be optimized independently. The separation properties and permeation rates of the membrane are determined exclusively by the top layer; the sub-layer functions as a mechanical support. The advantages of the higher fluxes provided by such membranes are so great that almost all commercial processes use such membranes.

There are two types of liquid membranes; supported liquid membranes and unsupported liquid membranes. Supported liquid membranes have a microporous structure which is filled with the liquid membrane phase; the microporous structure provides the mechanical strength and the liquid-filled pores the selective separation barrier. The microporous substructure should have a high porosity and a pore size small enough to support the liquid membrane phase sufficiently under hydrostatic pressure. Unsupported liquid membranes are composed of thin films of liquid stabilized by a surfactant in an emulsion type mixture. Figure 1.1 shows membrane classes according to their morphology. On the basis of mechanism of action, membranes are classified as adsorptive or diffusive, ion-exchange, osmotic or nonselective (inert) membranes [1].

1.1.2. Classification of membrane separation processes

The wide variety of membrane separation processes differ from one another in the type and configuration of the membrane, the mechanism of trans-membrane transport for various feed components, the nature of the process driving force and other features. Some processes which are well proven in full scale industrial applications, have been widely used for separation, purification and concentration of water-soluble solutes or water dispersible materials in industries such as pharmaceutical, chemical processing, food processing, oil industries,

wastewater treatment plant, etc. Other processes, which are still in experimental stage, are yet to get into industrial use.

Membrane separation processes may be classified and categorized by a number of criteria. It is a filtration technique in which a membrane acts as a selective barrier between two phases [1]. As a result of a driving force across the membrane, components are transported towards the membrane surface, where some components pass the membrane and others are retained at the membrane surface. Membrane processes are available for numerous applications, each with its own driving force and separation characteristics. Table 1.1 provides further information on these processes, such as membrane type, method of separation and range of applications [3, 4].

Pressure driven membrane separation processes differ mainly in the pore size of their membranes, which makes a particular membrane effective for the removal of a specific range of impurities. Reverse osmosis has the smallest membrane pore size and therefore is used to remove all ionic species. Nanofiltration is sometimes referred to as 'loose reverse osmosis' as it can remove divalent ions and low molecular weight contaminants while allowing monovalent ions to pass through. Ultrafiltration is used for removal of macromolecules such as proteins and small colloids, but not ionic species. Microfiltration is used to remove particulates, bacteria and other larger colloids only. Table 1.2 reports a summary of the main characteristics of the pressure driven processes in terms of pressure, pore size and removable components.

In pressure driven membrane systems the pressure of the feed solution permits passage of the major portion of the solution through a semi-permeable membrane. The portion of the feed solution that passes through the membrane is called permeate, or filtrate. The portion of the feed solution that does not pass through the membrane is called

concentrate or retentate. A simple schematic representation of a membrane process is shown in Figure 1.2.

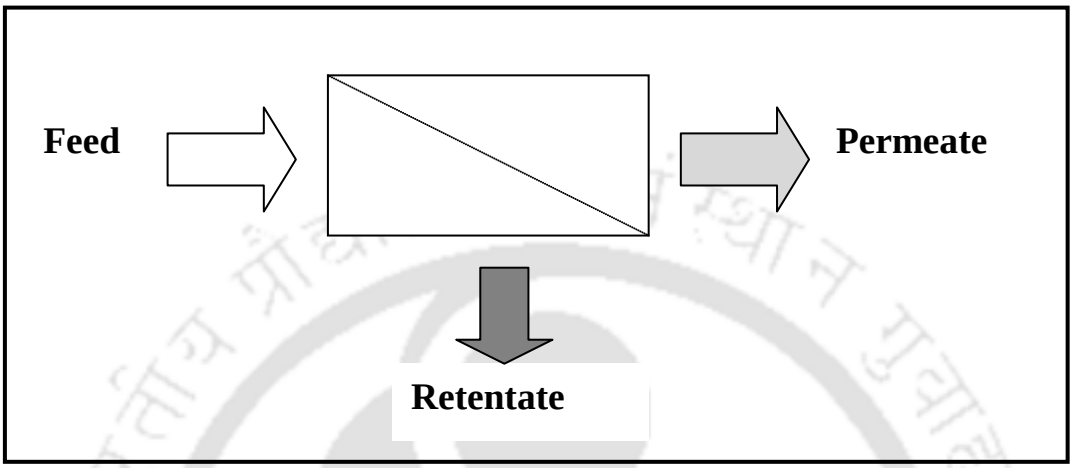

Figure 1.2: Schematic representation of a membrane process.

Table 1.1: Typical membrane separation processes: Operating principles, driving force and applications [3, 4].

Separation process	Membrane type	Driving force	Separation mechanism	Range of application	Size range (nm)
Micro filtration	Symmetric and asymmetric microporous membrane	Pressure difference (ΔP)	Sieving mechanism as a function of pore size and adsorption	Sterile filtration clarification	100-10000
Ultra filtration	Asymmetric microporous membrane	Pressure difference (ΔP)	Sieving mechanism	Separation of macromolecular solutions	10-100
Nano filtration	Asymmetric 'skin type' membrane	Pressure difference (ΔP)	Solution diffusion mechanism	Separation of divalent ions from solutions	0.5-5

Reverse osmosis	Asymmetric 'skin type' membrane	Pressure difference (ΔP)	Solution diffusion mechanism	Separation of salts and micro solutes from solutions	<1
Dialysis	Symmetric microporous	Concentration difference (ΔC)	Diffusion	Separation of salts and micro solutes from macro molecular solutions	<1
Electro dialysis	Cation and anion exchange membrane	Electric potential difference (ΔE)	Selective transport of ions or molecules according to electric charge	Desalting of ionic solutions	<1
Supported liquid membrane	Microporous membranes supporting adsorbed organic liquid	Concentration difference (ΔC)	Solution diffusion via carrier	Separation and concentration of metal ions and biological species	<1
Membrane distillation	Microporous membrane	Temperature difference (ΔT)	Vapour transport into hydrophobic membrane	Ultra pure water concentration of solutions	1-10
Pervaporation	Asymmetric membrane	Concentration difference (ΔC)	Solution diffusion mechanism	Separation of organics	<1

The UF membrane is considerably more porous i.e. its nominal pore size is larger compared to the reverse osmosis (RO) membrane. As a result, most soluble species including inorganic salts pass through the membrane with the water; but colloids, suspended solids and high molecular weight organic molecules (e.g. BSA) do not pass through the

membrane with the water. They are rejected and remain in the concentrate (retentate) stream. The porous nature of the UF membrane allows the process to be operated with high fluxes at relatively low pressures (e.g. 1 – 10 bars). This is possible because the osmotic pressure of colloids and high molecular weight organics is extremely low. The degree and quantity of the separation are a result of the pore size of the membrane and the molecular structure, size, shape and flexibility of the colloids and organic molecules. Pore sizes ranging from 0.001–0.01 μm allow separation from solution of molecules with a molecular weight between 500 Da and 3,00,000 Da.

Table 1.2: Characteristics of the pressure driven membrane processes [1].

Membrane processes	Transmembrane pressure (bar)	Pore size (nm)	Removable components
Microfiltration	1 - 2	100 - 1000	Suspended solids, bacteria
Ultrafiltration	2 - 10	1 - 100	Macromolecules, viruses, proteins
Nanofiltration	10 - 30	0.5 - 5	Micropollutants, bivalent ions
Reverse osmosis	35 - 100	< 1	Monovalent ions, hardness

1.2. Materials for ultrafiltration membranes

The most important class of material for ultrafiltration membranes includes the polymers. The choice of the polymeric material for a particular membrane is based on its chemical and physical properties originating from structural factors such as molecular weight, chain flexibility and chain interaction. Those factors also determine the membrane permeability [1].

Chemical properties describe how the material chemical structure changes under certain circumstances such as change in pH, temperature, etc. Physical properties include density, melting point, glass transition temperature, compressibility, etc [5].

The process of making the UF and MF membranes has to control both the surface characteristics and the supporting sub-structure. Polymers should have good mechanical properties to produce membranes, with a reasonable degree of flexibility. Also, they need to have good chemical resistance, tolerance limit of a wide pH range and high chlorine concentrations, enabling rigorous cleaning to be conducted if necessary. In addition, thermal resistance should be good, so that moderate elevated temperatures can be used without affecting the membrane properties or life [6].

Commercial thermoplastics and cellulose were primarily used as membrane materials for large scale production. Basically all polymers can be used as membrane material but the chemical and physical properties differ so much that only a limited number is used in practice. Since the initial development of the first asymmetric cellulose acetate membrane, significant progress has been made in the field of non-cellulosic membrane materials that are more durable, less susceptible to biodegradation and perform well within broad pH and temperature ranges. The materials most commonly used for the production of UF membranes by phase inversion method are:

- Cellulose acetate (CA)
- Aromatic Polyamide (PA)
- Polysulfone (PSF) and Polyethersulfone (PES)
- Polyvinylidene fluoride (PVDF)
- Polyacrylonitrile (PAN)
- Polypropylene (PP)
- Polyethylene (PE)

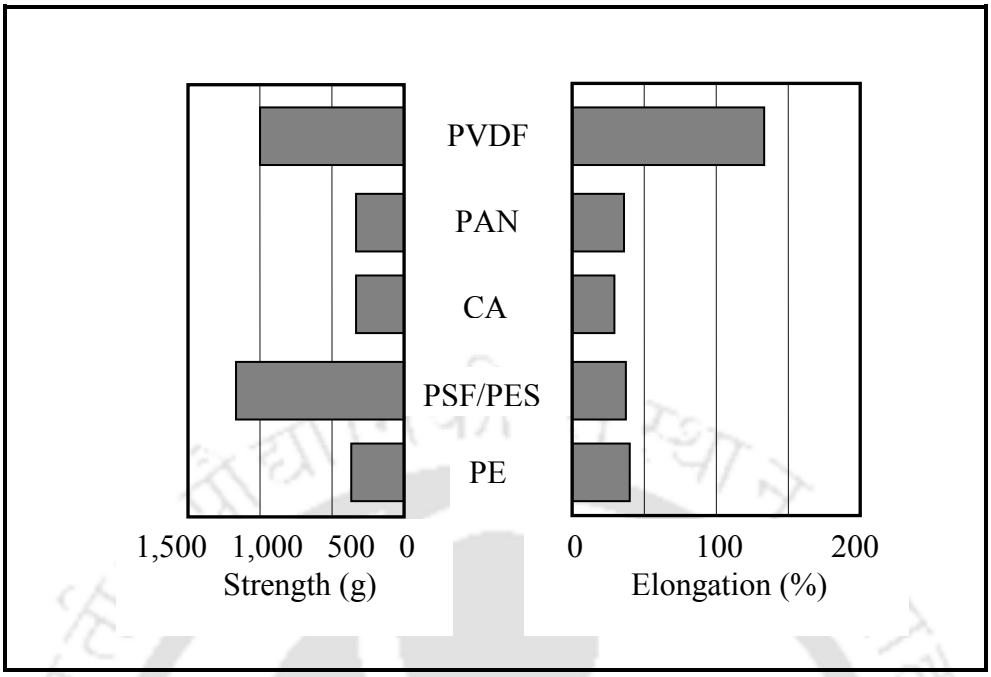

Figure 1.3: Comparison of physical stability of different membrane materials.

Figure 1.3 compares the common polymers in terms of strength and flexibility [7]. PES has similar mechanical properties to those of PSF. It shows that PSF and PVDF are the strongest polymers, whilst PVDF is more flexible. Of the polymers discussed above, the PSF/PES family has the widest chemical resistance, and can tolerate a pH range from 1.5 to 13, as well as moderate chlorine levels. PVDF tolerates acids, but is limited to pH 11 with caustic. However, its major advantage is a very high tolerance to chlorine, which makes it ideal for membrane reactors. Chlorine cleaning is preferred for PVDF membranes while PSF/PES may choose for caustic cleaning. PAN has similar pH tolerance to PVDF, combined with a moderate chlorine tolerance (almost similar to PSF/PES). CA is much more limited in its chemical resistance, since its natural hydrophilicity makes it susceptible to hydrolysis in the presence of acids below pH 4 and alkalis above pH 8. It tolerates chlorine, but is biodegradable which makes it sensitive to bacterial attack. The polyolefin family, PP and PE, has good tolerance to acid and caustic, but low tolerance to chlorine, particularly in the case

of PP. The lack of chlorine tolerance is a major limitation in the water industry, and this has limited the prospects for these membranes. Apart from this, solubility of PSF makes it ideal candidate for polymer blend membranes since other polymer can be co-dissolved. PSF has following advantages over other organic membrane materials [2]:

- ✓ High chemical resistance.
- ✓ Usability in a wide pH range.
- ✓ Soluble in solvents like DMAc and NMP, making it easily applicable for the conventional phase inversion processes.
- ✓ High thermal stability.
- ✓ Good mechanical strength and permeability.
- ✓ Ability to modify properties through blending with other polymers.

However, PSF membrane exhibits drawback mainly due to their hydrophobic nature which causes the adsorption and deposition of foulants (colloids, proteins and particles) on the surface of the membrane and inside the membrane pores. This leads to lower permeation flux and deterioration in performance [8, 9].

That's why various methods are adopted to make them hydrophilic and less prone to fouling. The methods include surface coating by adsorption, free radical or radiation grafting of hydrophilic polymers, plasma treatment, chemical conversion of polymer side chains to hydrophilic groups, blending with hydrophilic polymers, etc [2].

1.3. Membrane fouling

During UF, some constituents of the feed deposit on the membrane surface and/or in the membrane matrix resulting in gradual decrease in permeate flux. This process is often referred to as fouling of the membrane. The common definition of membrane fouling is

provided by the International Union for Pure and Applied Chemistry (IUPAC), which defined fouling as: 'Fouling is the process resulting in loss of performance of a membrane due to the deposition of suspended or dissolved substances on its external surfaces, at its pore openings, or within its pores' [10]. Mulder (1997) gave a second definition of fouling as: 'The (ir)reversible deposition of retained particles, colloids, emulsions, suspensions, macromolecules, salts etc. on or in the membrane' [1]. Wiesner and Aptel (1996) defined fouling as an irreversible flux reduction: 'A reduction in permeate flux that cannot be reversed' [11].

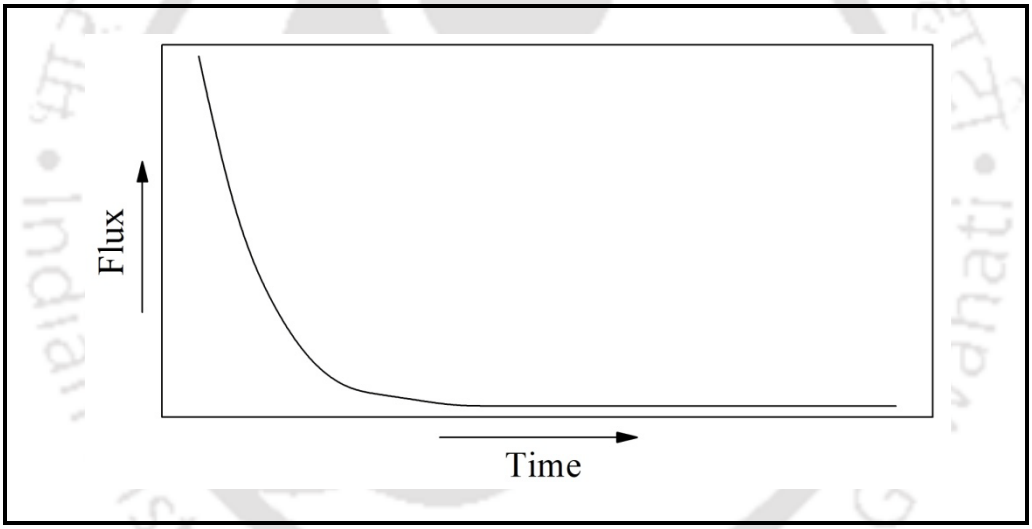

Figure 1.4: Flux declination with time at a constant TMP.

The easily removable part of the retained material is called the reversible part of the fouling layer, the remaining part is called the irreversible fouling layer. The feed constituents that are retained on or in the membrane surface are called foulants. The retention of feed constituents causes an increase of the total resistance over the membrane, resulting in a decreased flux at a constant TMP. The decrease in flux that is found during membrane filtration is schematically shown in Figure 1.4.

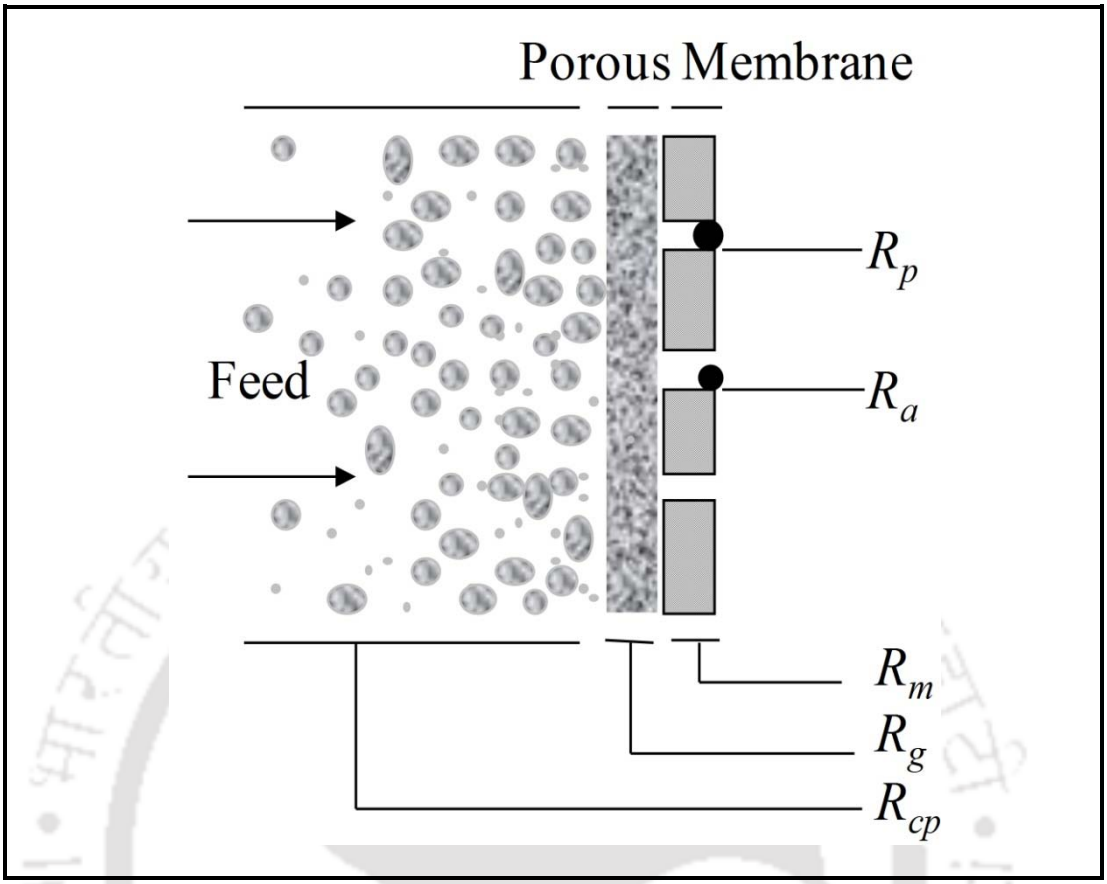

Figure 1.5: Overview of various resistances of a fouled membrane in pressure driven process; R_a = adsorption, R_p = pore blocking, R_m = membrane resistance, R_g = gel layer resistance, R_{cp} = concentration polarization.

Flux decline can be caused by several factors, such as plugging of the membrane pores, adsorption inside the membrane pores, concentration polarization and gel layer formation. All these factors induce additional resistances on the feed side to the transport across the membrane. Essentially, four 'fouling mechanisms' can be distinguished which are schematically shown in Figure 1.5. During membrane filtration, these mechanisms may occur simultaneously. The membrane resistance (R_m), is mainly involved in the initial period of filtration. After some time, accumulation of retained solutes near the membrane surface results in a highly concentrated layer which exerts a resistance towards mass transfer; this is the concentration polarization resistance (R_{cp}). When the concentration of the accumulated

solute molecules is sufficiently high, a gel layer is formed which exerts gel layer resistance (R_g). With porous membranes it is possible that some smaller solute molecules penetrate into the membrane pores and block them, leading to the pore-blocking resistance (R_p). Another resistance (R_a) may likely to arise due to adsorption of solute molecules upon the membrane surface as well as within the pores. Among these four resistances R_{cp} and R_g are responsible for reversible fouling (F_r), where as R_p and R_a are responsible for irreversible fouling (F_{ir}). F_r is caused by reversible solute deposition on the membrane surface, which can be removed by hydraulic cleaning of the membrane. F_{ir} is caused by irreversible solute adsorption and it cannot be keep away from hydraulic cleaning.

1.4. Antifouling mechanism by improved hydrophilicity of polymeric membrane surface

It is generally accepted that an increase in hydrophilicity offers better fouling resistance because many foulants such as protein are hydrophobic in nature [12]. A pure water layer is easily formed on highly hydrophilic surface, which can prevent the adsorption and deposition of hydrophobic foulants onto membrane surface, thus reducing fouling. In fact, numerous studies have been conducted to enhance surface hydrophilicity of membranes aiming at the improvement of antifouling performance. Similarly, the surface charge is also an important factor influencing membrane fouling. It is easy for us to understand that the electrostatic repulsive force but not the attraction force between the charged membrane surface and foulant in feeding solution is advantageous to reducing membrane fouling. In other words, the antifouling membranes should be developed according to the electrostatic character of foulants in practical situation. The surface-bound long-chain hydrophilic molecules (e.g. polyethylene glycol, PEG) were very effective in preventing adsorption of macromolecules such as protein onto membrane surface due to the steric repulsion mechanism [13]. When

hydrophilic polymer chains are grafted or created on membrane surface, this diffused hydrophilic layer will exert steric repulsion to hydrophobic proteins that reach the surface. Steric repulsion is due to the loss of configurational entropy resulting from volume restriction and/or osmotic repulsion between the overlapping polymer layers [13, 14].

1.5. Surface modification methods for polymeric membranes

1.5.1. Improvement of membrane preparation process

The surface modification of polymeric membranes can be achieved during preparation process, e.g., the introduction of hydrophilic or anti fouling modifiers by blending. The hydrophilic modifiers can be mainly classified into two categories: polymer material and inorganic nanoparticle.

1.5.1.1. Introduction of organic materials

The blending of organic material is a simple way to enhance the hydrophilicity of polymeric membranes. In this method, the additives are usually dissolved into membrane separation process. Water soluble polymers [14–18], charged polymer [19], surfactants [20], organic acids [21] and other hydrophilic polymer [9, 22, 23] have been used to prepare hydrophilic UF membrane through homogeneous blending.

1.5.1.2. Introduction of inorganic nanoparticles

Besides organic materials, the inorganic nanoparticle is another type of important modifier. Polymer-nanoinorganic particles composite membranes present an interesting approach for improving the separation, physicochemical, as well as anti- fouling properties of polymer membranes [24]. The introduction of nanoparticles into polymeric membranes to enhance

hydrophilicity has been proven to be an effective way and attracted much attention. The nanoparticles mixed into the polymeric membrane casting solution mainly include TiO_2 [25], SiO_2 [26], $Mg(OH)_2$ [27], ZnO [28], carbon naotubes [29], boehmite nanoparticles [30]. There are two ways of introducing nanoparticles into PVDF membranes during the preparation process: blending them in coagulation bath or in polymer solution.

1.5.2. Surface alteration of existing polymeric membranes

The surface modification of existing polymeric membranes is another effective and frequently used method to enhance hydrophilicity. In general, the aim is to form a hydrophilic layer on the existing polymeric membrane surface which can prevent the contact between membrane and pollutants, thus reducing membrane fouling. The surface modification can be mainly classified into two categories according to the interaction between modifiers and membranes: physical modification and chemical modification.

1.5.2.1. Physical modification

Here, the physical modification means that the hydrophilic modifiers exist on polymeric membrane surface via physical interaction but not covalent bonding. In other words, the chemical composition of polymeric membrane is unchanged. However, the chemical reaction may be required during the modification. The physical modification of PVDF membranes can be achieved by two ways: (1) The hydrophilic polymers is directly coated or deposited on membrane surface (further treatment is conducted sometimes). (2) The polymeric membrane is firstly immersed in or coated by a solution of chemically active monomers. Then, the monomers are immobilized onto membrane surface by cross linking or polymerization reaction without the chemical participation of base membrane. The hydrophilic polymers for

surface modification of polymeric membranes can be selected from commercial materials such as poly vinyl alcohol [31] and chitosan [32] etc.

1.5.2.2. Chemical modification

In chemical treatment, the polymeric membrane surface is modified through covalent bonding interaction. Generally, base polymer chains are firstly activated by chemical reaction or high-energy radiation, followed by the grafting of hydrophilic modifiers. The membrane surface properties can be improved while the membrane bulk is not significantly affected. Moreover, the covalent attachment of modifiers on membrane surface offers a long-term chemical stability, in contrast with physical surface coating. So far, the chemical modification of polymeric membranes is mostly focused on the pegylation [33], sulfonation [34, 35], O_3/O_2 pre activation [36, 37], electron beam radiation [38], plasma treatment [39] etc.

1.6. State of the art

With a brief overview of the contemporary research, this section outlines the research outcome of various literatures so as to identify few promising areas of research that needs to be addressed in this thesis. The state of the art has been presented for hydrophilic modification of polymeric ultrafiltration membranes.

1.6.1. Modification of polymeric membrane by blending hydrophilic polymer

Literature survey

Asymmetric membranes are increasingly used in various fields like ultrafiltration, nanofiltration, reverse osmosis and gas separation processes because of their high selectivity,

mechanical strength and permeability in high pressure applications [40]. Wet phase inversion method is the most common method for the fabrication of flat sheet asymmetric membrane. The key parameters for this technique are polymers-solvent-additives, their compositions and coagulant bath conditions i.e. temperature and composition [41].

Blending of polymers is an important alternate to obtain various polymeric membranes with desired properties and the process is less complicated and inexpensive. Water soluble polymers [14-18], charged polymer [19], surfactants [20] and other hydrophilic polymer [9, 22, 23] have been used to prepare hydrophilic UF membrane through homogeneous blending. Chakrabarty et al. [15, 17] prepared PSF membrane by using PVP and PEG of different molecular wt. as additive, in the case of PEG pure water flux (PWF) was increased with increase in molecular weight of PEG, but BSA rejection was not increased in same trend, it was highest for PEG 6000. For PVP they found that as the molecular weight of PVP was increased, membranes had more compact structure and consequently less PWF. Malek et al. [16] investigated the effect of PVP concentration on poly ether sulfone (PES) membrane and they found that addition of PVP to the casting solution strongly enhances the permeability of membrane to a specific point, after which higher concentration of PVP causes denser top layer and which lead to lower PWF. Sikder et al. [22] and Sivakumar et al. [23] reported the effect of different concentrations of CA in PSF membrane. They found that, as the CA concentration increased in the membrane casting solution, largest pore diameter of membranes significantly decreased and microfiltration performance get enhanced.

Some studies illustrated that the addition of hydrophilic polymer in casting solution could improve the performance and structure of the asymmetric membranes. Various literatures related to hydrophilic polymer addition is reported in Table 1.3.

Table 1.3: Literatures related to hydrophilic polymeric additives.

Polymer	Solvent	Hydrophilic polymer additive	Reference
PSF	NMP/DMAc	PVP	[15]
PSF	NMP/DMAc	PEG	[17]
PSF	NMP	PEGME	[42]
PSF	NMP	PEI/PVP/PEG	[43]
PSF	NMP	Chitosan	[44]
PSF	NMP	N-succinyl chitosan	[45]
PSF	NMP	PBI	[46]
PSF	N,N-dimethyl formamide)	PAA	[47]
PVDF	NMP	PEG+LiCl+Tween-80	[48]

Possible scope for further research

From the above literatures it may be found that although several authors have reported various additives to increase the hydrophilicity of PSF membrane, but the role of the mixture of two hydrophilic polymeric additives, i.e., polyvinyl pyrrolidone/polyacrylic acid (PVP–PAA) blend in PSF membrane has not been accounted yet. Therefore, in this work, the effect of addition of PVP–PAA blend in the casting solution of PSF membrane was studied. PAA was chosen as hydrophilic polymer additive in the present study because of its good compatibility with PVP. Membrane hydrophilicity is supposed to be increased by addition of PAA in membrane casting solution as PAA forms hydrogen bond with PVP.

1.6.2. Use of functional copolymers for the modification of polymeric membranes

Literature survey

Use of polymeric membrane in water purification [49], protein separation [50], biotechnology for gene and tissue engineering [51], food industry [52] for separation of fermentation and food products with high purity and yield is increasing day by day. Separation and purification of proteins is required for particular uses of it in the biotechnology, food, biomedical along with the pharmaceutical industries [53-56]. Proteins are the construction unit of human life and they participate in all the course of action that happens inside the cells. So, the proteins are widely used in aforesaid industries. Purified proteins can be obtained by UF, ion-exchange chromatography, centrifugation, adsorption and membrane absorber with electrophoretic membrane contactor [54, 57-59]. Among aforementioned techniques polymeric UF membranes are mainly used for efficient separation and purification of proteins. PES and PSF are favourable for membrane casting, because of good physicochemical constancy, resistance to chlorine and oxidation [60]. Solubility of PSF makes it more suitable for polymer blend membranes as others polymers can be simultaneously dissolved, this permit different properties (like hydrophilic, hydrophobic, thermo responsive, pH responsive, antifouling properties) of the finished membrane to be customized. To proceed for the aforesaid applications, many studies have been done to investigate the modification of polymeric membranes [9, 17-20, 23]. The modification of membranes with stimuli-responsive polymers, which can exhibit relatively large and abrupt property variations in reply to small change in external stimulus (like change in temperature, pH, ionic strength, electric field and concentration of specific chemical species), added a variety of new abilities to the membranes and broadened the application fields of membrane [61-62].

Much interest has been shown in the study of functional copolymers for the modification of polymeric membrane. Various functional copolymers have been mixed in casting solution of polymeric membrane to induce required property like hydrophilicity and pH sensitivity. Jiang et al. [63] have prepared PES membrane by blending a copolymer of acrylonitrile and acrylic acid. The membrane showed good pH sensitivity and pH effect was observed at the pH between 4.5 − 11. Blending of copolymers with polymeric membrane is a common technique for increasing the hydrophilicity of these membranes. Kim et al. [64] studied the effect of addition of poly(1-vinylpyrrolidone-co-acrylonitrile) copolymers, P(VP-AN) in PSF membrane. They observed that the contact angle between water and blend film reduced by increasing P(VP–AN) content in blend. It depicts that the hydrophilicity of PSF membrane could be improved by blending with P(VP-AN) copolymers. Cui et al. [65] prepared an amphiphilic copolymer of poly (methyl methacrylate-co-dimethylaminoethyl methacrylate) (P(MMA-co-DMA)) and then blended with polyvinyl chloride (PVC) to fabricate precursor membranes. They resulted with low pressure-driven nanofiltration (NF) membranes with high permeate flux. Park et al. [66] synthesized amphiphilic graft copolymers having PSF backbones and poly(ethylene glycol) (PEG) side chains. They observed that the graft copolymer delivered enhanced wettability, porosity and protein resistance compared to unmodified PSF membranes. Yoo et al. [67] prepared UF membranes from the miscible blends of PSF with poly(1-vinylpyrrolidone-co-styrene) copolymers. They observed that membranes prepared from the miscible blends of PSF and Poly(VP-S) exhibited higher water flux than the membranes prepared from PSF alone without any deficiency in solute rejection. Yi et al. [68] prepared F127-based (F127, PEO-b-PPO-b-PEO) amphiphilic block copolymers containing poly(N,N–dimethylamino-2-ethyl methacrylate) (PDMAEMA) end blocks (F127-b-PDMAEMAn). They resulted with improved water permeation results with smart properties that responded to temperature and pH stimulations

by the addition of copolymer. Zhao et al. [69] synthesized PSF-based triblock copolymer, their observation shows improved surface hydrophilicity and fouling-resistance of the fabricated membranes by the addition of block copolymer. Zhou et al. [70] prepared poly(vinyl chloride-co-poly(ethylene glycol)methyl ether methacrylate) membranes. Their observation depicted that membrane with copolymer showed very good antifouling property and restrained irreversible fouling, despite showing low membrane rejection to BSA molecules. Helin et al. [71] prepared anti-fouling UF membrane from polysulfone-graft-methyl acrylate copolymers. They observed improved hydrophilicity of graft copolymer membranes and also an enhancement of antifouling property for graft copolymer membranes. Effect caused by the addition of various copolymers such as poly(acrylic acid-co-butyl acrylate) microgels, Poly (acrylamide-co-acrylic acid) and poly(N-vinylcaprolactam-co-acrylic acid) on the hydrophilicity of membrane was also studied [72-74]. Researchers resulted with increased hydrophilicity and improved rejection capacity of polymeric membrane.

Possible scope for further research

It may be seen from the literature review that although lots of works have reported on numerous copolymers to increase the hydrophilicity of PSF membrane, but no work has been reported on the investigation of poly(VP-co-IAH) based copolymer in PSF membrane. So, keeping the main objective of preparation of hydrophilic membrane, this part of thesis focussed on the preparation and characterization of the pH responsive membrane using pH responsive copolymer with hydrophilicity. The objective of this research is to explore the use of synthesized copolymer for increasing the hydrophilicity of the PSF membrane and also examine the pH responsive behaviour of it. Therefore, in the present study an attempt was made to investigate the effects of hydrophilic copolymer poly(VP-co-IAH) on the membrane

morphology, hydrophilicity, water flux as well as permeation and rejection behaviour. Radical initiated copolymerization was used for the preparation of copolymer poly (VP-co-IAH) from N-vinyl pyrrolidone and isatoic anhydride. AIBN was used as initiator for the synthesis of copolymer. The PSF membrane was modified by blending poly (VP-co-IAH) in casting solution. Apart from giving pH sensitivity to the membrane, this copolymer also increases the hydrophilicity of the membrane. Due to hydrophilic in nature; it can improve the antifouling property of the membrane.

1.6.3. Racemic and enantiomeric effect of tartaric acid on the hydrophilicity of polysulfone membrane

Literature survey

Solubility of Dextro-tartaric acid (D-TA) and racemic tartaric acid (DL-TA) is different in water [75]. This fact can change the diffusion rate of solvent and non-solvent in coagulation bath (i.e. water) during wet phase inversion process and it can subsequently change the porosity of the membrane. Dissociation constants of acids are also slightly different which can affect the surface charge of the PSF membrane. Some literatures are available, addressing the enantiomeric and racemic effect of organic acid on membrane. Yang et al. [76] studied extractive resolution of racemic mandelic acid through a bulk liquid membrane containing binary chiral carrier. They developed a complex of di(2-ethylhexyl) phosphoric acid and O, O'-dibenzoyl-(2R, 3R)-tartaric acid (L-(-)-DBTA) for the extractive resolution of racemic mandelic acid and observed a separation factor (α) of 2.74.

Literature shows that even a small amount of organic acid can change the hydrophilicity of polymeric membrane. So, blending of different organic acids with PSF can be used for surface modification and consequently increasing the hydrophilic properties of the

membrane. Kumar et al. [77] prepared polysulfone-chitosan blend ultrafiltration membranes with 1 % acetic acid. Their observation resulted with improved antifouling property of BSA rejection through modified membrane. Xenobiotics removal at different solution pHs was studied by Ghaemi et al. [21]. They investigated the effect of various concentrations (0.25 to 1 wt %) of three different organic acids (i.e. ascorbic acid, citric acid and maleic acid) on the morphology and performance of PSF membrane. They observed that porosity was maximum for 0.5 wt % of all the organic acids in the PSF membrane. Citric acid offered highest retention efficiency of the solutes compared to other two acids. Ghaemi et al. [78] also studied the effect of amphiphilic fatty acids (palmitic, oleic, and linoleic acid) on the structure and performance of cellulose acetate nano filtration membranes. They observed that addition of palmitic acid represent higher rejection of nitrophenols compared to other fatty acids in all of the solution pHs. Mansourizadeh et al. [79] used Polyethylene glycol (PEG 200) and ethanol, glycerol and acetic acid as the additives in porous PSF hollow fibre membranes for CO_2 absorption. They found that all the additives resulted in enhanced surface porosity. Wei et al. [80] studied the effect of preadsorption of citric acid on surface modification of PSF based UF membrane. They observed that after modification the membrane surfaces became more hydrophilic and permeability also improved. The modified membranes showed enhanced BSA and PEG retentions and improved antifouling properties with higher flux recovery ratios during filtration of a complex pharmaceutical wastewater. Acrylic acid was also used with different hydrophilic polymers [81]. Sinha et al. [82] synthesized polyurethane macromolecules (PU) with end capping of citric acid, maleic acid, lactic acid and 4-hydroxy benzoic acid. Membranes blended with PU showed improved pore density, hydrophilicity and pure water flux compared to plain PSF membrane.

Possible scope for further research

In most of the literatures, polymeric membranes were modified by blending of different organic acids for increasing the hydrophilicity of PSF membrane. However investigation of enantiomeric and racemic effect of tartaric acid (TA) on the hydrophilicity of PSF membrane has not been reported yet. Therefore, in this part of thesis an attempt was made to investigate the effects of addition of D-TA and DL-TA into the casting solution of PSF membrane; i.e. blending of D-TA and DL-TA in PSF membrane and their performance in the removal of crystal violet dye (CVD) from aqueous solutions by molecular enhanced ultrafiltration (MEUF). However, different membrane processes were studied for the removal of CVD from aqueous medium. Enantiomeric and racemic effects of TA on the membrane morphology, hydrophilicity, water flux as well as permeation and rejection behaviour were also examined and explained well for BSA.

1.6.4. Impact of synthesized amino alcohol plasticizer on the morphology and hydrophilicity of polysulfone ultrafiltration membrane

Literature survey

Ultrafiltration is a pressure driven separation process with pore size in the range of 1 nm to 100 nm and can separate macromolecules like protein and colloids. PSF is largely used as membrane material for fabrication of membrane by phase inversion method. Generally two types of hydrophilic modifiers are used for modification of PSF membranes, inorganic nanoparticle and polymer material. Polymeric plasticizers can be also used for increasing the hydrophilicity and subsequently lifetime of membrane [83]. Mekonnen et al. [84] studied the effects of addition of plasticizers on plastics. They resulted with the fact that plasticizers are important additives which can enhance the performance of polymers. Lindström [85] et al.

studied the poly(vinyl chloride)/polyester blends based plasticizer with varying degrees of branching with respect to migration resistance during aging in water, thermal stability and protection of material characteristics. Their observation was that films plasticized with a little branched polyester could have maintained their mechanical and material properties throughout the aging. Zahran et al. [86] studied the effect of polymeric plasticizer on the lifetime of the membrane. They resulted with the fact that it extends the lifetime of PVC-membrane ion-selective electrodes. Khodaverdi et al. [87] fabricated Eudragit RS (ethylacrylate–methylmethacrylate–trimethyl ammonioethyl methacrylate chloride copolymers with ratios of 1:2:0.1) and different percentages of plasticizers membranes. Their observation was that adding suitable amount of plasticizer such as TEC or PEG 400 (20%) to the membranes the thermo-responsive behavior of the Eudragit RS films was attained. Stark et al. [88] studied the effect of molecular weight of plasticizer on plasticizer retention in PVC geomembranes. Their observation was that the plasticizer loss can reduce the flexibility of PVC geomembranes and to ensure long-term plasticizer retention, an average plasticizer molecular weight should be greater than or equal to 400.

Possible scope for further research

From the above discussed literature it can be infers that although lots of works have reported on numerous plasticizers to enhance the life time and other properties of membranes, but no work has been reported on the investigation of isatoic anhydrides (IAH) based plasticizer in PSF membrane. Therefore, in this section of thesis, different molecular weight PEG based hydrophilic amino alcohol plasticizer (AAP) were synthesized and used for the modification of PSF membrane to increase the hydrophilicity of the fabricated membrane. This work focused on fabrication and characterization of hydrophilic flat sheet PSF membrane by phase

inversion method. Amphiphilic AAP macromolecules were synthesized in a three necked round bottom flask (heated in an oil bath). Dioxane was taken as solvent.

1.7. Objectives of thesis work

Based on the above state of the art, the present PhD thesis incorporates the following main objectives

- Preparation of hydrophilic polysulfone membrane using polyacrylic acid with polyvinyl pyrrolidone
- Preparation and characterization of poly(vinyl pyrrolidone-co-isatoic anhydride) copolymer added pH responsive hydrophilic polysulfone ultrafiltration membrane
- Racemic and enantiomeric effect of tartaric acid on the hydrophilicity of polysulfone membrane
- Impact of synthesized amino alcohol plasticizer on the morphology and hydrophilicity of polysulfone ultrafiltration membrane

1.8. Organization of the thesis

Chapter 1 discusses the background of the problem undertaken in this work i.e. the problem associated with the hydrophobic tendency of polymeric UF membranes. The objectives of the present work are also highlighted in this chapter. **Chapter 2** gives a complete description of the experimentation involved in the fabrication and characterization of polymeric membranes by phase inversion method. **Chapter 3** describes the modification and characterization of PSF membrane by PVP-PAA additives. Effect of addition of two hydrophilic polymers was studied. Apart from that all the results were compared with Chakrabarty et al. [15]. They used same molecular weight PVP in their work. **Chapter 4** presents results obtained from the

addition of different weight % of poly (vinyl pyrrolidone-co-isatoic anhydride) copolymer in the polysulfone membrane casting solution and their effects on membrane morphology, water permeation, hydrophilicity as well as on the pH responsive behaviour. **Chapter 5** discusses the preparation and characterization of D-TA and DL-TA blended PSF membrane. This chapter gives a broad knowledge about the enantiomeric and racemic effect of TA on the morphology and hydrophilicity of PSF membrane. Application of the modified PSF membrane for crystal violet dye removal by MEUF process was also studied and explained in this chapter. **Chapter 6** converses the synthesis and characterization of novel amino alcohol plasticizer (AAP). Effect of these AAPs on membrane morphology, BSA transport and hydrophilicity were discussed in detail. **Chapter 7** summarized the inferences drawn from this work and provided some suggestions towards future research.

Chapter 2
Membrane preparation and characterization

This chapter gives a complete description of the experimentation involved in the preparation and characterization of polymeric membranes. The chapter also provides information regarding the materials used for the preparation of polysulfone membranes along with their sources from where these are obtained. It presents the detail of instruments used for characterization of synthesized polymeric material and modified membranes like FTIR, ATR-FTIR, NMR, SEM, FESEM, AFM, UV-VIS spectrophotometer and HPLC. It further elaborates the characterizations of the prepared membranes through measurement of pure water flux (PWF), equilibrium water content (EWC), compaction factor (CF), hydraulic permeability (P_m), ion exchange capacity (IEC), pH sensitivity, water contact angle as well as BSA flux and rejection through prepared membranes.

2.1. Materials

Base polymer used for the membrane preparation was PSF in all the cases. NMP was used as solvent for the preparation of membrane casting solution throughout the experiments except chapter 5, where DMAc was used as solvent. In the present study various kind of additives were used for the modification of polymeric membranes. Some additives were used directly like PVP, PAA and TA; whereas other additives were synthesized for specific membrane properties like amphiphilic, pH responsive and hydrophilic. Details of the chemicals used for membrane preparation and modification are tabulated in Table 2.1. All the chemicals were used without further purification. Deionized water purified by Millipore system (Millipore, France) was used as non- solvent in coagulation bath as well as for all other purposes.

Table 2.1: Chemicals used in this work.

Sr. No.	Chemicals (specification)	Brand
1.	Polysulfone (average molecular weight 35000 Da)	Sigma-Aldrich Co. USA
2.	N- methylpyrrolidone (reagent grade)	LOBA Chemie, India
3.	Polyethylene glycol (average molecular weight 400 Da, 1500 Da, 6000 Da and 20000 Da)	Sisco Laboratories, India
4.	Bovine serum albumin (68,000 Da)	Otto Chemie, India
5.	Polyvinyl pyrrolidone (average molecular weight 24000 Da, 40000 Da and 360000 Da)	Otto Chemie, India
6.	Dimethyl acetamide (synthesis grade)	LOBA Chemie, India
7.	Potassium bromide (FTIR grade)	LOBA Chemie, India
8.	D-tartaric acid	Otto Chemie, India
9.	DL-tartaric acid	Otto Chemie, India
10.	Isatoic anhydride	HiMedia Laboratories, India
11.	1, 4-Dioxane	Sigma-Aldrich Co. USA
12.	Poly acrylic acid (average molecular weight 18000 Da)	Otto Chemie, India
13.	Benzene	Sigma-Aldrich Co. USA
14.	N-vinyl pyrroloidone	Sigma-Aldrich Co. USA
15.	Crystal violet dye	CDH Laboratory, India
16.	Sodium dodecyl sulphate	Sisco Laboratories, India
17.	Azobisisobutyronitrile (AIBN)	Sigma-Aldrich Co. USA

2.2. Preparation of membrane

Flat sheet PSF based membranes were fabricated by the wet phase inversion method. The casting solution was stirred using a magnetic stirrer for 12-24 h at room temperature and then degassed for 12 h at room temperature for removal of air bubbles. The solution was then cast on a clean glass plate using a casting knife maintaining a uniform and constant thickness of 100-200 μm, in ambient conditions. Then without any delay the glass plate was immersed into the water bath (coagulation bath) at room temperature. The casted film instantaneously changed its colour and converted from transparent to white after the immersion in the water bath and then separated out from the glass plate. The prepared membrane sheets were then washed under running water to remove the additional amount of additive and then kept overnight in a deionized water bath to remove any residual solvent. Finally, the sheets were air dried at room temperature. Thereafter cutting them into the form of circular disks of diameter 0.03 m to place inside the membrane cell for filtration experiments [89]. Membrane preparation steps are shown in Figure 2.1.

2.3. Membrane characterization

The porosity and pore size distribution are important parameters deciding the membrane performance [90]. The prepared membranes were characterized by morphological analysis and permeation experiments. The morphology of the prepared membranes was studied by liquid-liquid displacement porosimetry (LLDP) method and microscopic observations. The performance of each membrane was evaluated in terms of water contact angle, equilibrium water content, compaction factor, hydraulic resistance, porosity, pure water flux, permeate flux, BSA rejection. Detail methods are elaborated in subsequent sections of the current chapter.

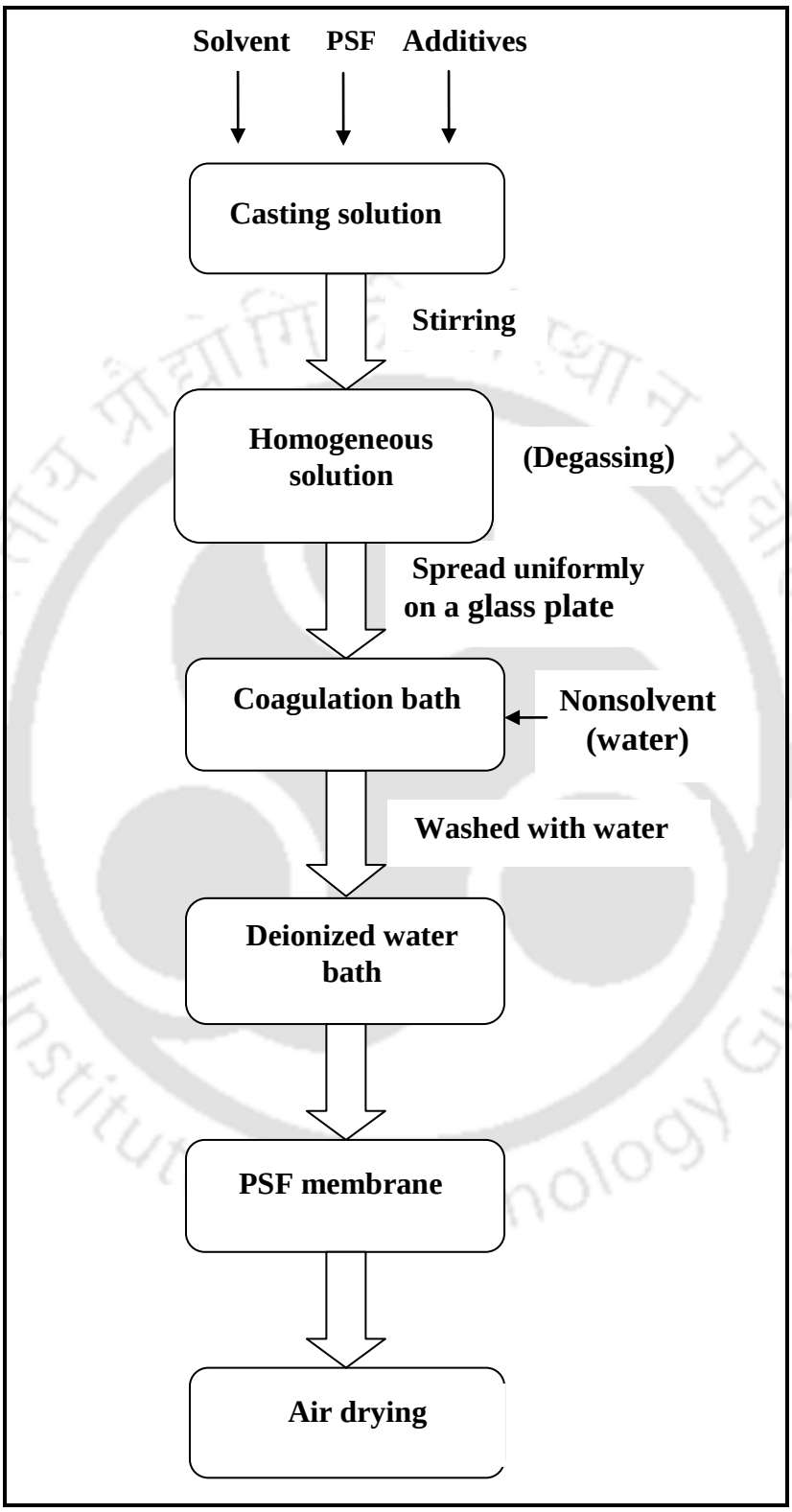

Figure 2.1: Steps of membrane preparation by phase inversion method.

2.3.1. Liquid-liquid displacement (LLDP) porosimetry method

The average pore size, number of pores and pore area distribution of the prepared membranes were determined by LLDP [1]. In this method, membrane was wetted with an appropriate penetrating liquid and then an immiscible liquid that does not wet the membrane was pressurized to pass through the pores displacing the previous liquid which was already occupying the pores. Water - isobutanol - methanol (25:15:7, v/v) was taken with surface tension of 0.35 mN/m and dynamic viscosity of 3.4 mPa s. The mixture was prepared by pouring proper amount of ultra pure water and mentioned alcohols in a separating funnel and shaking it vigorously. After that this mixture was allowed to stand overnight. The separated water reach phase was used to wet the membrane and alcohol reach phase was used as displacing liquid. The pore size distribution was obtained from the data of variation of flow with pressure [91]. The radius (r) was calculated by well known Cantor's equation:

$$r = \frac{2\sigma}{P} \tag{2.1}$$

Where, P is the transmembrane pressure and σ is the interfacial tension between the two liquids. The total hydraulic permeability coefficient (L_n) was obtained by:

$$L_n = \sum L_{i,k} = \sum \frac{J_{i,k}}{P_{i,k}} \tag{2.2}$$

Where $J_{i,k}$ is flux at pressure $P_{i,k}$ and $L_{i,k}$ is partial permeability coefficient of the pores with radius r_i and r_k evaluated at $P_{i,k}$, which corresponds to a mean radius $r_{i,k}$.

$$r_{i,k} = \frac{r_i + r_k}{2} \tag{2.3}$$

Combining equations (1) and (2), flux versus pressure data gives the permeability versus pore radius curve. Again, the pore number versus pore radius and pore area versus pore radius curves can be obtained using the following equations [92, 93]:

$$N_{i,k} = \frac{d\eta}{2\pi\sigma^4} P_{i,k}^3 J_{i,k} \tag{2.4}$$

$$\mathrm{A_{i,k}} = \pi \mathrm{r_{i,k}^2 N_{i,k}} \tag{2.5}$$

Where $N_{i,k}$ is the pore density, i.e. the number of pore having radius between r_i and r_k per unit area of the membrane surface, d is the length of the pore which is approximately equivalent to thickness of the skin layer and η is the viscosity of the alcohol rich mixture. $A_{i,k}$ is the area of the pores having radii between r_i and r_k. Both the equations are derived from the Hagen-Poiseuille's permeation equations assuming cylindrical pores and laminar flow. An average value of the thickness of the skin layer equal to 0.1 μm was considered in the present work even though it was likely to vary along the surface of the membrane. The total area A_t and the total number of pores per unit area of the membrane N_t was calculated as follows:

$$A_t = \sum A_{i,k} \tag{2.6}$$

$$N_t = \sum N_{i,k} \tag{2.7}$$

The mean pore radius r_m was calculated as [91]:

$$r_m = \frac{\sum N_{i,k} r_{i,k}}{\sum N_{i,k}} \tag{2.8}$$

The limitation of this methods is that the absolute values of the A_t, N_t and their distribution are likely to be associated with an error because of the deviation from the assumption of cylindrical pores and non-uniform thickness of membranes skin layer. However, the information may be useful in comparing the different membranes.

2.3.2. Microscopic observation

Microscopic observation was done by field emission scanning electron microscope (FESEM, Make: Zeiss LSM 510 Meta) and scanning electron microscope (SEM, Make: LEO 1430VP, UK) after the samples were coated with thin gold layer. The pore size on the membrane surface as well as skin layer thickness was measured with the help of image J software. These images directly provide the top layer visual information as well as cross sectional information of the membranes. A number of FESEM images were taken at different magnification for both top surface and cross section of the prepared membranes. Computerized analysis of FESEM [94] image was extensively performed for this study. Cross section images were taken by SEM with an acceleration voltage of 10 kV after the samples were coated with thin gold layer. The area average pore diameter (d_s) from FESEM analysis of the membrane is evaluated by assuming cylindrical porous texture of the membrane as [95]:

$$d_s = \left[\frac{\sum_{i=1}^{n} n_i d_i^{\,2}}{\sum_{i=1}^{n} n_i} \right]^{0.5} \tag{2.9}$$

2.3.3. Permeation experiments

The unstirred batch experiment was conducted in a 400 ml permeation cell made of stainless steel. Inside the cell, a flat circular disk shape membrane was placed over a perforated base

support. The membrane diameter was 3×10^{-2} m and the effective area of the membrane was 7.065×10^{-4} m^2. The permeating solution was collected from the bottom of the cell. The cell was pressurized using a nitrogen cylinder. The schematic of batch experimental setup is shown in Figure 2.2.

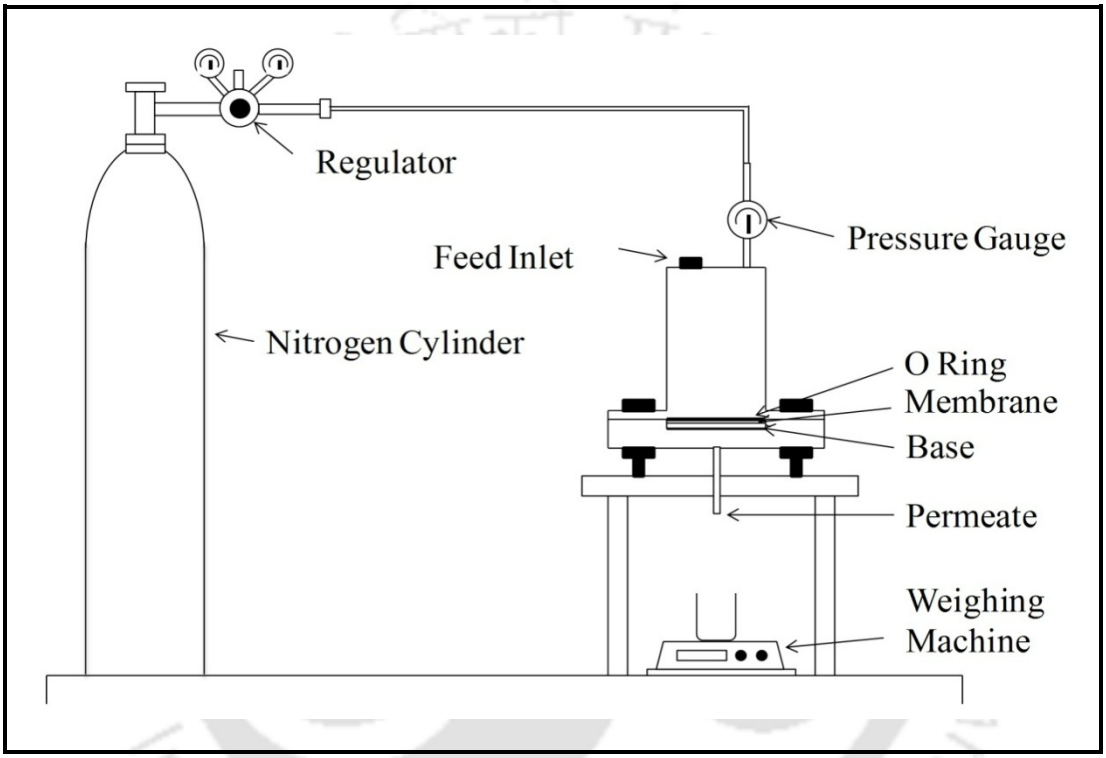

Figure 2.2: Schematic of experimental setup.

2.3.3.1. Compaction of membranes at constant pressure

Prepared membrane was compacted with deionized water for 1-4 h at a transmembrane pressure of 240-414 kPa which was higher than the maximum operating pressure in this study. The water permeation flux was at regular time interval after attaining flow stabilization through the membrane. The compaction factor (CF) was calculated as the ratio of initial pure water flux ($PWF_{initial}$) to steady state pure water flux ($PWF_{steady\ states}$).

2.3.3.2. Pure water flux (PWF) and hydraulic permeability (P_m)

Membrane hydraulic permeability has got significance particularly for membranes used in pressure driven separation processes. Pure water flux (PWF) was determined by allowing deionized water to pass through the compacted membrane. Flux values of pure water at different transmembrane pressures were measured under steady state condition using following equation:

$$J_w = \frac{Q}{A\,\Delta t} \tag{2.10}$$

Where, J_w is pure water flux (L/m^2 h), Q is volume of water permeated (L), A is effective membrane area (m^2) and t is permeation time (h). P_m (L/m^{2}h kPa) is evaluated from the slope of the plot of J_w vs P. Hydraulic permeability was calculated as:

$$P_m = \frac{J_w}{\Delta P} \tag{2.11}$$

2.3.4. Equilibrium water content (EWC) and porosity

EWC is directly related to the porosity of membrane. It also indicates the hydrophilicity or hydrophobicity of the membranes. EWC at room temperature was calculated as:

$$EWC\ (\%) = \frac{W_w - W_d}{W_w} \times 100 \tag{2.12}$$

The membrane porosity was determined as [15]:

$$Porosity = \frac{W_w - W_d}{\rho_w \times V} \tag{2.13}$$

Where, W_w and W_d is the weight of membrane in wet and dry state, respectively. ρ_w is the density of water and V is volume of the membrane. Membranes were weighed in electronic balance in wet state after mopping the surface water with a clean tissue paper. The wet membranes were dried by putting in a vacuum oven for 24 h at a temperature of 50-60˚ C and again they were weighed in dry state. For calculation of volume of membrane, thickness of membranes was measured by FESEM image at different place and the average was taken. The error was found within 2-3 %.

2.3.5. Hydrophilicity

The hydrophilic property of the membrane was evaluated by measuring the static contact angle between the de-ionized water and membrane films at ambient condition at room temperature using a digital camera (canon power shot) and a goniometer was used to determine the contact angle. Farbod et al. [96] had also used the same technique to measure contact angle. For measuring the contact angle, membrane coupons of about 2 cm × 2 cm areas were prepared by cutting the membrane sheet and then these samples were fixed at glass palates with the help of tape. Then, a drop DI water (20 µl) was placed on the surface using a micropipette. Static contact angle between the surface of membrane and water (deionized) droplet was also verified by drop shape analyzer (DSA-25, KRUSS GmbH, Hamburg). Membrane pieces of about 1cm × 1cm area were prepared and then these samples were kept at sample holder of the instrument using the tape. A little drop of DI water (4 µL) was located on the surface and the images were captured at 27^0C temperature.

2.3.6. Ion exchange capacity (IEC) of membranes

The ion exchange capacity (IEC) of membranes was determined by using standard titration method [97]. First, modified membranes were kept in 2M NaCl solution for 24 h at 30 ˚C in orbital shaker for the complete substitution of H^+ by Na^+. Then, the remaining solution was titrated with 0.01M NaOH solution using phenolphthalein indicator. Finally, the IEC value was calculated using the following equation:

$$IEC\ (mmol/g) = \left(\frac{0.01 \times 1000 \times V_{NaOH}}{W_d}\right) \quad (2.14)$$

Where V_{NaOH} is the volume of NaOH solution (L) consumed for titration and W_d is the weight of dry membrane sample.

2.3.7. ATR-FTIR of modified membranes

Fourier transform infrared (FTIR) analyses of the polymers were measured with FTIR spectrometer (IRAffinity-1, Shimadzu, Japan) with the help of an attachment called ATR-8200 HA (Shimadzu, Japan). For doing analysis, film samples were clamped firmly on the surface of attenuated total reflectance (ATR) crystal.

2.3.8. Ultrafiltration experiment and fouling studies

Ultrafiltration experiments were conducted in the batch cell explained in the preceding section to study the influence of molecular weight of PVP on solute separation and permeate flux behaviour of the prepared membranes. The protein, Bovine Serum Albumin (BSA), was dissolved in deionized water and the concentration was kept constant at 1000 mgL^{-1} for all the experiments. After the membrane was fixed in the membrane cell, the cell was filled

deionized water. Each membrane was initially pressurized for 60 min at pressure higher then operating pressure, then the pressure was reduced to the operating pressure and the water flux (J_{w1}) was measured. After that cell was emptied and refilled with 1.0 mg/mL BSA solution; the flux was recorded (J_p). The BSA rejection ratio was calculated by the following equation:

$$R\ (\%) = \left(1 - \frac{C_p}{C_f}\right) \times 100 \tag{2.15}$$

Where, C_p and C_f are the concentration in permeate and the feed in mg/mL, respectively. After ultrafiltration, the membrane was cleaned with deionized water and water flux was measured (J_{w2}). BSA concentration in permeate was determined spectrophotometrically using a UV-VIS spectrophotometer (Perkin-Elmer Precisel, Lamda-35) at wavelength of 280 nm. The concentration values were plotted against corresponding values of absorbance. The relation between absorbance versus concentration was found to be a linear one with R^2 = 0.9995. This relation was used for measuring concentration of unknown sample i.e. permeate. The calibration curve so formed is shown in Figure 2.3.

Membrane fouling causes flux loss (J_{w1}-J_p). To study the antifouling property, Wang et al. [9] defined some ratios to describe the fouling process. The first ratio is F_t, which is the degree of total flux loss caused by total fouling. F_t was calculated by following equation:

$$F_t = 1 - \frac{J_p}{J_{w1}} \tag{2.16}$$

F_r and F_{ir} are other two ratios. Where, F_r is reversible fouling and F_{ir} is irreversible fouling. F_r and F_{ir} were calculated by the following equations:

$$F_r = (J_{w2} - J_p)/J_{w1} \quad (2.17)$$

$$F_{ir} = (J_{w1} - J_{w2})/J_{w1} \quad (2.18)$$

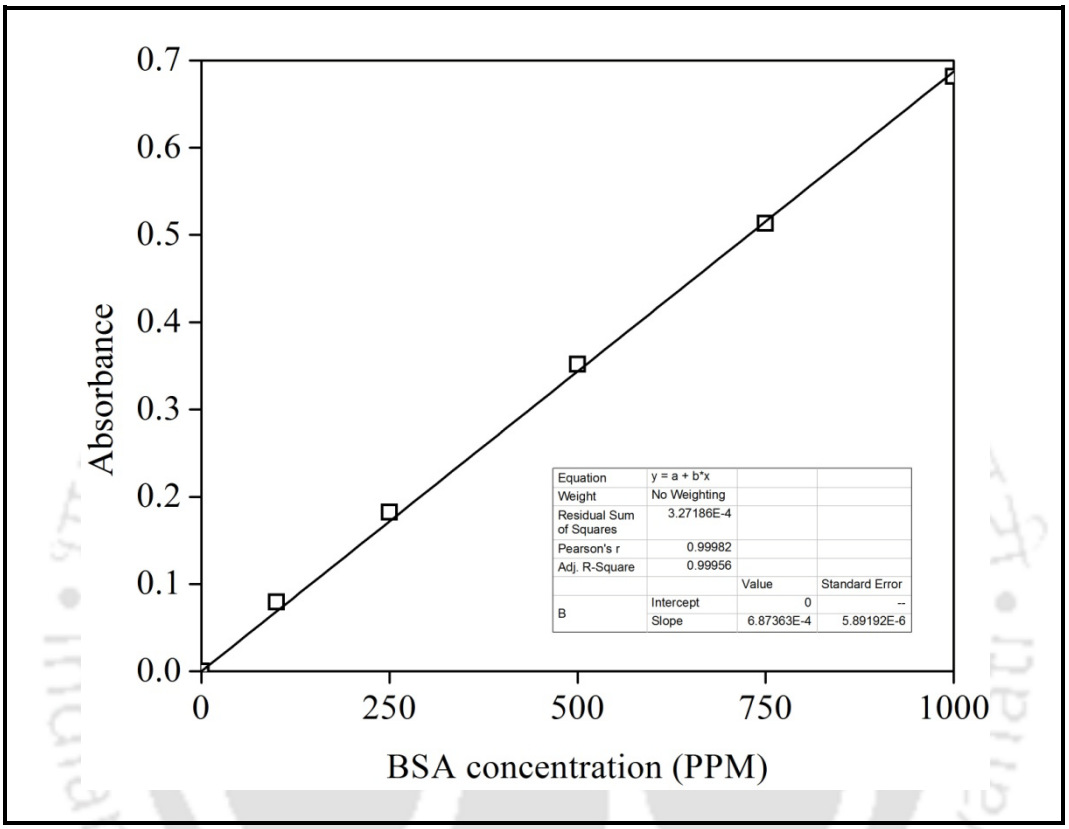

Figure 2.3: Calibration plot of BSA solution.

The reversible BSA adsorption on the membrane surface causes reversible fouling, which can be eliminated by hydraulic cleaning. Irreversible fouling caused by irreversible BSA adsorption, cannot be avoided by hydraulic washing. Thus F_t is sum of F_r and F_{ir}.

$$F_t = F_r + F_{ir} \quad (2.19)$$

With the help of J_{w1} and J_{w2}, flux recovery ratio ($Flux_{RR}$) was measured using the following equation:

$$Flux_{RR}(\%) = \frac{J_{w2}}{J_{w1}} \times 100 \tag{2.20}$$

2.4. Characterization of synthesized additive

For preparing hydrophilic polymeric membranes, different additives had been synthesized and blended with membrane casting solution. These additives are (a) polyvinyl pyrrolidone-polyacrylic acid (b) pH sensitive copolymer poly(vinyl pyrrolidone-co-isatoic anhydride) (c) Dexro-tartaric acid and DL- tartaric acid (d) hydrophilic amino alcohol plasticizer. These additives were characterized by various techniques, which are discussed below and the results of these characterization are reported in the respective chapters.

2.4.1. Proton nuclear magnetic resonance (^{1}H NMR) spectroscopy

Structure of the synthesized molecule was confirmed by NMR spectroscopy. ^{1}H NMR (600 MHz) spectra were recorded with Bruker Ascend 600 (Bruker Co., Japan) using $CDCl_3$ as solvent. To prepare NMR sample, the copolymer was first dissolved in $CDCl_3$ and NMP and filled in NMR tubes.

2.4.2. Fourier transform infrared (FTIR) spectroscopy

Fourier transform infrared (FTIR) analyses of the polymers were measured with FTIR spectrometer (IRAffinity-1, Shimadzu, Japan). To prepare FTIR sample, the copolymer was first dissolved in DMAc and cast on a KBr palette. The casted polymer solution was dried to remove the DMAc. FTIR analysis was done with 30 numbers of scans and apparatus resolution was set at 4.

2.4.3. Photon correlation spectroscopy (PCS)

The hydrodynamic size distribution and zeta potential of the crystal violet dye molecules with and without sodium dodecyl sulphate was done by PCS (Delsanano, Bckman Coulter, Switzerland). For the zeta potential analysis each sample was adjusted to a pH of 7.5. The zeta potential measurement of membrane surface was also done by PCS.

2.5. Determination of molecular weight cut off (MWCO)

MWCO values are the measures to determine qualitative pore sizes of the membranes while the pure water permeability is related to porosity (pore number density) of the membranes [98]. MWCO values were measured by passing aqueous solutions of polyvinyl pyrrolidone (PVP) of two different molecular weights (i. e. PVP 24000 Da and PVP 40000 Da) and a protein bovine serum albumin (molecular weight 68000 Da). Standard technique [99] was opted for finding the concentration of PVP in aqueous solution. High performance liquid chromatography (HPLC, series 200; make Shimadzu, Japan) was used to measure PVP concentration. Whereas, protein concentration was measured by UV- vis spectrometer. MWCO of the membranes was determined using rejection (% R) of polymer and protein solutes.

Chapter 3

Preparation of hydrophilic polysulfone membrane using polyacrylic acid with polyvinyl pyrrolidone

In this chapter flat sheet asymmetric polymeric membranes were prepared from homogeneous solution of Polysulfone (PSF) by phase inversion method using N-methyl-2-pyrrolidone (NMP) as solvent. This study examined the consequences of the addition of polyvinyl pyrrolidone (PVP) of different molecular weights with constant molecular weight of polyacrylic acid (PAA) on the morphology and permeation properties of PSF membranes. The surface structure and morphology of the prepared membranes were analyzed by field-emission scanning electron microscope (FESEM) and atomic force microscopy (AFM). The pore number, average pore size and area of pores for all the membranes were determined by liquid-liquid displacement porosimetry (LLDP) method. Performance of membranes was also investigated by the water permeation and bovine serum albumin (BSA) rejection efficiency. A detailed comparative study was also done with the reported lit. [15].

3.1. Experimental

3.1.1. Materials

PSF, NMP and PVP-PAA blend were used as base polymer, solvent and additives, respectively, in the membrane casting solution. Demineralised water was used as non-solvent in the coagulation bath. BSA was used as model foulant. Details of the entire chemical are reported in chapter 2 (Table 2.1).

3.1.2. Membrane preparation

Content of this chapter is published as below:

Nilay Sharma, Mihir Kumar Purkait, Preparation of hydrophilic polysulfone membrane using polyacrylic acid with polyvinyl pyrrolidone, J. Appl. Poly. Sci. 132 (2015) 41964, DOI: 10.1002/app.41964.

Flat sheet PSF membranes were prepared by phase inversion method (Figure 2.1). Different molecular weight of PVP i.e. 24,000 Da, 40,000 Da, and 360,000 Da and PAA with molecular weight of 18,000 Da was taken for the preparation of PVP-PAA blend. Constant concentration of this blend in casting solution of PSF membrane was added. Effects of PVP-PAA blend on the morphology, permeation characteristic and on the hydrophilicity of PSF membrane was investigated. Membrane casting solution contains PSF as base polymer, N-Methyl-2-pyrrolidone (NMP) as solvent and PVP-PAA as non solvent additives. Composition and nomenclature of different membranes are shown in Table 3.1. The prepared polymer solution was casted on a clean glass plate with a casting knife maintaining a uniform thickness of 100 µm, in ambient atmosphere. Detail method of membrane preparation is given in section 2.2 of chapter 2.

Table 3.1: Composition of various membranes casting solution.

Membrane	PSF (wt.%)	Additives (wt.%)			NMP (wt.%)	PAA (wt.%)
		PVP 24000	PVP 40000	PVP 360000		
PSF_1	14	4.8	-	-	78	3.2
PSF_2	14	-	4.8	-	78	3.2
PSF_3	14	-	-	4.8	78	3.2
PSf1[15]	12	5	-	-	83	0
PSf2[15]	12	-	5	-	83	0
PSf3[15]	12	-	-	5	83	0

3.2. Membrane characterization

3.2.1. Morphological studies

Microscopic observation was done by scanning electron microscope and field emission scanning electron microscope**.** Atomic force microscopy was used for finding the surface roughness parameters. These images directly provide the top layer visual information as well as cross sectional information of the membranes.

3.2.2. Characterization by permeation studies

Prepared membranes were compacted with deionized (DI) water for 4 h at transmembrane pressure of 240 kPa which was higher than the maximum operating pressure in this study. The water flux was calculated from the experimental permeate flow rate measured at 30 min interval until the flow stabilization through the membrane was achieved. The compaction factor (CF) was calculated as the ratio of initial pure water flux ($PWF_{Initial}$) to steady state pure water flux ($PWF_{Steady\ state}$) [15, 17]. Permeation set up details are presented in section 2.3.3 of chapter 2.

3.2.2.1. Pure water flux (PWF) and hydraulic permeability (P_m)

Hydraulic permeability, P_m has got significance particularly for membranes used in pressure-driven separation processes. Pure water fluxes (PWF) of different membranes were measured at different transmembrane pressures (ranging 0 – 240 kPa) using the equation 2.10. P_m ($L/m^2h\ kPa$) was evaluated from the slope of the plot of J_w vs P by using equation 2.11.

3.2.2.2. Equilibrium water content (EWC), porosity and hydrophilicity

EWC is directly related to the porosity of membrane. It also indicates the hydrophilicity or hydrophobicity of the membranes. EWC and porosity at room temperature were calculated by equations 2.12 and 2.13, respectively. The hydrophilic property of the membrane was

evaluated by measuring the static contact angle between the deionized water and membrane films at room temperature.

3.3. Results and discussion

3.3.1. Preparation of PAA-PVP blend

PAA-PVP blend was prepared by the blending of PVP (4.8 wt %) and PAA (3.2 wt %) in 78 wt % of NMP for 6 h. Magnetic stirrer was used for blending of both the polymers. After getting the uniform solution, PSF was added in the solution for obtaining the membrane casting solution.

3.3.2. FTIR spectroscopy analysis of PAA-PVP blend

Figure 3.1 shows the FTIR spectra of PAA, PAA-PVP blend and PVP. As shown in Fig. 3.1, spectra of PAA shows peaks at 2954 cm^{-1} and 3550 cm^{-1}, these are characteristic peaks of C-H stretch and –OH group, respectively present in PAA. In PAA-PVP spectra, peaks at 1297 cm^{-1} and 1700 cm^{-1} are characteristic peaks of C-N and C=O group present in PVP - PAA blend. Another peak at 3515 cm^{-1} is due to –OH group present in blend, because of the formation of hydrogen bond. So, FTIR analysis shows that the complexes were formed through hydrogen bonding between the carboxyl groups of the PAA and the carbonyl groups of the PVP. Peak at 1700 cm^{-1} and 2954 cm^{-1} in PVP spectra show the presence of C=O group and C-H stretching in the PVP.

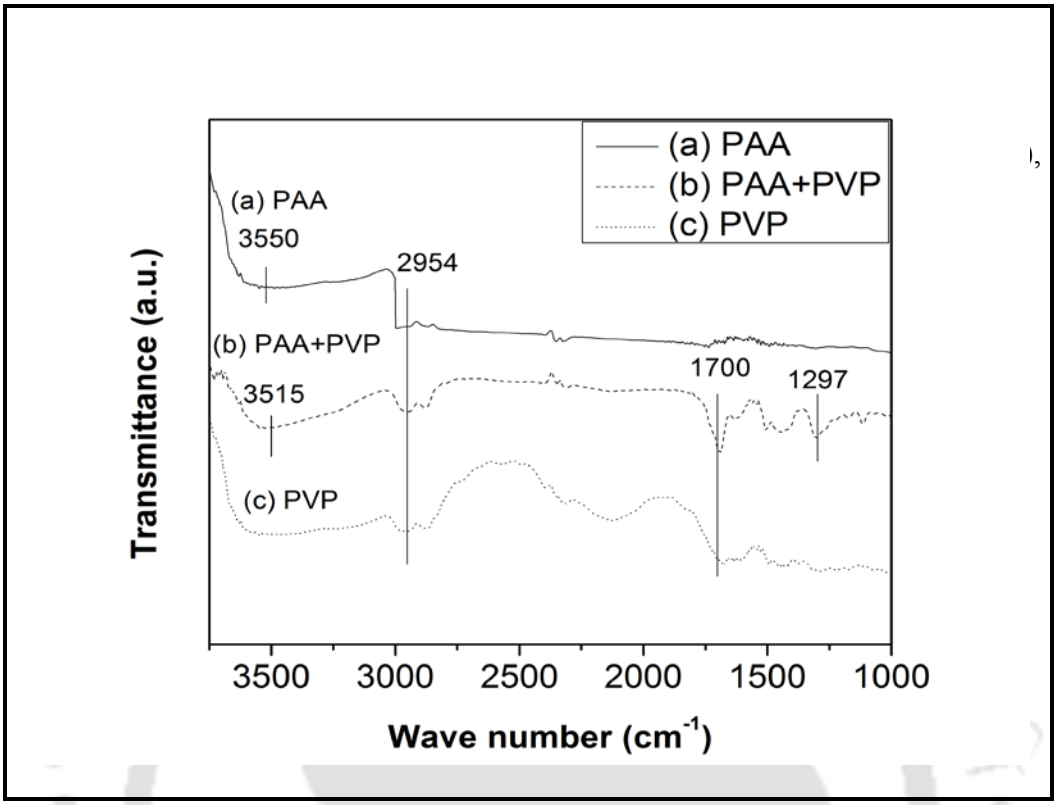

Figure 3.1: FTIR spectra of PAA, PAA-PVP blend and PVP.

3.3.3. Morphological studies

Qualitative information regarding surface and cross-sectional morphology of the membranes prepared was obtained through FESEM and SEM analysis, respectively. For determining surface roughness parameters AFM images were taken. FESEM images for the top surface (air side) of different membranes (Table 3.1) prepared by addition of different molecular weight of PVP with constant molecular weight of PAA, are shown in Figure 3.2 (a) and 3.2 (b), respectively. Higher magnification was required for top surface images to find the size of pores, so these images were taken by FESEM. On the other hand, cross-sectional morphologies of the prepared membranes were obtained through SEM analysis. In the case of cross-sectional morphology lower magnification was sufficient as only pore structure was observed.

3.3.3.1. SEM analysis

Figure 3.2 (a) shows the SEM images of the cross-sectional view of different membranes prepared with three different molecular weight of PVP with PAA in this study. From the images it can be seen that membranes so prepared were asymmetric porous structure. General structure shows a dense top layer and a porous sub-layer, which was very similar for all the membranes. The porous sub-layer seems to have finger-like structure. Similar observation was depicted by Chakrabarty et al. [15] for the system of PSF as base polymer with DMAc and NMP as solvent using different molecular weight of PVP as additive. Because of high interactive affinity of NMP for water, instantaneous demixing occurs, further leading to the creation of finger like cavities in the sub -layer of the prepared membranes [1]. Sinha et al. [42] also found the same result, for the system of PSF as polymer using NMP as solvent with different molecular weight of Polyethylene glycol methyl ether (PEGME) as additive.

3.3.3.2. FESEM analysis

FESEM images for the top surface (air-side) of different membranes are shown in Fig. 3.2 (b). The top surface formation was probably due to the spinodal demixing. This is due to the fact that during formation of top layer the diffusion process was so fast for the polymer solution to become highly unstable and cross the spinodal curve [100, 101]. This provides a top surface with much better interconnected pores. The interconnected pores can be taken as a continuous PSF lean (i.e. PVP - PAA rich) phase intertwined by a continuous PSF rich (i.e. PVP - PAA lean) phase which was responsible for the formation of the membrane matrix. Few round formations in Fig. 3.2 (b) depicted that although homogeneous solution is made for membrane preparation but still few polymeric particles remains insoluble in the casting solution. Image J software was used for determining the pore size from FESEM results, shown in Fig. 3.3. Average pore size was calculated as 37.12 nm, 35.85 nm and 30.65 nm for PSF_1, PSF_2 and PSF_3 membrane, respectively; which confirms that the membranes are in

UF range. It may also be seen that the pore size distribution for PSF_2 and PSF_3 is almost same, as maximum number of pores were of 30-35 nm size and for PSF_1 that value was nearly 40 nm.

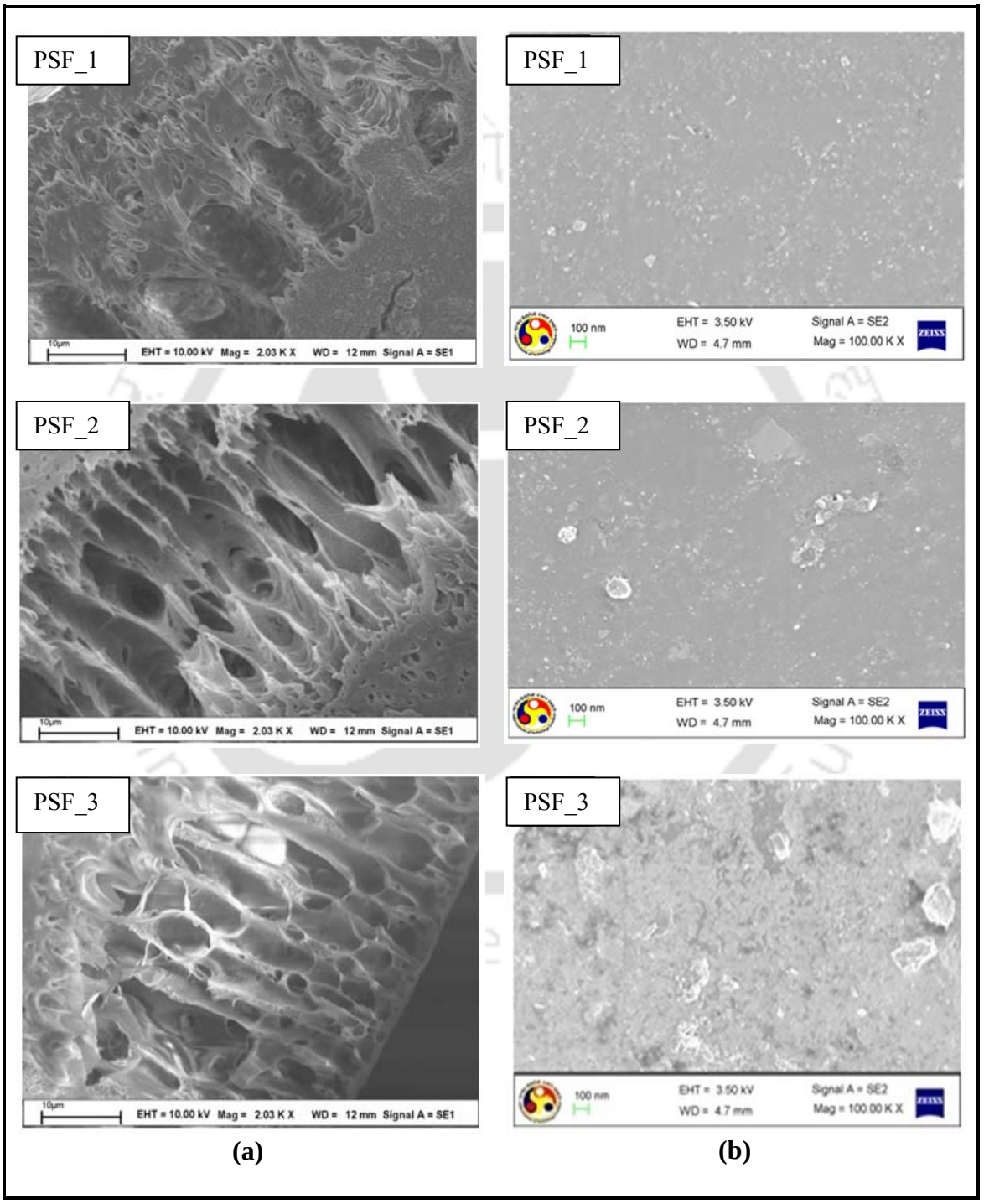

Figure 3.2: (a): SEM images of membrane cross section (b) FESEM images of membrane top surface.

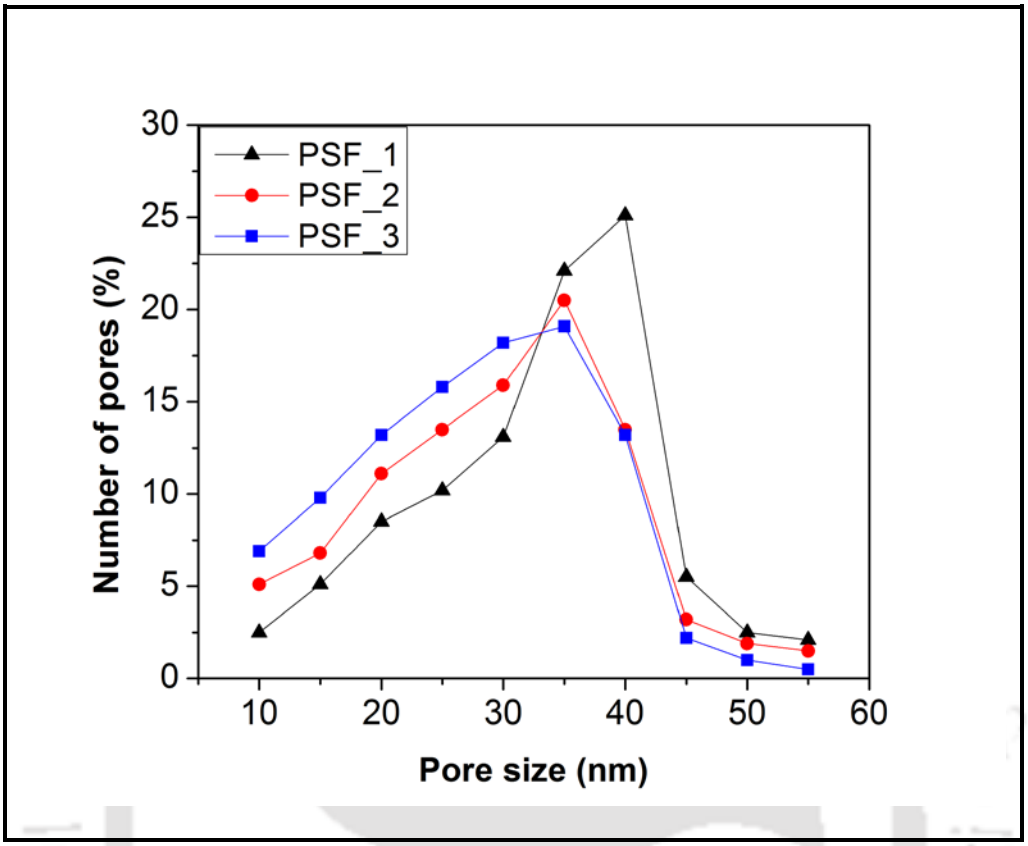

Figure 3.3: Pore size distribution of membranes by FESEM.

3.3.3.3. AFM analysis

Atomic force microscopy (AFM) was used to analyze the surface morphology and roughness of the membranes. Small squares of membranes (Approximately 1 cm^2) were cut and analyzed. The membrane surface was examined in a scan size of 2 µm × 2 µm. Fig. 3.4 shows the AFM images of the membranes. Root mean square (RMS) roughness (S_q), average roughness (S_a) and average height (S_z) were measured. RMS roughness is increasing with increase in molecular weight of PVP. It was measured as 5.81 nm, 10.36 nm and 15.70 nm for PSF_1, PSF_2 and PSF_3, respectively. It may be due to the fact that number of pores on the surface was increasing (i.e. porosity increasing) with increase in molecular weight of PVP. Table 3.2 shows the surface roughness parameters. It indicates increasing hydrophilicity

with increase in molecular weight of PVP as molecular weight of PAA was taken constant in this study.

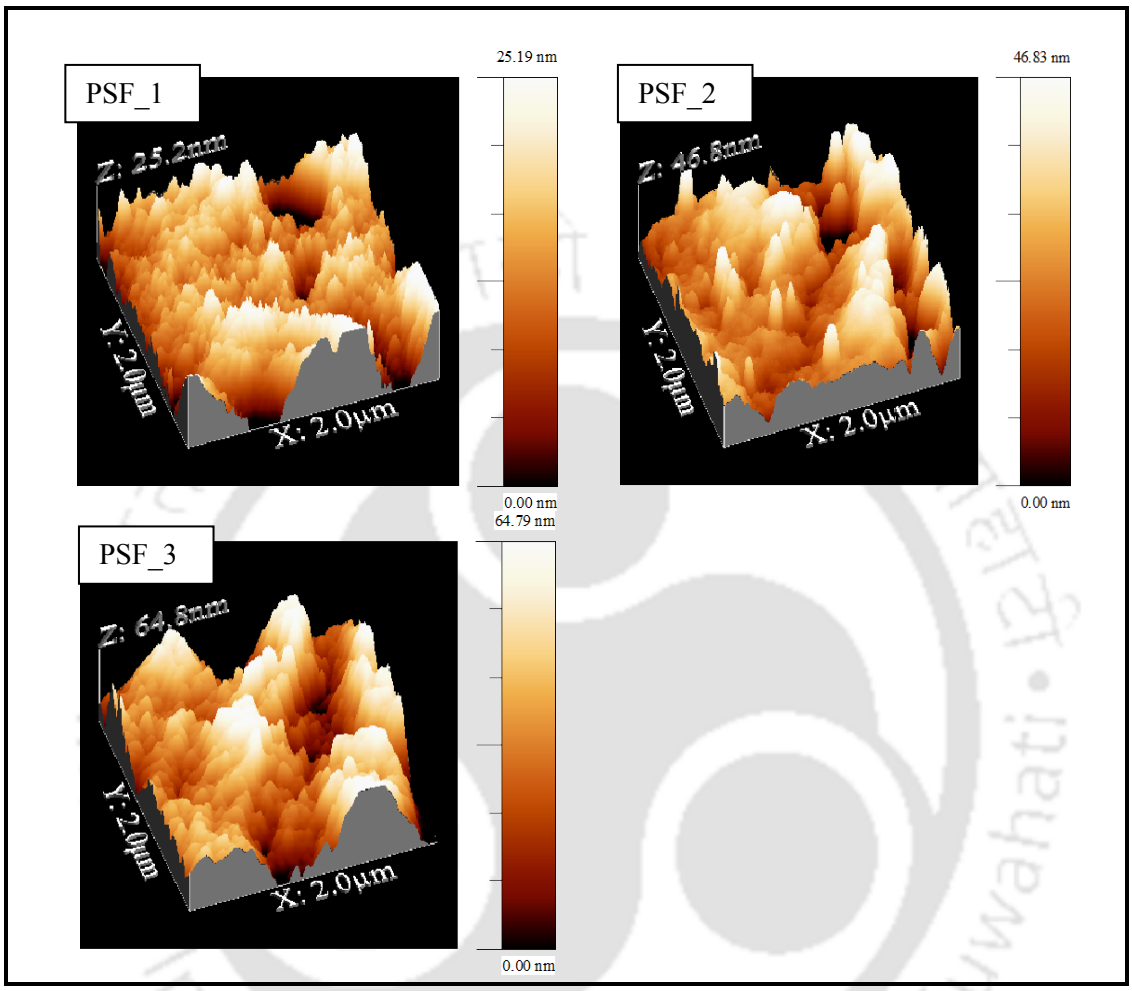

Figure 3.4: Three dimensional AFM surface images of PSF_1, PSF_2 and PSF_3.

Table 3.2: Surface roughness parameters of the membranes.

Membrane	RMS roughness (S_q) nm	Average roughness (S_a) nm	Average height (S_z) nm
PSF_1	5.81	4.52	12.70
PSF_2	10.36	8.14	23.75
PSF_3	15.70	12.68	32.37

3.3.3.4. Analysis of liquid–liquid displacement porosimetry results

The pore size, membrane permeability, pore number and pore area for each membrane were determined by Equations 2.1, 2.2, 2.4 and 2.5, respectively. Pore size distributions (PSD) of the membranes are shown in Figure 3.5. 27.5 % of the pores were in the size of around 2.5 nm for PSF_3. For PSF_1 and PSF_2 these numbers are 24 % and 24.1 %, respectively. Around 95 % of the pores were in the size of 2-5 nm for PSF_1, PSF_2 and PSF_3; which clearly brought them under UF range. PSD obtained from LLDP analysis was similar to the PSD observed by FESEM method. However, FESEM analysis using Image J software, bigger pores especially greater than 10 nm was measured on the surface of the membrane. It may be due to the fact that possibility this method may overrate the pore size by considering the wider pores on the surface [42]. Figure 3.6 depicts the variation of cumulative permeability (%) with pore size for PSF_1, PSF_2 and PSF_3 membranes. However, it is difficult and challenging to measure the accurate part of the larger pores (>100nm) and smaller pores (< 2 nm) by the LLDP method. Few larger pores are responsible for the membrane performance as a whole. Hagen–Poissuille equation explains that the enlarged pore radius can be responsible for increase in flux. Calvo et al. [102] observed the same results for UF membranes formed by track etched method. Number of pores calculated by LLDP method is placed in table 3.3. It is observed that, by the addition of PAA number of pores for all the membranes increases; especially adding the higher molecular weight PVP with PAA consequences in more porous membrane. It was observed that with increase in molecular weight of PVP number of pores for all the membranes increased, consequently more porous membrane were obtained. Number of pores per unit area (N_t) were found to be increased from 3.1×10^9 cm^{-2} to 16×10^9 cm^{-2} and these results were compared with Chakrabarty et al. [15] and found better in all aspects. The mean pore size r_m for membranes PSF_1, PSF_2, and PSF_3 was calculated as 4.98 nm, 4.58 nm and 1.8 nm, respectively.

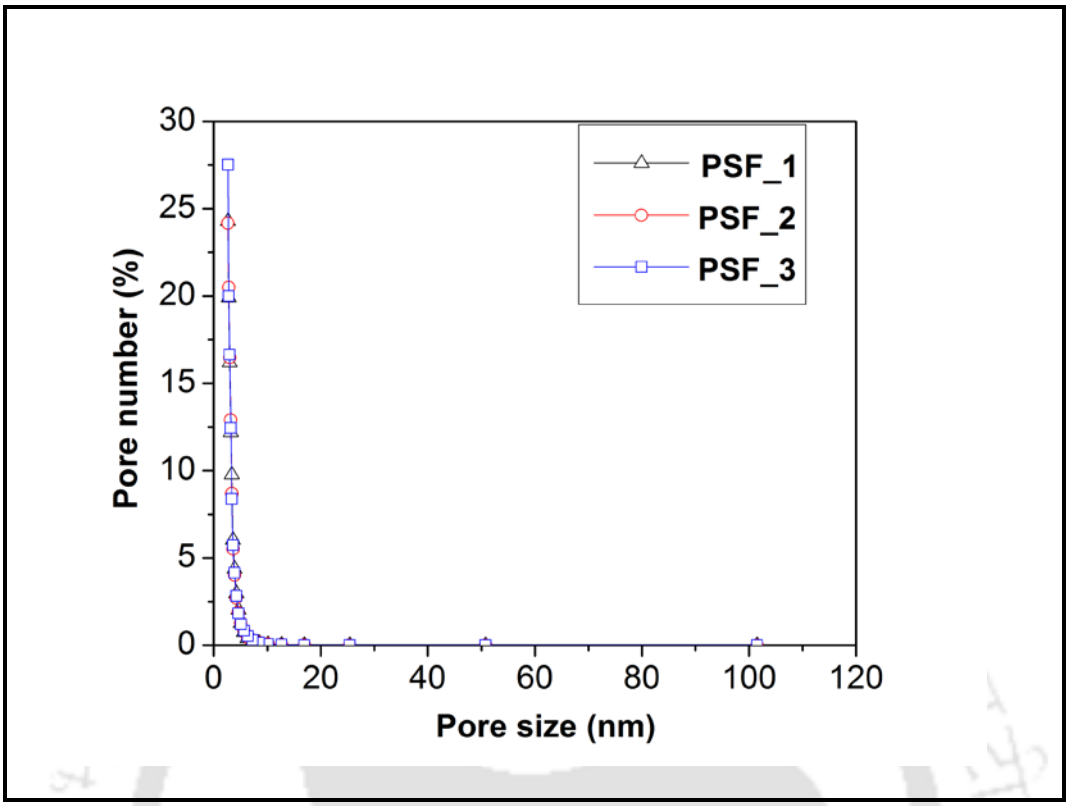

Figure 3.5: Pore size distribution of membranes PSF_1, PSF_2 and PSF_3 by LLDP.

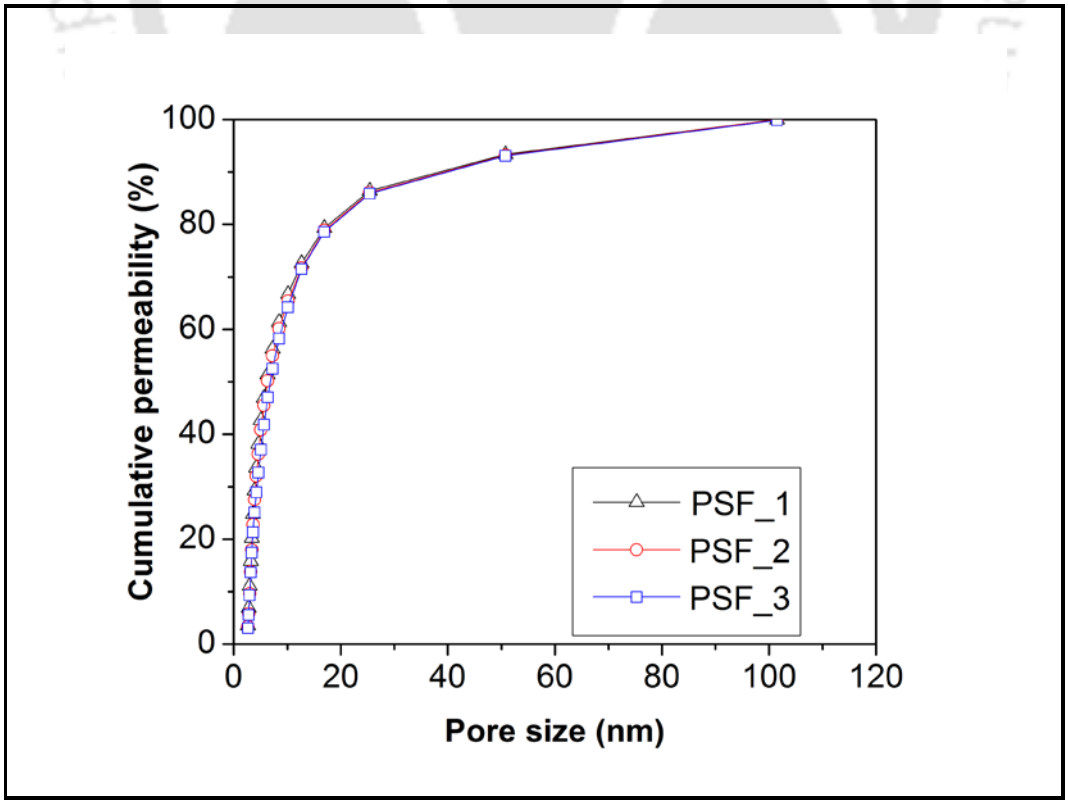

Figure 3.6: Variation of cumulative permeability (%) with pore size.

3.3.4. Permeation studies

PSF/PVP-PAA/NMP blended membranes were examined by permeation behaviour to observe the effect of PVP-PAA blend and different molecular weight of PVP. The membranes were characterized in terms of CF, hydraulic permeability and PWF. Effects of various parameters on EWC, hydraulic resistance and porosity were studied. Finally, the membranes were subjected to study for rejection as well as permeate flux behaviour with protein (BSA) at different pH. Results have been reported in subsequent sections.

3.3.4.1. Effect of molecular weight of PVP with PAA on CF

Compaction factor (CF) is an important parameter for relating the structure of the membrane, especially for the membrane sub-layer. Higher the CF, the membrane is more prone to be compacted because of the presence of large number of macrovoids in the sublayer. The effect of compaction time on PWF for all the membranes is shown in Fig. 3.7. For all the membranes, PWF is initially seen to decline sharply with time due to compaction and finally attain a steady state after around 3 h. This was due to the fact that the walls of the pores become denser, closer and uniform resulting reduction in pore size in addition to the flux for the duration of compaction [1]. From the figure it was found that the steady state PWF decreases with increase in molecular weight of PVP. For example, the steady state flux decreases from around 695 L/m^{2}h to 242 L/m^{2}h, when molecular weight increases from 24000 Da to 360000 Da. The CF for the membranes is presented in Table 3.3. It is seen that for PSF/NMP/PVP-PAA membranes (i.e. PSF_1, PSF_2 and PSF_3), the CF increases from 2.06 to 10.42 with increase in molecular weight of PVP. Similar observations were obtained by Chakrabarty et al. [15], Compaction factor increased from 1.76 to 6.67 for similar molecular weight of PVP, in their study. This may be due to the fact that addition of two

additives into the casting solution can either more enlarge or extra suppress the macrovoids in the membrane sublayer depending on their molecular weight as well as the type of solvent used [100]. In the present study, it is possible that for PSF/NMP/PVP-PAA system, increase in molecular weight of PVP has resulted in a membrane with a highly porous substructure due to presence of higher number of macrovoids which may be bigger than the pores formed by PVP alone. This fact can also be understood from the SEM figures (Fig. 3.2 (a)). This may be because of the reason; some PVP-PAA molecule present in the membrane matrix remained inside and gets swelled. Thus, slightly bigger pores were formed.

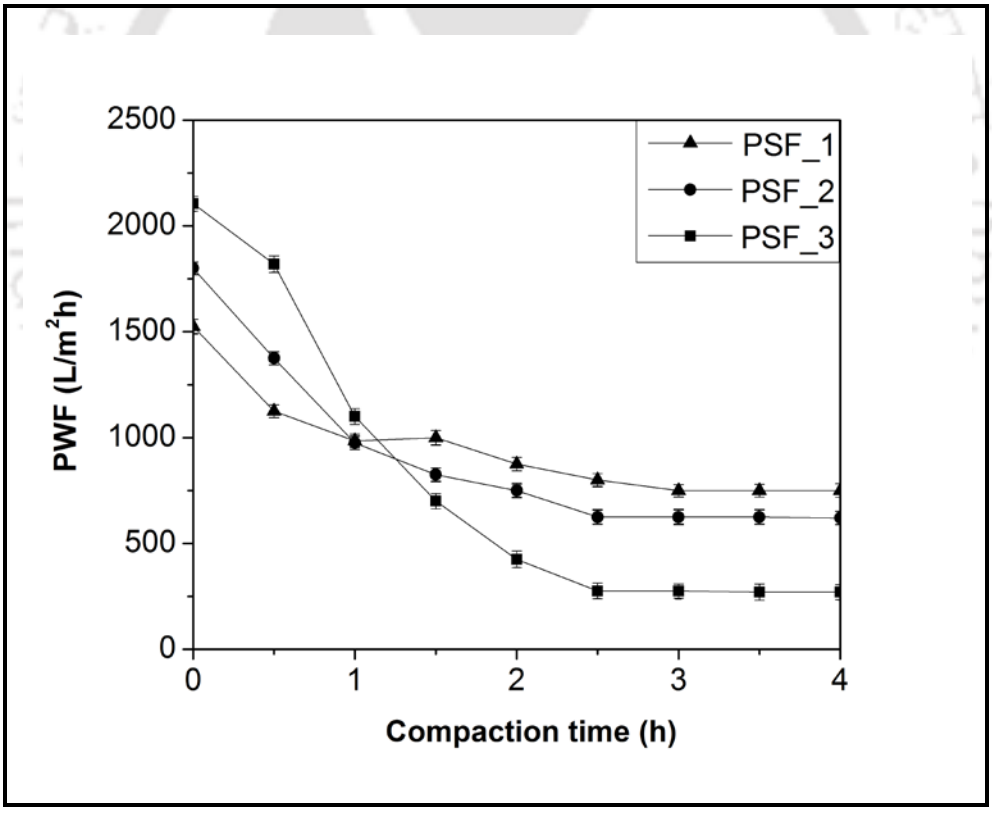

Figure 3.7: Flux profile during compaction at 240 kPa.

3.3.4.2. Effect of molecular weight of PVP on PWF and hydraulic permeability

Figure 3.8 depicts the effect of molecular weight of PVP on PWF at different transmembrane pressures. It was seen that within the range of 0 – 240 kPa, PWF (calculated using Eq. (2.10)) increases almost linearly with increase in transmembrane pressure, for all the membranes. It was also found that the PWF decreased with increase in molecular weight of PVP at a specific pressure which supports with the findings of the compaction study (Fig. 3.7). For example, at 137 kPa, the PWF decreases from around 501 Lm^{-2} h^{-1} to 275 Lm^{-2} h^{-1} when molecular weight of PVP increases from 24,000 Da to 360,000 Da.

Decline in flux with increase in molecular weight of PVP may be credited to the reduction in pore size at the top layer with higher molecular weight PVP. According to the literature [103, 104], although most of the additives are sluiced away during washing and coagulation time, but it is always not possible to remove the additives completely from the membrane matrix and it becomes more and more difficult with increase in molecular weight of additives i.e. PVP. Therefore, small amount of PVP which is hydrophilic in nature, may possibly to be entangled inside the membrane matrix lastingly. In this study, it may be possible that swelling of those trace amount of PVP - PAA molecules predominantly took place because of its hygroscopic and hydrophilic nature. This was happened due to pore blocking and consequently reduction in flux [105]. Swelling rate also increases with increase in molecular weight of PVP, later it caused the increased pore blocking. Higher molecular weight of PVP 360,000 Da containing membrane (PSF_3) had more suppressed sublayer which can be seen in Fig. 3.2 (a) that possibly to offer more resistance to water permeation consequential in lower flux. Comparison of present membrane morphology with literature [15] is presented in Table 3.3 and explained subsequently.

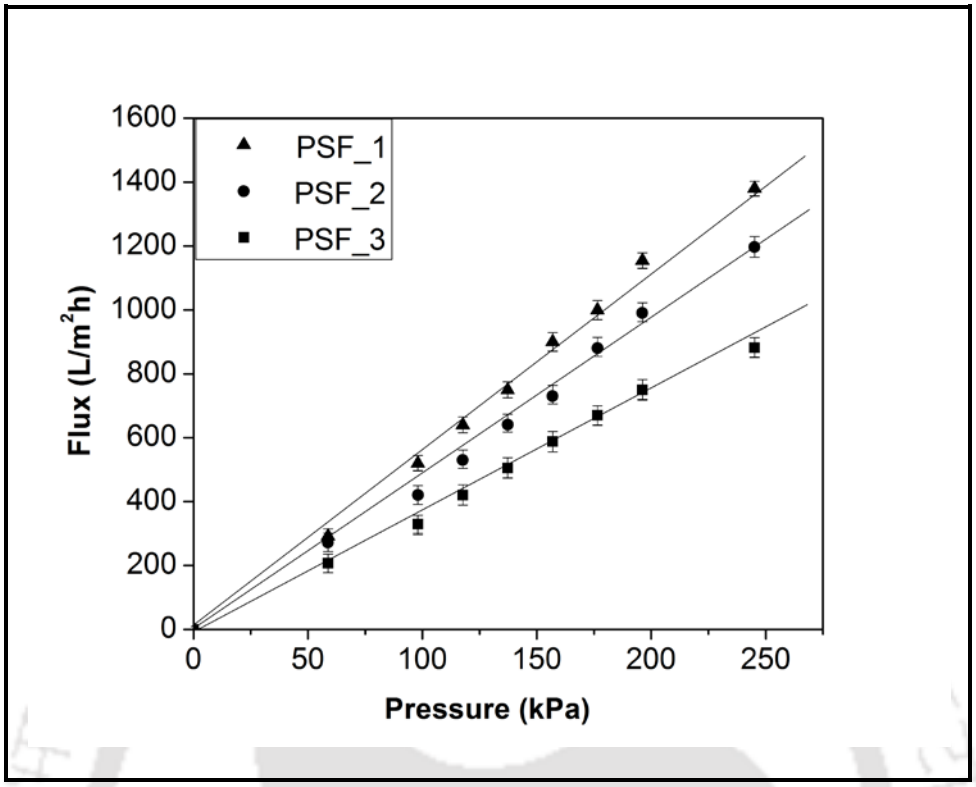

Figure 3.8: Effect of transmembrane pressure on PWF.

Table 3.3: Values of some characterization parameters of prepared membranes with different wt % of PVP with PAA.

Membrane	EWC (%)	Porosity	Contact angle (degree)	C.F.	Number of pores $N_t \times 10^{-9}$ (cm^{-2})
PSF_1	51.23	0.38	74±1	2.06	3.1±0.05
PSF_2	62.4	0.49	68±1	3.42	5.01±0.03
PSF_3	74.32	0.61	54±1	10.42	16±0.05
PSf1 [15]	46.8	-	-	1.76	2.6
PSf2 [15]	58.2	-	-	3.0	4.1
PSf3 [15]	73.4	-	-	6.67	9.8

3.3.4.3 Variation in EWC, porosity and hydrophilicity

EWC, Porosity and hydrophilicity of the membrane are important parameters in membrane preparation and separation processes. The EWC of all the membranes was calculated using Equation 2.12 and presented in Table 3.3. It has a strong relationship with PWF. It is an influential parameter for characterization of membrane and it was found from the calculations that increase in molecular weight of PVP, EWC of the membrane increases. The EWC for PVP 24000, PVP 40000 and PVP 360000 were 51.23 %, 62.4 % and 74.32 %, respectively. This increasing trend confirms the presence of increasing number of pores in the membrane with increase in the molecular weight of PVP (Table 3.3). The pores on the surface as well as cavities in the sublayer are responsible for accommodating water molecules in the membrane [106]. Chakrabarty et al. reported the similar trend with PSf/NMP/PVP and PSf/NMP/PEG membranes [15, 17]. Comparison with those literatures number of pores was found to be increased by addition of PAA in the membrane matrix. This may be because of the fact that water molecules may diffuse into the PVP - PAA molecule during immersion of membrane in water (wet phase inversion method) and disturb the network. Hydrogen bonds between PVP and PAA may have been broken and some PAA molecule came out to the surface of membrane caused more pores on the membrane surface.

Porosity of the membrane is another important parameter in membrane permeation and it is closely related to membrane performance. Porosity of the membrane was measured using Equation 2.13. Calculated values of porosity for membranes with different molecular weight of PVP and constant molecular weight of PAA are shown in Table 3.3. Porosity for PVP 24000, PVP 40000 and PVP 360000 is 0.38, 0.49 and 0.61, respectively. The porosity variation can be explained on the basis of kinetic and thermodynamic contemplation. With the addition of additives into the casting solution mainly two effects occur. Firstly, it causes thermodynamic improvement of the phase separation due to the reduced miscibility of the

casting solution in nonsolvent; this results in the immediate demixing. Secondly, it creates kinetic hindrance against phase separation due to increased viscosity of the solution; thus concluding in delayed demixing [1]. The viscosity of casting solution was measured as 0.136 Pa s, 0.151 Pa s and 0.176 Pa s for PSF_1, PSF_2 and PSF_3 membranes, respectively. With increase in viscosity, the ratio of nonsolvent inflow to solvent outflow increases, which according to the theory recommended by Young and Chen [107] consequences in a more porous membrane. The increase in membrane porosity with higher molecular weight of PVP was possibly due to decrease in miscibility of the casting solution in water. This in turn caused thermodynamic improvement in the demixing of casting solution. The small amount of PVP - PAA molecules left within the membrane matrix can be a cause of hydrophilic behaviour of membrane. Consequently, the entrapment of PVP - PAA molecules in membrane matrix improves the hydrophilic properties of membrane. Higher molecular weight of PVP tends to retained more residual of PVP - PAA.

Hydrophilicity of the membrane is important parameter for membrane permeation and separation processes and it is closely related to the morphology and PWF of the membrane. Surface hydrophilicity is often described by the contact angle [42, 108] measurement. In general, smaller the contact angle values higher the hydrophilicity. The values of contact angle of membranes are shown in Table 3.3. It can be found from Table 3.3 that contact angle decreases and porosity increases with the increase in molecular weight of PVP. The contact angle for PVP 24,000 is 74^0, for PVP 40,000 is 68^0, and for PVP 360,000 is 54^0. So, for membrane PSF_3, there is remarkable increase in hydrophilicity compared to membrane PSf3 [15]. The findings are uniform with morphology study of membranes. In case of porous membrane, contact angle depends upon porosity of the membrane. Higher the porosity lower will be the contact angle. Similar observation was also reported by Huang et al [109] during preparation of PVDF nanofibre membranes. All the three membranes were found better than

the corresponding membranes prepared by Chakrabarty et al. [15] with same molecular weight of PVP alone.

3.3.5. Ultrafiltration of BSA

Other than transmembrane pressure, the flux characteristics and rejection of the membranes mostly depend on the structure of the membrane and the properties of the feed solution. So, the prepared UF membranes were also characterized by measuring flux in permeation experiment and rejection by means of BSA solution (1000 mg/L). Change in permeate flux and rejection of BSA are the function of molecular weight of PVP as shown in Figs. 3.9 and 3.10. For all the membranes the feed solution was maintained at pH 4.8 (i.e. at IEP), at pH 7 and at pH 9.3. Morphological changes of the membrane including both top-layer and sub-layer due to the addition of PVP of different molecular weight with PAA is an important factor in protein transmission and rejection. Flux and rejection characteristics of BSA solution are also affected by the pH of the feed. Pore narrowing because of the protein adsorption (due to both hydrophobic and electrostatic interactions between the membrane surface and the protein molecules) may be reason of variation of flux and rejection of proteins by ultrafiltration membranes [110, 111].

3.3.5.1. Effect of molecular weight of PVP on the BSA flux and rejection

Figure 3.9 shows the average flux using BSA solution during 2 h ultrafiltration with respect to the molecular weight of PVP in membrane casting solution. The pH of the BSA solution was maintained at 4.8, 7 and 9.3. It may be seen from the figure that with increase in molecular weight of PVP from 24000 Da to 360000 Da, the flux slowly decreases from 12 to 2.2 L/m^{2}h, 47.5 to 28 L/m^{2}h and 31 to 16 L/m^{2}h when pH of BSA solution was 4.8, 7 and 9.3, respectively. This decreasing fashion offlux, irrespective of the pH of BSA, mig ht be due to

the formation of membranes with reduced average pore size on the top and suppressed sublayer due to addition of higher molecular weight PVP. The declination in BSA flux with increase in molecular weight of PVP could also be a consequence of increased susceptibility to pore plugging due to BSA adsorption. Initial flux declines are seen to be more pronounced and final fluxes are gradually lowered which is attributed to the loss of porosity by internal adsorption of protein leading to pore plugging [15].

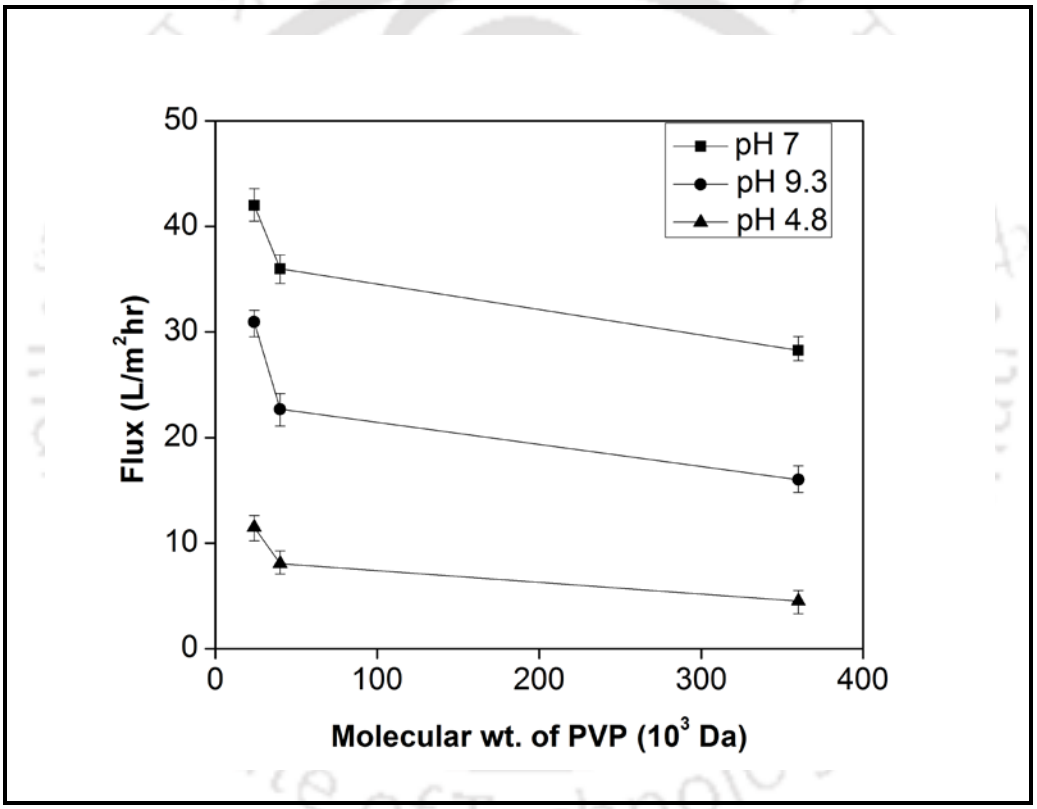

Figure 3.9: Effect of molecular weight of PVP on BSA flux at different pH at 150 kPa and concentration of BSA was 1000 mg/L for 2h UF.

Figure 3.10 depicts the result of the addition of different molecular weight of PVP in membrane casting solution on the BSA rejection at different solution pH of 4.8, 7 and 9.3. It can be seen from the figure that with the increase of molecular weight of PVP from 24000 Da to 360000 Da, the rejection increases from 65.5 % to 87.5 %, 35 % to 66 % and 5 % to 49 %

when pH of BSA solution was 4.8, 7 and 9.3, respectively. The protein rejection by ultrafiltration membranes can be explained with the concept of protein adsorption and subsequently pore contraction, as a result of both electrostatic and hydrophobic contacts between the membrane surface and the protein molecules [108, 110, 112]. Denser top layer of higher molecular weight of PVP with PAA also offered greater resistance towards the protein molecule for all pH values caused increasing tendency in percentage rejection. Lower molecular weight of PVP with PAA blended membrane has shown minimum rejection may be because of the fact that adsorption of protein on pore wall has less effect on pore narrowing due to their relatively high pore size compared to PVP 40,000-PAA and PVP 360,000-PAA. Chakrabarty et al. [15] observed the same results for a system of PSF/NMP/PVP.

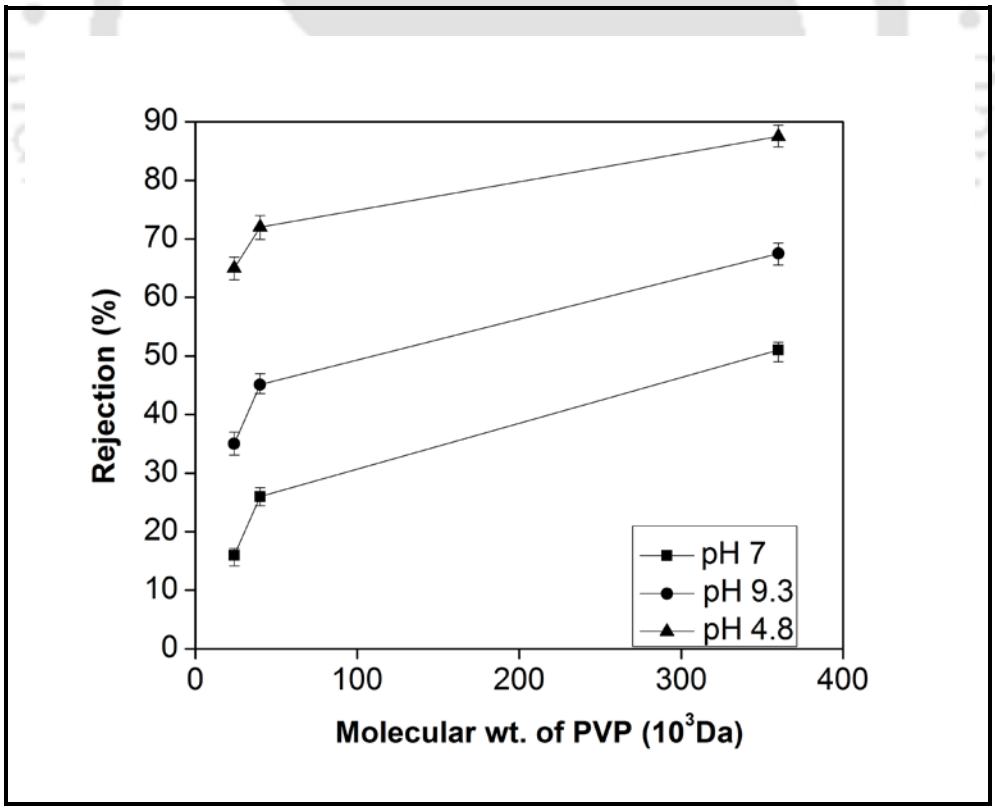

Figure 3.10: Effect of molecular weight of PVP on BSA rejection at 150 kPa and concentration of BSA was 1000 mg/L for 2h UF.

3.3.5.2. Effect of pH of BSA on flux and rejection

The BSA rejection strongly depends on pH. Rejection of BSA through different membranes was calculated by Equation 2.15. Flux was minimum and rejection was maximum at iso-electric point (IEP) of BSA solution. At IEP (i.e. at pH 4.8), BSA molecules have no charge and they are least soluble at its IEP. The BSA molecules rested in its most compact size when get deposited on the membrane surface and form slightest permeable layer [110, 112, 113]. This compact layer is accountable for least flux and highest BSA rejection. At neutral pH, BSA molecules have net negative charge and expand because of electrostatic repulsion; these effects would likely to give an additional permeable deposited layer and should give a lower rejection and higher flux than at pH 4.8. Change in BSA solution flux with pH can be explained by protonation and deprotonation capability of PAA, as its acid dissociation constant pKa is about ~ 4.9, carboxylic group of PAA deprotonated to carboxylate ions. These carboxylate ions provide high charge density in the PVP - PAA blended membranes, which results in expansion of PVP - PAA molecule and expansion of molecule blocks the membrane pores to some extent. Again on additional increment of pH, there is more loss of flux, which was because of the electro viscous effect [114]. This physical phenomenon occurs when an electrolyte solution is passed through a narrow capillary or pore with charged surface [115]. In this study at pH above 7, i.e. at pH 9.3 membranes and permeating liquid both have negative charge. As the pH increases, more negative charge comes to the permeating liquid, so membrane repels the permeating liquid from passing through the membrane pores and that feel more revulsion from the membrane and consequently more loss of flux. Higher rejection and lower flux at pH 9.3 compared to pH 7 can also be explained by Coulomb's law.

Summary

With increasing molecular weight of PVP in PVP-PAA blend number of pores per unit surface area (porosity) and EWC (%) of the prepared membranes was found to be increased. All the three membranes were found better than Chakrabarty et al. [15] in all aspects such as EWC (%), PWF, porosity, BSA rejection (%) at pH 9.3, number of pores N_t, (cm^{-2}) and area of pores, A_t (cm^2).

Chapter 4

Preparation and characterization of poly(vinyl pyrrolidone-co-isatoic anhydride) copolymer added pH responsive hydrophilic polysulfone ultrafiltration membrane

Flat sheet asymmetric polymeric membranes were prepared from homogeneous solution of polysulfone (PSF) by phase inversion method using N-methyl-2-pyrrolidone (NMP) as solvent and discussed in this chapter. Copolymer of vinyl pyrrolidone (VP) and isatoic anhydride (IAH), poly(VP-co-IAH) was used as the polymeric additive in the casting solution. Radical initiated copolymerization was used for the preparation of copolymer poly(VP-co-IAH) from N-vinyl pyrrolidone and isatoic anhydride. AIBN was used as initiator for the synthesis of copolymer. Morphology and structure of the resulting membranes were observed by field emission scanning electron microscope (FESEM). The pore number, pore permeability and their distribution and average pore size of the membranes were determined by the liquid-liquid displacement porosimetry (LLDP) method. The permeation performances of the membranes were evaluated in terms of pure water flux (PWF), hydraulic permeability and solute rejection, while hydrophilicity was evaluated in terms of porosity, equilibrium water content (EWC) and water contact angle. Solution of bovine serum albumin (BSA) was used to study the permeation performance of prepared membranes.

4.1. Experimental

4.1.1. Materials

PSF and NMP were used as base polymer and solvent respectively, in the membrane casting solution. Copolymer poly(VP-co-IAH) was used as additive in the casting solution and BSA

Content of this chapter has been submitted for publication as below:

N. Sharma, M.K. Purkait, Effect of synthesized copolymer poly(vinyl pyrrolidone-co-isatoic anhydride) on the pH responsive and hydrophilic behaviour of polysulfone ultrafiltration membrane, J. Membr. Sci.

was used as model foulant in UF experiments. Detail of all the materials used in the present chapter is given in Table 2.1 of chapter 2.

4.1.2. Membrane preparation

Flat sheet PSF membranes were prepared by phase inversion method as described in section 2.2 of chapter 2 with a thickness of 100 μm. Composition of different membrane casting solution is given in table 4.1.

Table 4.1: Composition of membrane casting solutions containing different wt % of poly(VP-co-IAH).

Membrane	Composition			
	Base polymer	Additive	Solvent	Additive
M_0	PSF (14 %)	poly(VP-co-IAH) (0%)	NMP (80%)	VP (6%)
M_2	PSF (14 %)	poly(VP-co-IAH) (2%)	NMP (84%)	VP (0%)
M_4	PSF (14 %)	poly(VP-co-IAH) (4%)	NMP (82%)	VP (0%)
M_6	PSF (14 %)	poly(VP-co-IAH) (6%)	NMP (80%)	VP (0%)

4.2. Membrane characterization

4.2.1. Microscopic study

Field emission scanning electron microscope (FESEM) was used for microscopic observation. Skin layer thickness and the pore size on the membrane surface were measured with the help of image J software. A number of FESEM images were taken at different magnification for both top surface and cross section of the prepared membranes. Computerized analysis of FESEM [94] image was extensively performed for this study. The

average pore size, number of pores and pore area distribution of the prepared membranes were determined by LLDP as discussed in section 2.3.1 of chapter 2.

4.2.2. Permeation experiments

Permeation experiments were performed as discussed in the section 2.3.3 of chapter 2. Initially all the membranes were compacted for 3 h at 275.8 kPa which was higher than the maximum operating pressure (150 kPa) in this chapter. Flux was collected after every half an hour interval until flow stabilization through the membrane was achieved. The compaction factor (CF) was calculated as the ratio of initial pure water flux ($PWF_{initial}$) to steady state pure water flux ($PWF_{steady\ states}$).

4.2.2.1. Pure water flux (PWF) and hydraulic permeability (P_m)

For pressure-driven membrane separation processes hydraulic permeability is an important parameter to be considered. Pure water flux (PWF) was measured by allowing deionized water to pass through the compacted membrane. Flux values of pure water at different transmembrane pressures (ranging 0–275.8 kPa) were measured under steady state condition using equation 2.10. P_m (L/m^{2}h kPa) is evaluated from the slope of the plot of J_w vs P. Hydraulic permeability was calculated by equation 2.11.

4.2.2.2. Equilibrium water content (EWC), porosity and hydrophilicity

EWC and porosity are also important parameters for the characterization of membrane. EWC is a measurement technique for porosity, since it is directly related to the porosity of membrane. It also gives indication about the hydrophilic or hydrophobic nature of the membranes. EWC and porosity at room temperature was calculated by equations 2.12 and 2.13, respectively. The hydrophilic property of the membrane was evaluated by measuring

the static contact angle between the de-ionized water and membrane films at ambient condition at room temperature. Contact angle measurement technique is discussed in section 2.3.5 of chapter 2.

4.2.3. Ultrafiltration experiment

Ultrafiltration experiments were performed in the stainless steel cell discussed in the preceding chapter to study the impact of different concentrations of copolymer on permeate flux and solute separation behaviour of the fabricated membrane. Bovine serum albumin (BSA) which is a type of protein was used for separation experiments. It was dissolved in deionized water at room temperature and the concentration was kept constant at 1000 mg/L for all the filtration experiments. The pH acts as a key factor in protein-membrane interface [110, 111]. Therefore, pH of the BSA solution was maintained at four values: 7 (neutral condition), 3 (acidic condition), 4.8 (i.e. at isoelectric) and 10 (i.e. basic condition) for finding the pH dependency of flux and rejection for all the membranes.

4.3. Result and discussion

4.3.1. Preparation and characterization of copolymer poly(VP-co-IAH)

4.3.1.1. Synthesis of poly (VP-co-IAH) copolymer

Radical initiated copolymerization was used for the preparation of copolymer poly(VP-co-IAH) by N-vinyl pyrrolidone (average molecular weight of 111 Da,) and isatoic anhydride (molecular weight 163 Da). AIBN was used as initiator for the synthesis of copolymer in 1, 4-dioxane. IAH and monomer of N-VP (the mass ratio = 4:6) were dissolved in 1, 4-dioxane with total concentration of 33 wt %. The AIBN was added to the solution at 0.4 % of the total weight of the N-VP and IAH. Mixture was reacted in a three necked round bottom flask

(heated in an oil bath) under nitrogen atmosphere at 65^0C. The reaction mixture was continuously stirred for 48 hours. After reaction, the product was cooled to room temperature and precipitated in acetone. The precipitate was rinsed a number of time with acetone for the removal of residual monomer and initiator. The copolymer was then dried at 40^0C under vacuum to constant weight for 2 days.

4.3.1.2. Investigation of FTIR-ATR spectra of copolymer poly(VP-co-IAH)

Figure 4.1 (a) depicts the FTIR spectra of synthesized copolymer. Peaks at 2940 cm^{-1} and 1618 cm^{-1} are characteristic peak of $–CH_2–$ and –NH stretch, respectively present in copolymer. Peaks at 1405 cm^{-1} and 746 cm^{-1} confirm the presence of C=O group and benzene ring structure, respectively in the copolymer.

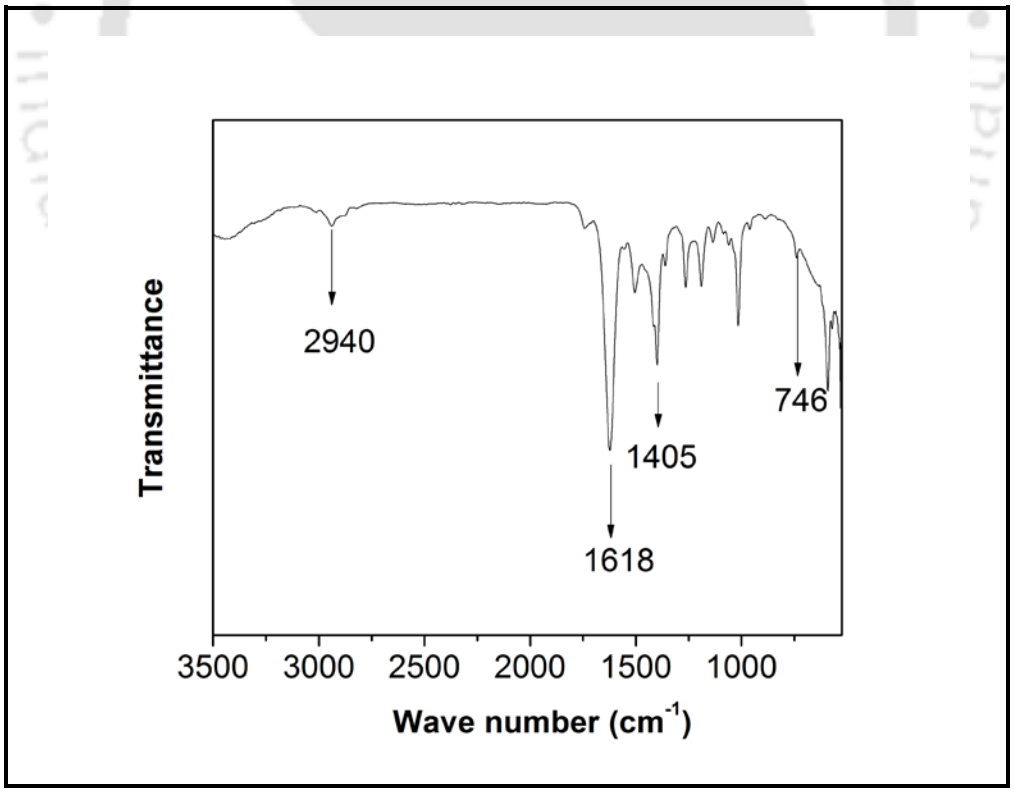

Figure 4.1 (a): FTIR spectra of copolymer poly(VP-co-IAH).

4.3.1.3. FTIR-ATR spectroscopy analysis of plain and copolymer poly(VP-co-IAH) containing membranes

Figure 4.1 (b) depicts the FTIR spectra of plain and poly(VP-co-IAH) containing membranes. FTIR analysis shows that the poly(VP-co-IAH) molecules were present in the membrane. As shown in Figure 4.1 (b) peak at 572 cm^{-1} is characteristic peak of –C-S stretching present in PSF. Peak at 864 cm^{-1} shows the presence of –C-O group in the PSF. Peaks at 1494 cm^{-1} and 1681 cm^{-1} are the characteristic peak of C-H and C=C stretching in the copolymer, respectively. 2180 cm^{-1} depicts the presence of –NH group in copolymer.

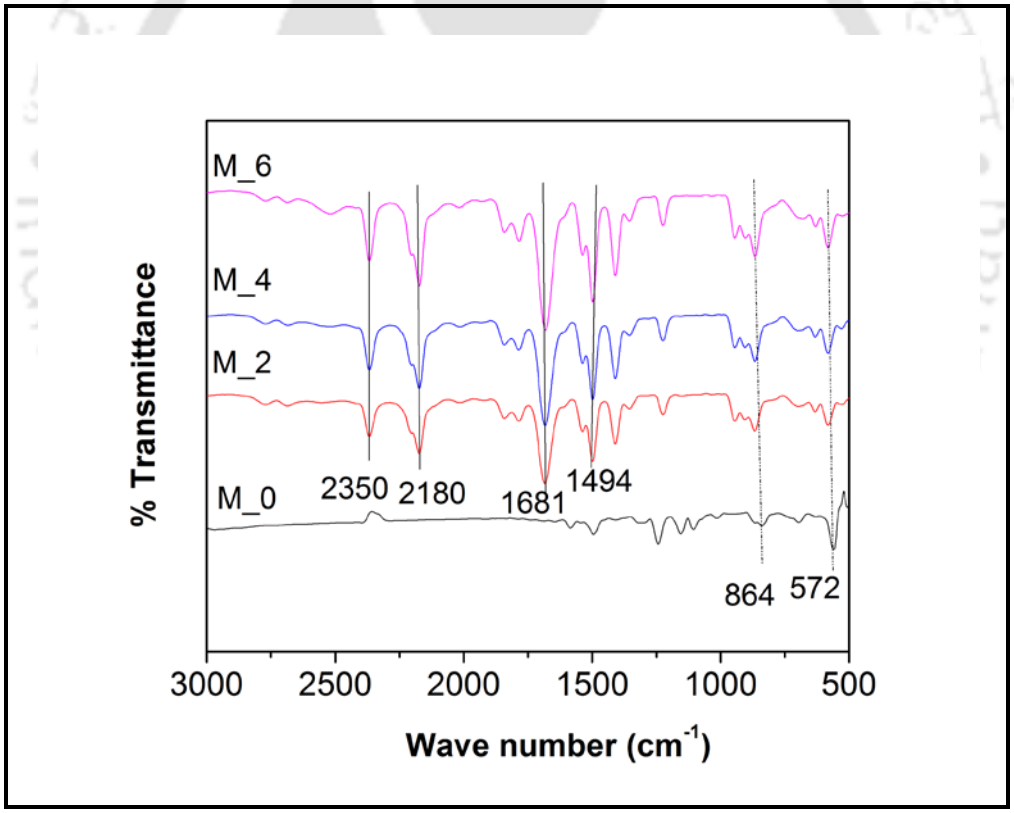

Figure 4.1 (b): FTIR spectra of membrane M_0, M_2, M_4 and M_6.

4.3.1.4. ^{1}HNMR analysis of copolymer poly(VP-co-IAH)

Figure 4.2 depicts the ^{1}H NMR spectra of copolymer. For poly(VP-co-IAH), shifts at δ= 1-2 and at δ= 2.2 show the presence of C–H and N–H bond present in copolymer. Shifts at δ= 6.9–7 confirms the presence of aromatic rings present in copolymer. Shift at δ= 7.4 shows CH_2 group of copolymer. Combined observations of FTIR spectra and NMR shifts confirm the formation of copolymer poly(VP-co-IAH).

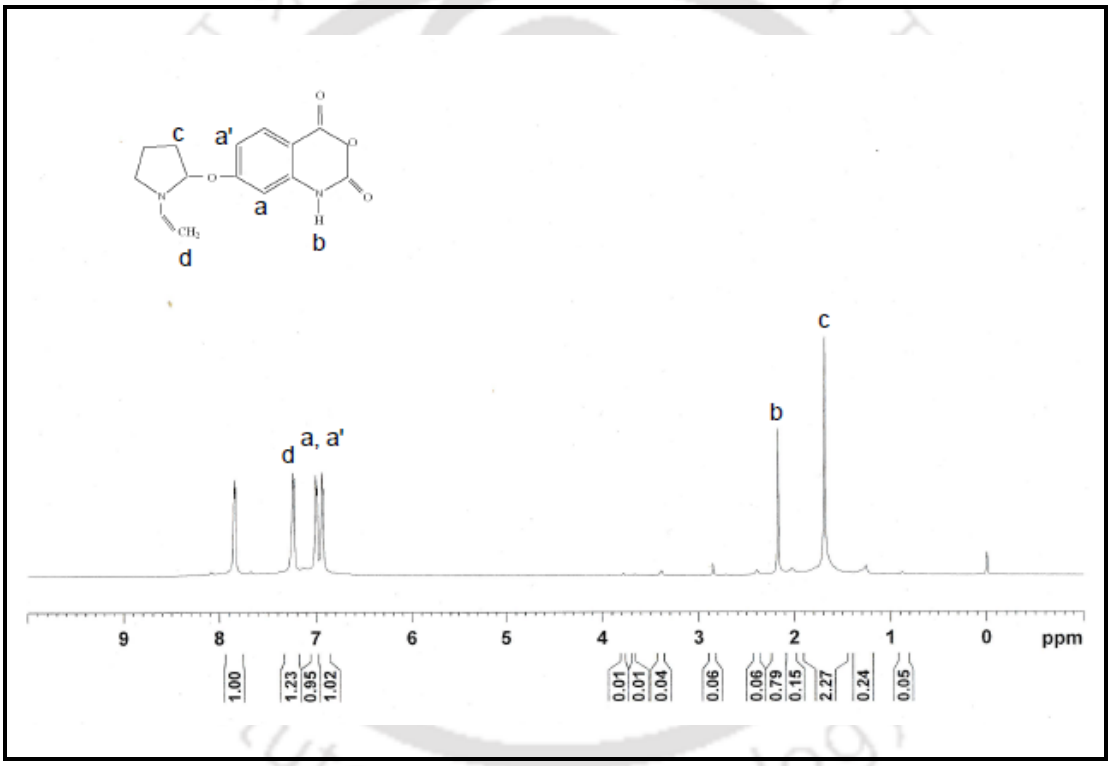

Figure 4.2: ^{1}H NMR spectra of copolymer.

4.3.2. Morphological study

Phase inversion process was opted for the preparation of plain PSF/NMP/VP and different amount of copolymer with PSF based membranes. High resolution FESEM was used for analyzing the surface and cross sectional morphology of the prepared membranes with different compositions. AFM images were taken for determining the surface roughness

parameters. Higher magnification was in favour of top surface images for finding the pore size on the surface of the membranes, so these images were taken at 100 KX magnification whereas, cross-sectional images were captured at 1 KX magnification by FESEM. quantitative information like average pore size, pore number, pore density and pore area was determined by liquid-liquid displacement porosimetry method.

4.3.2.1. FESEM study of cross section

Figure 4.3 depicts the cross sectional FESEM images of different membranes blended with various amount (in wt %) of copolymer. Cross sectional images clearly show that all the membranes have asymmetric structure. Except for membrane M_0, all the membranes possess dense uppermost skin layer with porous sub-layer and sponge like base layer. The permeable sub-layer consists of groove like structure. Hydrophilicity of NMP for water which consequences in immediate demixing is responsible for these structures [1]. But, by increasing the wt % of copolymer poly(VP-co-IAH) from 2 to 4 wt % in membrane, these grooves like configuration became prominent and longer cavities were developed beneath the top layer. It may be due to the fact that viscosity of membrane casting solution increased by the addition of poly(VP-co-IAH), which consequently resulted in faster demixing between non-solvent phase and polymer rich solvent phase during phase inversion [116]. However image for M_6 membrane shows shorter sub layer pores, it may be because of fact that after a certain concentration of copolymer in casting solution, it may enhance the viscosity at that level which can decline the phase separation between aforementioned phases during wet phase inversion process.

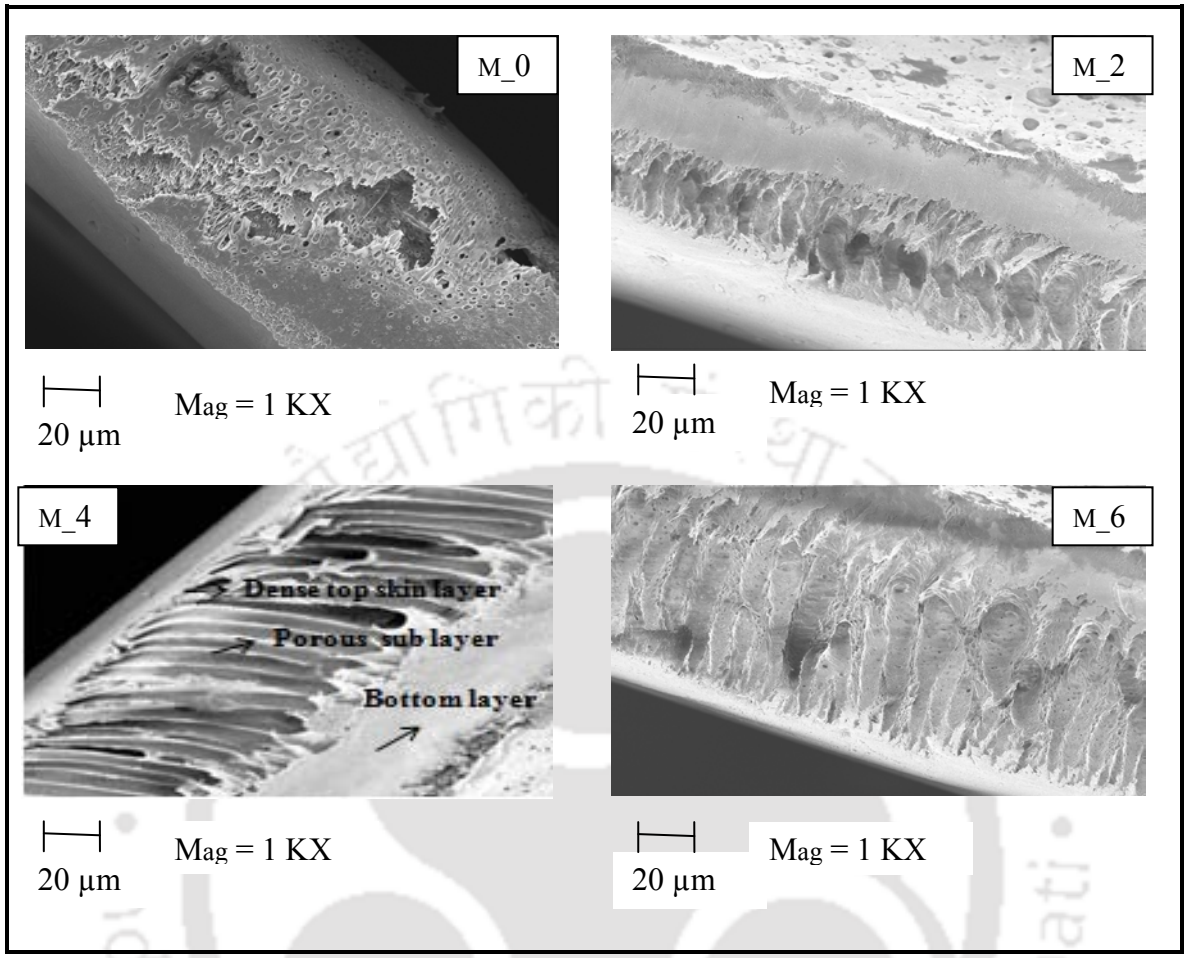

Figure 4.3: Cross sectional FESEM images of membrane M_0, M_2, M_4 and M_6.

4.3.2.2. FESEM study of top surface

Figure 4.4 depicts the FESEM images of top surface of the plain M_0 and different wt % of copolymer blended PSF membranes. It can be seen that, the plain PSF membrane's top surface is relatively less rough than the copolymer containing membranes. Surface roughness increases with the addition of copolymer and also with increased wt % of copolymer in blended membranes up to 4 wt %, after that the surface roughness reduces. This trend of roughness may be because of the fact that copolymer settles on the membrane surface. Number of these structures also enhanced up to 4 wt % of copolymer after that the surface become saturated and roughness decreases. Mean pore size on surface and macro-voids present in the support layer are important for determining flux and selectivity of membranes,

so managing the formation and size tuning of pores is significant [117]. Possibly spinodal demixing is responsible for the formation of top surface. Since, during formation of top layer the diffusion process became fast for the polymer solution to become highly unstable and cross the spinodal curve [100].

Pore size was determined using Image J software from FESEM results and shown in Figure 4.5 for various membranes. Average pore size was calculated as 19.75 nm, 15.68 nm 8.23 and 13.21 nm for M_0, M_2, M_4 and M_6 membrane, respectively. It may also be seen that the pore size distribution for M_2, M_4 and M_6 is almost same, as maximum number of pores were in the range of 5-10 nm size.

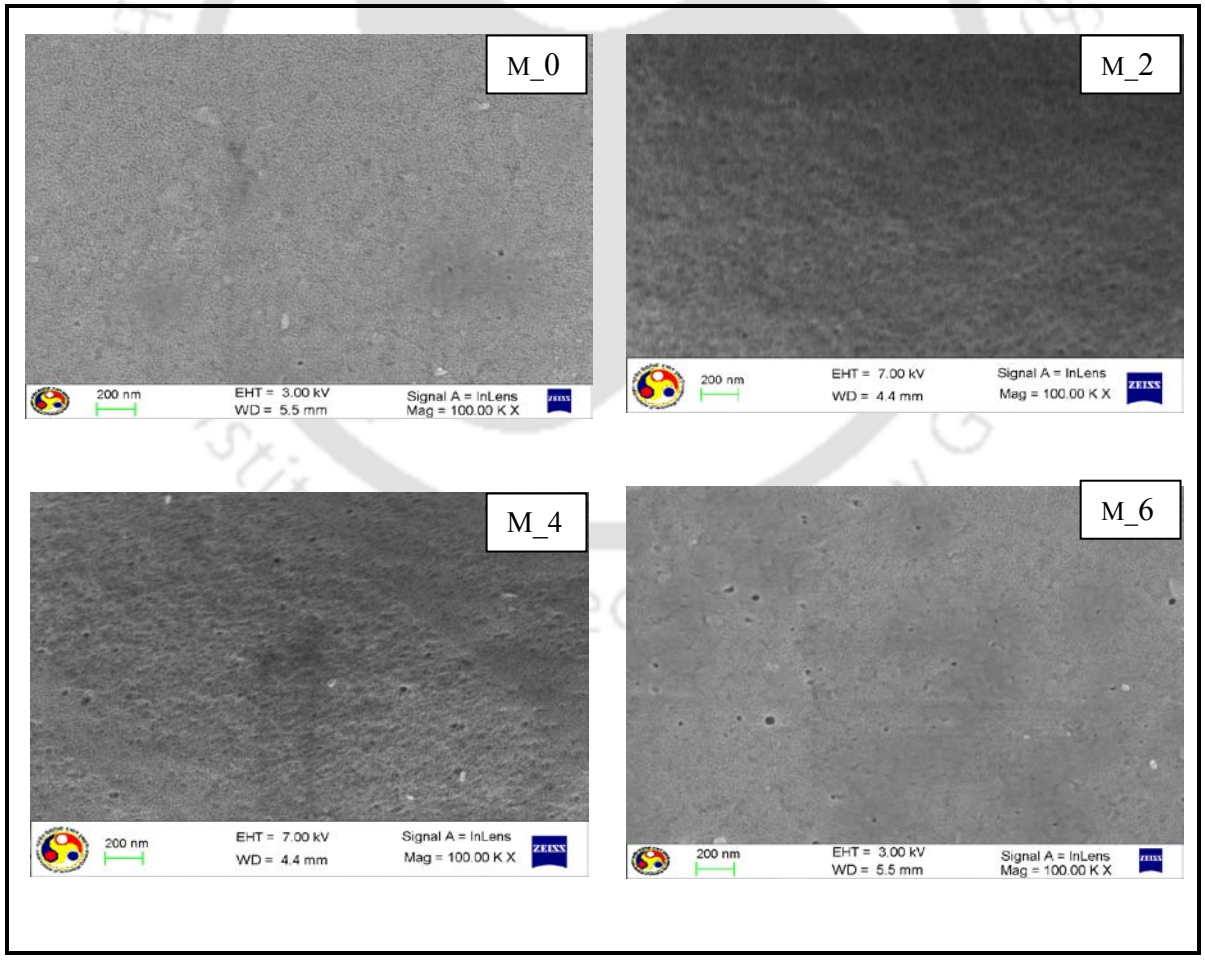

Figure 4.4: Cross sectional FESEM images of membrane M_0, M_2, M_4 and M_6.

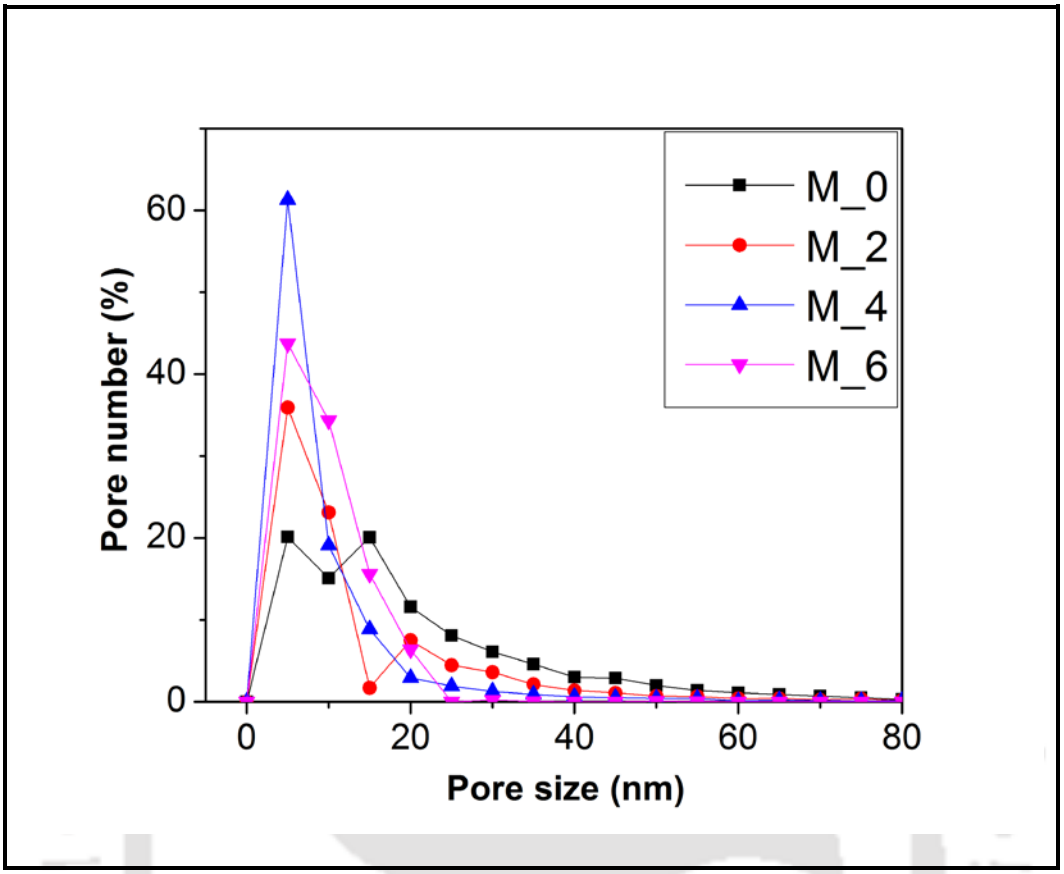

Figure 4.5: Pore size distribution of membranes by FESEM.

4.3.2.3. AFM studies

Figure 4.6 depicts the AFM images of plain PSF membrane and modified membranes with different wt % of copolymer. It is observed from AFM topography images and their 3D reproductions that plain PSF membrane has relatively smooth surface and as the wt % of copolymer increases in the membrane their top surface becomes rougher upto 4 wt %. Average height (S_z), root mean square (RMS) roughness (S_q) and average roughness (S_a) were measured. RMS roughness was increased with increasing the copolymer poly (VP-co-IAH) up to 4 wt % (Table 4.2). It can be described by the fact that porosity was increasing i.e. the number of pores on the surface was increasing [89, 118], due to the presence of copolymer. However, after 4 wt % the RMS roughness decreases since pore size increases. Contact angle values also support the findings of AFM image analysis. The reason for

increase in roughness is the addition of amphiphilic copolymer. The long chain of the poly(VP-co-IAH) stays with the bulk PSF phase and hydrophilic end group comes to the surface, also bulk phase amphiphilic molecules have tendency to migrate towards top surface during phase inversion process. This results in rougher surface as the wt % of amphiphilic copolymer increases upto 4 wt % [92, 119].

4.3.2.4. Effect of weight % of copolymer on hydrophilicity

Figure 4.7 depicts the contact angles of all the four membranes. It was found that contact angle decreases by the addition of copolymer for all the membranes. However it was lowest for membrane with 4 wt % copolymer i.e. more hydrophilic and consequently more porous membrane than plain and higher wt % copolymer containing membrane as shown in figure 4.6. Contact angle was measured as 76.25^0, 74.35^0, 61.65^0 and 64.85^0 for M_0, M_2, M_4 and M_6, respectively. Pore area and number of pores also increased by the addition of poly(VP-co-IAH). It is the indication of increased hydrophilicity with addition of copolymer in this study.

Table. 4.2. Surface roughness parameters of membranes by AFM analysis.

Membrane	Roughness parameters		
	S_a(nm)	S_q(nm)	S_z(nm)
M_0	3.4	4.2	8.9
M_2	5.1	6.2	12.8
M_4	5.2	8.7	14.1
M_6	5.2	6.5	13.7

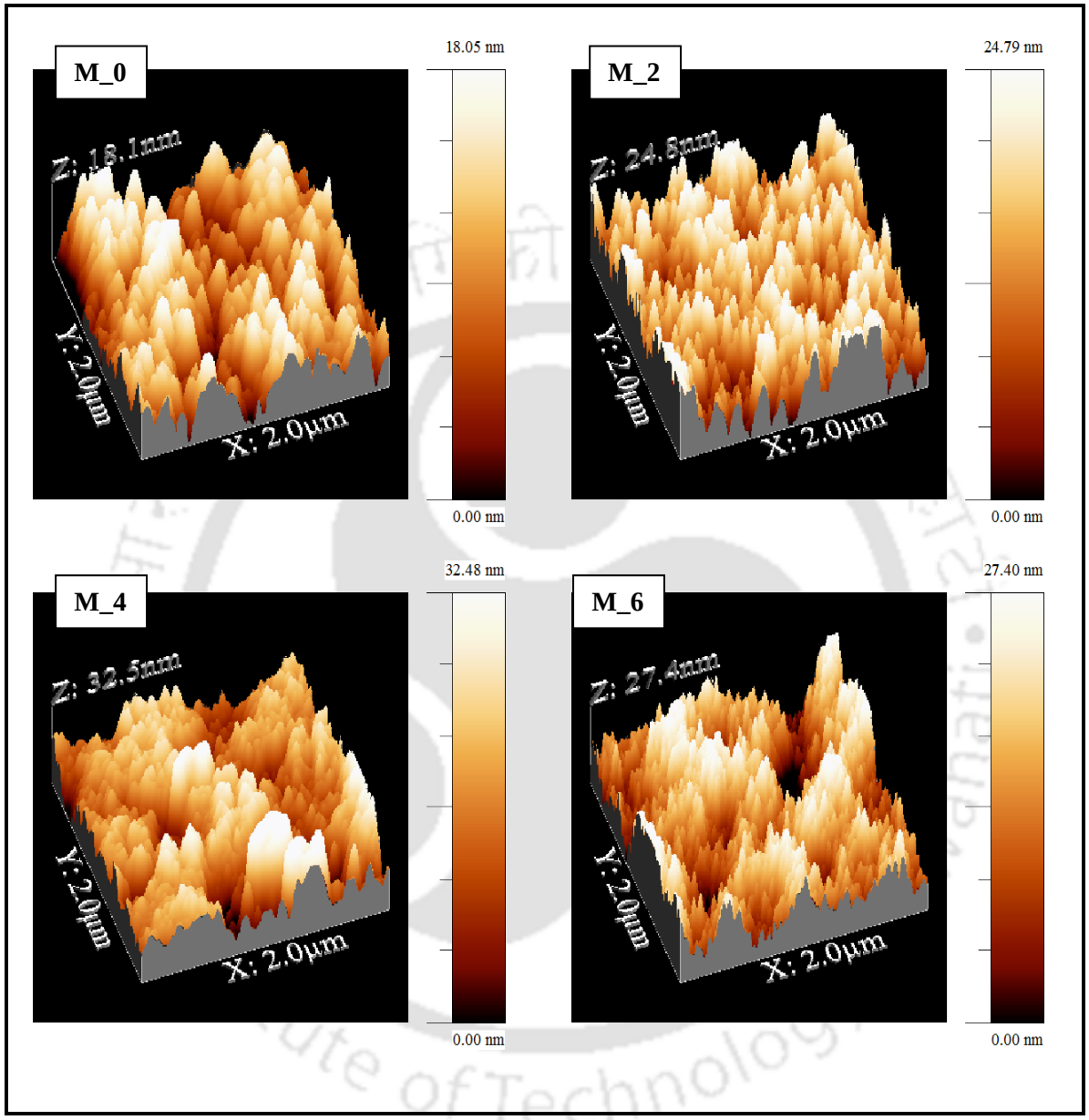

Figure 4.6: Effect of poly(VP-co-IAH) copolymer wt % on surface roughness of PSF membranes.

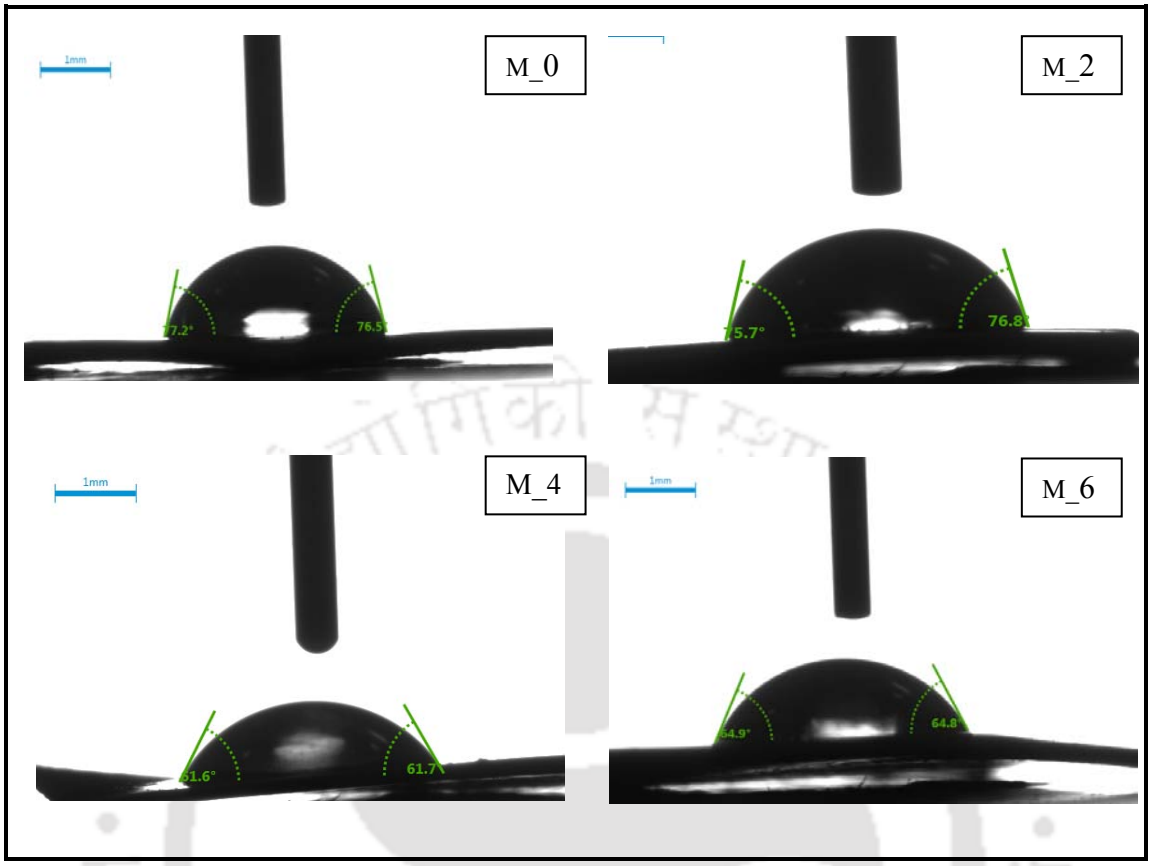

Figure 4.7: Contact angles for membrane M_0, M_2, M_4 and M_6.

4.3.3. Liquid–liquid displacement porosimetry studies

Figure 4.8 shows the pore size distribution by LLDP and flux profile for the prepared membranes. The pore size, membrane permeability, pore number and pore area for each membrane were determined by Equations 2.1, 2.2, 2.4 and 2.5, respectively. Trend of LLDP flux curve was nearly same for all the membranes. For starting the flow, minimum required pressure was 28 kPa. Wetting liquid (water rich) was replaced after this pressure by penetrating liquid (alcohol rich). Hence, by increasing the pressure on the membrane, smaller pores get opened and after substitution of the wetting liquid is completed in the pores, the flux starts to increase slightly as shown in the right side of Fig. 4.8. It was observed that flux

increases gradually at initial stage with rising pressure. However, flux was found to be increased rapidly from 166 kPa to 350 kPa and subsequently flux rising became gradual.

Comparable tendency in pore size distribution (in percentage) plot was also observed in left part of Fig. 4.8. Pores larger than 4 nm sizes were almost negligible. It was also found that most of the pores (around 62%) were less than 2 nm size. However, number of pores further decreased when size of pores was less than 2 nm. This trend was nearly similar for all the membranes. Pores having size less than 3 nm were around 96 % for all the fabricated membranes. This fact brought them under the UF category. Results of LLDP investigation were summarized in Table 4.3. It was observed that by increasing the wt% of copolymer, total number of pore per unit area (N_t) was found to be increased and consequences in more porous membranes. Total number of pores for Membrane M_0, M_2, M_4 and M_6 was calculated as 0.234×10^8 m^{-2}, 0.248×10^8 m^{-2}, 0.313×10^8 m^{-2} and 0.272×10^8 m^{-2}, respectively. Figure 4.9 and 4.10 shows the cumulative permeability and cumulative numbers of pores with respect to the pore radius, respectively by LLDP method. It was found that the permeability was increasing by the addition of copolymer. The total hydraulic permeability coefficient L_n for all the four membranes was calculated 1.9 ms^{-1} MPa^{-1}, 2.02 ms^{-1} MPa^{-1}, 2.56 ms^{-1} MPa^{-1} and 2.25 ms^{-1} MPa^{-1} for membrane M_0, M_2, M_4 and M_6, respectively. Average pore radius for membrane M_0, M_2, M_4 and M_6 was calculated as 1.94 nm, 1.92 nm, 1.81 nm and 1.86 nm, respectively. These observations point to the fact that addition of copolymer in membrane casting solution improves the performance of membranes. These results are in accordance with morphological analysis of the membranes.

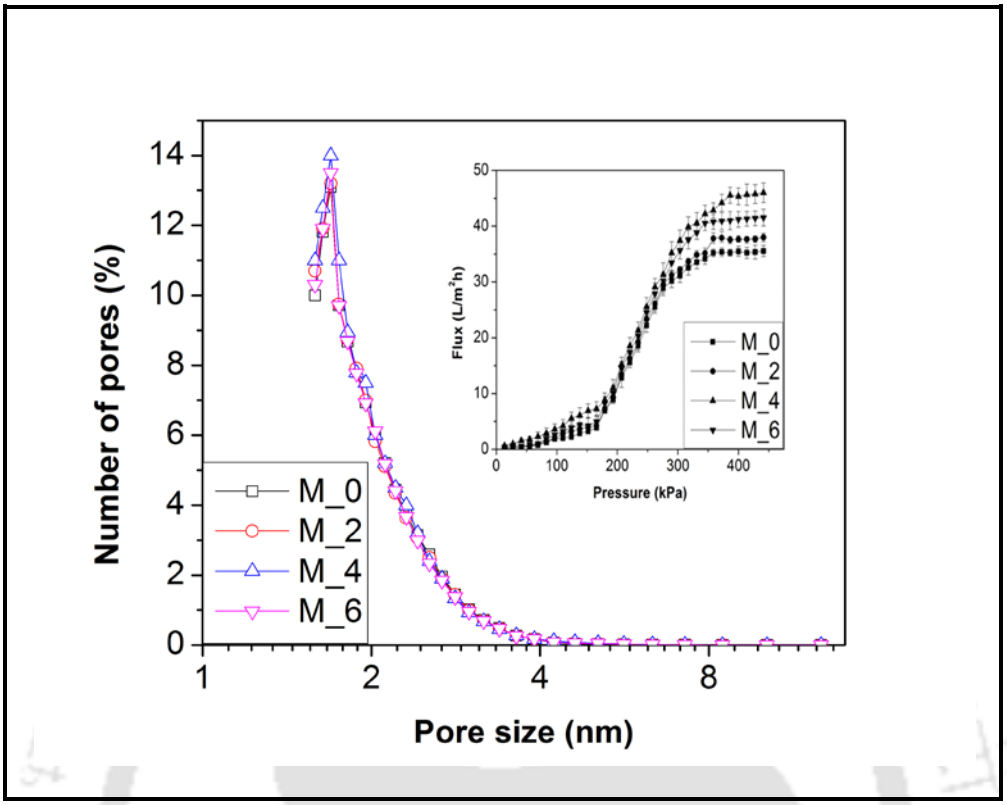

Figure 4.8: Pore size distribution of membrane M_0, M_2, M_4 and M_6 by variation with poly (VP-co-IAH) content in membranes through LLDP and flux profile during LLDP.

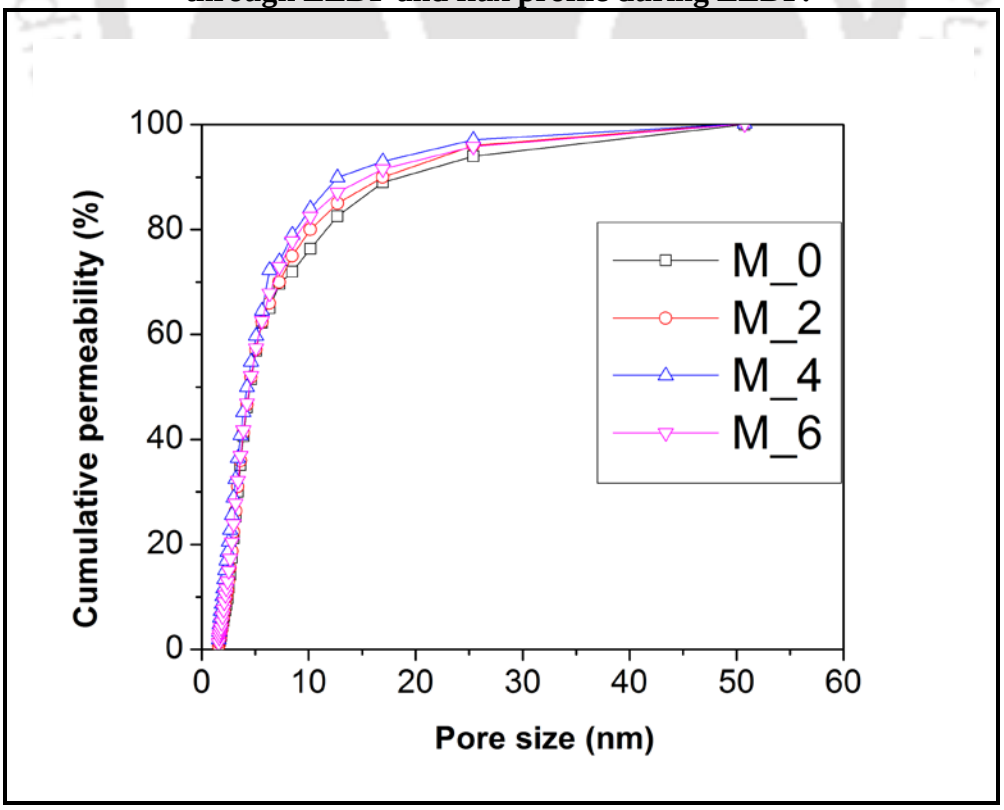

Figure 4.9: Cumulative permeability by LLDP method.

Table. 4.3. Characterization parameters of the membranes by LLDP method.

Membrane	L_n (ms^{-1} MPa^{-1})	r(nm)	Pore number $N_t(m^2)\times10^{-8}$	$A_t(m^2) \times 10^{10}$
M_0	1.9	1.94±0.03	0.234±0.02	2.76±0.01
M_2	2.02	1.92±0.02	0.248±0.04	2.87±0.02
M_4	2.56	1.81±0.03	0.313±0.03	3.21±0.01
M_6	2.25	1.86±0.01	0.272±0.04	2.95±0.01

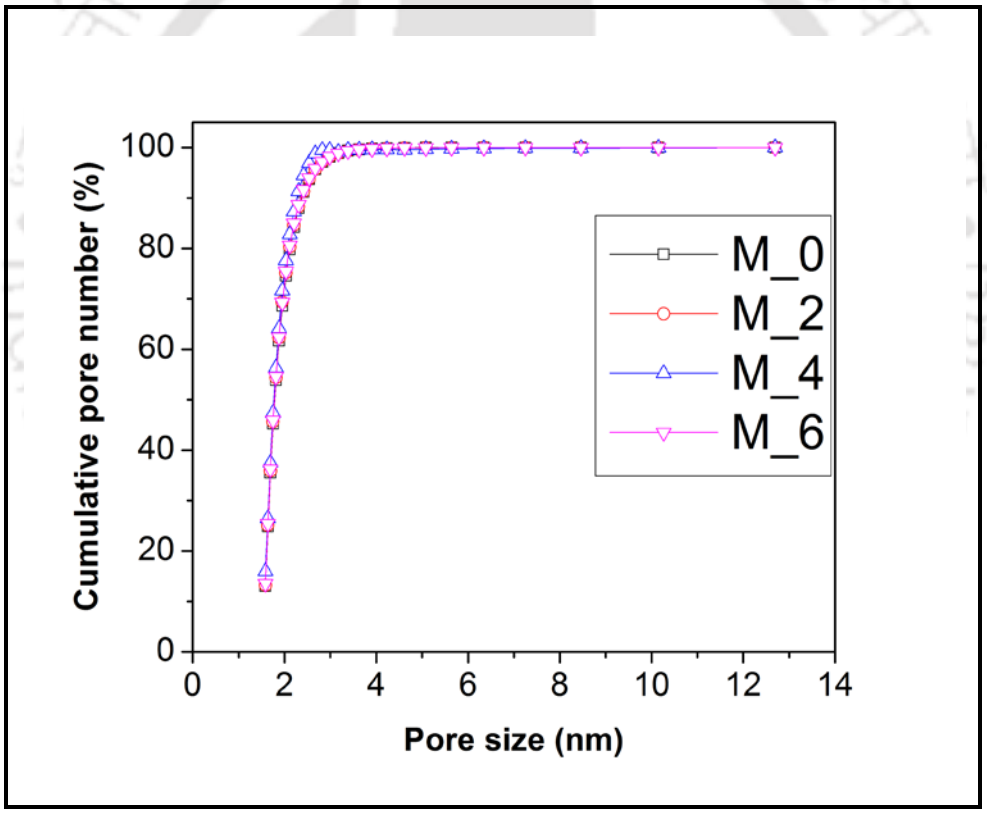

Figure 4.10: Change in cumulative pore number (%) with pore size.

4.3.4. Permeation studies

M_0, M_2, M_4 and M_6 membranes were examined by permeation behaviour for observing the effect of addition of copolymer poly(VP-co-IAH). Various characterization parameters such as PWF, CF and hydraulic permeability were measured. Lastly, the rejection performance and permeation behaviour of all the membranes at different pH were measured using BSA protein solution (1000 mg/L). Results have been reported in subsequent sections.

4.3.4.1. Effect of addition of copolymer poly(VP-co-IAH) on compaction factor

Membrane sub-layer described by compaction factor (CF). It is an important factor for finding the structure of the membrane. Increased CF shows the presence of large number of macrovoids in the sublayer those are likely to be compacted. Figure 4.11 depicts the compaction time versus PWF for all the membranes. Initially all the membranes were compacted for 3 h at 275.8 kPa and flux was collected after every half an hour interval. For all the membranes, PWF is initially seen to be declined with respect to time. Compaction is possibly responsible for this declination of flux and finally attains a steady state after around 2 h. It may be because of the fact that the pore size got reduced since the walls of the pores become closer and denser for the duration of compaction [1]. Steady state PWF was found to be increased with the addition of copolymer as shown in Figure 4.11. For instance, the steady state flux was increased from around 37.2 L/m^2h to 55.34 L/ m^2h for membrane M_0 and M_4, respectively. In other words by increase in wt % of copolymer up to 4 wt % steady state PWF increases. These results are in agreement with some previously done works [120-123]. After that concentration (i.e. 6 wt %) declination in flux was observed. It may be because of the fact that the viscosity of casting solution crossed the optimum limit and hampered the pore formation. However, all the copolymer containing membranes show higher flux than

plain membrane M_0. CF for the membranes is presented in Table 4.4. For the membranes M_0, M_2, M_4 and M_6 the CF was calculated as 3.3, 3.2, 2.7 and 2.9, respectively.

Table 4.4: Effect of copolymer poly(VP-co-IAH) on some characterization parameters of prepared membranes.

Membrane	C.F.	Permeability P_m (L/m^2hkPa)	EWC (%)	Porosity	Contact angle
M_0	3.3	0.16	47	0.38	76.25
M_2	3.2	0.17	53.1	0.42	74.35
M_4	2.7	0.28	56.6	0.57	61.65
M_6	2.9	0.22	54.4	0.46	64.85

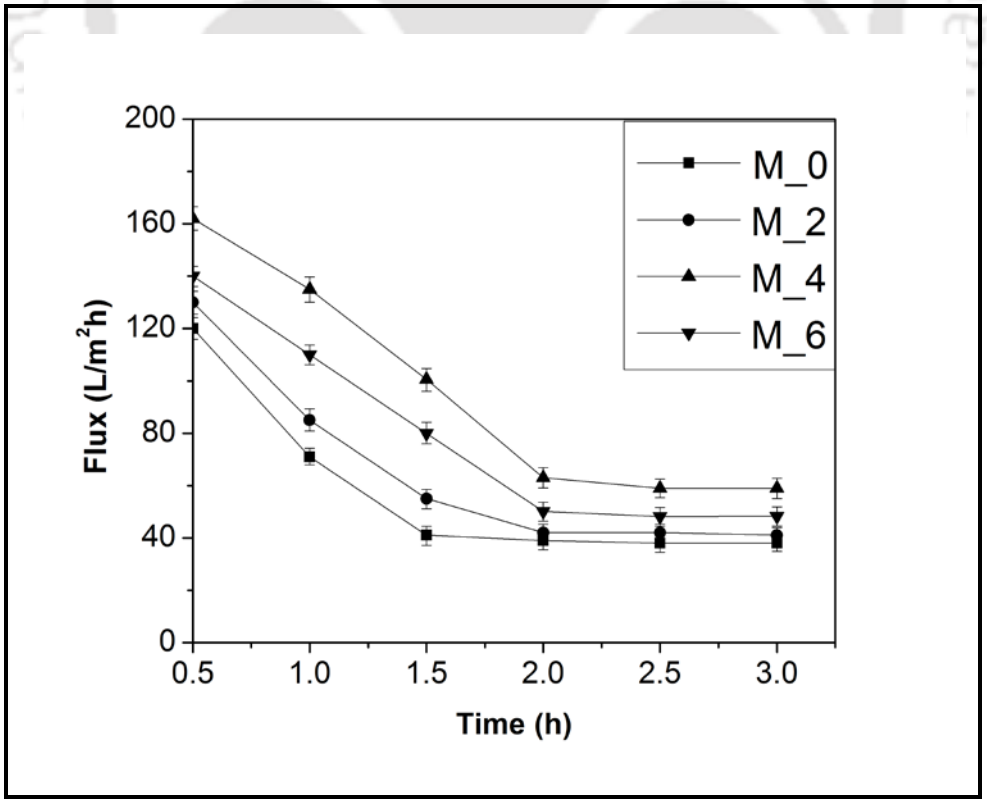

Figure 4.11: Flux profile during compaction for membranes at 275.8 kPa.

4.3.4.2. Effect of copolymer on PWF and Hydraulic Permeability

Figure 4.12 depicts the effect of transmembrane pressure on PWF for M_0, M_2, M_4 and M_6. These experiments were performed at different transmembrane pressures between 30 kPa to 275.8 kPa. It was observed for all the membranes that PWF increases almost linearly with increase in pressure. This was due to the rise in effective transmembrane pressure which is driving force for water permeation. These results confirm the findings of compaction studies as shown in figure 4.11, as well as the water contact angle measurements shown in figure 4.7. Flux profiles based on transmembrane pressure were used to determine the hydraulic permeability (P_m) of the membranes. It was found to be improved from 0.16 to 0.28 L/m^2 h kPa for the membrane M_0 to membrane M_4 (containing 4 wt % copolymer), respectively. Results of the pure water permeability and P_m analysis depict that addition of copolymer significantly reduces the chance of formation of relatively bigger pore as well as improves the pore forming capacity in the membranes; it is theoretically related to permeability [124]. These outcomes are consistent with the morphological analysis and hydrophilicity along with pore size distribution results of the membranes discussed in the previous sections. These observations are in accordance with the results of some previous works [120, 125-127].

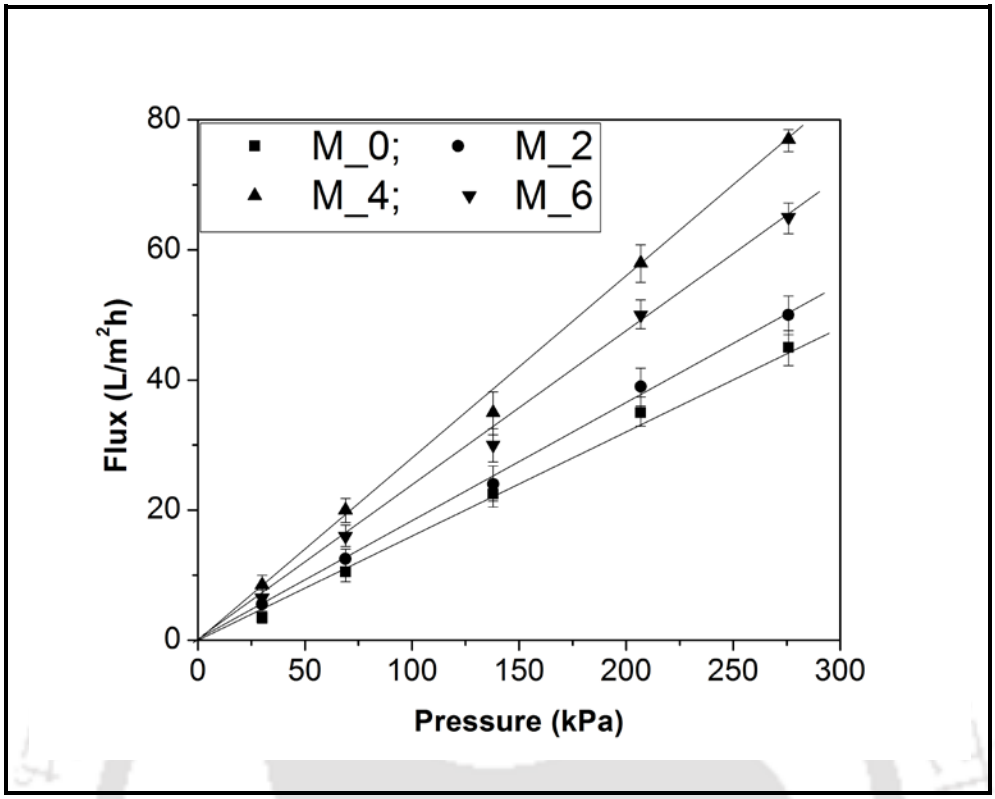

Figure 4.12: Effect of transmembrane pressure on PWF for M_0, M_2, M_4 and M_6 membranes.

4.3.4.3. Membrane characterization by EWC, porosity and hydrophilicity

Standard technique [15] was used for calculating the EWC of all the membranes and presented in Table 4.4. PWF is closely related to the EWC and it is a significant parameter for membrane characterization. It was observed that by the addition of poly(VP-co-IAH) with PSF membrane, EWC was increased. However, it was maximum for 4 wt % of copolymer. The EWC for membrane M_0, M_2, M_4 and M_6 was calculated as 47, 53.1, 56.6 and 54.4, respectively (Table 4.4). This increasing tendency approves the occurrence of increased number of pores in the membrane by the addition of copolymer. The pores present in the sublayer with the pores on the top surface provide space for accommodation of water molecules in the membrane. This may be because of the presence of hydrophilic copolymer in sublayer pores.

Hydrophilicity and porosity of membrane are significant factor for describing membrane permeation behaviour and separation processes and it has close contact with morphology and PWF of the membrane. Contact angle measurement gives insights about surface hydrophilicity [96]. In general term, value of hydrophilicity increases as contact angle decreases. The porosity (ε) of the membranes was determined by gravimetric method, using standard equation [15, 89]. Values of contact angle measured for all the membranes are shown in Table 4.4. It is confirmed from Table 4.4 that contact angle decreased and hydrophilicity got increased by the addition of copolymer in the membrane. The contact angle for M_0, M_2, M_4 and M_6 is 76.25^0, 74.35^0, 61.65^0 and 64.85^0, respectively. Similarly, Porosity also increases from 0.38 to 0.57 for membrane M_0 to M_4, respectively. Change in porosity can be explained on the basis of two facts one is kinetic and another is thermodynamic contemplation. As soon as additives are added into the casting solution two major effects take place. Firstly, phase separation due to the reduced miscibility of the casting solution in nonsolvent because of the thermodynamic improvement; this results in the instant demixing. Secondly, it produces kinetic obstruction to the phase separation due to increased viscosity of the solution [1]. M_4 depicted the maximum hydrophilicity by the addition of copolymer it may be because of the fact that 4 wt % of copolymer possess optimum viscosity for demixing [42, 74]. Figure 4.3 clearly depicts that without and with addition of copolymer in the membrane sublayer affects the formation of the pore. By the addition of copolymer and consequently formation of finger like cavities in the sublayer which are not formed in plain membrane M_0.

4.3.5. Ultrafiltration of BSA

Trans-membrane pressure is a key factor for finding the characteristic of flux other than that, the characteristics of flux and solute rejection behaviour through the membranes mostly assessed by the morphology of the membrane and the feed solution properties, specially its pH. So, membranes were also tested by flux measurement at different pH.

4.3.5.1. Effect of addition of copolymer on BSA flux at normal pH

Figure 4.13 shows the effect of addition of copolymer poly(VP-co-IAH) on the BSA flux through all the membranes at normal pH (i.e. pH 7). It was confirmed that maximum flux was found for membrane M_4. It may be attributed to the fact that by the addition of copolymer into the PSF casting solution, hydrophilic functional groups were increased. On the other hand, copolymer increased the top surface hydrophilicity of membranes consequently increase in flux. For example BSA flux for M_0, M_2, M_4 and M_6 were found as 6.8 L/m^2h, 11.7 L/m^2h, 18.3 L/m^2h and 15.1 L/m^2h, respectively. Moreover, addition of copolymer altered the membrane morphology as well as sub-layer pore structure (Figure 4.3) and hence porosity was increased. Varying morphology possesses a significant control over increment of BSA flux of the modified membranes.

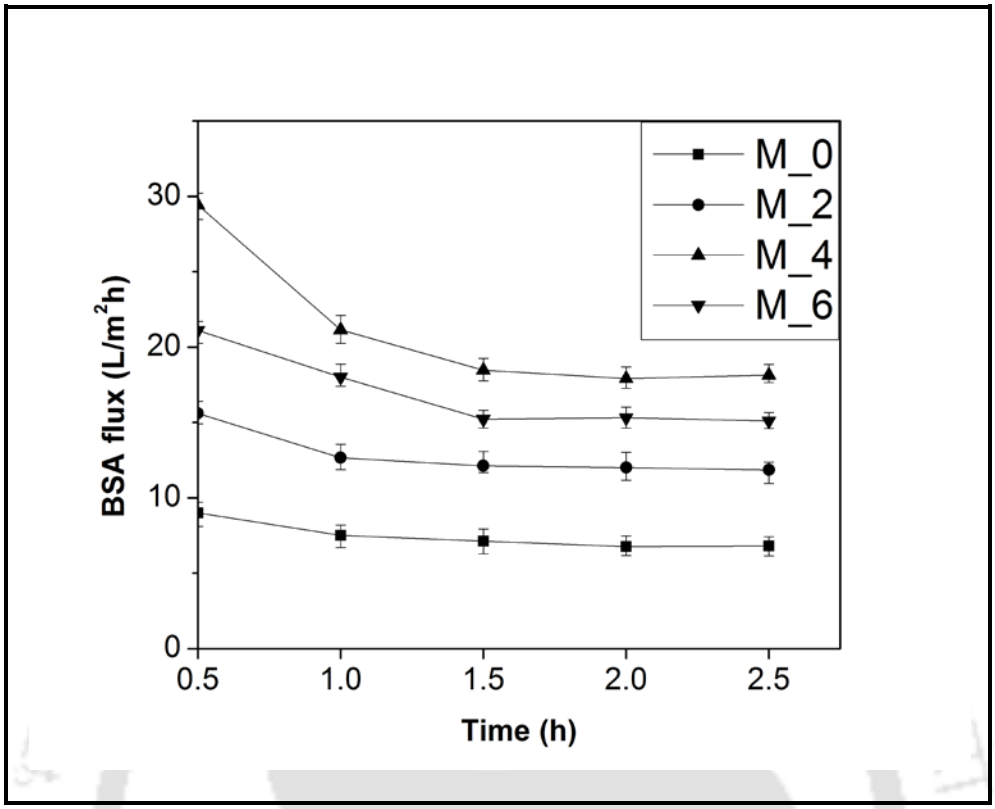

Figure 4.13: BSA Flux vs time for BSA concentration 1000mg/L and at Pressure 150 kPa.

4.3.5.2. Effect of addition of copolymer on BSA rejection at normal pH

Figure 4.14 depicts the effect of addition of different wt % of copolymer poly(VP-co-IAH) on the BSA rejection behaviour. BSA molecules have net negative charge at pH 7, in addition to the negative charge present in copolymer because of the $-COO^-$ group. This fact consequences in intense revulsion of BSA molecules from the membrane surface, which tends to reduced adsorption of protein molecules on the membrane surfaces [74]. These findings indicate that the total membrane fouling can be reduced by the induction of the $-COO^-$ groups.

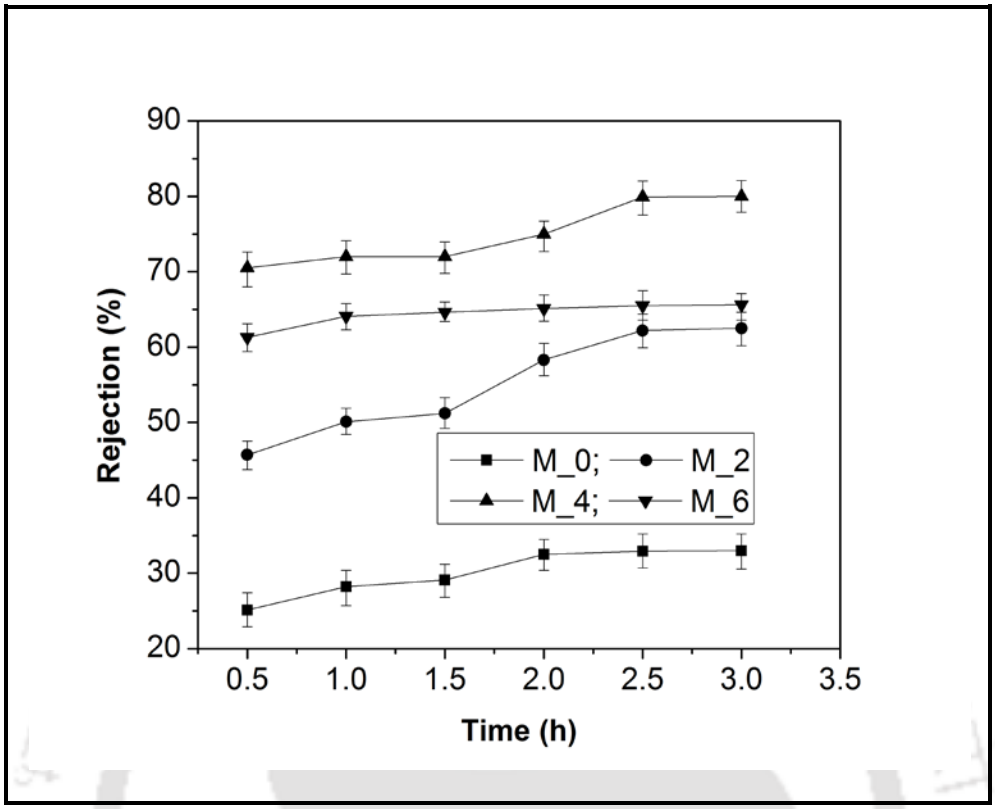

Figure 4.14: BSA Flux vs rejection (%) for BSA concentration 1000mg/L, at normal pH and at Pressure 150 kPa.

4.3.5.3. Effect of pH on the flux and rejection behaviour of BSA solution

Figure 4.15 depicted the effect of pH on BSA flux and rejection for all the four membranes. A significant variation in flux and rejection (%) was observed from the figures with change in pH of BSA solution. It depicts an evident difference between the unmodified membrane and membranes modified by the addition of copolymers. For unmodified membrane M_0, BSA rejection was lowest (10-56 %) for all pH values from 3 to 10. Moreover, for both modified and unmodified membranes, BSA rejection decreases at extreme acidic and basic pH. For example, BSA rejection for membrane M_0, M_2, M_4 and M_6 at pH 4.8 are 56.1 %, 59 %, 74.2% and 65.9%, respectively. Whereas, those values for membrane M_0, M_2, M_4 and M_6 at pH 3 are 17.5%, 28 %, 36.1 % and 33 % respectively. It was observed that flux was

maximum at pH 3. It may be because of the fact that retention and permeation performance of pH-responsive membrane is collective effort of both electrostatic interaction and pore size. pH variation can be responsible for the conformational change of poly (VP-co-IAH) copolymer and that result in change in pore size of the membrane [74]. At basic pH 10, elevated BSA rejection but reduced flux was observed, it may be because of the swelling of poly (VP-co-IAH) in skin layer of copolymer containing membranes and consequences in smaller pores, which gives lower flux and higher rejection. However at acidic pH 3, the pore size of skin layer became bigger because of the rupture of poly (VP-co-IAH) copolymer and fallout in lower rejection of BSA and higher flux [74].

Another key factor is the electrostatic interaction between BSA molecules and copolymer poly(VP-co-IAH) molecules. This factor can affect the rejection and permeation behaviour of the fabricated membrane. At isoelectric point (i.e. at pH 4.8) BSA molecules are least soluble and they have no net charge and consequently packed together and rested on the surface when get accumulated on the membrane surface and build up slightest permeable layer [110, 112, 113]. Moderate flux and subsequently highest BSA rejection was resulted due to this compact layer. While, below isoelectric point BSA molecules have net positive charge and vice versa above the pH 4.8. [89]. Thus, at basic pH BSA molecules have negative charge and synthesized copolymer molecules also possess negative charge as a result of the deprotonation of carboxylic group which consequences in higher rejection. Moreover, at pH 3 membranes hold no net charge and merely BSA molecules own positive charge. Also the pores are relatively bigger as discussed earlier, which consequences in lowest rejection of BSA among all the pHs.

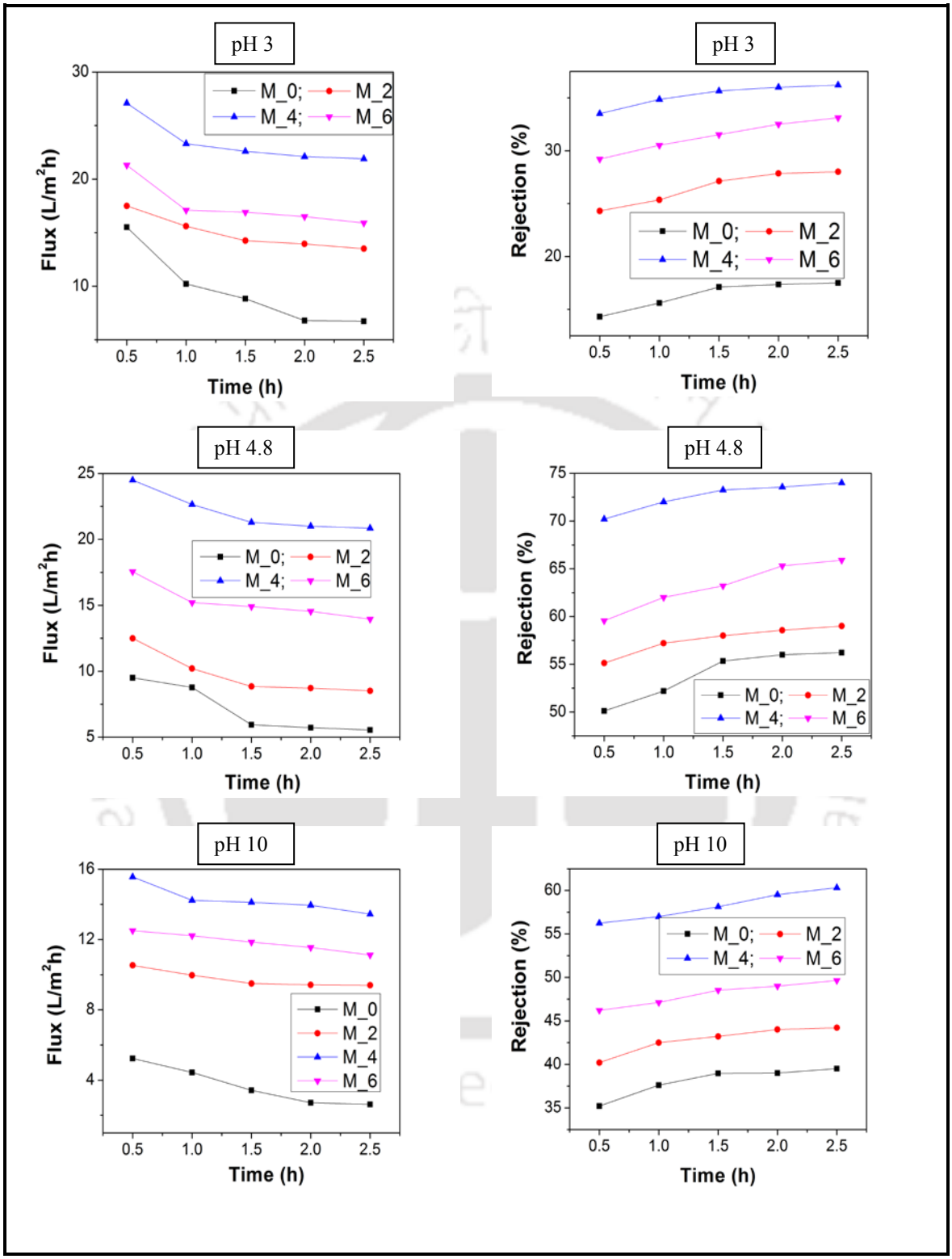

Figure 4.15: Effect of pH on flux and rejection of membrane.

Summary

AFM images of top surface confirm that surface roughness (RMS) increased by the addition of copolymer poly(VP-co-IAH) and consequences into the more porous membranes. Water contact angle images depict hydrophilic top surface for the copolymer poly(VP-co-IAH) containing membranes compared to the unmodified membranes. Copolymer containing membranes also exhibit the pH responsive behaviour.

Chapter 5
Racemic and enantiomeric effect of tartaric acid on the hydrophilicity of polysulfone membrane

This chapter discussed the effects of addition of D-TA and DL-TA into the casting solution of PSF membrane; i.e. blending of D-TA and DL-TA in PSF membrane and their performance in the removal of crystal violet dye (CVD) from aqueous solutions. Enantiomeric and racemic effects of TA on the membrane morphology, hydrophilicity, water flux as well as permeation and rejection behaviour were also examined and explained well for BSA. For the characterization of prepared membranes, morphological parameters were examined by scanning electron microscopy (SEM) for cross sectional view and field emission scanning electron microscope (FESEM) for top surface. Atomic force microscopy (AFM) was used for finding surface roughness parameters. Ion exchange capacity (IEC) and zeta potential of the membrane surface was measured for finding the charge density of the membrane. Equilibrium water content (EWC) and contact angle (CA) measurements were also performed to assess the membrane hydrophilicity.

5.1. Experimental

5.1.1. Materials

PSF and DMAc were used as base polymer and solvent respectively, in the membrane casting solution. D-tartaric acid (D-TA), DL-tartaric acid (DL-TA), potassium bromide (KBr), and BSA, CVD and SDS were used in this chapter. All the details of used chemical are provided in Table 2.1 of chapter 2.

Content of this chapter is published as below:

N. Sharma, M.K. Purkait, Enantiomeric and racemic effect of tartaric acid on polysulfone membrane during crystal violet dye removal by MEUF process, J. Water Proc. Eng. 10 (2016) 104–112.

5.1.2. Preparation of Flat Sheet Membranes

Wet phase inversion technique was used for the fabrication of flat film PSF membranes. PVP was used as pore former and D-TA and DL-TA were used as additives in the membranes. Flat sheet membranes were prepared by using different composition of PSF, D-TA, DL-TA, PVP and DMAc (as shown in Table 5.1). A constant concentration 18 wt % of the PSF was taken for all the membrane casting solutions. Membranes with varying compositions were defined as M1, M2, M3, M4 and M5. The casting solution was stirred at 350 rpm with the help of a magnetic stirrer for 8 h and further degassed for 12 h at room temperature. The solution was then casted on a clean glass plate with a casting knife maintaining uniform thickness of 100 μm in ambient atmosphere. Further details are given in section 2.2 of chapter 2.

Table 5.1: Composition of different membrane casting solution.

Membranes	PSF (wt.%)	PVP K-30 (wt%)	D-TA (wt%)	DL-TA (wt%)	DMAc (wt%)
M1	18	2	-	-	80
M2	18	2	1	-	79
M3	18	2	0.5	-	79.5
M4	18	2	-	1	79
M5	18	2	-	0.5	79.5

5.2. Membrane characterization

5.2.1. Surface Characterization of D-TA and DL-TA Blended Membranes

The presence of TAs in blended membranes was confirmed by comparing IR spectra of plain PSF membrane and TA blended PSF membrane. Microscopic observation of plain and blended membranes was done by field emission scanning electron microscope (FESEM) and scanning electron microscope (SEM). Cross section images were taken by SEM with an acceleration voltage of 10 kV after the samples were coated with thin gold layer. As top surface images required higher magnification, so these images were taken by FESEM with an acceleration voltage of 2-5 kV after the samples were coated with thin gold layer. Hydrophilic property of the membrane was evaluated by measuring the static contact angle between the DI water and membrane films at room temperature. Standard titration method was used to determine the ion exchange capacity (IEC) of different membranes [97]. The IEC value was calculated using the equation 2.14. Zeta potential of membrane surface, CVD and SDS added CVD solution was also measured. All the details of characterization techniques and instrument details are reported in section 2.3 of chapter 2.

5.2.2. Water permeation experiment

5.2.2.1. Membrane compaction and hydraulic permeability

For compaction study, prepared membranes were compacted with DI water for 1 h at a transmembrane pressure of 414 kPa and water permeation flux was measured at every 10 min interval through the membranes. The ratio of initial pure water flux ($PWF_{initial}$) to the steady state pure water flux ($PWF_{steady\ state}$) gives the value of compaction factor (CF). Water flux was measured by the equation 2.10. Flux values of pure water at different transmembrane pressures were measured under steady state condition. Permeability (P_m) ($L/m^2h\ kPa$) was

evaluated from the slope of the plot of J_w vs P. Hydraulic permeability was calculated by equation 2.11.

5.2.3. Membrane performance characterization by BSA ultrafiltration experiment

The solute separation and permeate flux behaviour of the prepared membranes were studied by BSA ultrafiltration experiments. BSA was dissolved in DI water and the concentration was kept constant at 1000 mgL^{-1} for all the experiments. The pH of the BSA solution (molecular weight 68000 Da) was kept at 3, 4.8, 7, 8 and 10. pH of the solution was adjusted by using 0.1 M NaOH and 0.1 M HCl solution. Each membrane was initially compacted for 1 h at 414 kPa, then the pressure was reduced to the working pressure of 208 kPa and membrane cell was filled with BSA solution; the flux was recorded. The BSA rejection ratio was calculated by the equation 2.15. UV-VIS spectrophotometer (Perkin-Elmer Precisel, Lamda-35) was used to find out the BSA concentration, at wavelength of 280 nm.

5.2.4. Membrane performance characterization by CVD ultrafiltration experiment

The solute separation and permeate flux behaviour of the prepared membranes were also studied by CVD (molecular weight 407.9 Da) ultrafiltration experiments. Micellar enhanced ultrafiltration (MEUF) technique was used for CVD separation. Anionic surfactant sodium dodecyl sulphate (SDS) (molecular weight 288.3) was taken for MEUF in this study. Transmembrane pressure is a key factor for finding the characteristic of flux. Other than that, the flux description and rejection of solute through the membranes mostly assessed by the morphology of the membrane and the properties of the feed solution, specially its pH. So,

fabricated UF membranes were also tested by measuring flux at different pH of CVD solution (20 mg L^{-1}). The pH of the CVD solution was kept at 3, 4.5, 7, 8 and 11. CVD was dissolved in DI water and the concentration was kept constant at 20 mg L^{-1} for all the experiments. Membrane M1, M2 and M4 were taken for UF studies. pH of the solution was adjusted by aforementioned technique discussed in section 5.2.3. Each membrane was initially compacted for 1 h at 414 kPa, then the pressure was reduced to the operating pressure of 150 kPa and membrane cell was filled with CVD solution; the flux was recorded. The CVD rejection ratio was calculated by the equation 2.15. UV-VIS spectrophotometer (Perkin-Elmer Precisel, Lamda-35) was used to find out the CVD concentration, at wavelength of 582 nm.

Effect of NaCl on SDS and CVD solution

In this experiment nine measuring cylinders were taken and in each cylinder 100 mg L^{-1} CVD solution was filled and pH was maintained at 11. In cylinder 1 there was no salt and SDS. Remaining eight cylinders have 8.2 mmol SDS (CMC level) concentrations and salt concentration was increasing from 10 g L^{-1} to 80 g L^{-1}.

5.3. Results and discussion

5.3.1. FTIR-ATR analysis of different membranes

Figure 5.1 shows the Chemical structures of D-TA and DL-TA, PVP and PSF. Figure 5.2 depicts the FTIR-ATR spectra of membranes M1, M2, M3, M4 and M5. Peak at 693 cm^{-1} is the characteristic band of the plane aromatic C-H bond in PSF membrane. Stretching at 845 cm^{-1} represents S-O-C group, symmetric and asymmetric stretching of sulfonate groups are presented by peaks 1144 cm^{-1} and 1243 cm^{-1}, respectively. Thus, confirming the presence of

polysulfone. Although, these peaks shifted little bit in blended membranes, this might be due to the changes in confrontation and interaction of molecules upon blending [128]. Peak at 2905 cm^{-1} shows the presence of TA with C-H stretching of methyl group. The strong absorption peaks between 1485-1595 cm^{-1} are related to the stretching of benzene ring skeletal. Peak found at 1665 cm^{-1} in FTIR-ATR spectra of PSF is related to amide C=O groups of PVP molecules which added as the pore former to PSF casting solution. These results indicate that the TA was blended well in the PSF membrane.

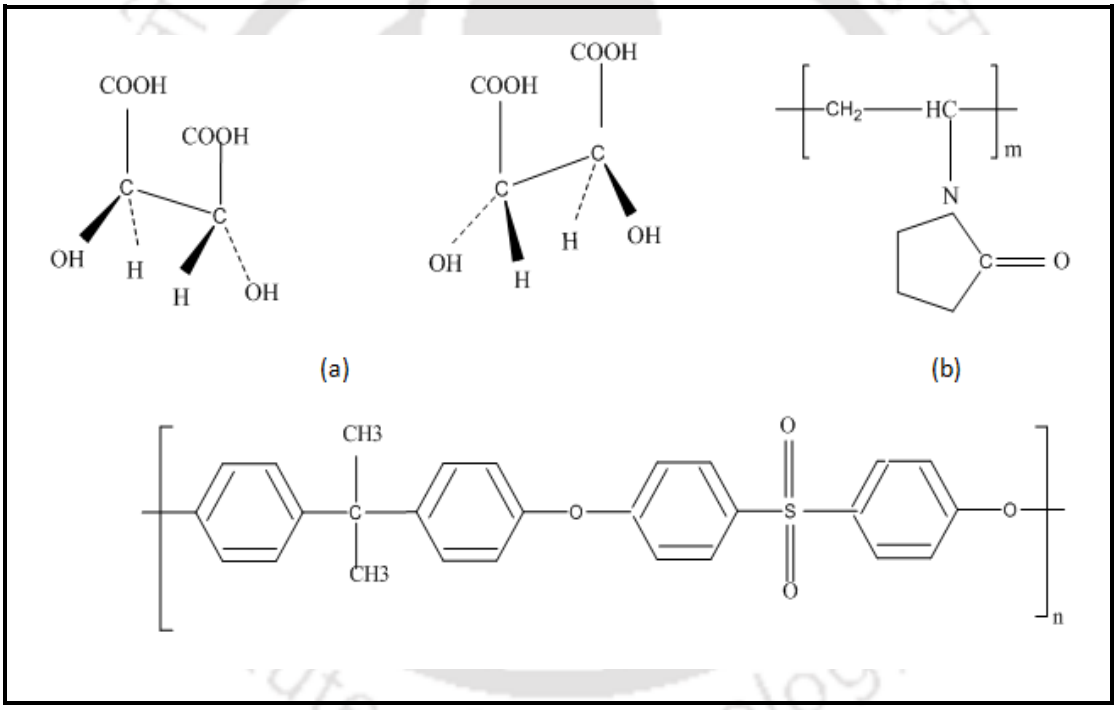

Figure 5.1: Chemical structures of (a) D-TA and DL-TA (b) PVP and (c) PSF.

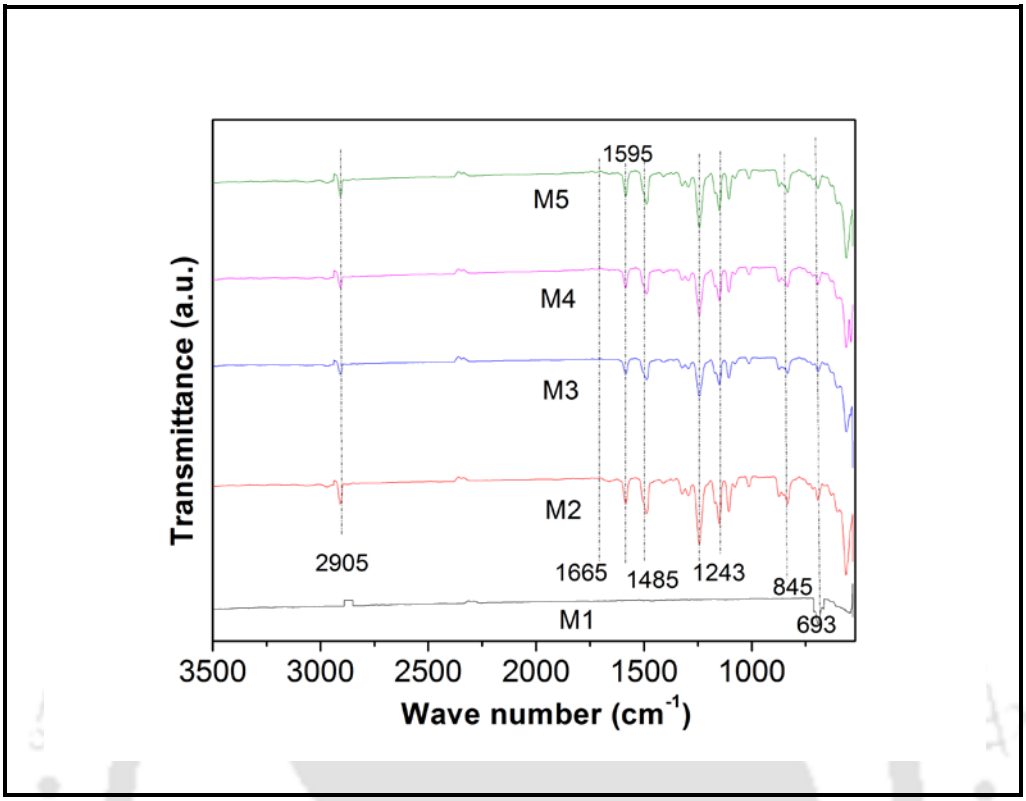

Figure 5.2: FTIR–ATR spectra of M1, M2, M3, M4 and M5 membranes.

5.3.2. Structure of membrane

5.3.2.1. SEM image analysis

SEM images shown in Fig. 5.3 depict the cross-sectional view of the fabricated membranes. Images clearly show that prepared membranes were porous structure which was asymmetric in nature. The figure also depicted dense top layer and a porous sub-layer. The porosity of the prepared membranes increases by the addition of D-TA. This information may be explained by two facts viz. (i) interactions between polymer chains got reduced as TA molecules and polymer came into contact and interacted with each other. (ii) Solvent (DMAc) outflow decreased and non-solvent (water) inflow increased due to the hydrophilicity of added TA to the casting solution [21, 129]. Hence, membranes with higher porosity were formed. Increased demixing rate of the casting solution may be the reason of thinner top-layer in

addition to the larger groove-like pores in the sub-layer compared to plain PSF membrane [130]. This fact can also be explained by the information that addition of an additive into the casting solution causes kinetic hindrance against phase separation by increasing the viscosity of the solution and causes delayed demixing [1, 131]. Further, increase in viscosity increases the ratio of nonsolvent inflow to solvent outflow which resulted in a more porous membrane [107]. The porous sub-layer seems to possess finger-like structure. Since, DMAc is highly soluble in water and shows high interactive affinity with water, instantaneous demixing occurs during membrane preparation by wet phase inversion method which further results in the creation of finger like structure in the sub-layer of the fabricated membranes [111]. Throughout the process, the concentration of non-solvent in the polymer solution slowly increases until the demixing gap is reached [101].

5.3.2.2. FESEM analysis

FESEM images for the top surface (air-side) of fabricated membranes are depicted in Fig. 5.4. Spinodal demixing may be the cause of formation of dense top surface. FESEM images were analyzed for determining the pore size on the membrane surface, using Image J software [105]. Fig. 5.5 shows the pore size distribution of all the three membranes. It may be noted that the pore size distribution trend (PSD) for M1 and M2 is almost identical whereas for M4 the PSD is different. Mean pore size was measured as 27.96 nm, 21.17 nm and 36.43 nm for M1, M2 and M4, respectively. These pore size values made it confirm that all the membranes were in UF range. It was confirmed that addition of DL-TA increased the pore size whereas, addition of D-TA reduced the pore size of the membrane. However, both TAs gave better results than PSF membrane in terms of rejection.

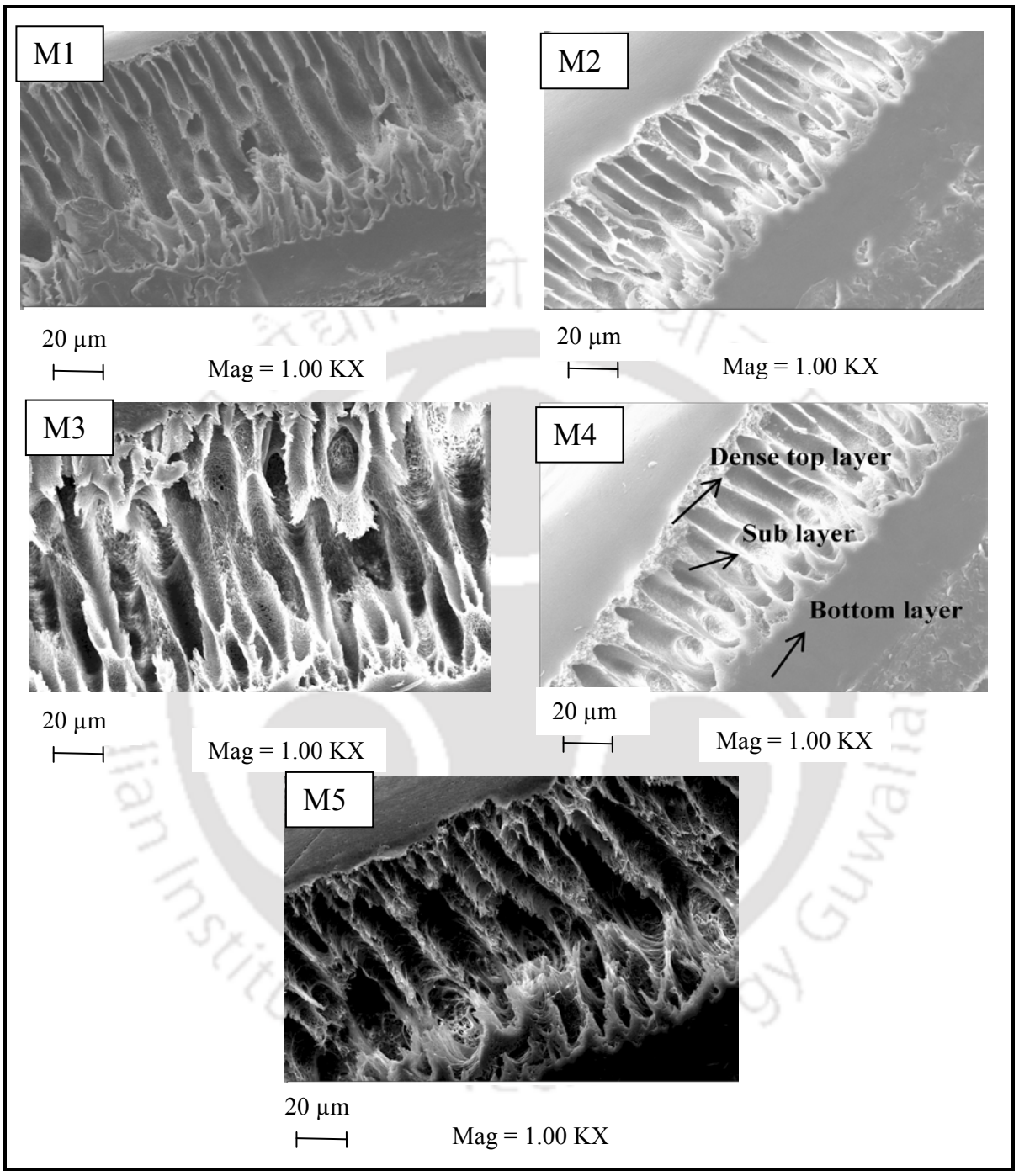

Figure 5.3: SEM images of membrane cross section for M1, M2, M3, M4 and M5.

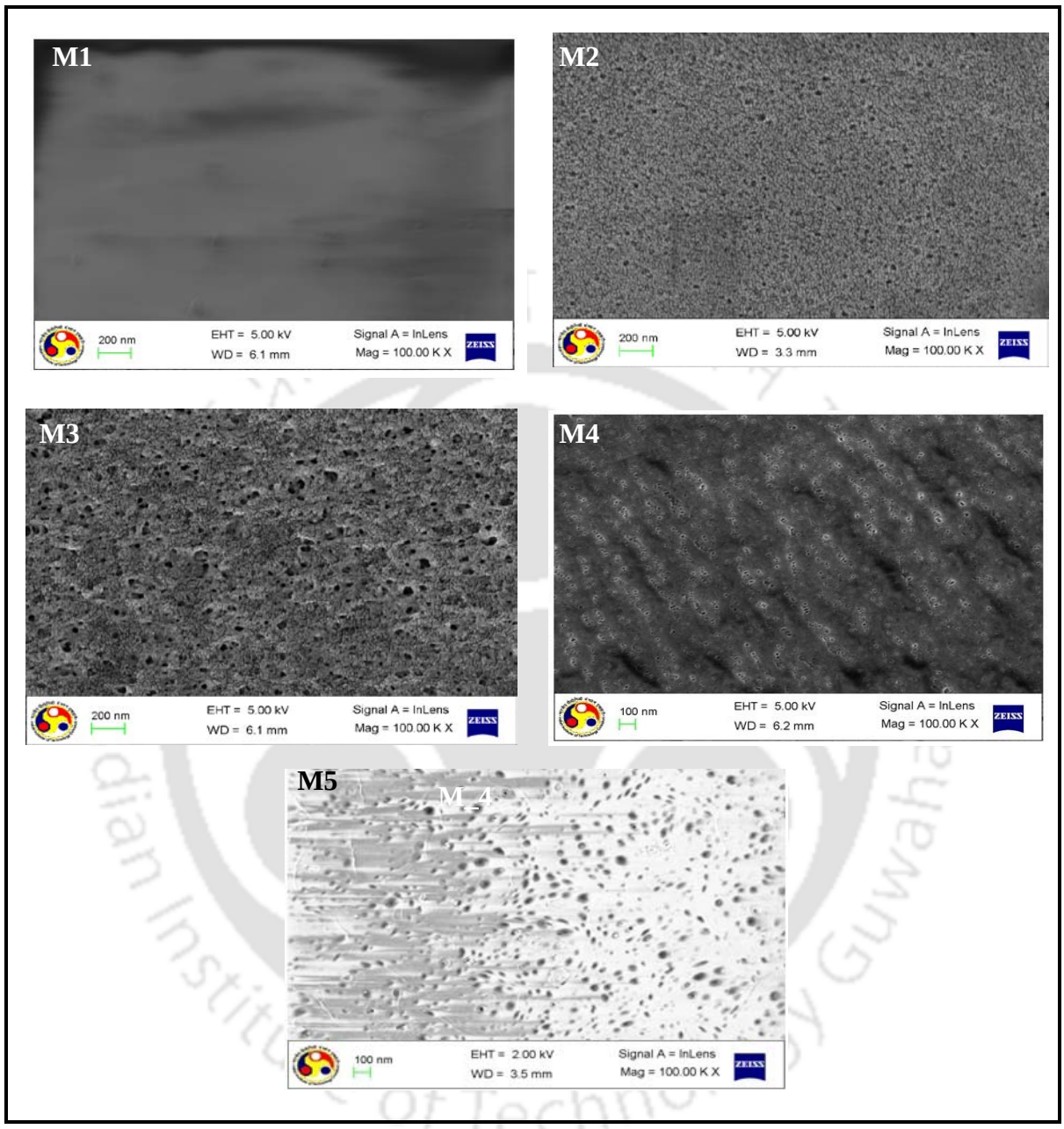

Figure 5.4: FESEM images of top surface of the membrane M1, M2, M3, M4 and M5.

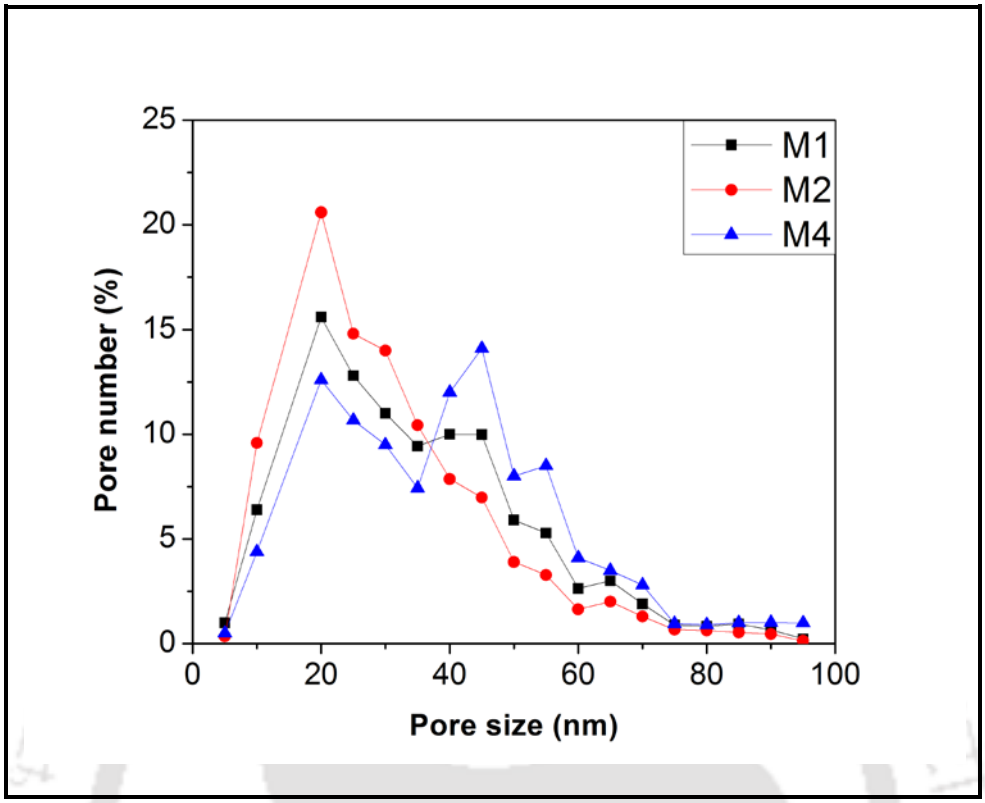

Figure 5.5: Pore size distribution of membrane M1, M2 and M4 by FESEM.

5.3.2.3. AFM analysis

Surface morphology and roughness of the membranes were analyzed by atomic force microscopy (AFM). Small squares of membranes (Approximately 1.5 cm^2) were taken and analyzed. Fig. 5.6 depicts the AFM images M1, M2, M4 and M5 membranes. Average height (Sz), root mean square (RMS) roughness (Sq) and average roughness (Sa) were measured. RMS roughness was increased with the addition of D-TA and decreased by DL-TA. Further it was found that D-TA containing membrane shows highest RMS roughness than plain and DL-TA containing membranes (Table 5.2). It may be due to the fact that surface porosity was increasing by the addition of D-TA. Table 5.2 shows different surface roughness parameters. Contact angle also decreased with the addition of D-TA and was measured as 68^0, 55^0 and 71^0 for M1, M2 and M4, respectively. Pore area and number of pores also increased by

blending of D-TA and decreased by the addition of DL-TA. M2 membrane was more porous and pore size is less than M4. It may be because of the higher solubility of D-TA as compare to the DL-TA in water at a particular temperature. During wet phase inversion process it got diffused faster than DL-TA in the non solvent (i.e. water in the coagulation bath) and subsequently creates smaller pores on the top layer. Thus, membrane M2 is more porous than that of M4 membrane.

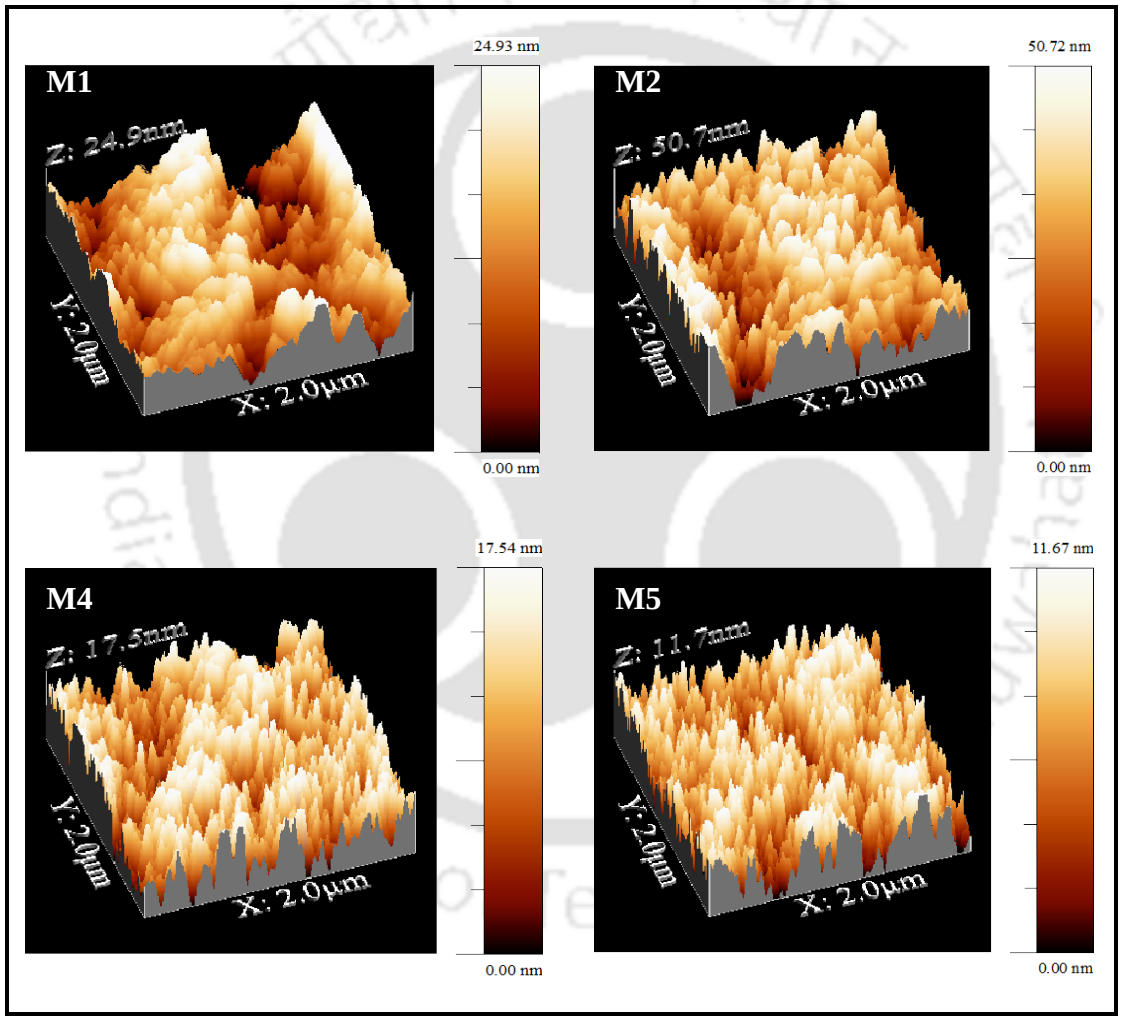

Figure 5.6: AFM images of membranes M1, M2, M4 and M5.

Table 5.2: Results of surface roughness parameters for the membranes.

Membrane	RMS roughness (S_q) nm	Average roughness (S_a) nm	Average height (S_z) nm
M1	5.8	4.7	12.4
M2	12.1	9.9	25.5
M3	-	-	-
M4	4.2	3.5	8.8
M5	2.8	2.3	5.9

5.3.3. Determination of molecular weight cut off (MWCO)

MWCO values are the measures to determine qualitative pore sizes of the membranes while the pure water permeability is related to porosity (pore number density) of the membranes [38]. MWCO values were measured by passing aqueous solutions of polyvinyl pyrrolidone (PVP) of two different molecular weights (i. e. PVP 24000 Da and PVP 40000 Da) and a protein bovine serum albumin (molecular weight 68000 Da). Detailed procedure for finding the MWCO is discussed in section 2.5 of chapter 2. Fig. 5.7 depicts the plot of rejection vs. molecular weight for M1, M2 and M4 membranes. The value of molecular weight at rejection 90% was taken as MWCO of membrane assuming that there is a linear correlation between the rejection and molecular weight of solute. Linear correlations between rejection and PVPs of different molecular weights were observed for all the membrane samples. The MWCO value was found to be about 68 KDa, 75 KDa and 81 KDa for the membrane M1, M2 and M4, respectively. MWCO value was lowest for membrane M2 among all the membranes.

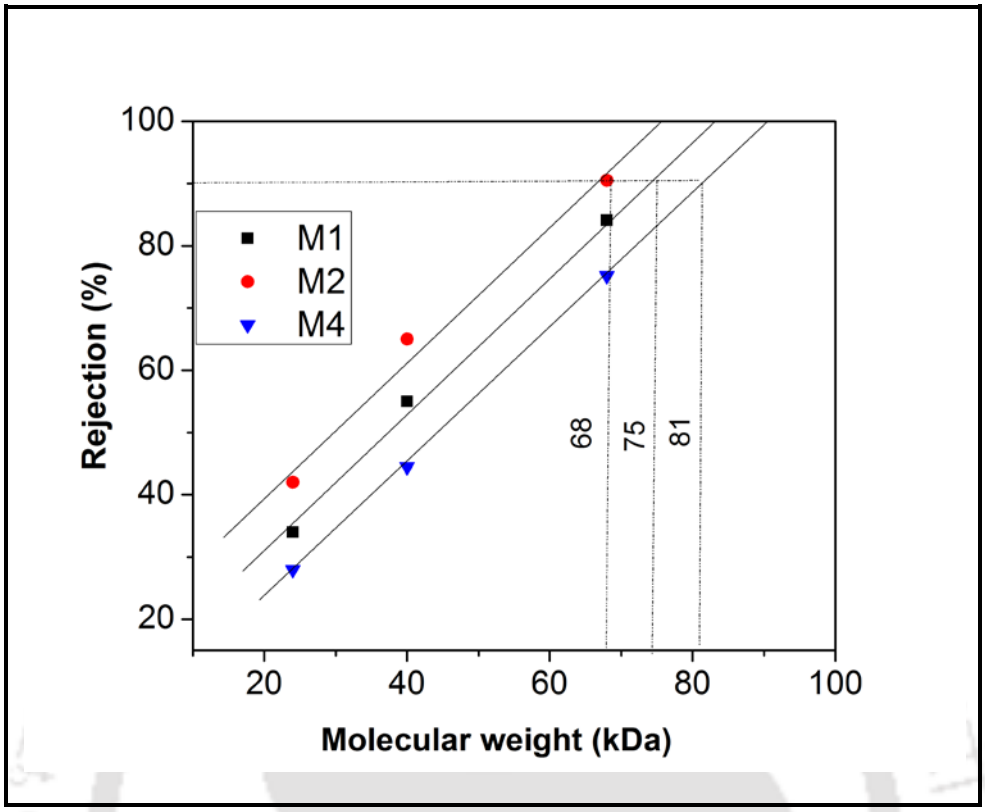

Figure 5.7: Rejection (%) vs. molecular weight for determining MWCO value of the membranes.

5.3.4. Analysis of liquid–liquid displacement porosimetry results

Figure 5.8 shows the LLDP flux profile for prepared membranes. Radius of the pore, permeability of the membranes, pore number per unit area and area of the pores for each membrane were calculated using equation 2.1 2.2, 2.4 and 2.5, respectively. Pore size distribution of the membranes observed by LLDP is shown in Fig. 5.9. Around 47 % of the pores were in the size of 2-3 nm for M2. For M1, M3, M4 and M5 these numbers are 34%, 35.5 %, 32 % and 30.5 %, respectively. It can be seen from the figure 5.9 that the pores approximately 94 % for all the five membranes are in the range of 3-5 nm which clearly brought them under UF range. Fig. 5.10 depicts the Variation in cumulative permeability (%) with pore size (nm). Though, larger pores play major role in overall permeability; as contribution from the small number of larger pores (>50 nm) can be quite high compared to

the smaller size pores (<5 nm) though they are majority in number [15]. Hagen–Poissuille equation explains that the enlarged pore radius can be responsible for increase in flux. Calvo et al. [101] observed the same results for UF membranes formed by track etched method. However, it is difficult and challenging to measure the accurate part of the larger pores (>50nm) and smaller pores (< 2 nm) by the LLDP method. Results obtained by LLDP method are placed in table 5.3. Fig. 5.11 depicts the variation of cumulative pore number (%) with pore size (nm) for membranes prepared with D-TA and DL-TA. It was observed that, by the addition of D-TA number of pores increases for both the membranes; however addition of DL-TA resulted in less porous membranes. Pores were found 3.51×10^{8} m^{-2}, 4.52×10^{8} m^{-2} and 1.72×10^{8} m^{-2} for membrane M1, M2 and M4, respectively. The mean pore size r_m was slightly decreased by the addition of D-TA whereas it was increased to some extent by the addition of DL-TA. It was calculated as 2.8 nm, 2.48 nm, 2.49 nm, 2.91 nm and 3.1 nm for M1, M2, M3, M4 and M5, respectively.

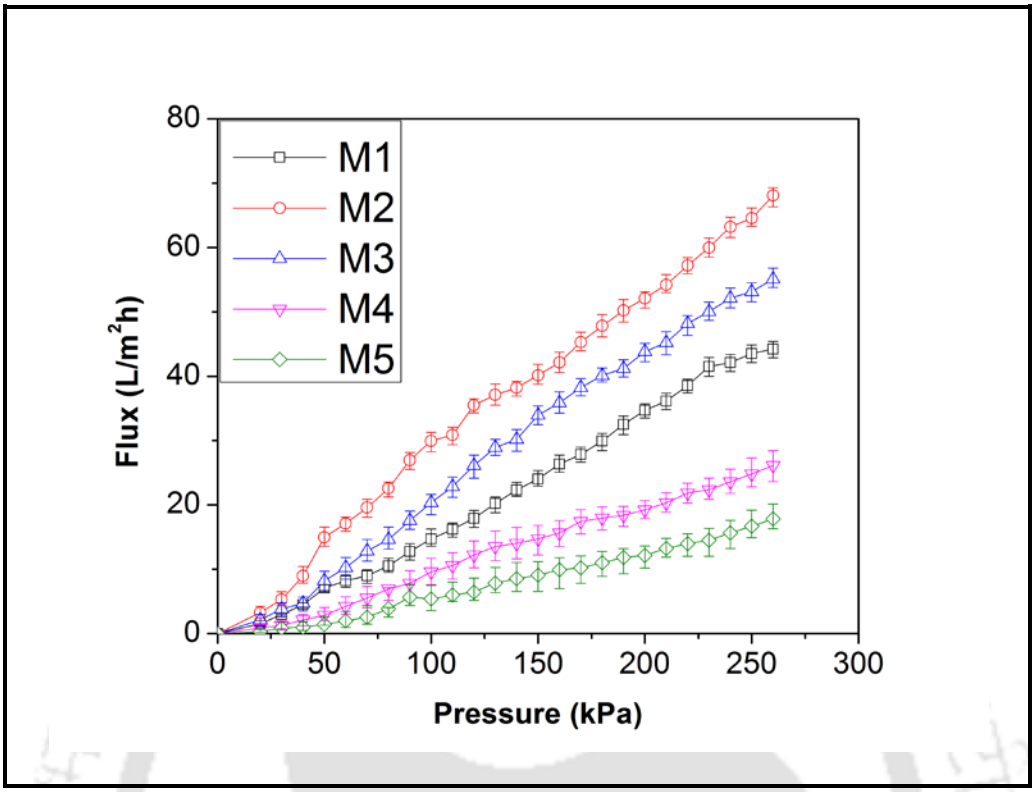

Figure 5.8: LLDP flux profile for membranes M1, M2, M3, M4 and M5.

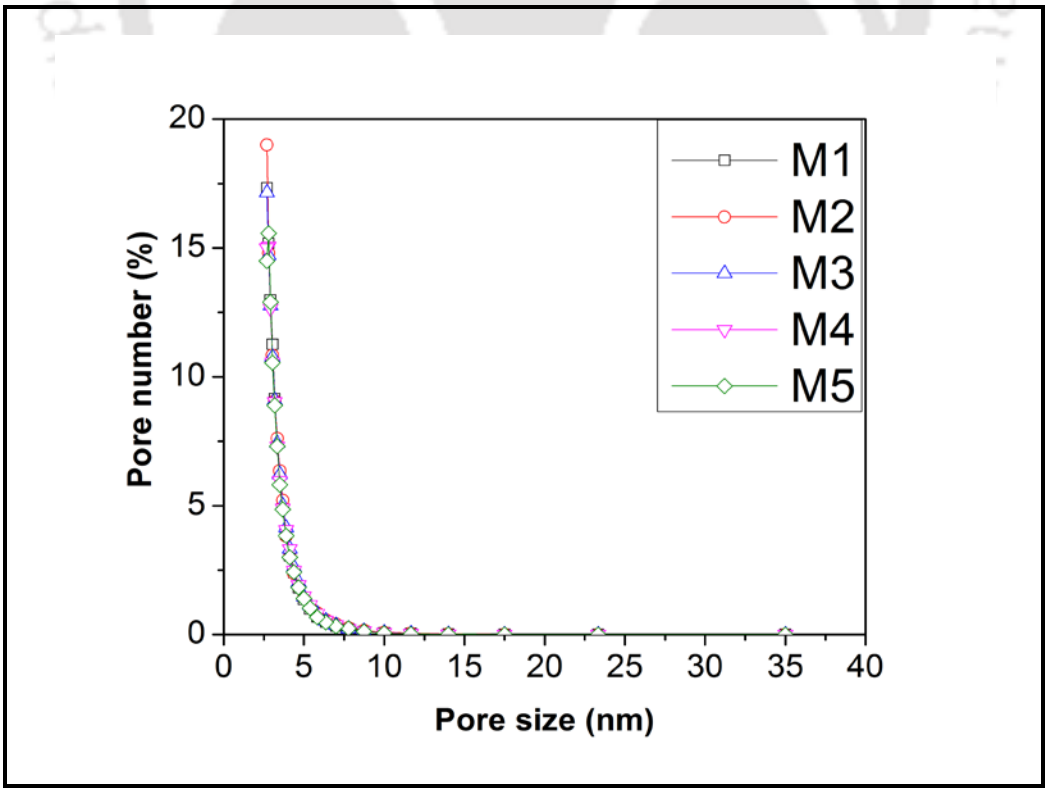

Figure 5.9: Pore size distribution of membranes by LLDP.

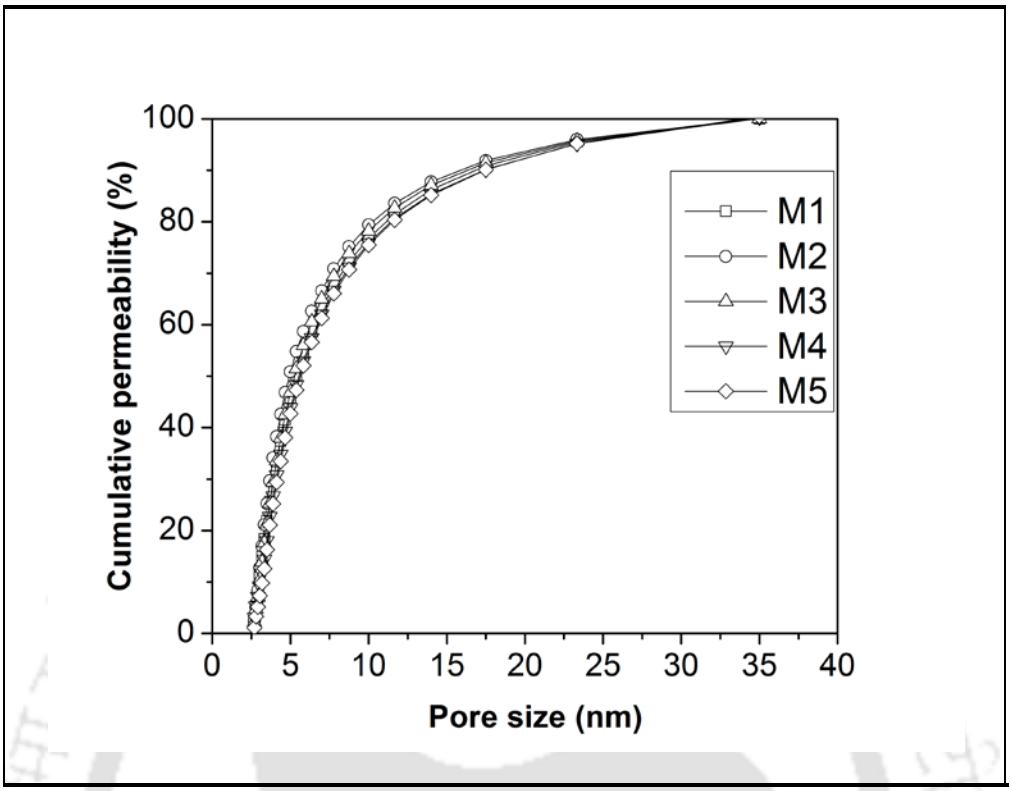

Figure 5.10: Variation in cumulative permeability with respect to pore size (nm).

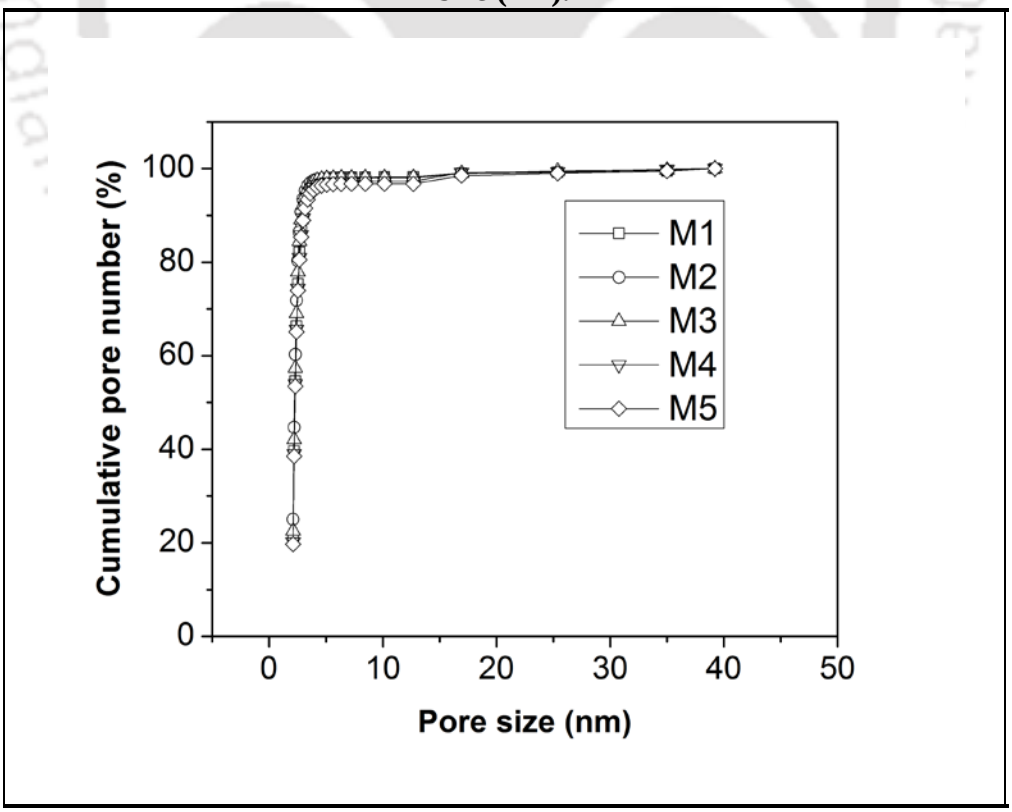

Figure 5.11: Variation of cumulative pore number (%) with pore size (nm) for membranes M1, M2, M3, M4 and M5.

Table 5.3: Effect of D-TA and DL-TA on some characterization parameters.

Membranes	Mean pore size (nm)	Pore area $A_t(m^2) \times 10^9$	Pore number $N_t(m^2) \times 10^{-8}$	Contact angle (^{0})	Permeability (L/m^2h kPa)
M1	2.8±0.03	8.64±0.02	3.51±0.02	68±1.5	0.16
M2	2.48±0.04	8.73±0.03	4.52±0.03	55±1	0.32
M3	2.49±0.02	8.6±0.02	4.43±0.01	59±1	0.24
M4	2.91±0.05	4.57±0.05	1.72±0.04	71±2	0.13
M5	3.1±0.06	3.89±0.07	1.29±0.05	73±1.5	0.08

5.3.5. Permeation studies

Fabricated membranes were checked by permeation behaviour for observing the effect of the addition of D-TA and DL-TA. The membranes were tested in terms of PWF and hydraulic permeability. Effects of solubility of both the tartaric acids and applied pressure were studied on EWC and porosity. Lastly, the membranes were checked for its rejection in addition to permeate flux performance with BSA and CVD at different pHs. Research outcomes have been discussed in subsequent sections.

5.3.5.1. Compaction behaviour of membranes

The effect of compaction time on PWF for all the 5 membranes (i.e. M1, M2, M3, M4 and M5) is shown in Fig.5.12. Flux was found as 84.76 L/m^2h, 161.03 L/m^2h and 53.19 L/m^2h for M1, M2 and M4, respectively. Flux decreased drastically up to 0.33 h; finally attain a steady state after around 0.33 h. It was observed that the steady state PWF decreased with addition of DL-TA whereas, it increased by the addition of D-TA for respective TA containing the membranes. For example, the steady state flux increases from around 84.76 L/m^2h to 161.03 L/m^2h, when $D\text{-}TA_1$ was added to the membrane whereas it decreases from 84.76 L/m^2h to

53.19 L/m^{2}h by the addition of DL-TA$_1$ to the membrane. The CF for the membranes is presented in Table 5.3. It is seen that for PSF/DMAc/PVP/D-TA membranes possess lowest CF than DL-TA containing membranes as well as without any acid containing membrane. The CF was calculated as 1.74, 1.41, 1.48, 1.81 and 1.96 for M1, M2, M3, M4 and M5, respectively. This may be attributed to the fact that addition of two additives into the membrane casting solution can either extra enlarge or in addition suppress the macrovoids present in the membrane beneath the top layer (i.e. sublayer) depending on their molecular weight and the type of solvent used [103].

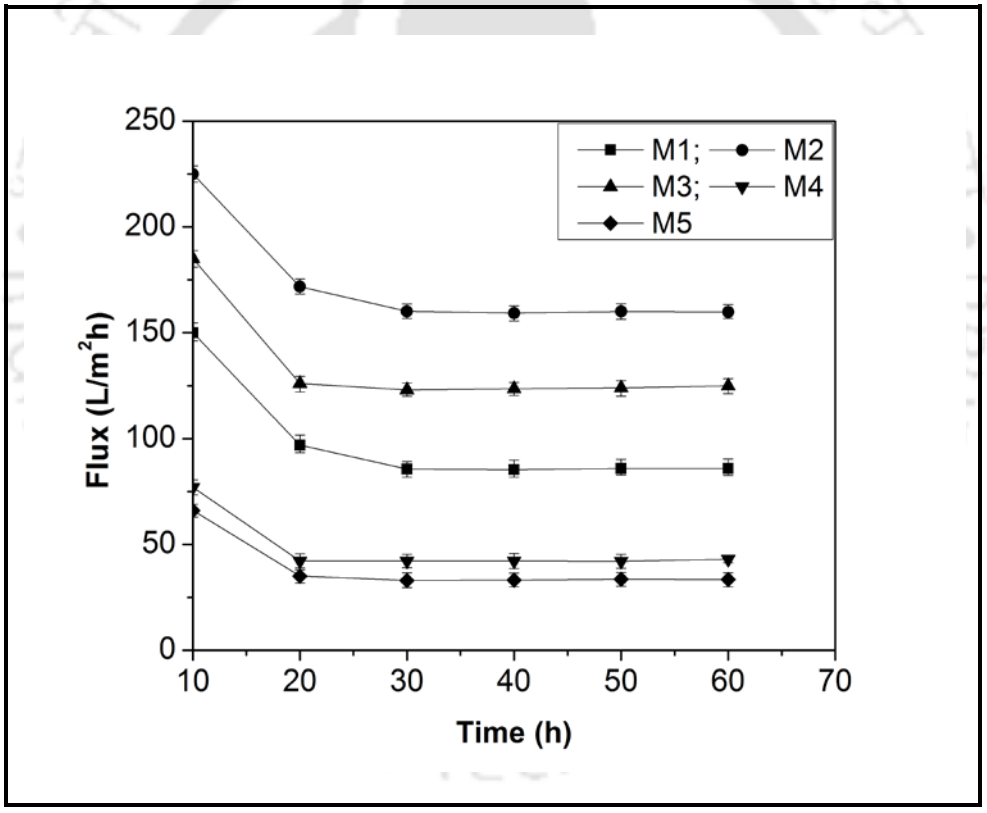

Figure 5.12: Flux profile during compaction at 414 kPa.

5.3.5.2. Effect of the addition of D-TA and DL-TA on PWF and hydraulic permeability

Figure 5.13 depicts the effect of addition of D-TA and DL-TA or enantiomeric and racemic effect of organic acid on PWF at different trans membrane pressures (TMP). PWF (calculated

using Eq. (2.10)) increases almost linearly with increase in TMP, for all the membranes. It was also found that the PWF decreased by addition of DL-TA in membrane at a certain pressure, these observations support the results of the compaction study (Fig. 5.12). For example, at 200 kPa, the PWF decreases from 57.79 $Lm^{-2}h^{-1}$ to 19.97 Lm^{-2} h^{-1} for membrane M2 and M4, respectively.

Hydraulic permeability (P_m) is also an important consideration for finding the hydrophilicity of membranes. It was observed that P_m was increased by the addition of D-TA. Whereas, it was found to be decreased by the addition of DL-TA. P_m for M1, M2, M3, M4 and M5 was calculated as 0.16, 0.32, 0.24, 0.13 and 0.08, respectively. Enhanced P_m and subsequently increase in flux by the addition of D-TA may be due to the solubility of it in water, as it is more soluble than DL-TA; Increase in hydraulic permeability and therefore elevated flux by the addition of D-TA may due to the fact that it is highly soluble in water and since having less molecular size it creates smaller pores on the top layer. It does not remain inside the pores with or without PVP and increased the sublayer pore size thus, pores present in per square area on the top surface were more as shown in FESEM images (Fig. 5.4). The result clearly indicates that addition of D-TA and DL-TA influences the formation of pores in the membranes, which affect the permeability as the latter is conceptually related to its pores for UF membranes [112].

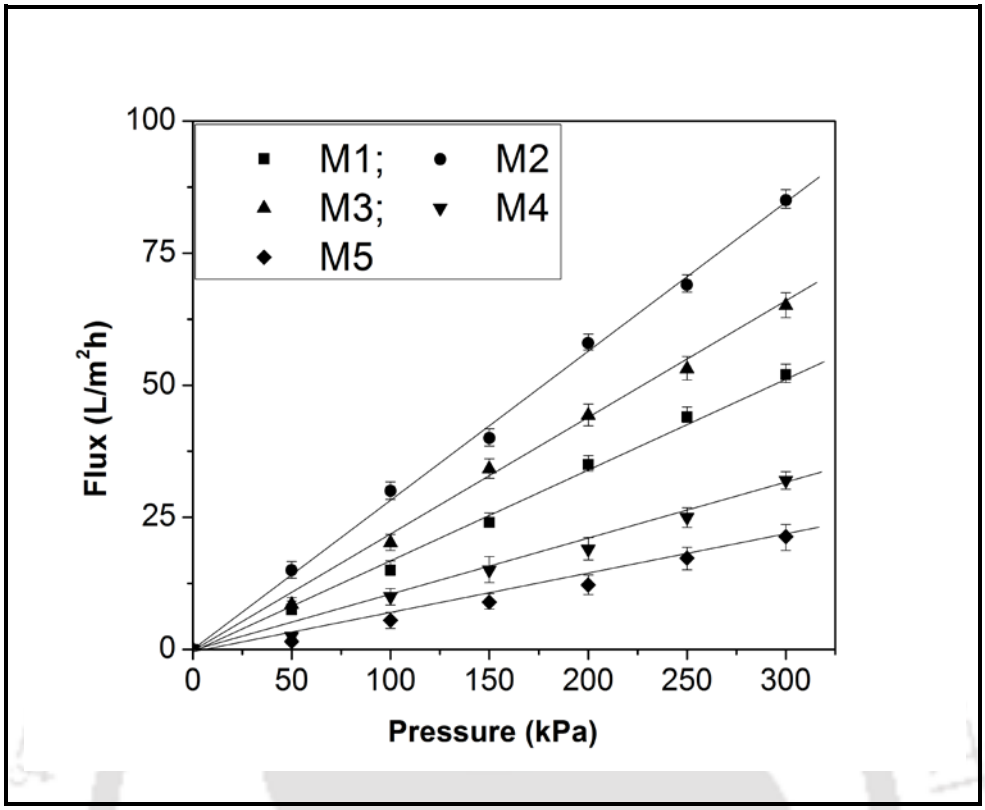

Figure 5.13: Effect of transmembrane pressure on PWF.

5.3.5.3. Effect of addition of D-TA and DL-TA on EWC, hydrophilicity and porosity

EWC, hydrophilicity and porosity of the membrane are important parameters in membrane permeation and separation processes. It is closely related to PWF and morphology of the membrane. The EWC of all the membranes was calculated using Equation 2.12 and presented in Table 5.4. It may be found from the Table 5.4 that by the addition of D-TA, EWC of the membrane increases and decreases by the addition DL-TA. The EWC for M1, M2, M3, M4 and M5 is 65%, 69%, 66.5%, 63% and 59.9%, respectively. This increasing trend confirms the presence of increasing number of pores in the membrane with D-TA as discussed in section 5.3.5.2.The pores on the surface as well as cavities in the sub layer are responsible for accommodating water molecules in the membrane [23]. The EWC value of the membranes

also coincides with PWF of different membranes as both the values increases for membrane containing 1 wt % of D-TA.

Role of hydrophilicity and porosity of the membrane is undoubtedly significant in membrane permeation process. These are based on the morphology and subsequently affect the PWF through membrane. Surface hydrophilicity is principally described by the contact angle (CA) measurement [96]. CA is a straightforward way to detect the relative hydrophilicity/hydrophobicity of the membrane surface. Generally it is a common phenomenon that as the value of contact angle decreases the hydrophilicity increases. Porosity of the membranes was measured using standard method [15, 89]. Values of contact angle of membranes are shown in Table 5.3. Contact angle decreased and permeability increased with the addition of D-TA. The contact angle for M1, M2, M3, M4 and M5 was 68^0, 55^0, 59^0, 71^0 and 73^0, respectively. Similarly, permeability for M1, M2 and M4 was 0.16, 0.32 and 0.13, respectively. Increase in permeability by blending with D-TA and decrease in it by the mixing of DL-TA may be due the lower solubility of DL-TA than that of D-TA as discussed in the preceding section. The change in porosity (from 0.35 to 0.38 for M1 and M2, respectively) was due the difference in viscosity of the casting solution.

Table 5.4: Values of some characterization parameters of membranes blended with D-TA and DL -TA.

Membranes	EWC (%)	Compaction factor	Zeta Potential at pH 7.5 (mV)
M1	65.0	1.74	-7.91
M2	69	1.41	-20.86
M3	66.5	1.48	-19.41
M4	63	1.81	-18.19
M5	59.9	1.96	-17.21

5.3.6. Ultrafiltration of BSA

5.3.6.1. Effect of concentration of D-TA and DL-TA on BSA rejection

Figure 5.14 shows the effect of addition of D-TA and DL-TA on the rejection of BSA at normal pH (i.e. pH 7) and 208 kPa pressure. It was confirmed that BSA rejection increased by the addition of both D-TA and DL-TA. So, addition of different quantities of D-TA and DL-TA with PVP (i.e. 40000 Da) was studied. It was observed that by increasing the concentration of D-TA and DL-TA the rejection was found to be increased, it may be attributed to the reason that after addition of additives into the PSF casting solution, hydrophilic functional groups of both TAs were increased. On the other hand, addition of DL-TA reduced the rejection as compared to D-TA added membranes because of the formation of larger pores on the top surface of membranes. Though, BSA molecules soaked in the sublayer of the membrane. For example rejection (%) for M1, M2, M3, M4 and M5 was 78.2%, 90.5%, 87.8%, 86% and 81.1% respectively. Moreover, addition of different forms of organic acid altered the membrane morphology as well as skin-layer thickness (Fig. 5.3) and hence higher porosity was formed by the addition of D-TA and reduced porosity by the addition of DL-TA.

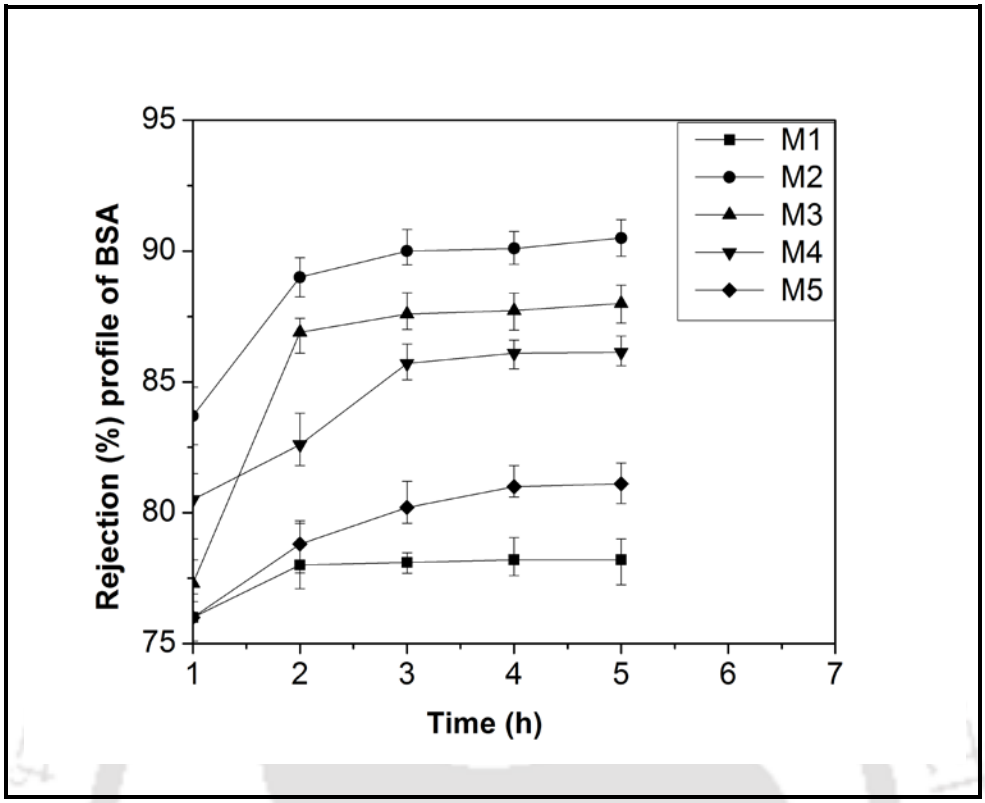

Figure 5.14: BSA Rejection profile for M1, M2, M3, M4 and M5 at normal pH (i.e. pH 7) and 208 kPa pressure.

5.3.6.2. Effect of pH of BSA solution on the flux and rejection

Membrane M2 was chosen for the flux and rejection studies at different pH conditions because it gave best results for each parameter. Fig. 5.15 shows the flux and rejection (%) profile at different pH (3, 4.8, 7, 8 and 10). It was observed that flux was maximum at pH 3 and lowest at pH 10. Whereas, rejection (%) was maximum at pH 10 and minimum at pH 3. As the zeta potential of membrane surface was negative at pH 7.5 (mV) (Table 5.4). More negative ions were present on the membrane surface at pH 10. Electrostatic charge repulsion (ECR) resulted in lowest flux and highest rejection at pH 10.

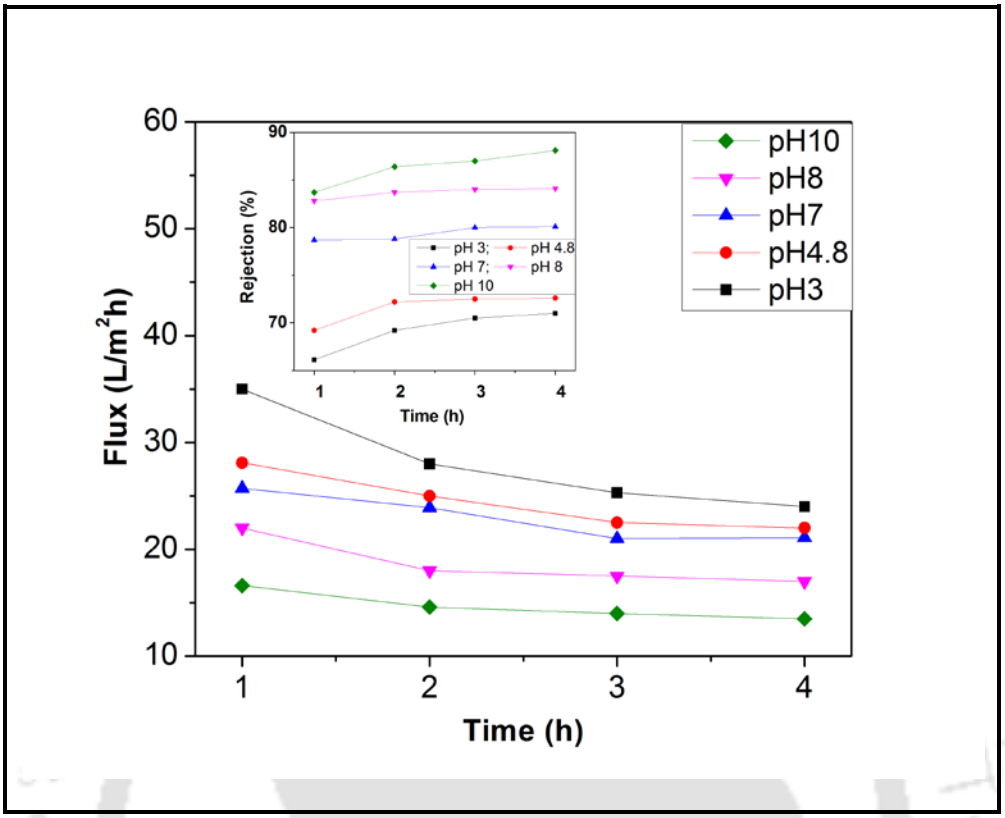

Figure 5.15: Effect of pH on BSA flux and rejection for membrane M2 at 208 kPa pressure.

5.3.7. Ultrafiltration of CVD

5.3.7.1. Effect of addition of D-TA and DL-TA on the performance of PSF membrane for CVD separation

Figure 5.16 shows the effect of addition of both TAs on flux and the rejection (% R) of CVD through the membranes M1, M2 and M4 at normal pH (i.e. pH 7). The rejection was found to be increased by the addition of both the TAs; it may be attributed to the fact that after addition of additives into the PSF casting solution, hydrophilic functional groups of both TA's were increased. On the other hand, addition of DL-TA depicted lower rejection than D-TA containing membrane because of the formation of bigger pores on the top surface of membranes. However, dye molecules impregnated in the sublayer of the membrane. For example rejection (%) for M1, M2 and M4 were found as 67.5%, 80.5% and 74.7%, respectively. Moreover, addition of different forms of organic acid altered the membrane

morphology as well as skin-layer thickness (Fig. 5.3). Curve for flux was constant up to 2 h then the slope of the curve changed and flux declined this may be because of the pore blocking i.e. CVD molecules were adsorbed on the surface of membranes. This trend of flux decline is therefore, considered to be because of the pore blocking. Particle size distribution of the CVD was measured by dynamic light scattering. Average size of CVD molecules was measured as 1.6 nm. So, dye molecules can pass through the membrane pores as the pore size distribution (Fig. 5.5) shows some bigger pores on the membrane surface. Separation of organic molecules by UF membranes can be credited to some mechanisms which include segregation by size, adsorption on the membrane surface and electrostatic charge repulsion (ECR) [21]. ECR between membrane surface and solutes to be removed; plays important role for removal of these charged organic solutes. Small charged solutes are mainly separated by such ECR than what perhaps assumed by the help of size exclusion effects [132-135]. Chemical structure of PSF membrane shows no dissociable functional groups; however, negative charge on the PSF membrane surface can be achieved by anionic adsorption which may be attributed to the breaking of carboxylic acid groups existing on the membrane surface by addition of PVP as well as addition of TA during preparation of membrane. Zeta potential of membrane M1, M2 and M4 was measured (at pH 7.5) as -7.91 mV, -20.86 mV and -18.19 mV, respectively. These values of zeta potential clearly indicate that more negative ions should be present on PSF membrane at higher solution pH and it becomes additionally negative with increasing pH as also reported by Ghaemi et al. [21].

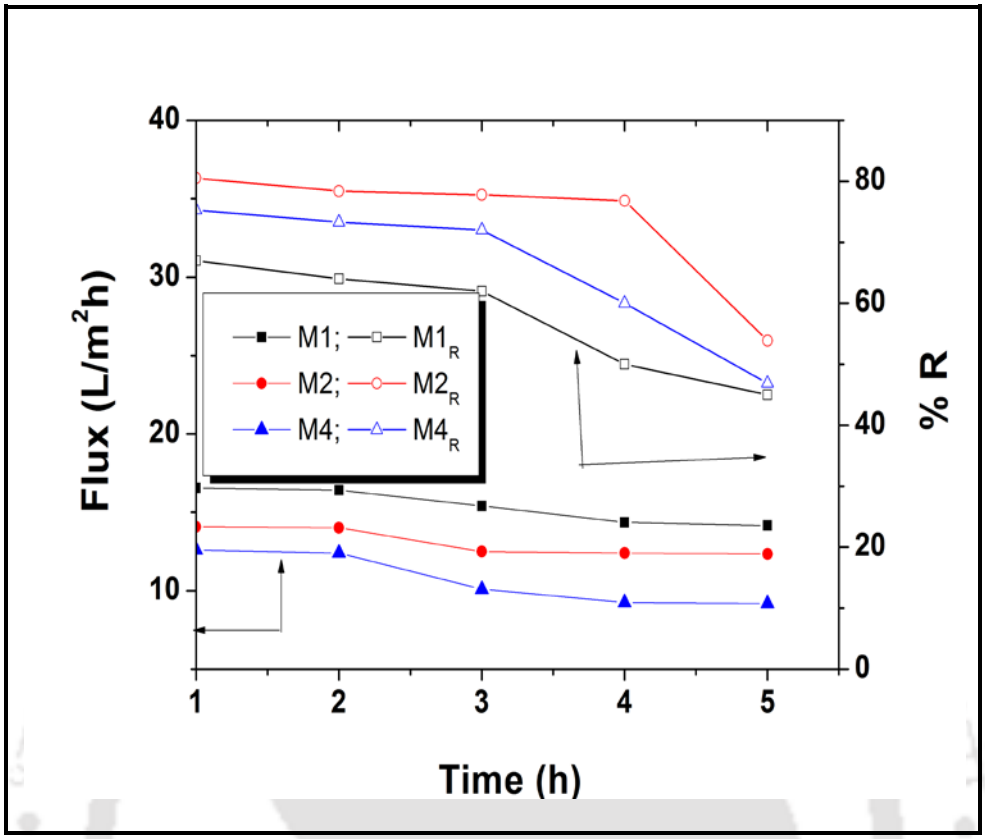

Figure 5.16: Flux and % Rejection at normal pH, at 20 mg/L CVD concentration and at 150 kPa.

5.3.7.2. Effect of the addition of anionic surfactant sodium dodecyl sulphate (SDS) on the flux and rejection of CVD

SDS is used for the micellar-enhanced ultrafiltration (MEUF) in the present study. In this technology surfactant micelles help to solubilize organic or inorganic contaminants from aqueous stream. Fig. 5.17 depicts the effect of the addition of SDS in CVD removal. CVD concentration was 20 mg L^{-1} and SDS was taken at its critical micellar concentration (CMC) 8.2 mM [136]. In aqueous solutions surfactant-dye interaction has been studied in the literature [137-139]. Spectral studies have shown that both electrostatic and hydrophobic forces play important role in association between ionic dyes and ionic surfactants [140]. In the case of oppositely charged dyes with surfactants interaction is responsible mainly by

coulombic force. If hydrophobic interaction can dominate electrostatic repulsion then only inter-action between surfactants and dyes of same charge happens [140]. Fig. 5.17 shows that the rejection of CVD is less in absence of surfactant. Since the size of CVD molecules is lesser than the pores of membrane. On the other hand, when surfactant SDS was mixed in dye solution, the retention of CVD increased up to 99%. Hence, it is clear that the dye molecules were solubilized on the surfactant micelles and afterward retained by the UF membrane [140].

Fig. 5.17 also shows the variation of the permeate flux with and without surfactant. Flux was found more without SDS. It may be because of the fact that during UF, the micelles were formed by surfactant molecules are obviously bigger in size and hence, retained and accumulated on the membrane surface, consequently resulted in an elevated surfactant concentration near the membrane surface than the bulk surfactant concentration [140], Purkait et al. also reported similar observations [141]. Concentration polarization on the membrane is responsible for reduced permeate flux.

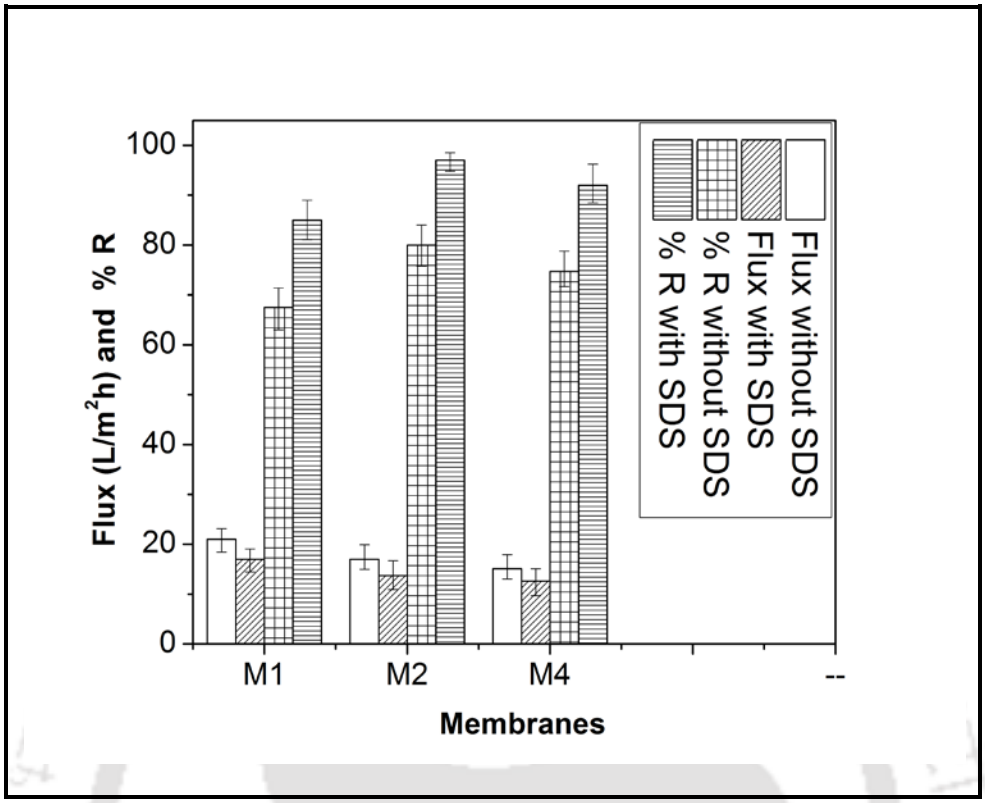

Figure 5.17: Flux and % Rejection after addition of SDS in CVD solution at 150 kPa pressure for M1, M2 and M4 membrane.

5.3.7.3. Effect of pH on the flux and rejection of CVD

Figure 5.18 depicts the effect of pH on flux and rejection of CVD for membrane M1, M2 and M4. Increasing rejection trend was observed with the increase of solution pH. This may be explained based on the extent of ionic interaction occurring in the feed solution over the membrane surface. The Zeta potential of CVD, SDS and CVD-SDS solution at pH 7.5 was measured as 11.29 mV, -37.44 mV and -22.66 mV, respectively. CVD molecules are solubilized over the membrane surface due to Coulombic forces. On the other hand, the electrostatic charge repulsion is prevailing between micelles and the negatively charged membrane surface (Table 5.4) which reduces the possibilities of micelles to get deposited. Thus CVD along with SDS is rejected. The increase in pH increases the negative charge of solution [142-144] which influences the flux and rejection during UF. For instance rejection

was increased from 86 % to 99.2 % for M2 by increasing pH from 3 to 11. The effect of pH on the permeate flux has been also studied. Fig. 5.18 shows that the flux decreased gradually when pH increased from 3 to 11. Flux was declined from 18.2 $Lm^{-2}h^{-1}$ to 9.5 $Lm^{-2}h^{-1}$ by increasing the pH from 3 to 11 for membrane M2. This can be attributed to the fact that more negative charge was there on the membrane surface at higher pH and offered resistance for permeation, consequently reduced flux was achieved. In order to make MEUF economical, recovery of surfactant may be adopted by precipitation method [145-146]. Therefore, addition of D-TA and DL-TA in PSF membrane can be useful for the removal of CVD by MEUF.

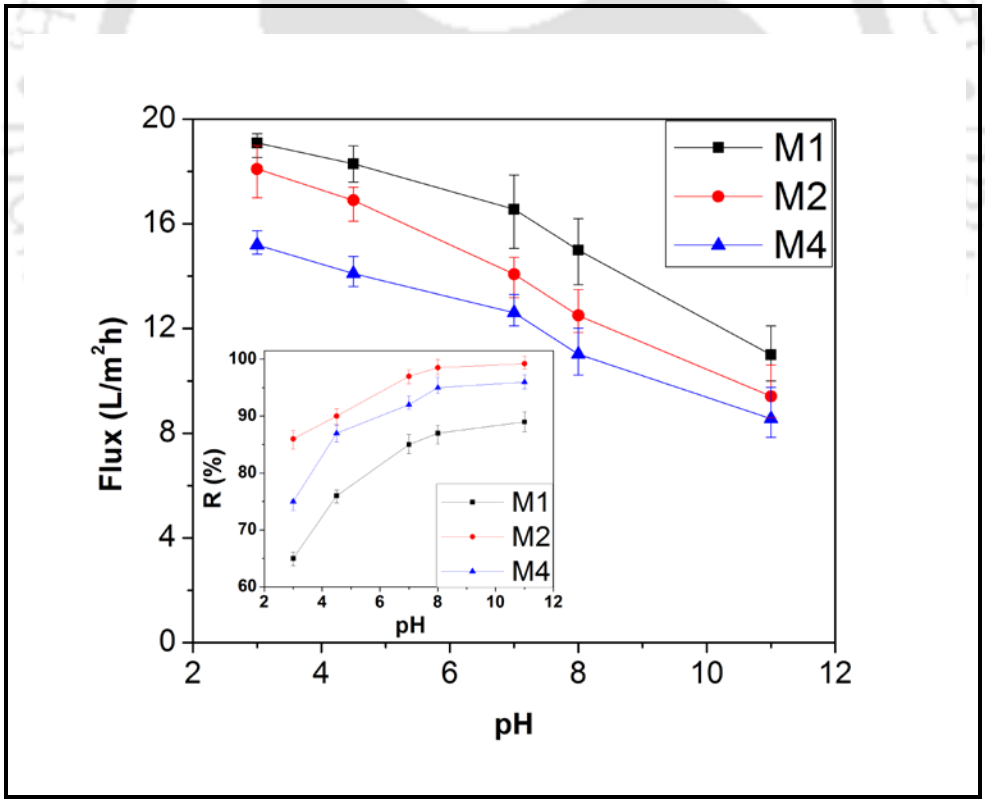

Figure 5.18: Effect of pH on CVD flux and rejection by MEUF at 150 kPa pressure for M1, M2 and M4 membrane.

5.3.7.4. Effect of salt concentration on the MEUF performance

Textile effluent possesses high salt concentration. Therefore, effect of salt concentration on precipitation of micelles was studied and shown in Table 5.5. It was observed that micellar precipitation started at NaCl/SDS ratio of 3.65 along with CVD. Dye removal increases with the increase of NaCl/SDS and most of the dye molecules were precipitated at the ratio of 8.53. It may be concluded by this experiment that the MEUF of CVD containing effluent using SDS is applicable for NaCl/SDS loading of up to 3.65 (g/mmole). Beyond this ratio, micellar precipitation will be started and concept of MEUF will be unacceptable. In order to observe the MEUF performance of synthetic CVD solution, NaCl/SDS ratio of 2.44 was chosen and experiments was conducted using 20 mg L^{-1} of CVD at pH of 11 (Fig. 5.19). 95 % rejection of CVD was observed with flux of 3.7 $Lm^{-2}h^{-1}$ for membrane M2. This is to be noted here that the flux is well below that of without salt condition (Fig. 5.18).

Figure 5.19 depicts the flux and rejection behaviour of membrane M1, M2 and M4 at pH 11, 20 mg L^{-1} of CVD concentration and salt loading about 20 g L^{-1} with SDS at the level of CMC. This experiment was done to know the performance of membrane for realistic application. It was observed that the flux was declined about three folds and rejection (%) was slightly decreased than the normal pH with same dye concentration and without any salt loading (Fig 5.18). This is because of the fact that the osmotic pressure is increased due to the high salt concentration in the feed solution [147]. Again, addition of salt increases the feed solution viscosity in the membrane pores [148]. Reduced flux can also explained by the fact that addition of NaCl to the solution reduces the CMC of SDS which increases the aggregation number and volume of micelles thereafter. On the other hand, pore swelling due to increased salt concentration decreases the membrane rejection behaviour [147-149].

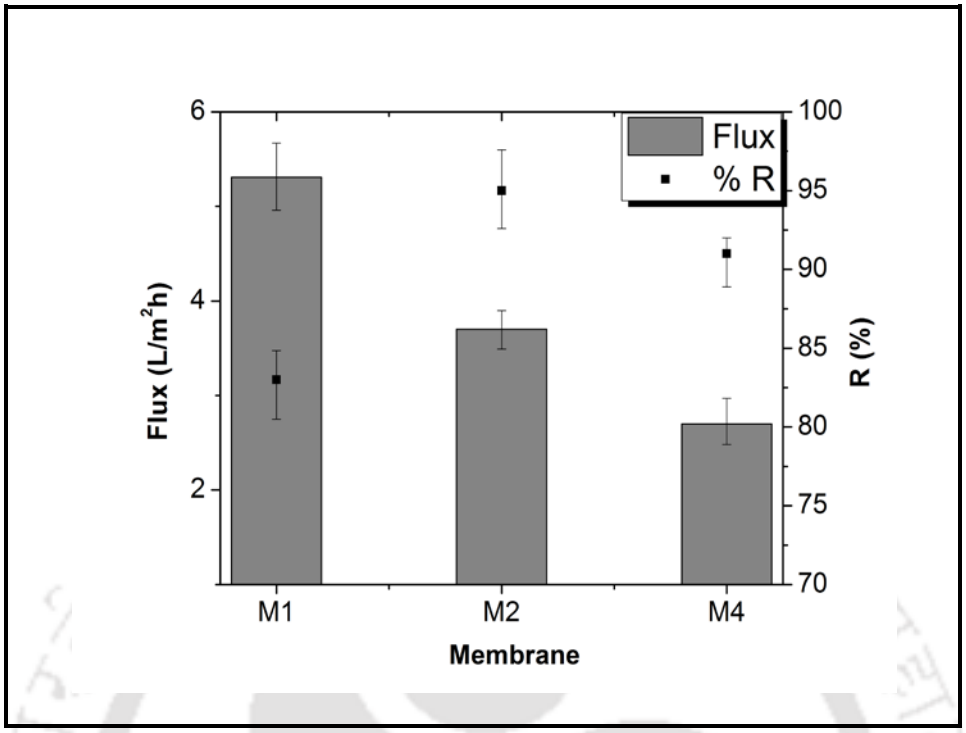

Figure 5.19: Flux and rejection through the membranes after 1 h at pH 11, 20 mg/L CVD and 20 g/L salt concentration with SDS at CMC level for M1, M2 and M4 membrane.

Table. 5.5: Effect of salt concentration in SDS solution. pH: 11, SDS: 8.2 m mol, CVD: 100 mg/L, time: 24 h.

Observation	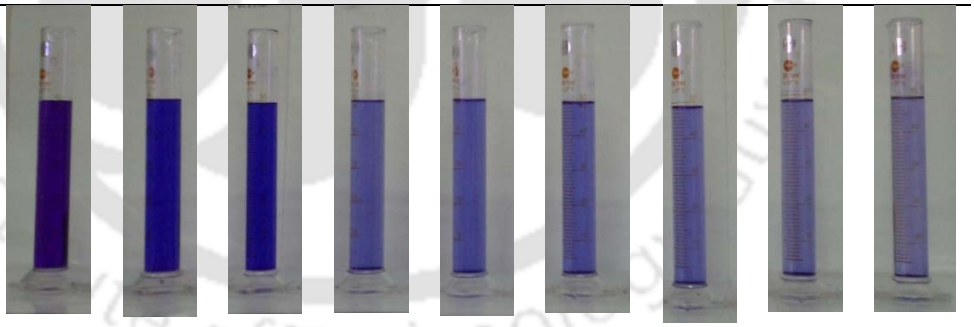								
Sample	1	2	3	4	5	6	7	8	9
SDS (mmol)	0	8.2	8.2	8.2	8.2	8.2	8.2	8.2	8.2
NaCl (g/L)	0	10	20	30	40	50	60	70	80
NaCl/SDS (g/mmol)	--	1.22	2.44	3.65	4.87	6.09	7.31	8.53	9.75
Precipitation	NP	NP	NP	PS	P	P	P	P	P
dye Removal (%)	0	10.4	10.6	31.2	35.1	38.6	40.1	54.2	60.9

NP: No precipitation; PS: Precipitation Started; P: Precipitation

Table 5.6: Literatures related to crystal violet dye removal

Type of membrane	Flux (L/m^{2}h)	Pressure (kPa)	Rejection (%)	Ref.
NF	7.55	415	95	[150]
Composite hollow fiber NF	5.57	70	99.2	[151]
Liquid emulsion membrane	-	-	95	[152]
NF	11	700	98	[153]
Advanced oxidation Process followed by MF	13.2	276	100	[154]
MEUF	14.1	150	99.2	[118]

Summary

Maximum porosity was observed for PVP with D-TA (1 wt %). Porosity was found to be increased by the addition of D-TA, however, it got reduced by the addition of DL-TA. Hydraulic permeability, EWC and hydrophilicity were increased by the addition of D-TA and decreased by the addition of DL-TA. It may be summarised that enatiomeric and racemic effects play an important role in the morphology, hydrophilicity and rejection behaviour of membranes.

Chapter 6

Impact of synthesized amino alcohol plasticizer on the morphology, hydrophilicity and fouling of polysulfone ultrafiltration membrane

In this chapter polysulfone (PSF) ultrafiltration membranes with increased hydrophilicity were prepared using the amino alcohol plasticizer (AAP). The AAP were synthesized by the reaction of polyethylene glycol (PEG) and isatoic anhydride (IAH). Different molecular weight of PEG and IAH (molecular weight 163 Da) were used for preparing the AAP. Asymmetric membranes were fabricated by blending of these plasticizers in membrane casting solution. Proton NMR and FTIR analysis was done to confirm the chemical structure of synthesized AAP. Morphology and surface chemical features were analyzed with SEM, FESEM, AFM, FTIR-ATR and water contact angle. Blended membranes showed enhanced pore density, pure water flux and hydrophilicity compared to plain membrane. Permeation experiments showed significant change in pure water flux through modified membrane with lowest molecular weight PEG based AAP. UF performance and anti fouling property of modified membranes were investigated.

6.1. Experimental

6.1.1. Materials

Polysulfone (PSF), of polyethylene glycol (PEG) (average molecular weight 400 Da, 1500 Da, 6000 Da and 20000 Da), isatoic anhydride (IAH) benzene and 1, 4-Dioxane. N-methylpyrrolidone (NMP), potassium bromide (KBr), $CDCl_3$ and Bovine serum albumin

Content of this chapter is published as below:

N. Sharma, M K Purkait, Impact of synthesized amino alcohol plasticizer on the morphology and hydrophilicity of polysulfone ultrafiltration membrane, J. Membr. Sci. 522 (2017) 202–215.

(BSA) were used for this chapter. Additional detail of all the chemicals is given in Table 2.1 of chapter 2.

6.1.2. Synthesis and characterization of amino alcohol plasticizer

Four kinds of amino alcohol plasticizer (AAP) were synthesized by the reaction of four different molecular weights of PEG with IAH. For preparing the amino alcohol plasticizer 6.52 wt % IAH and 22.4 wt % of a PEG were taken in a three necked round bottom flask (heated in an oil bath). Dioxane was taken as solvent. Mixture was heated up to 60^0C to form the monoamino alcohol. The reaction pathway is shown in Figure 1. The reaction product was then filtered and heated under vacuum at 55^0C for 24 h to remove dioxane. The concentrate was diluted with an equivalent amount of benzene and washed with dilute hydrochloric acid which was saturated with sodium chloride. Removal of benzene was done by applying the heat (65^0C) and vacuum for 12 h to yield the amino alcohol plasticizer. FTIR and ^{1}H NMR spectroscopy were performed as described in section 2.4.2 and 2.4.1, respectively of chapter 2.

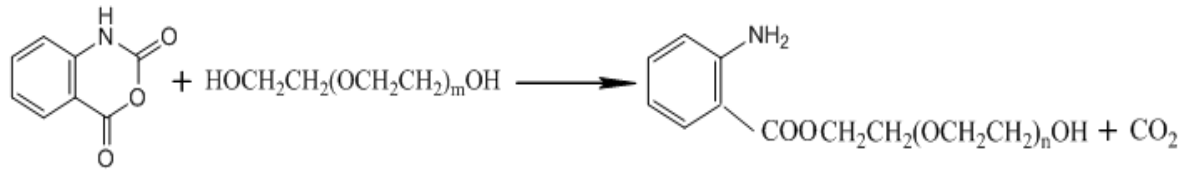

Fig. 6.1: Synthesis route of plasticizer.

6.1.3. Fabrication of blended flat sheet membranes by phase inversion method

Flat sheet membranes were prepared by phase inversion method using AAP by different molecular weight of PEG (as shown in Table 6.1). AAP-1, AAP-2, AAP-3 and AAP-4 were prepared by 400 Da, 1500 Da, 6000 Da and 20000 Da PEG, respectively. Concentration of PSF was kept constant at 14 wt % and concentration of AAP was 8 wt % of casting blend. The membrane casting solution was stirred at a speed of 200 rpm using a magnetic stirrer for 12 h at 40^0C temperature. After getting uniform casting solution, it was degassed for 24 h for eliminating the air bubbles. Further, steps of membrane preparations are presented in section 2.2 of chapter 2. Membrane thickness was maintained as 200 μm.

It is expected during wet phase inversion process, that the hydrophobic part of plasticizer molecules situated at the upper interface will be slanted in the direction of the liquid, which provides a more hydrophilic environment. However, as the casting solution immersed in a coagulation bath and as soon as phase inversion has been driven, plasticizer molecules are rearranged up-side down [82]. Solvent outflows from the casting solution; consequently, hydrophobic nature of the polymer system increases. Finally, the hydrophobic part intermingle with PSF which has hydrophobic character whereas, the hydrophilic parts supposed to be leaned toward the top surface [82, 92]. By the rearrangement of hydrophilic and hydrophobic part of AAP, a hydrophilic layer is formed on the top surface of membrane; which reduces the adsorption of BSA and subsequent fouling.

Table 6.1: Composition of different membrane casting solution containing AAP.

Membranes	PSF (wt.%)	PEG 400 (wt%)	AAP (wt %)	NMP (wt%)
m1	14	8	0	78
m2	14	0	8 (AAP-1)	78
m3	14	0	8 (AAP-2)	78
m4	14	0	8 (AAP-3)	78
m5	14	0	8 (AAP-4)	78

6.2. Membrane characterization

6.2.1. Surface characterization of AAP blended membranes

The presence of functional groups of AAP in modified membrane was confirmed by comparing IR spectra of plain PSF membrane and modified PSF membrane. Attenuated total reflectance - Fourier transform infrared spectra (ATR-FTIR) for the membranes were measured with FTIR instrument using attachment ATR-8200 HA (Shimadzu, Japan). Morphological study of the membranes was done by field emission scanning electron microscope (FESEM). Cross section and top surface images were taken by FESEM with an EHT voltage of 10 kV and by FESEM with an EHT voltage of 2 kV after the coating of thin gold layer, respectively.

Change in hydrophilicity or hydrophobicity of the modified membranes compared to plain membrane were observed by measuring the static contact angle between water and membrane surface. Lower the water contact angle (WCA) higher the hydrophilicity of the membranes. For each sample 4 angles were measured at different part of membranes and average was taken. Static contact angle between the surface of membrane and water

(deionized) droplet was also verified by drop shape analyzer (DSA-25, KRUSS GmbH, Hamburg). Membrane pieces of about 1cm × 1cm area were prepared and then these samples were kept at sample holder of the instrument using the tape. A little drop of DI water (4 μL) was located on the surface and the images were captured at 27^0C temperature.

6.2.2. Pore size distribution experiment

Pore size distribution of the membranes was determined by liquid-liquid displacement porosimetry (LLDP) method. This method gives the number of pores, average pore size and pore size distribution of the fabricated membranes. For this method, it is assumed that all the pores are cylindrical and thickness of the membrane layer is uniform [1]. Water – isobutanol - methanol (25:15:7, v/v, surface tension of 0.35 mN/m and dynamic viscosity of 3.4 mPa s) was taken in separating funnel and mixed vigorously. Then, this mixture was allowed to settle overnight. In the separating funnel water reach phase was separate in the lower part and taken out to wet the membrane. The remaining alcohol reach phase was used as permeating liquid. The variation in flow with change in pressure gives the pore size distribution.

6.2.3. Pure water permeation experiment

Prepared membranes were compacted with deionized water at a transmembrane pressure of 275.8 kPa for 3 h and after that pressure were reduced to the operating pressure of 150 kPa. Flux was measured at regular interval of 0.5 h. The compaction factor (CF) was calculated as the ratio of initial pure water flux to steady state pure water flux. Pure water flux (PWF) was determined by allowing deionized water to pass through the compacted membrane. PWF was measured by the equation 2.10. Flux values of pure water at different transmembrane pressures were measured under steady state condition. Permeability (P_m) (L/m^{2}h kPa) was

evaluated from the slope of the plot of J_w vs P. Hydraulic permeability was calculated by equation 2.11.

6.2.4. Ultrafiltration performance and fouling behaviour experiment

Ultrafiltration experiment was conducted to study the solute separation, permeate flux and fouling behaviour of the prepared membranes. BSA was dissolved in DI water and the concentration and pH were kept constant at 1000 mgL^{-1} and 7 respectively for all the experiments. Each membrane was initially compacted for 30 min at 275.8 kPa, then the pressure was reduced to 150 kPa and the water flux (J_{w1}) was measured for 1 h duration. Afterwards water permeation, cell was refilled with BSA solution and flux was measured (J_p). The BSA rejection ratio was calculated by the equation 2.15.

After 2 h of ultrafiltration and later hydraulic cleaning of the membrane, water flux was measured (J_{w2}). With the help of J_{w1} and J_{w2}, flux recovery ratio ($Flux_{RR}$) was measured. After the first round of BSA rejection and membrane cleaning, water flux was measured, that is used to calculate first flux recovery ratio ($Flux^1_{RR}$). Again, BSA rejection experiment was done for 2 h and all the operation was repeated to calculate the second flux recovery ratio ($Flux^2_{RR}$). Fouling of membrane causes flux loss $(J_{w1}\text{-}J_p)$ and the flux loss caused by total fouling (F_t), reversible fouling (F_r) and irreversible fouling (F_{ir}) are calculated by equations 2.16, 2.17 and 2.18 respectively.

6.3. Results and discussion

6.3.1. FTIR and NMR spectroscopy analysis of AAP

Figure 6.2 depicts the FTIR spectra of all the four AAP prepared by different molecular weight of PEG. Peaks at 3452 cm^{-1} and 2945 cm^{-1} are characteristic peaks of AAP due to –

OH group and –CH_2– group present in amino alcohol plasticizer. Peaks at 1630 cm^{-1} and 1412 cm^{-1} attributed to the –NH_2 and –CH_2 groups, respectively; those exist in AAP. Figure 6.3 depicts the ^1H NMR spectra of synthesized AAP-1, AAP-3 and AAP-4 with their chemical structure. For both the AAPs shift at δ= 1.4 (c) shows the presence of –CH_2 group in AAP. Shifts at δ= 2.8 (b) and δ= 3.0–4.0 (d), due to the presence of –NH_2 and –OH respectively. Shift at 6.5-7.5 (a, a') depicts the existence of aromatic group in AAP. Combining the FTIR spectra and NMR shifts, the results signified typical AAP structure had been obtained. Amino alcohol plasticizer with compounds containing -NH_2 and –OH groups was formed.

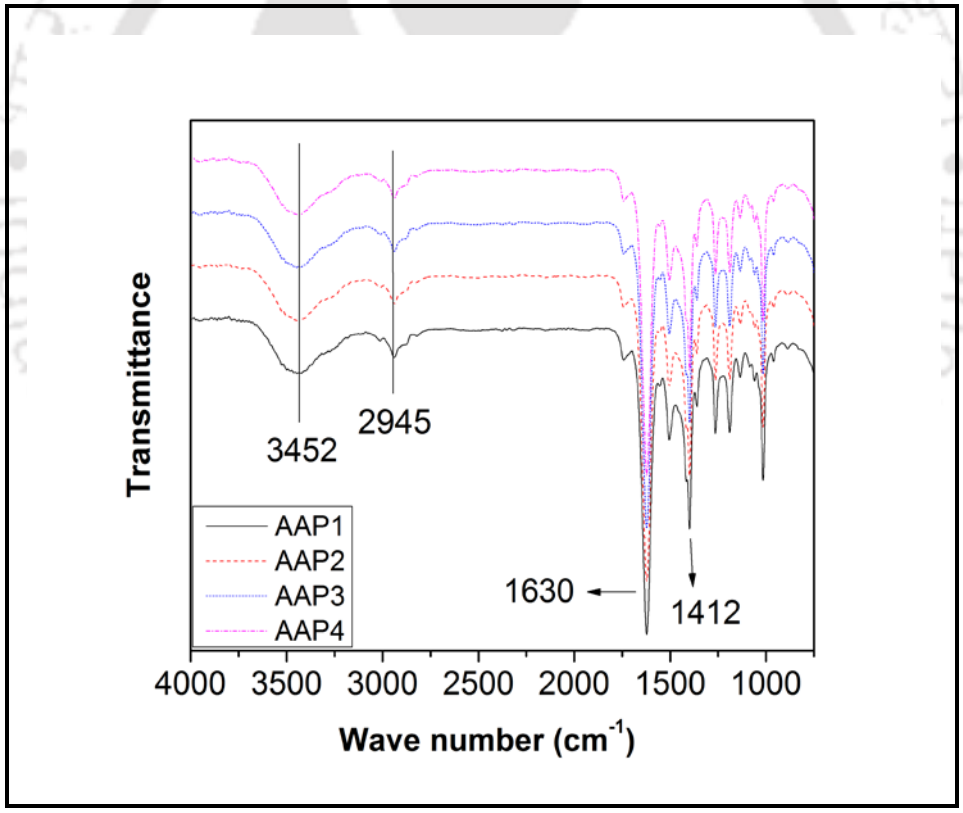

Figure 6.2: FTIR spectroscopy of different AAPs.

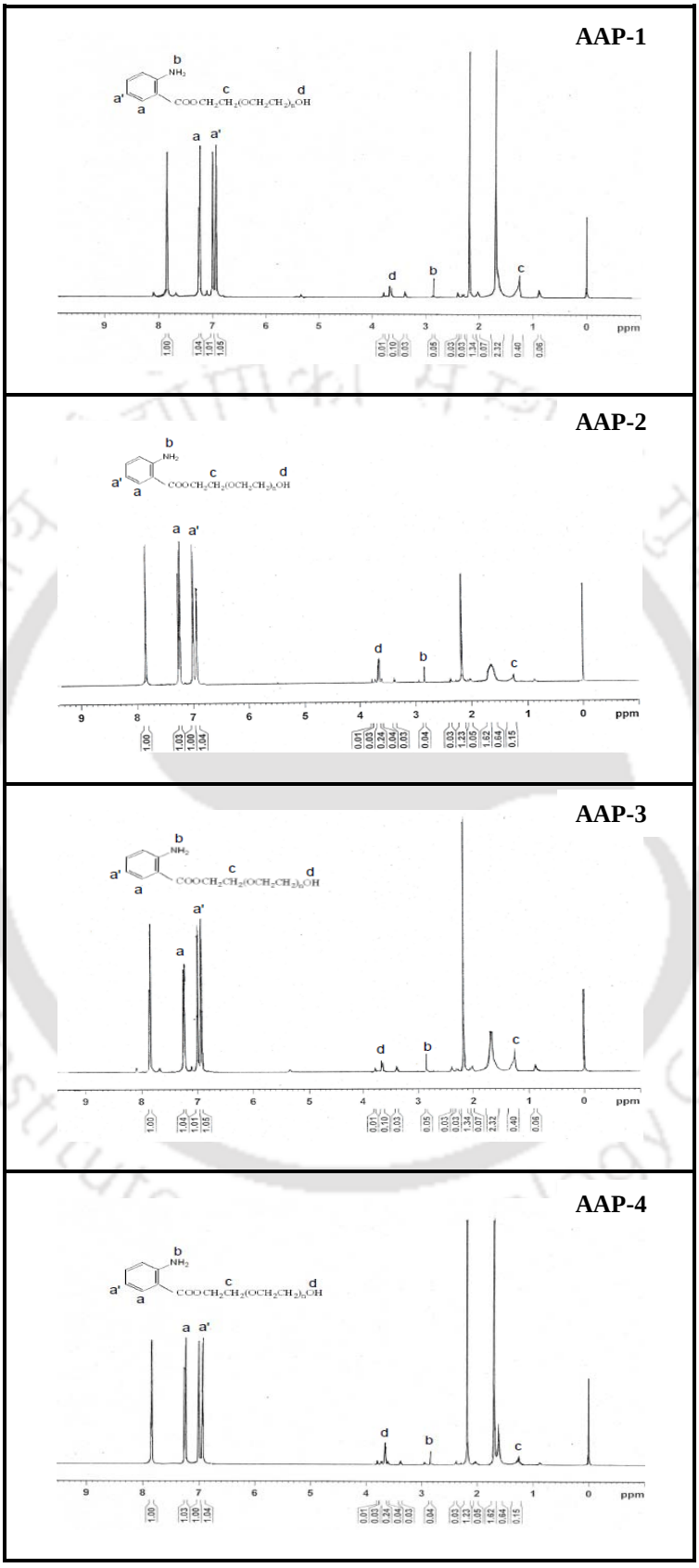

Figure 6.3: ^{1}H NMR specrta of synthesized AAPs.

6.3.2. Surface and morphological characterization of modified PSF membranes

6.3.2.1. ATR-FTIR analysis of plain and blended membranes

Figure 6.4 shows ATR-FTIR spectra of plain and blended PSF membranes surfaces fabricated with different AAPs. Peaks at 1598 cm^{-1} and 1485 cm^{-1} are the characteristic peaks of C=O and $–CH_2–$ group present in AAP. The peak at 1155 cm^{-1} due to S=O group present in PSF, thus verifying the presence of PSF. Peaks at 1240 cm^{-1}, 1097 cm^{-1} and 821 cm^{-1} confirm the occurrence of $COOCCH_2$, C-OH and benzene ring which are present in AAP. It was noted that by increasing molecular weight of PEG in AAP the intensity of peaks was falling. It may be due to fact that higher molecular weight of PEG based AAP were retained in lesser amount on the membrane surface.

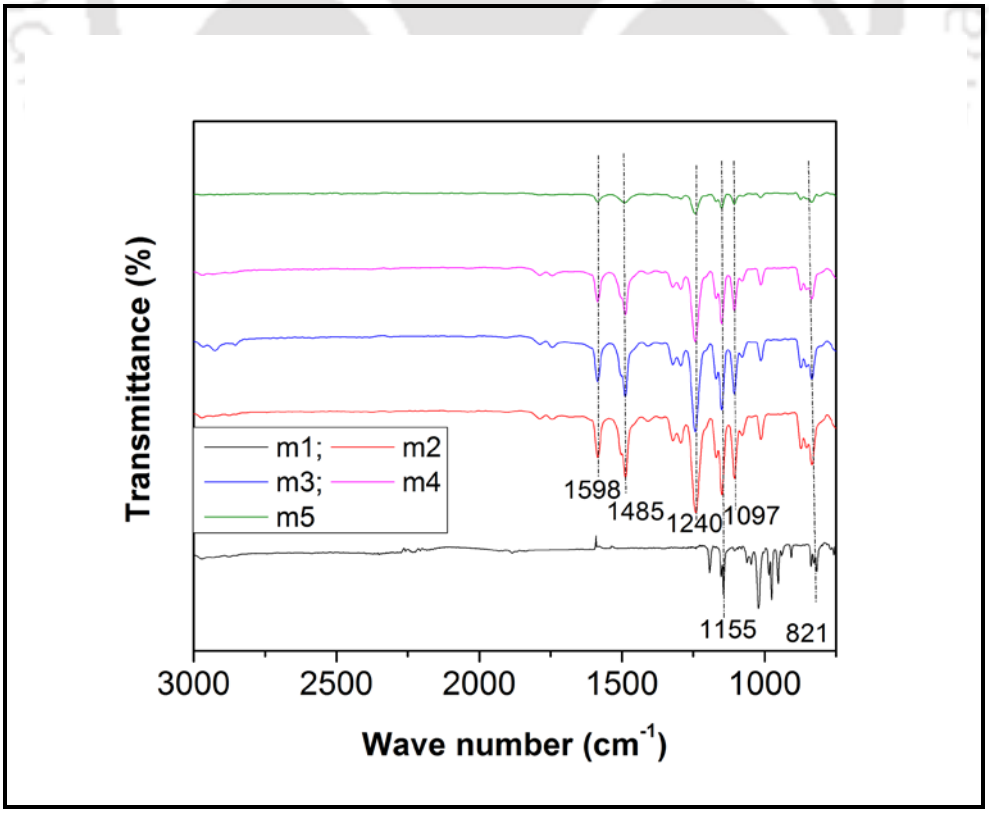

Figure 6.4: ATR-FTIR of membrane with different AAP.

6.3.2.2. Microscopic studies

FESEM images were used for finding the size of pores. Higher magnification was in favour for finding the size of pores. On the other hand, presence of AAP was confirmed by SEM image analysis.

SEM studies

Figure 6.5 shows the cross sectional images of the prepared membranes m1, m2, m3 and m4. Lower magnified images confirm finger like cavities thus, addition of AAP did not alter the typical asymmetric porous structure and both the membranes have a permeable sub-layer. Instantaneous demixing is responsible for this type of structures [116] and subsequently results in porous sublayer. Modified membrane depicts longer and more uniform finger like structure as compared to the membrane without AAP. It consequences in more permeable AAP membranes than the unmodified membrane. It has found that structure of membrane is formed by the relative diffusion rate of non-solvent and solvent as well as driving force between them [155, 156]. Since, the AAP has hydrophilic property; the addition of these plasticizers affects the diffusion rate of the non-solvent and solvent. AAP content membranes fallout in finger like cavities in sublayer below the dense top layer during phase inversion.

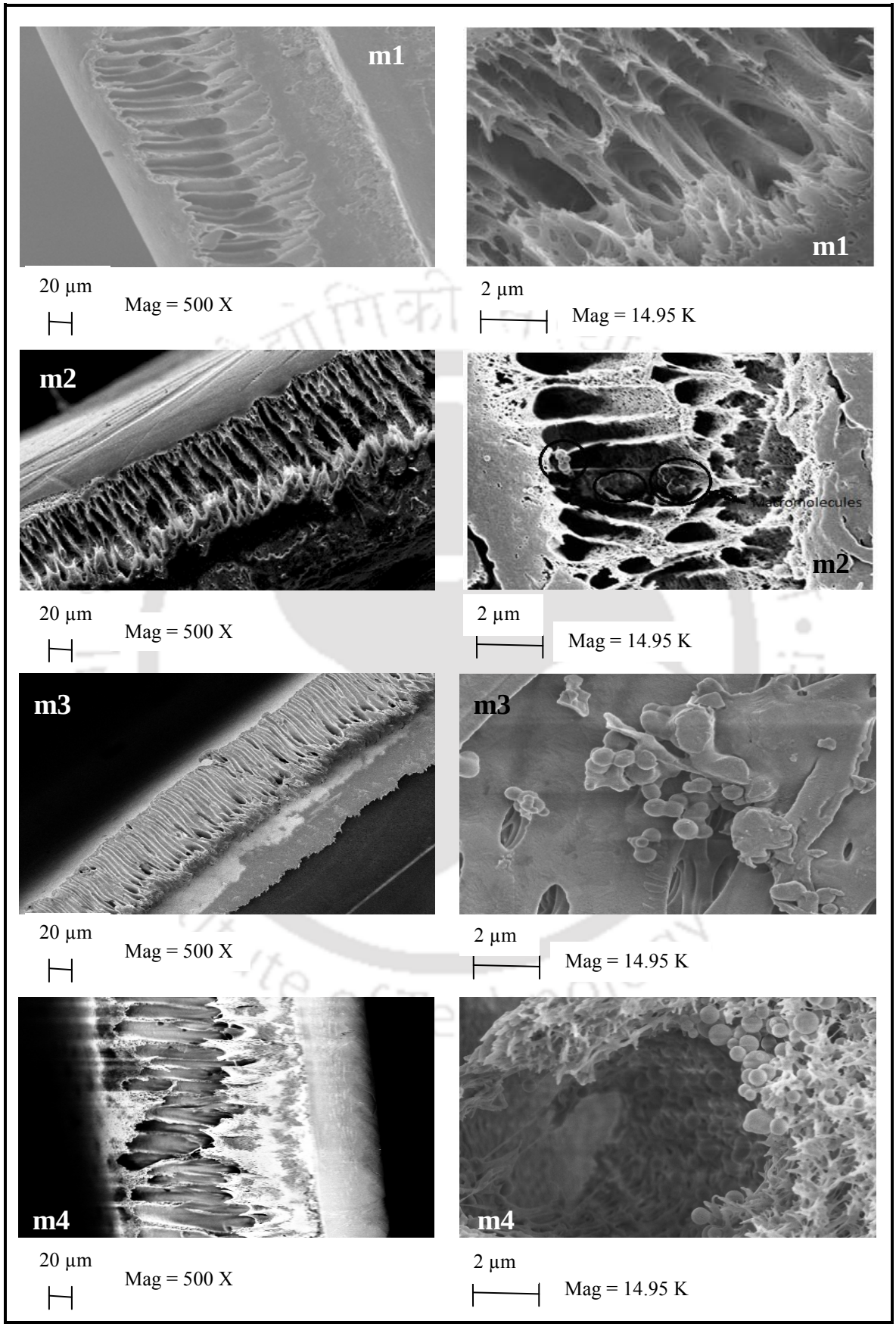

Figure 6.5: Cross sectional SEM images of m1, m2, m3 and m4 membranes.

FESEM studies

The top surface of membranes m1, m2 and m5 were imaged using FESEM (Figure 6.6). It depicts the top surface FESEM images with 50 KX magnifications. It was confirmed that m2 membrane has notably smaller pore size. It may be because of the fact that the degree of transmission and diffusion of solvent and non solvent at top surface was more as compared to sublayer. Mean pore size on surface and macro-voids present in the support layer are important for determining flux and selectivity of membranes, so managing the formation and size tuning of pores is significant [157]. Possibly spinodal demixing is responsible for the formation of top surface. Membrane m1 shows uniform surface with nano metric pores because of enough time for phase separation. The AAP containing membrane has pores below 5 nm with a higher number per unit area, on the surface. In supplement dark area and white particles appeared because of incomplete phase separation between PSF and AAP, which furthermore confirmed through contact angle values. It can be described by the fact that porosity was increasing since the number of pores on the surface was increasing by the addition of AAP. Figure 6.7 depicts and pore size distribution (PSD) of m1, m2 and m5 membranes obtained by FESEM. Image J software was used for measuring the size of the pores from FESEM images; PSD clearly shows that number of smaller sized pore increased by the addition of AAP for both the membranes m2 and m5. Trend of PSD was almost same for m1, m2 and m5. However, m2 possesses largest amount of smaller pores. Average pore size was calculated (using equation 2.9) as 21.33 nm, 8.67 nm and 17.15 nm for m1, m2 and m5 membranes, respectively. It was observed that maximum pores present in membranes m2 and m5 were less than 5 nm, however for membrane m1 the number of pores less than 5 nm was only around 20 % and bigger sized pores were more on m1 membrane. Suyatma et al. [158] found the same result; they studied effects of hydrophilic plasticizers on mechanical, thermal and surface properties of chitosan films.

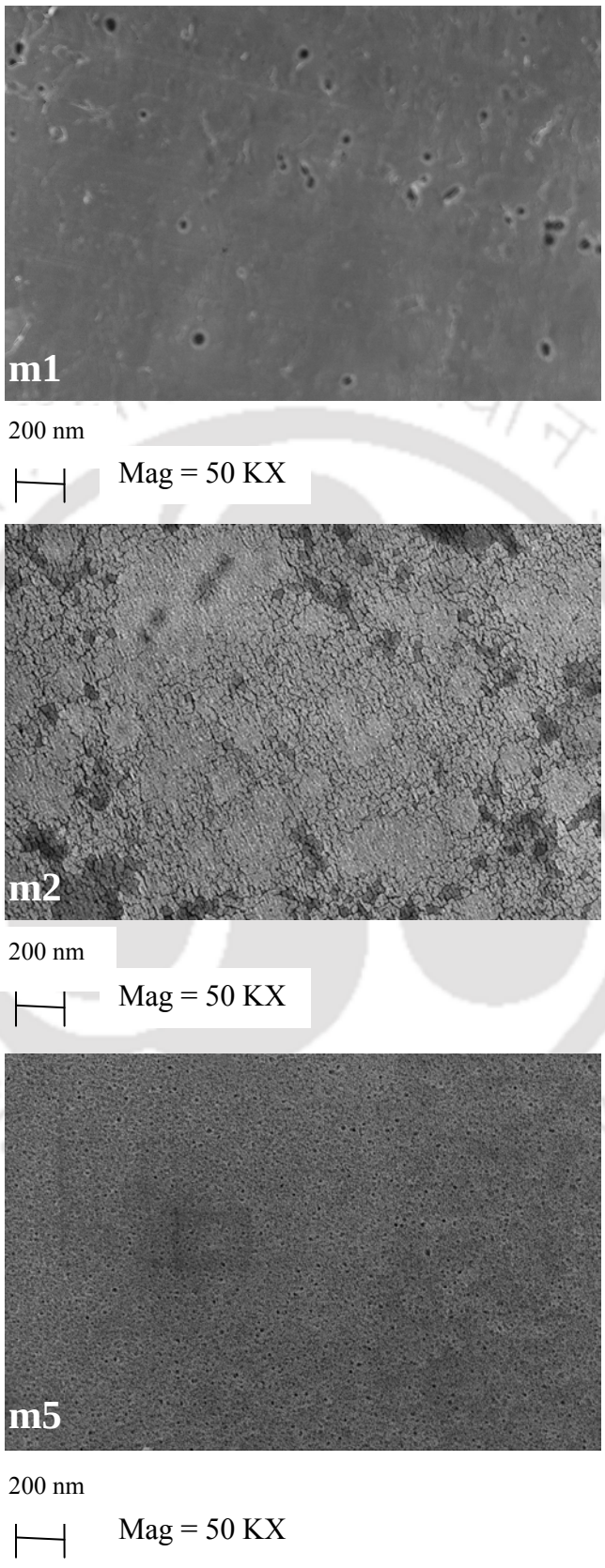

Figure 6.6: Top surface FESEM image of plain and modified membranes.

Furthermore, it was found that amphiphilic plasticizer improves the permeation performance of membrane by working as pore forming agent. Zhao et al. and Lv et al also found similar type of results [159, 160].

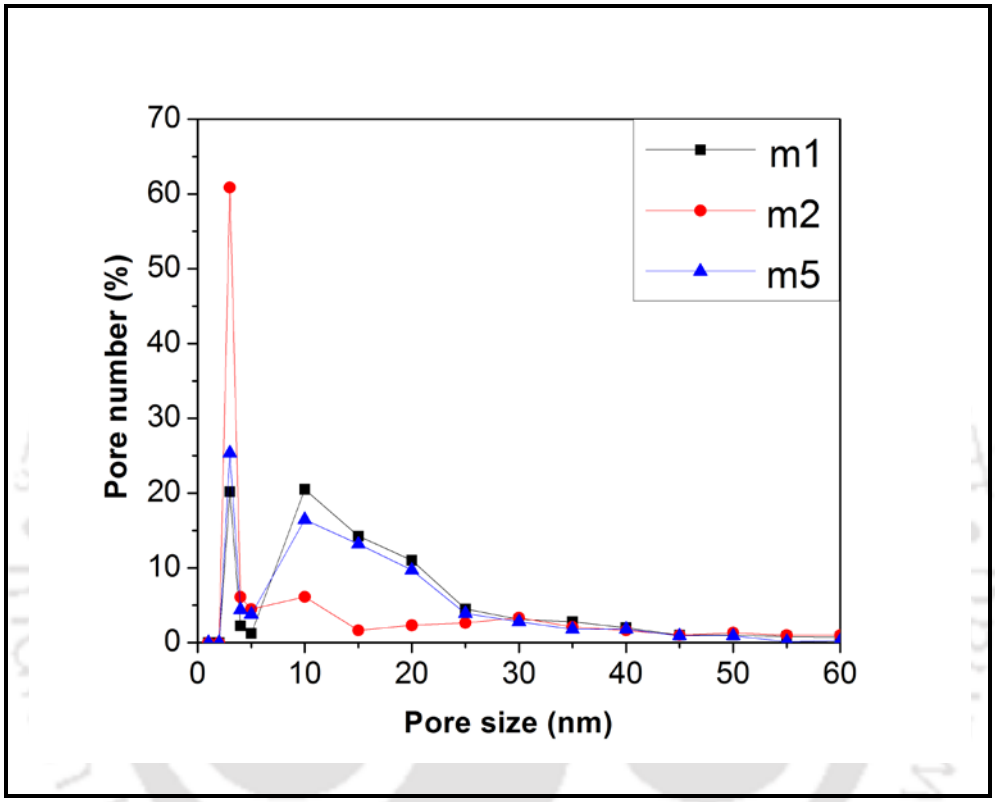

Figure 6.7: Pore size distribution of m1, m2 and m5 membranes by FESEM.

6.3.2.3. Pore size distribution study

Effect of different AAP on pore size distribution was carried out by LLDP methods. This method estimates the pore size distribution of the membranes in wet state i.e. similar to the condition of UF operation. Pore size, pore density, total number of pores and average pore size of all the membranes were determined using equations. 2.1, 2.4, 2.7 and 2.8, respectively. Fig. 6.8 shows the LLDP flux profile for m1, m2, m3, m4 and m5 membranes.

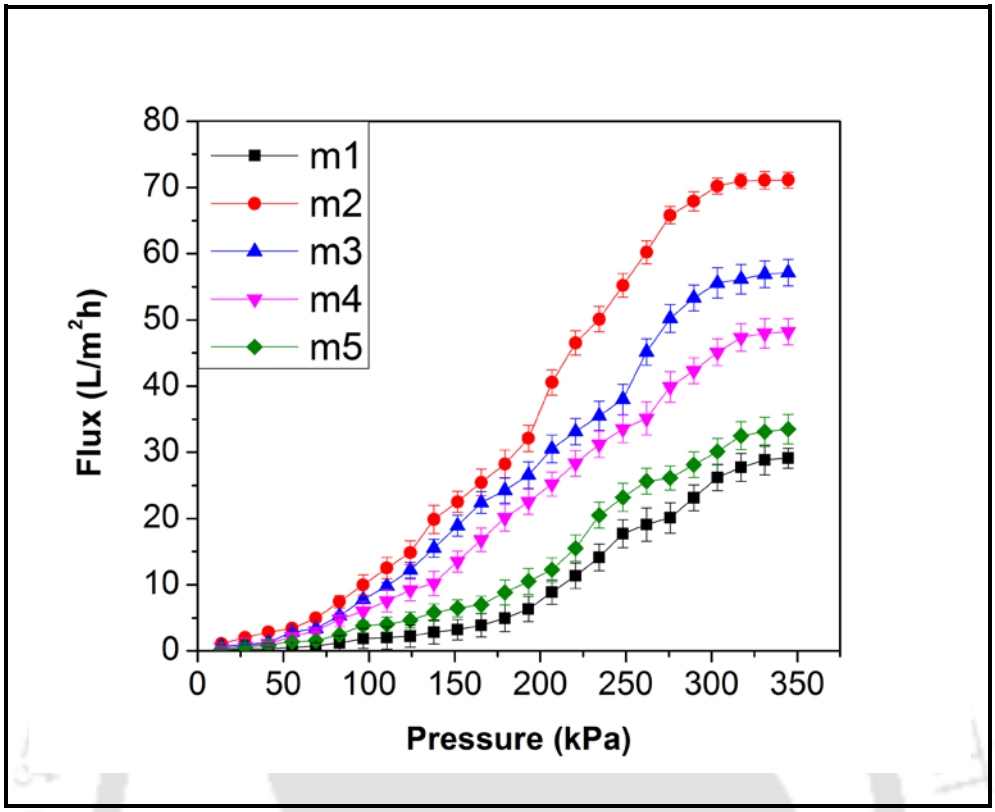

Figure 6.8: LLDP flux profile for membranes prepared with different molecular weight based AAP.

PSD of the membranes observed by LLDP is shown in Fig. 6.9. Around 23.3 % of the pores were in the size of 3-4nm for m2. For m1, m3 m4 and m5 these numbers are 18.4 %, 21.2 %, 20.5 and 20 %, respectively. Pore size distributions obtained from LLDP analysis was analogous to the PSD observed by FESEM method. However, FESEM analysis using Image J software, bigger pores especially greater than 10 nm was also measured on the surface of the membrane. It may be due to the fact that possibility this method may overrate the pore size by considering the wider pores on the surface [42]. Figure 6.10 and 6.11 depict membrane permeability and numbers of pores which were drawn with respect to the pore radius as cumulative curves, respectively. It can be seen from both the figures that the pores approximately 92 % for all the five membranes are in the range of 3-5 nm which clearly brought them under UF range. However, a few larger pores are responsible for the membrane

performance as a whole. Hagen–Poissuille equation explains that the enlarged pore radius can be responsible for increase in flux. Calvo et al. [102] observed the same results for UF membranes formed by track etched method. Results obtained by LLDP method are placed in table 6.2. It is observed that, by the addition of AAP number of pores for all the membranes increases; especially adding the lower molecular weight based AAP consequences in more porous membranes. The total hydraulic permeability coefficient L_n for all the five membranes was calculated 1.04 ms^{-1} MPa^{-1}, 3.97 ms^{-1} MPa^{-1}, 3.03 ms^{-1} MPa^{-1}, 2.45 ms^{-1} MPa^{-1} and 1.48 ms^{-1} MPa^{-1} for m1, m2, m3, m4 and m5, respectively. Number of pores per unit area was also found to be increased by the addition of AAP in the membrane casting solution. It was increased from 1.08×10^{8} m^{-2} to 3.34×10^{8} m^{-2} for membrane m1 and m2, respectively. The mean pore size r_m for all the five membranes was slightly decreased by the addition of AAP. It was calculated as 2.45 nm, 2.30 nm, 2.34 nm, 2.39 nm and 2.41 nm for m1, m2 m3, m4 and m5, respectively. Total pore area per unit area of membrane was calculated with the help of equations 2.5 and 2.6. From the LLDP flux data and by use of equation 2.4, pore number per unit area of different membranes were calculated which is shown in the Figure 6.9. Nature of LLDP flux profile is almost same for all the membranes. After the start of flow, penetrating liquid (alcohol rich) starts to swap the wetting liquid (water rich) in largest pores. Further, with the increase in pressure penetrating liquid swaps the wetting liquid in the smaller pores and as soon as all the pores of the membrane are opened by swapping the wetting liquid in the pores, the flux starts to remain almost constant (Figure 6.8). Cumulative permeability and cumulative pore number with respect to pore size (nm) are shown in figure 6.10 and 6.11, respectively.

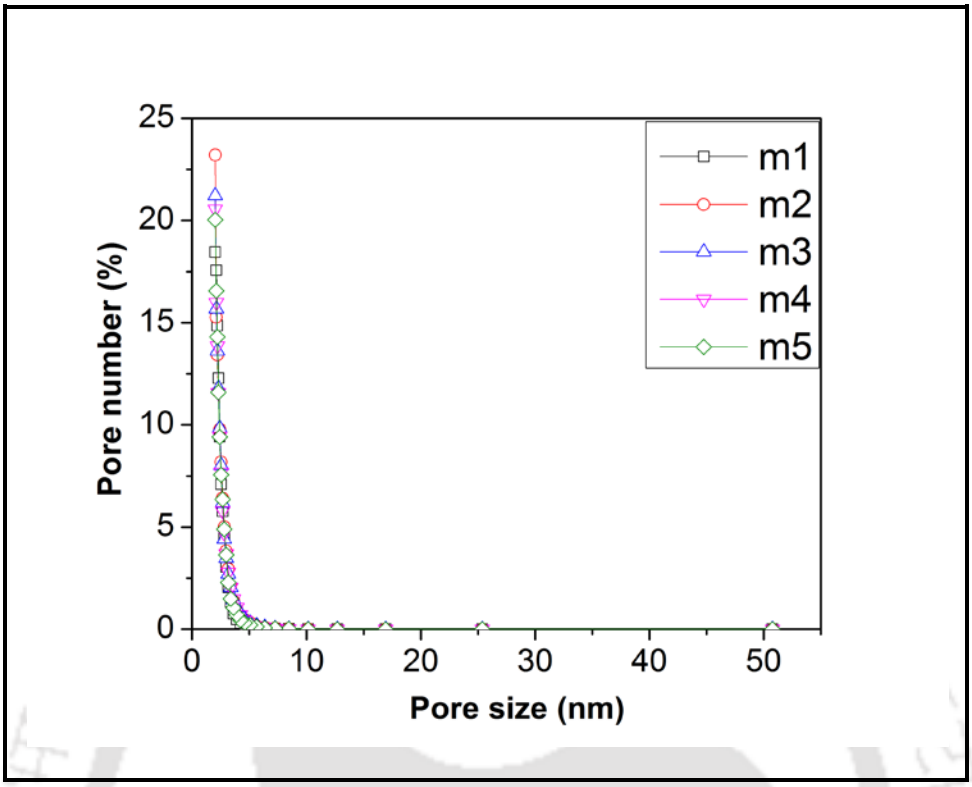

Figure 6.9: Pore size distribution in percentage for m1, m2, m3, m4 and m5 membranes by LLDP method.

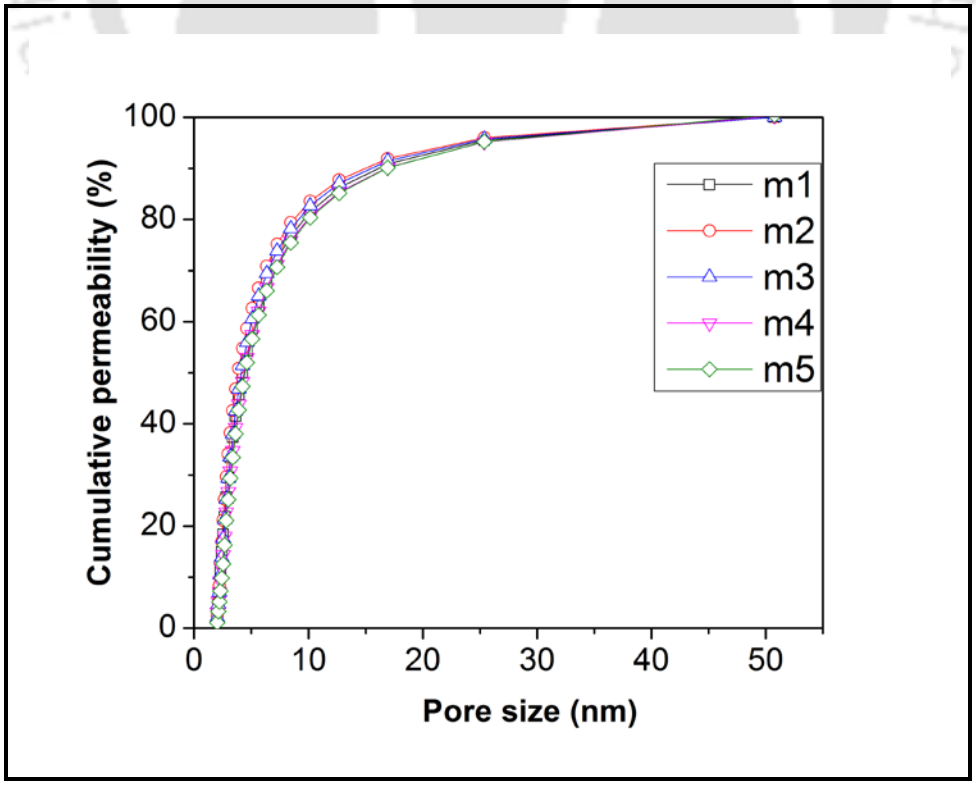

Figure 6.10: Change in cumulative permeability (%) with pore size.

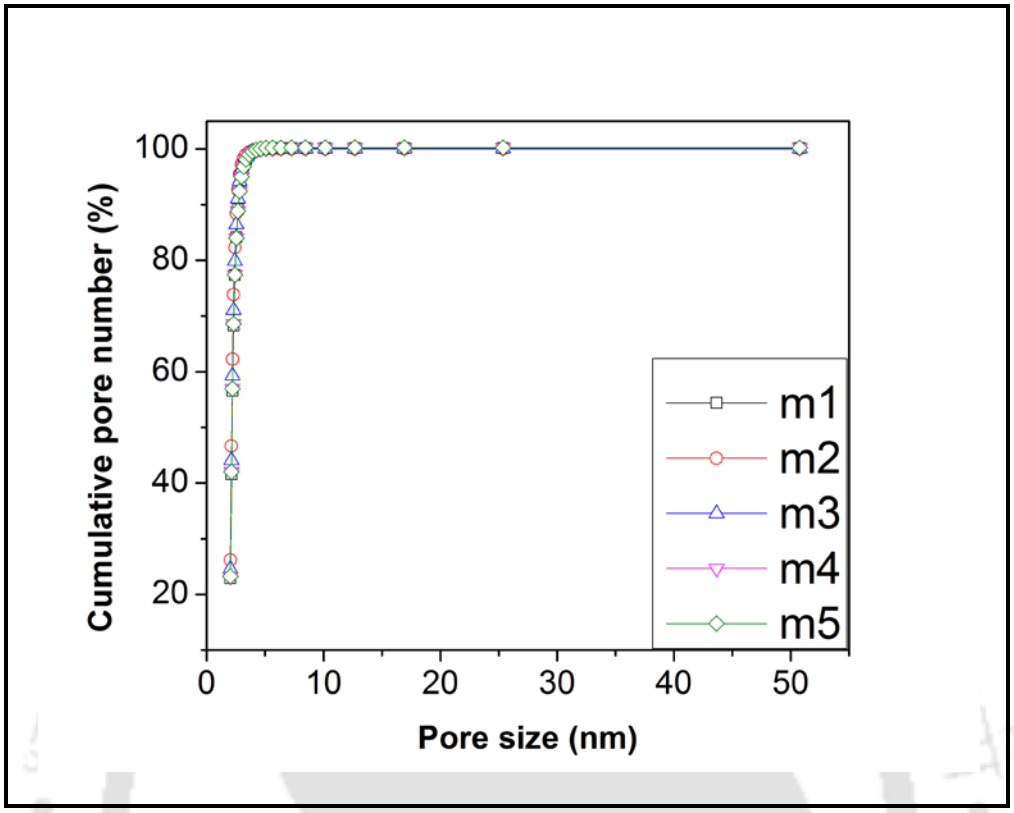

Figure 6.11: Effect of AAP on cumulative pore size distribution in percentage.

These results illustrate that AAP content in membrane casting solution enhances the pore forming process, which is discussed in previous section. Also, these results are in complete agreement with morphological study of the membranes.

6.3.3. Pure water permeation and hydraulic permeability studies

Membranes prepared by blending of four different AAP were tested through permeation experiments. Various characterization parameters such as PWF, CF and hydraulic permeability were measured.

6.3.3.1. Effect of addition of AAP on CF

Membrane sub-layer described by compaction factor (CF), it is an important factor for finding the structure of the membrane. Presence of large number of macrovoids in the

sublayer is the reason of the compaction. PWF for all the membranes during compaction is shown in figure 6.12. Initially all the membranes were compacted for 3h at 275.8 kPa and flux was collected after every half an hour interval. For all the membranes, PWF is initially seen to be declined with respect to time. Compaction is possibly responsible for this declination of flux and finally attains a steady state after around 2 h. It may be because of the fact that the pores become denser resulting lessening in pore size [1]. Figure 6.12 depicted that the addition of increased molecular weight of PEG based AAP, steady state PWF decreases. For example, the steady state flux decreases from around 110 L/m^{2}h to 34.9 L/ m^{2}h, when molecular weight of PEG increases from 400 Da to 20,000 Da. However, all the AAP containing membrane shows higher flux than plain membrane m1. It is seen that for m1, m2, m3, m4 and m5 membranes the CF was calculated as 3.8, 2.1, 3.2, 3.5 and 3.7, respectively.

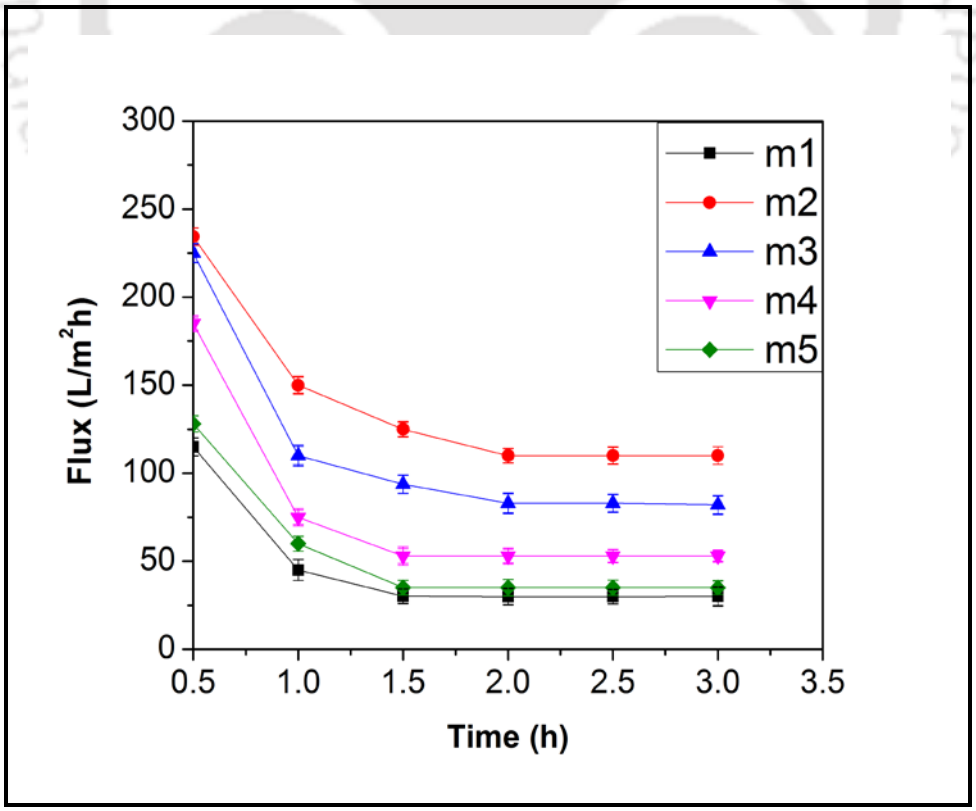

Figure 6.12: Flux profile during compaction for membranes at 275.8 kPa.

6.3.3.2. Effect of AAP on PWF, hydrophilicity and Hydraulic Permeability

Figure 6.13 depicts the effect of transmembrane pressure on PWF for m1, m2, m3, m4 and m5. These experiments were performed at different transmembrane pressures between 55 kPa to 275.8 kPa. It was observed for all the membranes that PWF increases almost linearly with increase in pressure. These results confirm the findings of compaction studies as shown in figure 6.12, as well as the water contact angle measurements shown in figure 6.14. Flux profiles based on transmembrane pressure were used to determine the hydraulic permeability (P_m) of the membranes (equation 2.11). It was found to be increased from 0.08 to 0.36 L/m^2 h kPa for the plain membrane to the membrane m2 modified with the AAP-1. These outcomes are consistent with the morphological analysis, hydrophilicity and PSD results of the membranes discussed in the preceding sections.

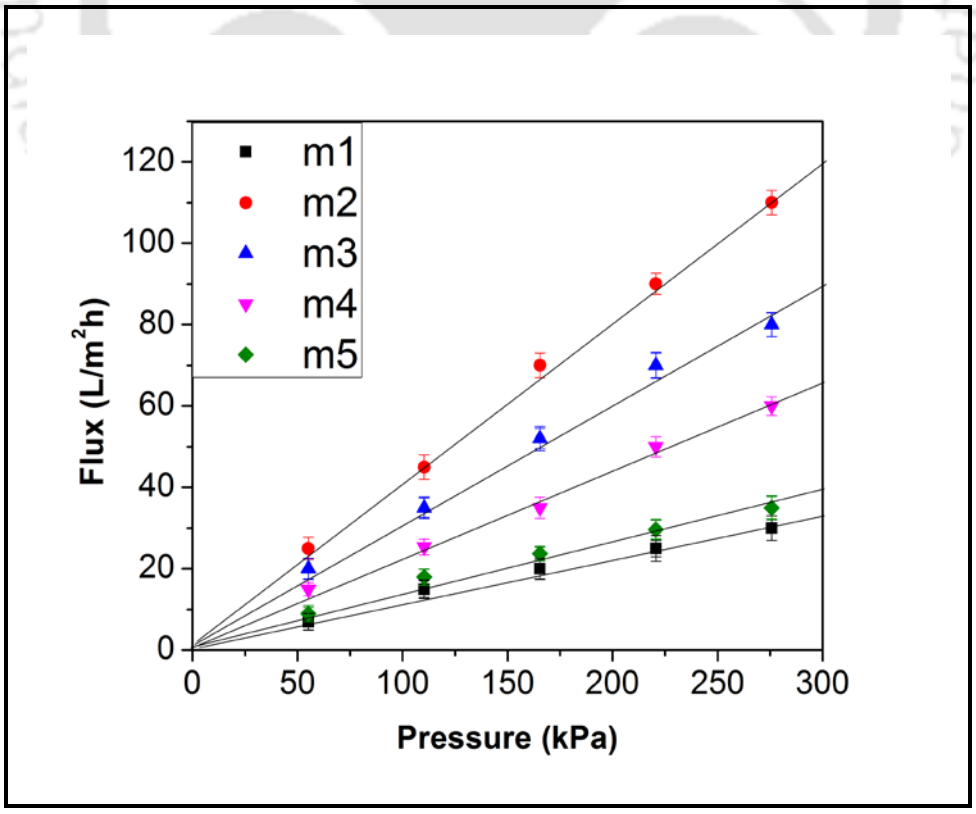

Figure 6.13: Effect of different molecular of PEG based AAP on hydraulic permeability.

Figure 6.14 depicts the images of contact angles for all the five membranes. Hydrophilic behaviour of the membrane is explained by water contact angle (WCA) measurement. Lower the WCA value higher will be the hydrophilicity of the membranes and more hydrophilic membranes are less prone towards fouling. Contact angle measurement gives insights about surface hydrophilicity [40]. It was found that lower molecular weight PEG based plasticizer containing membranes show lower contact angle than higher molecular weight PEG based plasticizer containing membranes i.e. more hydrophilic and consequently more porous membrane. Hołda et al. [161] observed the same results in their study based on influence of high molecular weight additives. The contact angle was also found to be decreased by the addition of AAP, prepared by different molecular weight of PEG. However, membrane m2 shows lowest contact angle as shown in figure 6.14. It was measured as 72^0, 62^0, 67^0, 69^0, and 70.5^0 for m1, m2, m3, m4 and m5 respectively. Pore area and number of pores also increased by the addition of AAP (table 6.2). It is the indication of increased hydrophilicity by the addition of AAP in this study.

Table 6.2: Effect of AAP on some characterization parameters.

Membrane	N_t (m^{-2}) × 10^{-8}	A_t (m^2) × 10^9	r_m (nm)	CF	Porosity
m1	1.08±0.06	2.03±0.04	2.45±0.05	3.8	0.34
m2	3.34±0.05	5.54±0.05	2.30±0.04	2.1	0.61
m3	2.59±0.06	4.45±0.05	2.34±0.05	3.2	0.54
m4	2.13±0.03	3.82±0.05	2.39±0.03	3.5	0.47
m5	1.37±0.04	2.49±0.05	2.41±0.06	3.7	0.39

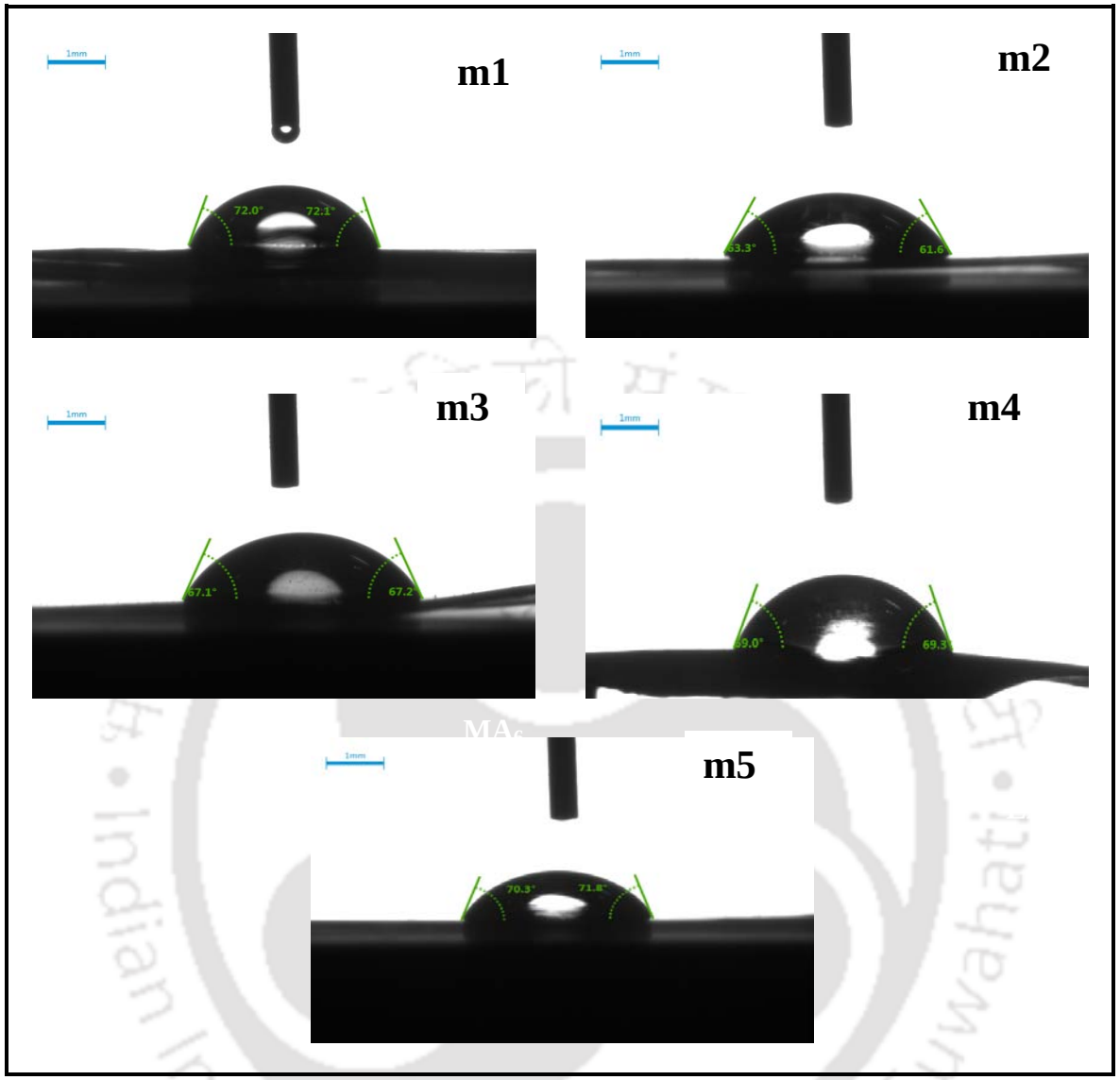

Figure 6.14: Images of contact angles for membrane m1, m2, m3, m4 and m5.

6.3.3.3. Membrane characterization by EWC and porosity

Equation 2.12 was used for calculating the EWC of all the membranes and presented in Table 6.3. PWF is closely related to the EWC and it is a significant parameter for membrane characterization. It was observed that by the addition of AAP prepared by different molecular weight of PEG, EWC (%) was increased. However, by increase in molecular weight of PEG, EWC of the membrane decreased. The EWC for membrane m1, m2, m3, m4 and m5 was calculated as 33.3, 64.5, 55, 54.1 and 37.5, respectively. This increasing tendency approves

the presence of increasing number of pores in the membrane by the addition of AAP (Table 6.2). The pores present on the top surface and also in the sublayer provide space for accommodation of water molecules in the membrane. This may be because of the presence of hydrophilic AAP in sublayer pores.

Porosity of membrane is significant factor for describing membrane permeation behaviour and separation processes and it has close contact with morphology and PWF of the membrane. Membranes porosity was measured using equation 2.13. Table 6.2 depicts the calculated values of porosity of all the membranes. It is confirmed from Table 6.2 that porosity got increased by the addition of AAP in the membrane. Porosity for m1, m2, m3, m4 and m5 is calculated as 0.34, 0.61, 0.54, 0.47 and 0.39, respectively. Change in porosity can be explained on the basis of two facts one is kinetic and another is thermodynamic contemplation. As soon as additives are added into the casting solution two major effects take place. Firstly, separation of phase because of the reduced miscibility of the casting solution in nonsolvent because of the thermodynamic improvement. Secondly, it produces kinetic obstruction to phase separation since the viscosity of the solution got increased; as a result delayed demixing occurs [1]. AAP prepared with PEG (molecular weight of 400 Da) depicted the maximum hydrophilicity, it may be because of the fact that the lower molecular size as compared to PEG 1500 Da, PEG 6000 Da and PEG 20000 Da. Figure 3 clearly depicts that without and with addition of AAP in the membrane sublayer affects the widths of the pore. Addition of AAP narrows the sublayer pores which are longer than plain m1 membrane.

Table 6.3: Values of some characterization parameters for all the 5 membranes.

Membrane	L_n (ms^{-1} MPa^{-1})	EWC (%)	WCA (^{0})	IEC
m1	1.04	33.3	72	0.07
m2	3.97	64.5	62	0.36
m3	3.03	55	67	0.11
m4	2.45	54.1	69	0.10
m5	1.48	37.5	71	0.10

6.3.4. Ultrafiltration and fouling studies using BSA

Feed solution properties and morphology of the membrane affect the flux characteristics and rejection of solute through the membranes, specially its pH. So, fabricated UF membranes were also tested in terms of flux and rejection at different pH with BSA solution (1000 mg/L).

6.3.4.1. Reversible and irreversible fouling study

Membrane fouling can be classified in two types; these are as reversible and irreversible fouling. Reversible adsorption and deposition of protein causes reversible fouling. This type of fouling can be removed by simple hydraulic cleaning. But irreversible protein adsorption causes irreversible fouling that can only be eliminated by chemical cleaning or enzymatic degradation [101]. To find out these fouling values, pH of 7 was used during experiments. The summarizing of total fouling (F_t), reversible fouling (F_r) and irreversible fouling (F_{ir}) as a function of different molecular weight of PEG based AAP.

The time dependent flux of membranes modified by the blending of different AAPs is shown in Figure 6.15. DI water flux was measured from 0 - 60 min, 180 - 240 min, 360 - 420 min and BSA flux was measured from 60 - 180 min and 240 - 360 min. Water permeation results were showing, a slight loss of flux through initial time of water permeation and after that it remains constant for all the membranes, but during BSA permeation, a severe flux loss was seen in initial permeation for all the membranes. It may be seen from Figure 6.15, as time passes, the difference between the pure water flux of plain membrane and modified membranes (blended with lower molecular weight based AAP) increases. For membrane modified with lower molecular weight based AAP, flux becomes higher compared to other membranes. Membrane containing AAP-1 had the highest flux at the end of experiment. It may be because of the fact that AAP-1 contains more number of hydrophilic –OH group. The more hydrophilic the membrane was, the less decrease in the flux. Initial loss of flux during UF of BSA may be because of the deposition or adsorption of BSA molecules on the surface of membranes or inside the pores. So, the fouling resistance membrane should successfully oppose the deposition or adsorption of foulants to their surface or pore as reported in literatures [108, 162].

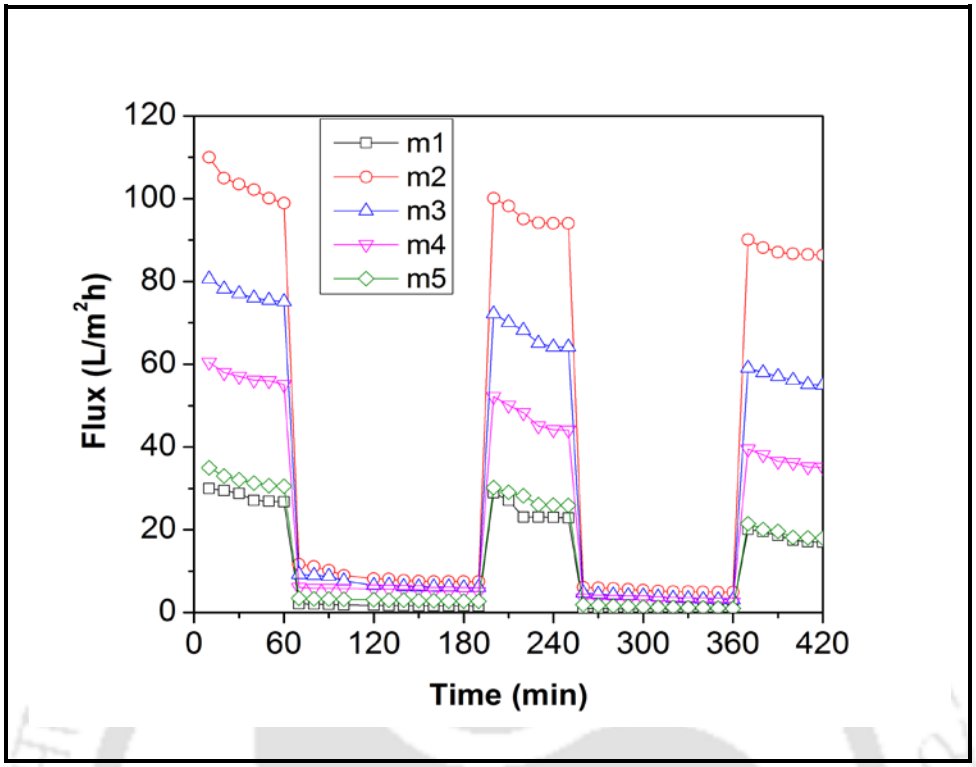

Figure 6.15: Effect of Different AAPs on time dependent flux; millipore water: 0-60 min, 180-240 min and 360-420 min; BSA solution: 60-180 min and 240-360 min.

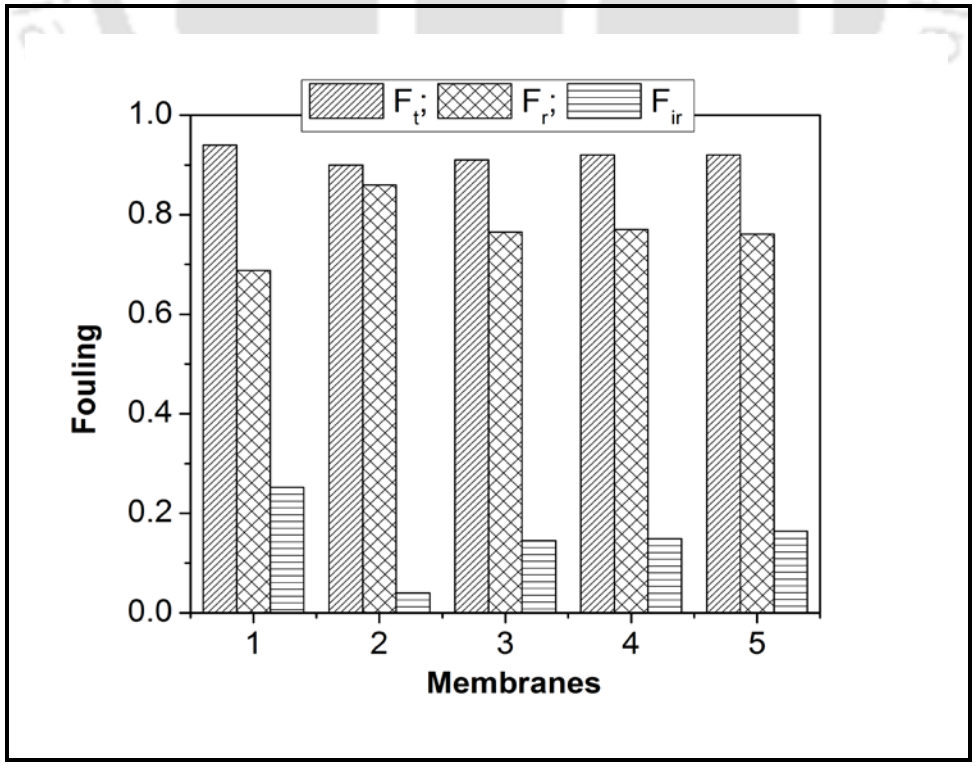

Figure 6.16: Effect of AAPs on fouling parameters.

For investigating the fouling resistant behaviour of the membrane, F_r and F_{ir} values were calculated from Figure 6.15 by using equations 2.17-2.19 and are shown in Figure 6.16. It can be seen in figure 6.16 that by the addition of hydrophilic AAP-1, AAP-2, AAP-3 and AAP-4 in modified membranes, F_{ir} values are reduced significantly as compared to plain membrane and therefore, the F_r values are increased. Furthermore the sequence of flux recovery ratio and fouling values are consistent with hydrophilicity and BSA rejection trend of membranes. In this case also, the hydrophilic segment of the AAP could form hydration layer on the membrane surface through hydrogen bonding, exhibiting anti fouling property and efficiently prevent adsorption deposition of foulants. Sinha et al. [82] also observed the similar result by the blending of amphiphilic polyurethane macromolecules with PSF membrane. However, it can be remarked that F_r values increased after addition of amphiphilic AAP. The possible reason could be accumulation of more BSA on membrane surface due to comparatively increased BSA rejection. Even though increased F_r value, the value of total fouling showed a reducing trend due to remarkable decrease in F_{ir} value. So, these trends suggest that anti fouling property, especially irreversible fouling of modified PSF membrane was enhanced appreciably via blending of amphiphilic AAPs.

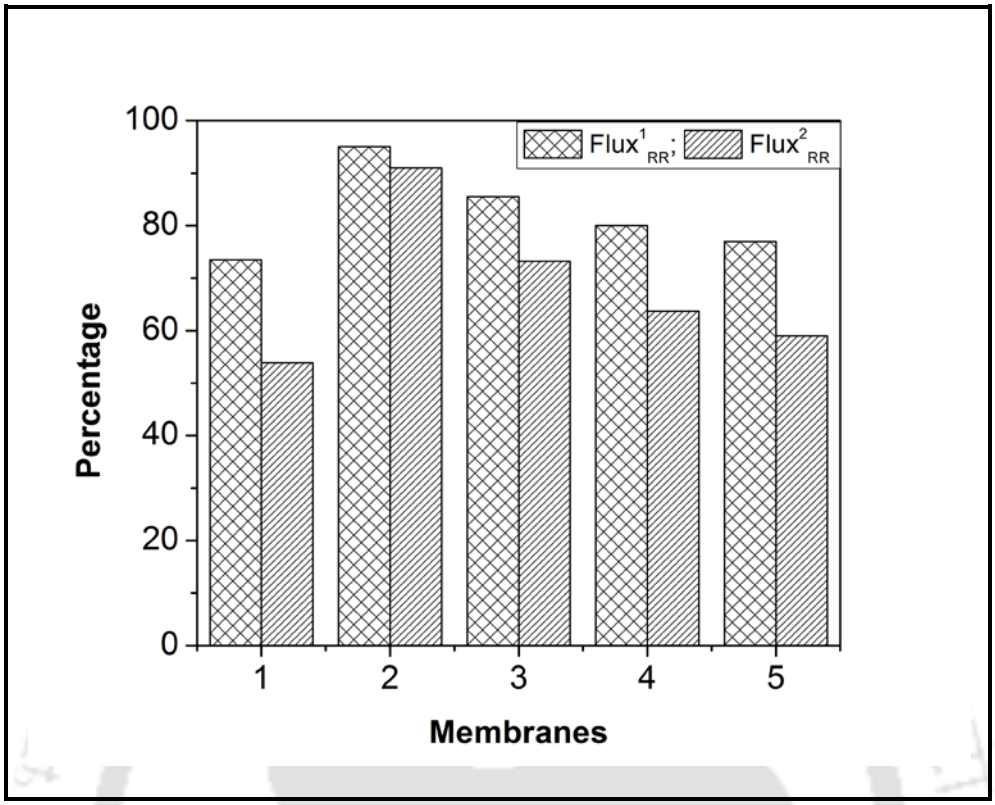

Figure 6.17: Effect of AAP on flux recovery ratio.

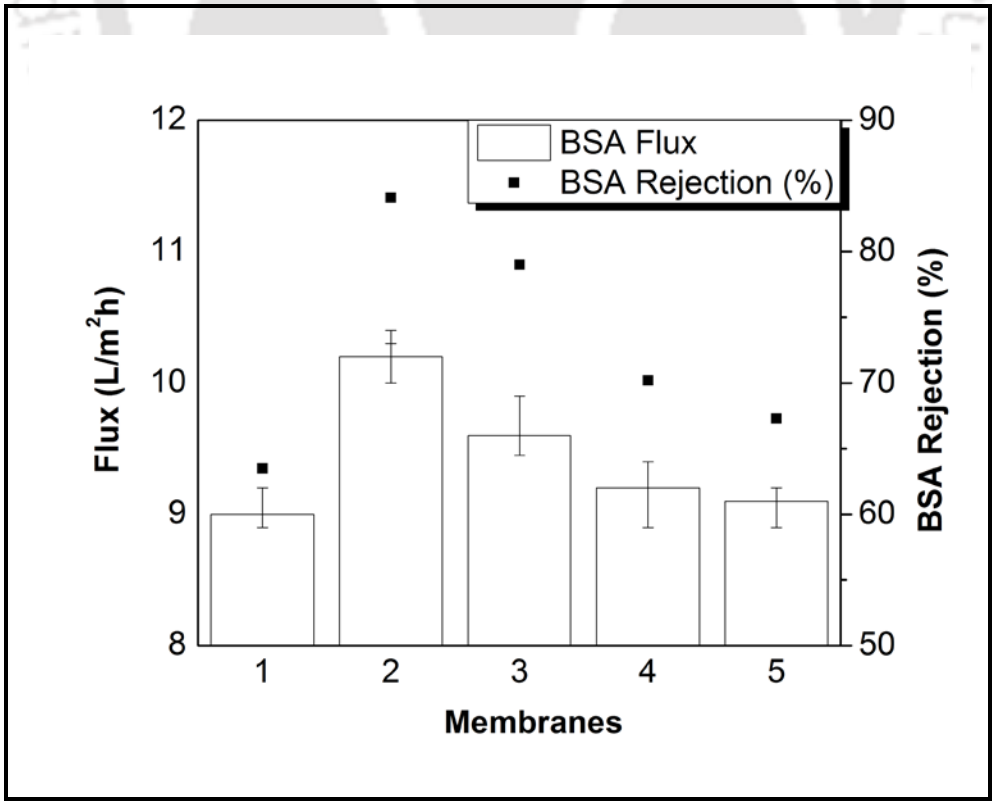

Figure 6.18: Effect of different AAPs on BSA flux and rejection.

Figure 6.18 shows the BSA rejection and flux for different membranes. It is already reported in the preceding section that amphiphilic AAP not only enhances the hydrophilicity but also pore forming capacity. So, the flux as well as BSA rejection was higher for modified membranes. In case of different AAPs, AAP-1 has most number of -OH groups; hence membrane m2 had highest flux as well as flux recovery ratio. Second time flux recovery ratio ($Flux^2_{RR}$) for plain membrane m1 is lower than $Flux^1_{RR}$, In case of membrane m2, the difference between $Flux^1_{RR}$ and $Flux^2_{RR}$ it is not much (Figure 6.17). The main reason is, plain membrane had already some amount of deposited or adsorbed BSA on their surface, which again increased after second round of BSA ultra filtration. $Flux^2_{RR}$ value came close to $Flux^1_{RR}$ value, for the AAP with the decreased molecular weight of PEG. Similarly for different additive, results are in line with hydrophilicity study of membranes.

Summary

AAP-1 (synthesized by lower molecular weight of PEG) provided more hydrophilic membrane than other AAP prepared by higher molecular weight PEG. Hydrophilicity of the modified membranes m2, m3, m4 and m5 were found to be increased by the addition of amphiphilic AAP. Presence of AAP also increases the ion exchange capacity of membranes.

Chapter 7
Conclusion, summary and scope of future work

This chapter comprises three segments; first segment is conclusions, which includes the results drawn from several works presented in this thesis. Second segment covers the winding up of all the chapters and presents the final verdict on all the works done in the thesis under the part called as summary. Third and last section discusses the ideas for the future work.

7.1. Conclusions

The thesis deals with the preparation and characterization of hydrophilic polysulfone based ultrafiltration membranes. Different type of membranes were prepared using four modifying agent or additives separately viz. (i) hydrophilic polymer PVP-PAA, (ii) pH responsive copolymer poly(VP-co-IAH), (iii) organic acid (D-TA and DL-TA) and (iv) hydrophilic amino alcohol plasticizer. Among these additives, two additives were synthesized and characterized by FTIR and NMR. Modified membranes were characterized by FESEM, SEM, AFM, LLDP, ATR-FTIR as well as in term of porosity and equilibrium water content. In some case ion exchange capacity was also determined for prepared membranes. The major conclusions from the different studies are presented below.

Preparation of hydrophilic polysulfone membrane using polyacrylic acid with polyvinyl pyrrolidone (Refer Chapter 3):

With increasing molecular weight of PVP in PVP-PAA blend, observations may be summarized as follows:

- The number of pores per unit surface area (porosity) of the prepared membranes was found to be increased from 0.38 to 0.61 (Refer page 61).

- The EWC increased which might be depicted as indication of increase in hydrophilicity and number of pores of the membranes (Refer Table 3.3).
- Rejection of BSA was found more irrespective of the molecular weight of PVP at pH 4.8 (IEP of BSA). Highest rejection was observed as 87.5 % by PSF_3 membrane at pH 4.8.
- All the three membranes were found better than Chakrabarty et al. [15] in all aspects such as EWC (%), PWF, porosity, BSA rejection (%) at pH 9.3, number of pores N_t, (cm^{-2}) and area of pores, A_t (cm^2).

Preparation and characterization of poly(vinyl pyrrolidone-co-isatoic anhydride) copolymer added pH responsive hydrophilic polysulfone ultrafiltration membrane (Refer Chapter 4):

Effects of wt % of poly(VP-co-IAH) on membrane morphology, hydrophilicity, permeability and BSA rejection were studied and on the basis of that the following details are found:

- AFM images of top surface confirm that surface roughness (RMS) increased 35.39 % by the addition of copolymer poly(VP-co-IAH) and consequences into the more porous membranes. (Refer Figure 4.6).
- Cross sectional images taken by FESEM depicted that the fabricated membrane modified with poly(VP-co-IAH) had a porous structure beneath the dense top layer and finger like cavities were formed which was not present in M_0 membrane (Refer Figure 4.3).
- Water contact angle images depict hydrophilic top surface for the copolymer poly(VP-co-IAH) containing membranes compared to the unmodified membranes (Refer Figure 4.7).

- Copolymer poly(VP-co-IAH) containing membrane were rated in the following order in terms of BSA separation and hydrophilicity: M_4 > M_6 > M_2 > M_0.

Racemic and enantiomeric effect of tartaric acid on the hydrophilicity of polysulfone membrane (Refer Chapter 5):

The results of the study showed that with increase in wt. % of enantiomeric tartaric acid (D-TA) and racemic tartaric acid (DL-TA) from 0.5 to 1% in membrane casting solution, following observations were found:

- Maximum porosity was observed for PVP with D-TA (1 wt %). Porosity was found to be increased by the addition of D-TA, however, it got reduced by the addition of DL-TA.
- Size of pores on the membrane surface was reduced 24.3% by the addition of D-TA but increased 23.34% with DL-TA which was confirmed by the FESEM images.
- The hydraulic permeability, EWC and hydrophilicity were increased by the addition of D-TA and decreased by the addition of DL-TA (Refer Table 5.3 and 5.4).
- IEC of the membranes was improved 20.5% by the addition of both D-TAs and DL-TA.
- Effect of pH on the membrane permeation and rejection behaviour revealed the fact that flux was increased with decrease in pH. Whereas, rejection was found to be increased by increasing the pH from 3 to 11. (Refer Figure 5.15 and 5.18).
- Highest rejection 99.2% was achieved by membrane M2 with SDS at basic pH 11 for CVD removal. (Refer Figures 5.17).

Impact of synthesized amino alcohol plasticizer on the morphology, hydrophilicity and fouling of polysulfone ultrafiltration membrane (Refer Chapter 6):

Effects of different molecular weight of PEG based amino alcohol plasticizer (AAP) on membrane morphology and properties were observed and following inferences were made.

- AAP-1 (synthesized by lower molecular weight of PEG) provided more hydrophilic membrane than other AAP prepared by higher molecular weight PEG did.
- Water contact angle images show that the AAP containing membranes have increased hydrophilic top surface as compared to the unmodified membrane m1.
- FESEM images of top surface and LLDP data revealed that AAP enhances the pore formation and therefore pore density of the modified membranes get increased by the addition of AAP (Refer Figures 6.6, 6.7 and 6.9).
- Hydrophilicity of the modified membranes m2, m3, m4 and m5 were found to be increased by the addition of amphiphilic AAP; Plain and AAP containing membranes were rated in the following order in terms of BSA separation and hydrophilicity: m2 > m3 > m4 > m5 > m1.
- Cross sectional FESEM photographs showed that addition of AAP improves finger like structure and presence of AAP was also confirmed (Refer Figure 6.5).
- The hydrophilicity, PWF and EWC (%) were seen to be increased by 14 %, 72.7 % and 48.4 %, respectively for membrane with AAP-1 compared to plain membrane.
- Presence of AAP in membranes also increases the ion exchange capacity of membranes (Refer Table 6.3).
- Presence of AAP reduces the irreversible fouling of the modified membranes and maximum of ≈ 91% flux recovery ratio was achieved for modified membrane with AAP-1 (Refer Figure 6.17).

7.2. Summary

Hydrophilic behaviour of all the prepared membranes are compared and summarised in Table 7.1. Modified membranes were compared on the basis of water contact angle, EWC (%), route mean square roughness (RMS), IEC (mmol/g) and BSA rejection (%).

Table 7.1: Comparative analysis of all the prepared membranes.

Membrane composition	Type of additives	Membrane name	Water contact angle (°)	Equilibrium water content (%)	Root mean square roughness (RMS)	IEC (mmol/g)	BSA rejection (%)
As in Table 3.1 of Chapter 3	Water soluble polymer	PSF_1	74	51.2	5.8	0.73	65
		PSF_2	68	62.4	10.3	1.36	72.5
		PSF_3	54	74.3	15.7	2.40	85.4
As in Table 4.1 of Chapter 4	Functional copolymer	M_0	76.25	47	4.2	0.16	56.1
		M_2	74.35	53.1	6.2	0.32	58.9
		M_4	61.65	56.6	8.7	0.47	74.2
		M_6	64.85	56.4	6.5	0.34	65.7
As in Table 5.1 of Chapter 5	Enantiomeric and racemic tartaric acid	M1	68	65.0	5.8	1.47	78
		M2	55	69.0	12.1	1.85	90.5
		M3	59	66.5	7.6	1.80	87.5
		M4	71	63.0	4.2	1.75	86
		M5	73	59.9	2.8	1.59	80.9
As in Table 6.1 of Chapter 6	Hydrophilic plasticizer	m1	72	33.3	Nil	0.07	60.1
		m2	62	64.5	Nil	0.36	75.3
		m3	67	55	Nil	0.11	72
		m4	69	54.1	Nil	0.10	65.3
		m5	71	37.5	Nil	0.10	62

It is clear from Table 7.1 that all the membranes have one common BSA rejection property i.e. hydrophilicity or water contact angle (WCA) and some membranes have other hydrophilic properties i.e. ion exchange capacity (IEC). It can be seen that membranes PSF_3, M_4, M2, and m2 have the highest hydrophilicity among all the prepared membranes. These membranes have BSA rejection in the range of 74.2% to 90.5%. The possible reason is hydrophilicity. Membrane M_4 and m2 have almost same WCA value of ≈62˚, membrane M2 has WCA value of 55˚and also it has highest BSA rejection due to zeta potential of the membrane (Refer Table 5.4). So, it can be said that zeta potential is also an important parameter in hydrophilic behaviour, as it can reduce the BSA adsorption by inducing electrostatic repulsion. Among above mentioned membranes, PSF_3 and M2 have BSA rejection around 85.4 and 90.5 %, respectively. Membrane PSF_3 shows lowest WCA among all the membranes. However, BSA rejection is lower than M2 membrane; it may be due the electrostatic repulsion property of membrane M2. Membrane M_4 and m2 have rejection of 74.2 % and 75.3%, which is lower as compared to other two mentioned membranes; may be because of their lessen hydrophilicity. Overall, it can be concluded that the membrane M2 is the best performing membrane, as it has highest BSA rejection. Also hydrophilicity of M2 membrane is on the higher side; as WCA is nearly equal to the membrane PSF_3. In case of membranes PSF_3, hydrophilic polymer blend (PVP-PAA) was used as hydrophilic additive (8 wt % concentration) in membrane casting solution. In this membrane the molecular weight of PVP was highest. Because of more viscosity it gave highest porosity. Due to amphiphilic behaviour, these additives provide more hydrophilicity to the membrane. Migrate towards top surface of membranes during phase inversion process of membrane. In case of M_4 membrane, 4 wt % of poly(VP-co-IAH) copolymer was used in the membrane casting solution. One of the components of copolymer gives hydrophilicity to the membrane surface, while second component provides IEC capacity to the membrane. So,

this additive offers both hydrophilicity as well as IEC to the membranes. 1 weight % D-TA was added in membrane M2. MWCO was lowest and zeta potential was highest for membrane M2. Therefore, it offered highest rejection for both BSA and CVD. During MEUF process oppositely charged CVD molecules are solubilized over the micellar surface. Thus, by the increment of size the solutes separated after trapping with the micelles. AAP-1 was used as hydrophilic agent in membrane m2. AAP-1 contains more number of hydrophilic –OH group. The more hydrophilic the membrane was, the less decrease in the flux. Membrane m2 shows highest $Flux^1_{RR}$ and $Flux^2_{RR}$. It also demonstrates the lowest F_{ir} among all the membranes.

7.3. Recommendations on future work

This section highlights some of the new areas of research, that can be carried out to further the preparation and applicability of polymeric membranes. Some of the important areas of recommended research are suggested as an extension of the present study:

- PVP 360000 provided better result than other molecular weight of PVP with PAA, so the effect of different wt. % of PVP 360000 with PAA on PWF, BSA flux and on fouling behaviour can be studied.
- Polymeric membrane can be modified by adding other organic acids for finding their enantiomeric and racemic effects on membrane morphology, hydrophilicity and fouling resistant behaviour.
- Other anhydrides such as maleic anhydride can be used with monomer N-vinyl pyrrolidone for synthesizing hydrophilic copolymer for improving the hydrophilicity of polymeric membranes.

- Other anhydride and hydrophilic monomer based plasticizer can be synthesized, as both are hydrophilic in nature and may improve the fouling resistance of the polymeric membranes.
- Extension of the present UF experiments and fouling study in other modes of operations like cross-flow to obtain more realistic idea upon the performance of the prepared membrane in industrial applications.
- Hollow fibre membrane module study can also be done for these set of membranes.

References

[1] M. Mulder, Basic Principles of Membrane Technology, Kluwer Academic Publishers, Dordrecht, 1991.

[2] Munir Cheryan , Ultrafiltration and Microfiltration Handbook, Technomic Publishing Co. Inc. Lancaster, Pennsylvania, U.S.A, 1998.

[3] S. P. Nunes and K.V. Peinemann (Eds.), Membrane Technology in the Chemical Industry, Wiley-VCH Verlag GmbH., 2001.

[4] Application of membrane technologies for liquid radioactive waste processing, International Atomic Energy Agency, Vienna, Technical Reports Series No. 431, 2004.

[5] T. Matsuura, Synthetic Membranes and Membrane Separation Processes, CRC Press. Inc., Corporate Blvd., N.W., Boca Raton, Florida 33431, 2000.

[6] G. Pearce, Introduction to membranes: Membrane selection, Filtration and Separation, April 2007.

[7] A. J. G. Abrahamse, E. Cornelissen, J. A. M. Hofman, Fiber failure frequency and causes of hollow fiber integrity loss, Desalination 194 (2006) 251-258.

[8] Y.L. Su, C. Li, W. Zhao, Q. Shi, H.J. Wang, Z.Y. Jiang, S.P. Zhu, Modification of polyethersulfone ultrafiltration membranes with phosphorylcholine copolymer can remarkably improve the anti-fouling and permeation properties, J. Membr. Sci. 322 (2008) 171–177.

[9] Y. Wang, T. Wang, Y. Su, F. Peng, H. Wu, Z. Jiang, Remarkable reduction of irreversible fouling and improvement of the permeation properties of poly(ether sulfone) ultrafiltration membranes by blending with pluronic F127, Langmuir 21 (2005) 11856–11862.

[10] W. J. Koros, Y. H. Ma, T. Shimidzu, Terminology for membranes and membrane processes; IUPAC recommendations, J. Membr. Sci. 120 (1996) 149–159.

[11] M. R. Wiesner, and P. Aptel. Mass transport and permeate flux and fouling in pressure driven processes (Ch. 4). In: Water Treatment Membrane Processes. Mallevialle, J., Odendaal, P.E. and Wiesner, M.R. (eds.), McGraw-Hill, New York. 1996.

[12] Y. Kim, D. Rana, T. Matsuura, W. Chung, K. C. Khulbe, Relationship between surface structure and separation performance of poly(ether sulfone) ultrafiltration membranes blended with surface modifying macromolecules. Sep. Purif. Technol. 72 (2010) 123–132.

[13] P. Wang, K. L. Tan, E. T. Kang, K. G. Neoh, Plasma induced immobilisation of poly (ethylene glycol) onto poly (vinylidene fluoride) microporous membrane, J. Membr. Sci. 195 (2002) 103–114.

[14] J. Wang, C. J. Pan, N. Huang, H. Sun, P. Yang, Y. X. Leng, J. Y. Chen, G. J. Wan, P. K. Chu, Surface characterization and blood compatibility poly(ethylene terephthalate) modified by plasma surface grafting, Sur. Coat. Technol. 196 (2005) 307–311.

[15] B. Chakrabarty, A. K. Ghoshal, M. K. Purkait, Preparation, characterization and performance studies of polysulfone membranes using PVP as an additive, J. Membr. Sci. 315 (2008) 36–47.

[16] S. A. A. Malek, M. N. A. Seman, D. Johnson, N. Hilal, Formation and characterization of polyethersulfone membranes using different concentrations of polyvinylpyrrolidone, Desalination 288 (2012) 31–39.

[17] B. Chakrabarty, A. K. Ghoshal, M. K. Purkait, Effect of molecular weight of PEG on membrane morphology and transport properties, J. Membr. Sci. 309 (2008) 209–221.

[18] A. Idris, N. M. Zain, M. Y. Noordin, Synthesis, characterization and performance of asymmetric polyethersulfone (PES) ultrafiltration membranes with poly- ethylene glycol of different molecular weights as additives, Desalination 207 (2007) 324–339.

[19] W. R. Bowen, T. A. Doneva, H. B. Yin, Polysulfone sulfonated poly (ether ether) ketone blend membranes: systematic synthesis and characterization, J. Membr. Sci. 181 (2001) 253–263.

[20] A. Rahimpour, S. S. Madaeni, Y. Mansourpanah, The effect of anionic, non-ionic and cationic surfactants on morphology and performance of polyethersulfone ultrafiltration membranes for milk concentration, J. Membr. Sci. 296 (2007) 110–121.

[21] N. Ghaemi, S. S. Madaeni, A. Alizadeh, P. Daraei, M.M.S. Badieh, M. Falsafi, V. Vatanpour, Fabrication and modification of polysulfone nanofiltration membrane using organic acids: morphology, characterization and performance in removal of xenobiotics, Sep. Purif. Technol. 96 (2012) 214–228.

[22] J. Sikder, C. Pereira, S. Palchoudhury, K. Vohra, D. Basumatary, P. Pal, Synthesis and characterization of cellulose acetate–polysulfone blend microfiltration membrane for separation of microbial cells from lactic acid fermentation broth, Desalination 249 (2009) 802–808.

[23] M. Sivakumar, D. Raju, R. Rangarajan, Studies on cellulose acetate polysulfone ultrafiltration membranes II. Effect of additive concentration, J. Membr. Sci. 268 (2006) 208–219.

[24] Z. L. Xu, L. Y. Yu, L. F. Han, Polymer nanoinorganic particles composite membranes: a brief overview, Front. Chem. Eng. China 3 (2009) 318–329.

[25] A. Razmjou, J. Mansouri, V. Chen, The effects of mechanical and chemical modification of TiO_2 nanoparticles on the surface chemistry , structure and fouling performance of PES ultrafiltration membranes, J. Membr. Sci. 378 (2011) 73–84.

[26] A. L. Ahmad, M. A. Majid, B.S. Ooi, Functionalized PSf/SiO_2 nanocomposite membrane for oil-in-water emulsion separation, Desalination 268 (2011) 266–269.

[27] C. Dong, G. He, H. Li, R. Zhao, Y. Han, Y. Deng, Antifouling enhancement of poly(vinylidene fluoride) microfiltration membrane by adding $Mg(OH)_2$ nanoparticles, J. Membr. Sci. 387-388 (2012) 40–47.

[28] S. Balta, A. Sotto, P. Luis, L. Benea, B. Van Der Bruggen, J. Kim, A new outlook on membrane enhancement with nanoparticles: The alternative of ZnO, J. Membr. Sci. 389 (2012) 155–161.

[29] V. Vatanpour, M. Esmaeili, M. H. D. A. Farahani, Fouling reduction and retention increment of polyethersulfone nanofiltration membranes embedded by amine-functionalized multi-walled carbon nanotubes, J. Membr. Sci. 466 (2014) 70–81.

[30] V. Vatanpour, S. Siavash, L. Rajabi, S. Zinadini, A. Ashraf, Boehmite nanoparticles as a new nanofiller for preparation of antifouling mixed matrix membranes, J. Membr. Sci. 401-402 (2012) 132–143.

[31] J. R. Du, S. Peldszus, P. M. Huck, X. Feng, Modification of poly (vinylidene fluoride) ultrafiltration membranes with poly (vinylalcohol) for fouling control in drinking water treatment, Water Res. 43 (2009) 4559–4568.

[32] A. Chanachai, K. Meksup, R. Jiraratananon, Coating of hydrophobic hollow fiber PVDF membrane with chitosan for protection against wetting and flavor loss in osmotic distillation process, Sep. Purif. Technol. 72 (2010) 217–224.

[33] Q. Shi, Y. Su, S. Zhu, C. Li, Y. Zhao, Z. Jiang, A facile method for synthesis of pegylated polyethersulfone and its application in fabrication of antifouling ultrafiltration membrane, J. Membr. Sci. 303 (2007) 204–212.

[34] M. J. Han, G. N. B. Baroña, B. Jung, Effect of surface charge on hydrophilically modified poly (vinylidene fluoride) membrane for microfiltration, Desalination 270 (2011) 76–83.

[35] G. Arthanareeswaran, P. Thanikaivelan, M. Raajenthiren, Fabrication and Characterization of CA / PSf / SPEEK Ternary Blend Ultrafiltration Membranes, Ind. Eng. Chem. Res. 47 (2008) 1488–1494.

[36] Y. W. Chen, L. Ying, W. H. Yu, E. T. Kang, K. G. Neoh, Poly (vinylidene fluoride) with grafted poly(ethyleneglycol) side chains via the raft mediated process and pore size control of the copolymer membranes, Macromolecules 36 (2003) 9451–9457.

[37] Y. Chang, Y. J. Shih, R. C. Ruaan, A. Higuchi, W. Y. Chen, J. Y. Lai, Preparation of poly (vinylidene fluoride) microfiltration membrane with uniform surface copolymerized poly (ethyleneglycol) methacrylate and improvement of blood compatibility, J. Membr. Sci. 309 (2008) 165–174.

[38] F. Liu, B. K. Zhu, Y. Y. Xu, Improving the hydrophilicity of poly (vinylidene fluoride) porous membranes by electron beam initiated surface grafting of AA/SSS binarymonomers, Appl. Surf. Sci. 253 (2006) 2096–2101.

[39] D. Tyszler, R.G. Zytner, A. Batsch, A. Brügger, Reduced fouling tendencies of ultrafiltration membranes in wastewater treatment by plasma modification, Desalination 189 (2006) 119–129.

[40] M.C. Porter, Hand book of Industrial Membrane Technology, Noyes Publications, New Jersey, 1990.

[41] A. Bottino, G. Camera-Roda, G. Capannelli, S. Munari, The formation of micro-porous polyvinylidene difluoride membranes by phase separation, J. Membr. Sci. 57 (1991) 1–20.

[42] M. K. Sinha, M. K. Purkait, Increase in hydrophilicity of polysulfone membrane using polyethylene glycol methyl ether, J. Membr. Sci. 437 (2013) 7–16.

[43] A. Pagidi, R. Saranya, G. Arthanareeswaran, A.F. Ismail, T. Matsuura, Enhanced oil–water separation using polysulfone membranes modified with polymeric additives, Desalination 344 (2014) 280–288.

[44] R. Kumar, A. M. Isloor, A.F. Ismail, Preparation and evaluation of heavy metal rejection properties of polysulfone/chitosan, polysulfone/N-succinyl chitosan and polysulfone/N-propylphosphonyl chitosan blend ultrafiltration membranes, Desalination 350 (2014) 102–108.

[45] R. Kumar, A. M. Isloor, A.F. Ismail, T. Matsuura, Performance improvement of polysulfone ultrafiltration membrane using N-succinyl chitosan as additive, Desalination 318 (2013) 1–8.

[46] E. Eren, A. Sarihan, B. Eren, H. Gumus, F. O. Kocak, Preparation, characterization and performance enhancement of polysulfone ultrafiltration membrane using PBI as hydrophilic modifier, J. Membr. Sci. 475 (2015) 1–8.

[47] H.S. Choi, T. Hinob, M. Shibata, Y. Negishi, H. Ohya, The characteristics of a PAA-PSf composite membrane for separation of water-ethanol mixtures through pervaporation, J. Membr. Sci. 72 (1992) 259-266.

[48] H. B. Li, W. Y. Shi, Y. F. Zhang, D. Q. Liu, X. F. Liu, Effects of Additives on the Morphology and Performance of PPTA/PVDF in Situ Blend UF Membrane, Polymers 6 (2014) 1846-1861.

[49] P.L. Clech, V. Chen, A.G. Fane, Fouling in membrane bioreactors used in wastewater treatment, J. Membr. Sci. 284 (2006) 17–53.

[50] R. Ghosh, Z. F. Cui, Protein purification by ultrafiltration with pre-treated membrane. J. Membr. Sci. 167 (2000) 47–53.

[51] A. Barbetta, M. Dentini, E.M. Zannoni, M.E. De Stefano, Tailoring the porosity and morphology of gelatin-methacrylate polyHIPE scaffolds for tissue engineering applications, Langmuir 21 (26) (2005) 12333–12341.

[52] D. Wu, M.R. Bird, The fouling and cleaning of ultrafiltration membranes during the filtration of model tea component solutions, J. Food Process Eng. 30 (2007) 293–323.

[53] V. Orr, L. Zhong, M. Moo-Young, C.P. Cho, Recent advances in bioprocessing application of membrane chromatography, Biotechnol. Adv. 31 (2013) 450–465.

[54] M. Kumar, M. Ulbricht, Novel ultrafiltration membranes with adjustable charge density based on sulfonated poly(arylene ether sulfone) block copolymers and their tunable protein separation performance, Polymer 55 (2014) 354–365.

[55] M.M. Rohani, A.L. Zydney, Role of electrostatic interactions during protein ultra filtration, Adv. Colloid Interf. Sci. 160 (2010) 40–48.

[56] M.E. Avramescu, M. Girones, Z. Borneman, M. Wessling, Preparation of mixed matrix adsorber membranes for protein recovery, J. Membr. Sci. 218 (2003) (1-2), 219–233.

[57] M.N. Sarvi, T.B. Bee, C.K. Gooi, B.W. Woonton, M.L. Gee, A.J. Connor, Development of functionalized mesoporous silica for adsorption and separation of dairy proteins, Chem. Eng. J. 235 (2014) 244–251.

[58] M.J. Santos, J.A. Teixeira, L.R. Rodrigues, Fractionation of the major whey proteins and isolation of b-Lactoglobulin variants by anion exchange chromatography, Sep. Purif. Technol. 90 (2012) 133–139.

[59] S. Galier, H.R. Balmann, The electrophoretic membrane contactor: A mass-transfer-based methodology applied to the separation of whey proteins, Sep. Purif. Technol. 77 (2011) 237–244.

[60] Y. Zhang, Z. Jin, X. Shan, J. Sunarso, P. Cui, Preparation and characterization of phosphorylated Zr-doped hybrid silica/PSF composite membrane, J. Hazard. Mater. 186 (2011) 390–395.

[61] A. Pich, A. Tessier, V. Boyko, Y. Lu, H. P. Adler, Synthesis and Characterization of Poly (N-vinylcaprolactam)-Based Microgels Exhibiting Temperature and pH-Sensitive Properties, Macromolecule 39 (2006) 7701–7707.

[62] X. Jiang, G. Lu, C. Feng, Y. Li, X. Huang, Poly(acrylic acid)-graft-poly(N-vinylcaprolactam): A Novel pH and Thermo Dual-Stimuli Responsive System, Polym. Chem. 4 (2012) 3876–3884.

[63] B.S. Jiang, J. Li, Preparation and characterization of pH-sensitive polyethersulfone hollow fiber membrane for flux control, J. Membr. Sci. 344 (2009) 297–303.

[64] J.W. Kim, E.J. Moon, C.K. Kim, New miscible blends composed of polysulfone membrane and poly(1-vinyl pyrrolidone-co-acrylonitrile) copolymers and their phase behaviour, Polymer 46 (2005) 5662–5672.

[65] Y. Cui, Z..K.Yao, K. Zheng, S.Y. Du, B.K. Zhu, L.P. Zhu, C.H. Du, Positively-charged nanofiltration membrane formed by quaternization and cross-linking of blend PVC/P(DMA-co-MMA) precursors, J. Membr. Sci. 492 (2015) 187–196.

[66] J.Y. Park, M.H. Acar, A. Akthakul, W. Kuhlman, A. M. Mayes, Polysulfone-graft-poly(ethylene glycol) graft copolymers for surface modification of polysulfone membranes, Biomaterials 27 (2006) 856–865.

[67] J.E. Yoo, J.H. Kim, Y. Kim, C.K. Kim, Novel ultrafiltration membranes prepared from the new miscible blends of polysulfone with poly(1-vinylpyrrolidone-co-styrene) copolymers, J. Membr. Sci. 216 (2003) 95–106.

[68] Z. Yi, L.P. Zhu, Y.Y. Xu, X.L. Li, J.Z.Yu, B.K. Zhu, F127-based multi-block copolymer additives with poly(N,N-dimethylamino-2-ethyl methacrylate) end chains:

The hydrophilicity and stimuli-responsive behaviour investigation in polyethersulfone membranes modification, J. Membr. Sci. 364 (2010) 34–42.

[69] Y. Zhao, L.P. Zhu, Z.Yi, B. K. Zhu, Y.Y. Xu, Improving the hydrophilicity and fouling-resistance of polysulfone ultrafiltration membranes via surface zwitterionicalization mediated by polysulfone-based triblock copolymer additive, J. Membr. Sci. 440 (2013) 40–47.

[70] Z. Zhou, S. Rajabzadeh, A. R. Shaikh, Y. Kakihana, T. Ishigami, R. Sano, H. Matsuyama, Preparation and Characterization of Antifouling Poly(vinyl chloride-co-poly(ethylene glycol)methyl ether methacrylate) Membranes, J. Membr. Sci. 498 (2016) 414–422.

[71] H. Helin, L. Na, W. Linlin, Z. Hui, W.Guangxi, Y. Zonghuan, L. Xiangwei, T. Lianyi, Anti-fouling ultrafiltration membrane prepared from polysulfone-graft-methylacrylate copolymers by UV-induced grafting method, J. Env. Sci. 20 (2008) 565–570.

[72] Y. He, X. Chen, S. Bi, W. Fu, C. Shi, L. Chen, Conferring pH-sensitivity on poly (vinylidene fluoride) membrane by poly (acrylic acid-co-butyl acrylate) microgels React. Funct. Poly. 74 (2014) 58–66.

[73] S. Roy, C.M. Hussain, S. Mitra, Poly(acrylamide-co-acrylic acid) hydrophilization of porous polypropylene membrane for dehumidification, Sep. Purifi. Tech. 107 (2013) 54-60.

[74] M.K. Sinha, M.K. Purkait, Preparation and characterization of stimuli-responsive hydrophilic polysulfone membrane modified with poly (N-vinylcaprolactam-co-acrylic acid), Desalination, 348 (2014) 16-25.

[75] S.H. Yalkowsky and Y. He, Handbook of Aqueous solubility data, second edition, 2003.

[76] L. Yang, X.Q. Chen, F.P. Jiao, Extractive Resolution of racemic mandelic acid through a bulk liquid membrane containing binary chiral carrier, J. Braz. Chem. Soc. 20 (2009) 1493-1498.

[77] R. Kumar, A.M. Isloor, A.F. Ismail, A. Suraya, Rashidc and T. Matsuura, Polysulfone–Chitosan blend ultrafiltration membranes: preparation, characterization, permeation and antifouling properties, RSC Adv. 3 (2013) 7855-7861.

[78] N. Ghaemi, S.S. Madaeni, A. Abdolhamid, H. Rajabi, P. Daraei, M. Falsafi, Effect of fatty acids on the structure and performance of cellulose acetate nanofiltration membranes in retention of nitroaromatic pesticides, Desalination 301 (2012) 26-41.

[79] A. Mansourizadeh, A.F. Ismail, Effect of additives on the structure and performance of polysulfone hollow fiber membranes for CO2 absorption, J. Membr. Sci. 348 (2010) 260–267.

[80] X. Wei, Z. Wang, J. Wang and S.A. Wang, novel method of surface modification to polysulfone ultrafiltration membrane by preadsorption of citric acid or sodium bisulphate, Membr. Water Treat. 3 (2012) 35-49.

[81] J. Li, S. Nie, L. Wang, S. Sun, F. Ran and C. Zhao, One-pot synthesized poly(vinyl pyrrolidone-co-methyl methacrylate-co-acrylic acid) blended with poly(ether sulfone) to prepare blood-compatible membranes, J. Appl. Poly. Sci. (2013) DOI: 10.1002/app.39463.

[82] M.K. Sinha, M.K. Purkait, Preparation of fouling resistant PSF flat sheet UF membrane using amphiphilic polyurethane macromolecules, Desalination 355 (2015) 155-168.

[83] V.K. Thakur, M.K. Thakur Handbook of Polymers for Pharmaceutical Technologies, Processing and Applications, Scrivener Publishing, 2015.

[84] T. Mekonnen, P. Mussone, H. Khalil, D. Bressler, Progress in bio-based plastics and plasticizing modifications, J. Mater. Chem. A 1 (2013) 13379-13398.

[85] A. Lindström, M. Hakkarainen, Designed Chain Architecture for Enhanced Migration Resistance and Property Preservation in Poly(vinyl chloride)/Polyester Blends, Biomacromolecules 4 (2007) 1187-1194.

[86] E. M. Zahran, A. New, V. Gavalas, L.G. Bachas, Polymeric plasticizer extends the lifetime of PVC-membrane ion-selective electrodes, The Analyst 139 (2014) 757-763.

[87] E. Khodaverdi, F. S. M. Tekie, S. S. Amoli, F. Sadeghi, Comparison of Plasticizer Effect on Thermo-responsive Properties of Eudragit RS Films, AAPS Pharm. Sci. Tech. 13 (3) (2012) 1024–1030.

[88] T. D. Stark, H. Choi, P.W. Diebel, Influence of plasticizer molecular weight on plasticizer retention in PVC geomembranes, Geosynth. Int. 12 (2005) 99-110.

[89] N. Sharma, M.K. Purkait, Preparation of hydrophilic polysulfone membrane using polyacrylic acid with polyvinyl pyrrolidone, J. Appl. Poly. Sci. 132 (2015). DOI: 10.1002/app.41964.

[90] H. Kamusewitz, M. Schossig-Tiedemann, M. Keller, D. Paul, Characterization of polymeric membranes by means of scanning force microscopy (SFM) in comparison to results of scanning electron microscopy (SEM), Surf. Sci. 377–379 (1997) 1076–1081.

[91] G. Cappanelli, F. Vigo, S. Munari,Ultrafiltration membrane-Characterization technique, J. Membr. Sci.15 (1983) 289–313.

[92] P. Abaticchio, A. Bottino, G. Capannelli, S. Munari, Characterization of ultrafiltration polymeric membranes, Desalination 78 (1990) 235–255.

[93] S. Munari, A. Bottino, G. Capannelli, P. Moretti, Membrane morphology and transport properties, Desalination 53 (1985) 11–23.

[94] K.J. Kim, A.G. Fane, C.J.D. Fell, T. Suzuki, M.R. Dickson, Quantitative microscopic study of surface characterization of ultrafiltration membranes, J. Membr. Sci. 54 (1990) 89–102.

[95] B.K. Nandi, R. Uppaluri, M.K. Purkait, Preparation and characterization of low cost ceramic membranes for micro-filtration applications, Appl. Clay Sci. 42 (2008) 102–110.

[96] M. Farbod, S. Rezaian, An investigation of super-hydrophilic properties of TiO_2/SnO_2 nano composite thin films, Thin Solid Films 520 (2012) 1954–1958.

[97] Z. Jiang, X. Zheng, H. Wu, F. Pan, Proton conducting membranes prepared by incorporation of organophosphorus acids into alcohol barrier polymers for direct methanol fuel cells, J. Power Sources 185 (2008) 85–94.

[98] S.K. Maurya, K. Parashuram, P.S. Singh, P. Ray, A.V.R. Reddy, Preparation of polysulfone–polyamide thin film composite hollow fibre nanofiltration membranes and their performance in the treatment of aqueous dye solutions, Desalination 304 (2012) 11-19.

[99] S.A. Jones, G.P. Martin, M.B. Brown, Determination of polyvinyl pyrrolidone using high-performance liquid chromatography, J. Pharma. Biomed. Analy. 35 (2004) 621-624.

[100] J. Reuvers, C.A. Smolders, Formation of membranes by means of immersion precipitation. Part II. The mechanism of formation of membranes prepared from the system cellulose acetate-acetone-water, J. Membr. Sci. 34 (1987) 67–86.

[101] K. Kimmerle, H. Strathmann, Analysis of the structure-determining process of phase inversion membranes, Desalination 79 (1990) 283–302.

[102] J. I. Calvo, A. Bottino, G. Capannelli, A. Hernández, Comparison of liquid–liquid displacement porosimetry and scanning electron microscopy image analysis to

characterize ultrafiltration track-etched membranes, J. Membr. Sci. 239 (2004) 189–197.

[103] P.S.T. Machado, A.C. Habert, C.P. Borges, Membrane formation mechanism based on precipitation kinetics and membrane morphology: flat and hollow fiber polysulfone membranes J. Membr. Sci. 155 (1999) 171-183.

[104] I.M. Wienk, R.M. Boom, M. A. M. Beerlage, A. M. W. Bulte, C.A. Smolders, Recent Advances in the formation of phase inversion membranes made from amorphous or semi-crystalline polymers, J. Membr. Sci. 113 (1996) 361–371.

[105] M.K. Chun, C.S. Cho, H.K. Choi, Characteristics of poly(vinyl pyrrolidone)/poly(acrylic acid) interpolymer complex prepared by template polymerization of acrylic acid: Effect of reaction solvent and molecular weight of template, J. Appl. Poly. Sci. 94 (2004) 2390-2394.

[106] C. Feng, R. Wang, B. Shi, G. Li, Y. Wu, Factors affecting pore structure and performance of poly(vinylidene fluoride-co-hexafluoro propylene) asymmetric porous membrane, J. Membr. Sci. 277 (2006) 55–64.

[107] T.H. Young, L.W. Chen, A diffusion-controlled model for wet-casting membrane formation, J. Membr. Sci. 59 (1991) 169–181.

[108] Q. Li, Q. Bi, H. Lin, L. Bian, X. Wang, A novel ultrafiltration (UF) membrane with controllable selectivity for protein separation, J. Membr. Sci. 427 (2013) 155–167.

[109] F. L. Huang, Q. Q. Wang, Q. F. Wei, W. D. Gao, H. Y. Shou, S. D. Jiang, Dynamic wettability and contact angles of poly(vinylidene fluoride) nanofiber membranes grafted with acrylic acid, eXPRESS Polymer Letters 4 (9) (2010) 551–558.

[110] D. A. Musale, S. S. Kulkarni, Relative rates of protein transmission through poly (acrylonitrile) based ultrafiltration membranes, J. Membr. Sci. 136 (1997) 13–23.

[111] A. Higuchi, Y. Ishida, T. Nakagawa, Surface modified polysulfone membranes: Separation of mixed proteins and optical resolution of tryptophan, Desalination 90 (1993) 127–136.

[112] A. G. Fane,C. J. D. Fell, A. G. Waters, The relationship between membrane surface pore characteristics and flux for ultrafiltration membranes, J. Membr. Sci. 9 (1981) 245–262.

[113] R. Ghosh, Z.F.Cui, Fractionation of BSA and lysozyme using ultrafiltration: effect of pH and membrane pretreatment, J. Membr. Sci. 139 (1998) 17–28.

[114] M. K. Sinha, M. K. Purkait, Preparation and characterization of novel pegylated hydrophilic pH responsive polysulfone ultrafiltration membrane, J. Membr. Sci. 464 (2014) 20–32.

[115] R.J. Hunter, Zeta Potential in Colloid Science, Academic Press, London, 1981.

[116] R. Kumar, A. M. Isloor, A. F. Ismail, T. Matsuura, Synthesis and characterization of novel water soluble derivative of Chitosan as an additive for polysulfone ultrafiltration membrane, J. Membr. Sci. 440 (2013) 140–147.

[117] S. Zhang, K.Y. Wang, T.S. Chung, H. Chen, Y.C. Jean, G. Amy, Well-constructed cellulose acetate membranes for forward osmosis: Minimized internal concentration polarization with an ultra-thin selective layer, J. Membr. Sci. 360 (2010) 522–535.

[118] N. Sharma, M.K. Purkait, Enantiomeric and racemic effect of tartaric acid on polysulfone membrane during crystal violet dye removal by MEUF process, J. Water Proc. Eng. 10 (2016) 104–112.

[119] M. Taniguchi, J. P. Pieracci, G. Belfort, Effect of undulation on surface energy: a quantitative assessment, Langmuir 17 (2001) 4312–4315.

[120] R.Wang, T. Xiang,W. Yue, H. Li, S. Liang, S. Sun, C. Zhao, Preparation and characterization of pH-sensitive polyethersulfone hollow fiber membranes modified

by poly(methyl methylacrylate-co-4-vinyl pyridine) copolymer, J. Membr. Sci. 423–424 (2012) 275–283.

[121] C. Cheng, L. Ma, D. Wu, J. Ren, W. Zhao, J. Xue, S. Sun, C. Zhao, Remarkable pH-sensitivity and anti-fouling property of terpolymer blended Polyethersulfone hollow fiber membranes J. Membr. Sci. 378 (2011), 369–381.

[122] W. Zou, Y. Huang, J. Luo, J. Liu, C. Zhao, Poly (methyl methacrylate–acrylic acid–vinyl pyrrolidone) terpolymer modified polyethersulfone hollow fiber membrane with pH sensitivity and protein antifouling property, J. Membr. Sci. 358 (1–2) (2010) 76–84.

[123] L. Li, Z. Yin, F. Li, T. Xiang, Y. Chen, C. Zhao, Preparation and characterization of poly(acrylonitrile-acrylic acid-N-vinyl pyrrolidinone) terpolymer blended polyether sulfone membranes J. Membr. Sci. 349 (2010) 56–64.

[124] Y. Wang, T. Wang, Y. Su, F. Peng, H. Wu, Z. Jiang, Remarkable Reduction of Irreversible Fouling and Improvement of the Permeation Properties of Poly(ether sulfone) Ultrafiltration Membranes by Blending with Pluronic F127, Langmuir 21 (2005) 11856–11862.

[125] P. Guo,W.Y. Guan, L. Liang, P. Yao, J. Colloid Interface Sci., Self-assembly of pH-sensitive random copolymers: Poly(styrene-co-4-vinylpyridine), J. Colloid Interf. Sci. 323 (2008) 229–234.

[126] Y. Kim, D. Rana, T. Matsuura, W. Chung Influence of surface modifying macromolecules on the surface properties of poly (ether sulfone) ultra-filtration membranes, J. Membr. Sci. 338 (2008) 84–91.

[127] Q. Wei, J. Li, B.S. Qian, B.H. Fang, C.S. Zhao, Preparation, characterization and application of functional polyethersulfone membranes blended with poly (acrylic acid) gels, J. Membr. Sci. 337 (2009) 266–273.

[128] R. M. Silverstein, F. X. Webster, Spectrometric identification of organic compounds, 6th Edition, John Wiley & Sons, Inc. Canada, 1998.

[129] A. EL- Gendi, H. Abdalla, S. Ali, Construction of Ternary Phase Diagram and Membrane Morphology Evaluation for Polyamide/Formic acid/Water System, Australian J. Basic and Appl. Sci. 6 (5) (2012) 62-68.

[130] J.F. Blanco, J. Sublet, Q. T. Nguyena, P. Schaetzel, Formation and morphology studies of different polysulfones-based membranes made by wet phase inversion process, J. Membr. Sci. 283 (2006) 27-37.

[131] H. Strathmann, K. Kock, P. Amar, R.W. Baker, The formation mechanism of asymmetric membranes, Desalination 16 (1975) 179–203.

[132] X. Hu, Y. Li, H. Sun, X. Song, Q. Li, X. Cao, Z. Li, Effect of divalent cationic ions on the adsorption behaviour of zwitterionic surfactants at the silica/solution interface. J. Phys. Chem. B 114 (2010), 8910.

[133] D.F. Parsons, B.W. Ninham, Charge reversal at surfaces in divalent electrolytes: the role of the ionic dispersion interaction, Langmuir 26 (2010) 6430.

[134] C. Schneider, M. Hanisch, B. Wedel, A. Jusufi, M. Ballauff, Experimental study of electrostatically stabilized particles: colloidal stability and charge reversal, J. Colloid Interf. Sci. 358 (2011) 62-67.

[135] I. Szilagyi, D. Rosicka, J. Hierrezuelo, M. Borkovec, Charging and stability of anionic latex particles in the presence of linear PEI, J. Colloid Interf. Sci. 360 (2011) 580.

[136] P.H. Elworthy and K.J. Mysels, The surface tension of sodium dodecyl sulfate solutions and the phase separation model of micelle formation, J. Colloid Interf. Sci. 21 (1966) 331-347.

[137] M. Sarkar, S. Poddar, Studies on the interaction of surfactants with cationic dye by absorption spectroscopy, J. Colloid Interf. Sci. 221 (2000) 181-185.

[138] R. Sabat´e, M. Gallardo, A. de la Maza, J. Estelrich,ASpectroscopy study of the interaction of pinacyanol with n-dodecyltrimethyl ammonium bromide micelles, Langmuir 17 (2001) 6433-6437.

[139] S.G¨okt¨urk, M.Tuncay, Spectral studies of safranin-O in different surfactant solutions, Spectrochim. Acta, Part A: Mol. Biomol. Spectrosc. 59 (2003) 1857-1866.

[140] N. Zaghbani, A. Hafiane, M. Dhahbi, Separation of methylene blue from aqueous solution by micellar enhanced ultrafiltration, Sep. and Purifi. Tech. 55 (2007) 117-124.

[141] M.K. Purkait, S. DasGupta, S. De, Micellar enhanced ultrafiltration of phenolic derivatives from their mixture, J. Colloid Interf. Sci. 285 (2005) 395-402.

[142] M. Dai, The effect of zeta potential of activated carbon on the adsorption of dyes from aqueous solution, J. Colloid Interf. Sci. 164 (1994) 223-228.

[143] K. Wojciechowskia, E. Klodzinska, Zeta potential study of biodegradable antimicrobial polymer, Colloids and Surfaces A: Physicochem. Eng. Aspects 483 (2015) 204–208.

[144] B. Tanhaei, M.P. Chenar, N. Saghatoleslami, M. Hesampour, T. Laakso, M. Kallioinen, M. Sillanpää, M. Mänttäri, Simultaneous removal of aniline and nickel from water by micellar-enhanced ultrafiltration with different molecular weight cut-off membranes, Sep. Purif. Tech. 124 (2014) 26–35.

[145] M.K. Purkait, S. DasGupta, S. De, Separation of aromatic alcohols using micellar-enhanced ultrafiltration and recovery of surfactant, J. Membr. Sci. 250 (2005) 47–59.

[146] M.K. Purkait, S. DasGupta, S. De, Removal of dye from wastewater using micellar-enhanced ultrafiltration and recovery of surfactant, Sep. Purif. Technol. 37 (2004) 81–92.

[147] G. Bargeman, J.M. Vollenbroek, J. Straatsma, C.G.P.H. Schroen, R. M. Boom, Nanofiltration of multi-component feeds. Interactions between neutral and charged components and their effect on retention, J. Membr. Sci. 247 (2005) 11–20.

[148] W.R. Bowen, H.N.S. You sef, Effect of salts on water viscosity in narrow membrane pores, J. Colloid Interf. Sci. 264 (2003) 452–457.

[149] A. Bouchoux, H.R. Balmann, F. Lutin, Nanofiltration of glucose and sodium lactatesolutions: variations of retention between single- and mixed-solute solutions, J. Membr. Sci. 258 (2005) 123–132.

[150] S. Chakraborty, B.C. Bag, S. Das Gupta, S. De, J. K. Basu, Separation and Fractionation of Dye Solution by Nanofiltration, Sep. Sci. Tech. 38 (2007) 219-235.

[151] Y. Zheng, G. Yao, Q. Cheng, S. Yu, M. Liu, C. Gao, Positively charged thin-film composite hollow fiber nanofiltration membrane for the removal of cationic dyes through submerged filtration, Desalination 328 (2013) 42-50.

[152] C. Das, M. Rungta, G. Aryab, S. DasGupta, S. De, Removal of dyes and their mixtures from aqueous solution using liquid emulsion membrane, J. Hazard. Mater. 159 (2008) 365-371.

[153] S.R. Panda, S. De, Preparation, characterization and performance of ZnCl2 incorporated polysulfone (PSF)/polyethylene glycol (PEG) blend low pressure nanofiltration membranes, Desalination 347 (2014) 52-65.

[154] S. Jana, M.K. Purkait, K. Mohanty, Removal of crystal violet by advanced oxidation and microfiltration, Appl. Clay Sci. 50 (2010) 337-341.

[155] R. M. Boom, I. M. Wienk, T. Boomgaard, C. A. Smolders, Microstructures in phase inversion membranes. Part 2. The role of a polymeric additive, J. Membr. Sci. 73 (1992) 277–292.

[156] J. H. Kim, K. H. Lee, Effect of PEG additive on membrane formation by phase inversion, J. Membr. Sci. 138 (1998) 153–163.

[157] S. Zhang, K.Y.Wang, T.-S.Chung, H.Chen, Y.C.Jean, G.Amy, Well-constructed cellulose acetate membranes for forward osmosis: Minimized internal concentration polarization with an ultra-thin selective layer, J. Membr. Sci. 360 (2010) 522–535.

[158] N. E. Suyatma, L. Tighzert, A. Copinet, J. Agric. Effects of hydrophilic plasticizers on mechanical, thermal, and surface properties of chitosan films, Food Chem. 53 (10) (2005) 3950–7.

[159] W. Zhao, Y.L. Su, Ch. Li, Q. Shi, X. Ning, Z.Y. Jiang, Fabrication of antifoul- ing polyethersulfone ultrafiltration membranes using Pluronic F127 as both surface modifier and pore-forming agent, J. Membr. Sci. 318 (2008) 405–412.

[160] C. Lv, Y. Su, Y. Wang, X. Ma, Q. Sun, Z. Jiang, Enhanced permeation performance of cellulose acetate ultra filtration membrane by incorporation of Pluronic F127, J. Membr. Sci. 294 (2007) 68–74.

[161] A. K. Hołda, I. F. J. Vankelecom, Integrally skinned PSf-based SRNF-membranes prepared via phase inversion-Part B: Influence of low molecular weight additives, J. Membr. Sci. 450 (2014) 512–521.

[162] J.H. Huisman, P. Pradanos, A. Hermandez, The effect of protein–protein and protein-membrane interactions on membrane fouling in ultrafiltration, J. Membr. Sci. 179 (2000) 79–90.

Appendix

A. Error analysis

The errors in experimentally measured quantities and in parameters calculated from those measurements are important in that they determine the accuracy of calculation and predictions using those quantities. There are two types of errors viz. systematic error and random error. Systematic errors are the results of faulty assumptions or improper experimental measuring techniques. In this work, care was taken in eliminating systematic errors by appropriately designing the experiments and adopting qualified methods for analysis of the data. On the other hand, random errors result from variation in the precision of measuring parameters and the slight variations that occur in successive measurements made by the same observer under nearly identical conditions. Random errors cannot be eliminated. The focus of the error analysis presented in this section is on the random errors.

In most of the experiments performed in this work, the quantities that are measured directly are concentrations and permeate flow rates which are used to determine the rejection (%) and permeate flux, respectively.

A.1. Error in measurement of BSA concentration in permeate

BSA concentration in the aqueous phase was determined by measuring the absorbance value at a specific wavelength in the UV-Vis spectrophotometer. A calibration curve was prepared by taking the absorbance values against the corresponding known values of concentrations of BSA as discussed in section 2.3.8 of Chapter 2. From Figure 2.3, which is the calibration curve between absorbance and concentration of BSA, it is seen that the standard deviation of the predicted value from actual value of concentration is 0.9995. Thus, every measurement of BSA concentration in permeation is associated with an error of 0.05 % whose effect on rejection values of BSA can be ignored.

A.2. Error in the measurement of permeate flux

The errors in the values of permeate flux are related to the errors in the measurements used to calculate those values. In this section, statistical analysis is used for the estimation of uncertainty associated with the values of permeate flux. Determination of standard deviation is generally considered to be one of the best methods to estimate the uncertainty which is based on the following method:

If u_1, u_2, ..., u_N are the N results of the measurements of a particular quantity u, then the mean value of u (i.e. $\bar{u}$), is defined by

$$\bar{u} = \frac{u_1 + u_2 + ... + u_N}{N} = \frac{1}{N}\sum_{i=1}^{N} u_i \qquad \text{(A.1)}$$

The uncertainty in the result is usually expressed as "root-mean-squared-deviation", which is denoted as Δu, which is computed using the following Eq. (A.2):

$$\Delta u = \sqrt{\frac{(u_1 - \bar{u})^2 + (u_2 - \bar{u})^2 + ... + (u_N - \bar{u})^2}{N-1}} \qquad \text{(A.2)}$$

In the present work, all the membranes were cleaned thoroughly following each experiment. Besides, before each experiment, performance of all the membranes were checked through pure water flux (PWF) measurement; hence uncertainties involved in the PWF measurements are reported here. The uncertainties involved in different experimental measurements for (PWF) for membranes PSF_1, PSF_2 and PSF_3 are estimated and shown in Table A.1.

Table A.1. Values of uncertainties estimated in PWF measurements for membranes PSF_1, PSF_2 and PSF_3.

Membranes	Run 1	Run 2	Run 3	$\bar{u}$	Δu	Uncertainties (%)
PSF_1	754.1	749.8	753	752.3	2.23	0.29
PSF_2	622	618.5	626	622.16	3.75	0.60
PSF_3	270	272	267	269.66	2.51	0.93